Open Water Workgroup Progress Report

Delta Mercury Control Program

Prepared by:

The Open Water Workgroup:

Department of Water Resources

Division of Environmental Services

Bay Delta Office

California State Lands Commission

Central Valley Flood Protection Board

U.S. Army Corps of Engineers

U.S. Bureau of Reclamation

The Open Water Technical Group

Department of Fish and Wildlife

Reed Harris Environmental Ltd.

Moss Landing Marine Lab

U.S. Geological Survey

October 20, 2015

Table of Contents

Executive Summary 14

Background 14

Modeling 14

Field and Laboratory Linkage and Studies 19

Inlet/Outlet 22

Gust Chamber 23

Bale Chamber 24

Pore Water 24

Next Steps 25

Field and Laboratory 25

Modeling 26

Literature Cited 27

1. Introduction 29

1.1. Background 30

1.2. Field and Laboratory Study Background 32

1.2.1. Inlet/Outlet Mass Balance Study 34

1.2.2. Gust Chamber Study 35

1.2.3. Bale Chamber Flux Study 35

1.2.4. Pore Water Flux Study 35

1.3. Delta and Yolo Bypass Modeling-Background 36

1.4. Literature Cited 37

2. Non-modeling Activities 38

2.1. State Agencies 38

2.1.1. California State Lands Commission and Central Valley Flood Protection Board 38

2.2. Federal Agencies 39

2.2.1. US Army Corps of Engineers and US Bureau of Reclamation 39

3. Model and Field Data Linkages 40

3.1. Literature Cited 43

4. Inlet/Outlet Mass Balance Field Study 44

4.1. Introduction 44

4.2. Methods 47

4.2.1. Sampling Locations and Analytes 47

4.2.2. Water Flow Calculations- 50

4.2.3. Load Calculations 51

4.3. Results and Discussion 51

4.3.1. QA/QC Samples 51

4.3.2. Yolo Bypass Flows and Water Balance 54

4.3.3. Total Mercury, Methylmercury, and TSS Concentrations, Loads, and Mass Balance 57

4.3.4. Mercury Sources and Sinks 58

4.3.5. Next Steps-Inlet/Outlet Study 59

4.4. Literature Cited 60

4.5. Appendix A Computation of Stairstep's Modeled Flows for December Inlet/Outlet Sampling Event 69

4.6. Literature Cited 70

4.7. Appendix B Laboratory QA/QC for Inlet/Outlet Samples Collected December 22-23, 2014 73

5. Gust Chamber Erosion Experiments 76

5.1. Introduction 76

5.2. Field Methods 76

5.3. Data analysis 84

5.4. Next Steps 90

5.5. Literature Cited 91

5.6. Appendix A Comparison of Gust and Bale Erosion Chamber Results 92

5.7. Literature Cited 96

5.8. Appendix B Utilization of both Gust and Bale Chamber Results for Sediment and Mercury Mobilization, Respectively 97

6. Bale Chamber-Particulate and Dissolved Flux Rates-Pilot Study 98

6.1. Introduction 98

6.2. Methods 99

6.3. Results 102

6.3.1. Particulate Experiment--Concentration Data 102
6.3.1.1. TSS and MeHg 102
6.3.1.2. Hg 103
6.3.2. Diffusion Experiment--Concentration Data 103
6.3.2.1. TSS and MeHg 103
6.3.2.2. Hg 104
6.3.3. Erosion Rates 104
6.4. Discussion 104
6.5. Summary 106
6.6. Next Steps 107
6.7. Literature Cited 109
7. Sediment-water Exchange of Total Mercury and Methylmercury in the Yolo Bypass Pilot Study (Pore Water Flux) 121
7.1. Introduction 121
7.2. Methods 123
7.3. Results and Discussion 129
7.3.1. Analytical quality assurance and quality control (QA/QC) 129
7.3.2. Incubated core flux study 129
7.3.3. Mercury in sediment and pore water 131
7.3.4. Benthic diffusive fluxes 135
7.3.5. Micro depth profiles 136
7.3.6. Comparison of measured and diffusive fluxes 139
7.3.7. Significance of sediment water exchange study 139
7.3.8. Summary of findings and recommendations for next set of pore water samples to be collected winter of 2015/16 142
7.4. Literature Cited 144
7.5. Appendix A 146
8. Model Progress 150
8.1. DSM2-Hg Model Development Progress 150
8.1.1. DSM2-Hg Domain 151
8.1.2. Data 153
8.1.3. Delta Mercury Model Development: Overview 156
8.1.4. Delta Mercury Model Development: General Transport Module 160

8.1.5. Delta Mercury Model Development: Mercury Module 163
8.1.6. Delta Mercury Model Development: Suspended Sediment Module 164
8.1.7. Delta Mercury Model Development: Bed Sediment Module 165
8.1.8. Delta Mercury Model Development: Integration and Testing 168
8.1.9. Delta Mercury Model Calibration and Application 169
8.2. Yolo Bypass Dynamic Mercury Cycling Model 170
8.2.1. D-MCM Yolo Bypass Model Domain 170
8.2.2. Data Assembly for D-MCM Simulations of Yolo Bypass 171
8.2.3. Development of D-MCM Grid for the Yolo Bypass 176
8.2.3.1. Land use 177
8.2.3.2. THg and MeHg concentrations in sediments 179
8.2.3.3. Agricultural disking 180
8.2.3.4. Hydrological factors 181
8.2.3.5. D-MCM grid development 182
8.2.3.6. Using TUFLOW hydrodynamic model outputs in D-MCM simulations of Yolo Bypass. 184
8.3. Linkage Analysis between DSM2-Hg and D-MCM 186
8.4. Literature Cited 189
9. Next Steps 199
9.1. Field and Laboratory Experiments 199
9.1.1. Next Steps—Inlet/Outlet Study 199
9.1.2. Next Steps—Gust Chamber 199
9.1.3. Next Steps—Bale Chamber 199
9.1.4. Next Steps—Pore Water Diffusive Flux 200
9.2. Next Steps—Modeling 200
9.2.1. Next Steps--DSM2-Hg Modeling 200
9.2.2. Next Steps--D-MCM Yolo Bypass Modeling 202

List of Tables

Table ES- 1. Linkage between D-MCM Yolo Bypass Model and Field and Laboratory Studies. .. 21

Table 3-1. Linkage between D-MCM Yolo Bypass Model and Field and Laboratory Studies. 42

Table 4-1. Flow Estimation Methods for Each Sampling Location. 50

Table 4-2. Field and Filter Blanks. 52

Table 4-3. Field Duplicates. 53

Table 4-4. Yolo Bypass Water Volume and Balance for December 22-23, 2014. 56

Table 4-5. THg, MeHg, and TSS Concentration Data and Daily Average Flow Data for the December 2014 Sampling Event. 64

Table 4-6. Total Mercury, Methylmercury, and Total Suspended Sediment Loads for the December 22-23, 2014 Sampling Events. 65

Table 4-7. Total Hg, MeHg, and TSS Mass Balance for the December 22-23, 2014 Sampling Event. 67

Table 4-8. Laboratory Method Blanks. 73

Table 4-9. Laboratory Replicates. 73

Table 4-10. Lab Control Standards and Duplicates. 74

Table 4-11. Matrix Spikes and Duplicates. 75

Table 5-1. Sites for Erosion Experiments in Yolo Bypass, Dates, and Initial Critical Shear Stress. 80

Table 6-1. Bale Chamber Particulate Study. MeHg concentration vs. velocity for cores collected from Wild Rice and Un-disked Seasonal Wetland Soils. Kd = 1000 * dry weight pMeHg concentration (ng/g)/dMeHg (ng/L). 110

Table 6-2. Hg and TSS results-Particulate experiments. 111

Table 6-3. MeHg and TSS concentrations--Diffusion experiments. 112

Table 6-4. dHg and TSS data--Diffusion experiments. 113

Table 6-5. Comparison of erosion results from Gust and Bale Chambers. 114

Table 7-1. Sampling Dates and Locations. 124

Table 7-2. Results of Analytical Quality Control Samples for THg and MeHg in Sediment and Water. 129

Table 7-3. Sediment-Water Fluxes (F_M) for MeHg and THg Determined using Incubated Cores Collected from Wild Rice (WR) and Un-disked Seasonal Wetland (UDSW) Fields with Overlying Water from either the Sacramento River (Sac) or Cache Creek (Cache). Negative values Indicate Flux into the Sediment. 131

Table 7-4. Fluxes of MeHg and THg by Location and Study. Negative Values Indicate Flux into the Sediment. 131

Table 7-5. Sediment-Water Estimated Diffusive Fluxes (FD) for MeHg and THg Determined using Pore water to Overlying Water Gradients in Cores Collected from Wild Rice (WR) and Un-disked seasonal Wetland (UDSW) Fields with Overlying Source Water from either the Sacramento River (Sac) or Cache Creek (Cache). Negative Values Indicate Flux into the Sediment. 136

Table 7-6. Ancillary Measurements taken during the Incubated Core Flux Study and the Average and Standard Deviation for each Time Series. 146

Table 7-7. Sample Name, Time Collected, Water Volume in Core at Time of Sampling, Mercury Concentration, and Mercury Mass in Core Overlying Water for Wild Rice (WR) Incubated Core Experiment. 147

Table 7-8. Sample Name, Time Collected, Water Volume in Core at Time of Sampling, Mercury Concentration, and Mercury Mass in Core Overlying Water for Un-disked Seasonal Wetland (UDSW) Incubated Core Experiment. 148

Table 7-9. Sample Name, Date Collected, MeHg, and THg, and Percent Moisture for Pore water and Sediment Samples. 149

Table 8-1. Summary of Information Sources reviewed for Mercury Simulations in the Delta. 154

Table 8-2. List of Data Sources Reviewed for use in Yolo Bypass Mercury Simulations. 172

List of Figures

Figure ES- 1. Domains for the two mercury models being developed for the open water portion of the DMCP. 15

Figure ES- 2. Progress, key steps, and milestones associated with the development of the DSM2-Hg model. 16

Figure ES- 3. Progress on development of the DSM2 General Transport Model (DSM2-GTM).. 17

Figure ES- 4. Progress, key steps, and milestones associated with the development of the Yolo Bypass D-MCM 18

Figure ES- 5. Draft revised open water modeling and field/laboratory schedule. 28

Figure 1-1. Geographical extent of the Delta Mercury Control Program. 30

Figure 4-1. Stage at the Toe Drain at Lisbon gage during the month of December 2014. 45

Figure 4-2. Pictures showing the inundation of the Yolo Bypass along the Toe Drain. 46

Figure 4-3. Photo of the Toe Drain at ½ Lisbon sampling location on December 23, 2014. 47

Figure 4-4. Water sampling locations and flow monitoring stations for the December 2014 event. 49

Figure 4-5. Hydrographs for the flow monitoring stations used to calculate loads. 55

Figure 4-6. Flow data for the sum of Knight's Landing Ridge Cut and Cache Creek Settling Basin 56

Figure 4-7. a) Hg, and b) MeHg concentrations for samples collected in the Yolo Bypass, December 22-23, 2014. 61

Figure 4-8. Total suspended solids concentrations for samples collected in the Yolo Bypass.... 62

Figure 4-9. Particulate THg and MeHg concentrations (ng/g) for selected Toe Drain sites. Note: Dry weight concentrations were calculated by dividing the particle phase concentration (ng L^{-1}) by TSS (g/L). 62

Figure 4-10. Apparent partitioning of MeHg and THg at selected Toe Drain sites. 63

Figure 4-11. a) Hg, and b) MeHg loads in the Yolo Bypass, December 22-23, 2014. 66

Figure 4-12. Conceptual model of MeHg imports and exports from the Yolo Bypass mini-flood sampling event, December 22-23, 2014. 68

Figure 4-13. Conceptual model of THg imports and exports from the Yolo Bypass mini-flood sampling 68

Figure 4-14. Comparison between SCHISM modeled and observed flows in 2009 for the Toe Drain below the junction. 71

Figure 4-15. Comparison between SCHISM modeled and observed flows in 2009 for the Toe Drain at Liberty Cut. 71

Figure 4-16. Modeled flow on the upper Toe Drain above the Stairstep, below the Stairstep, and entering the Stairstep during the December 2014 Event. 72

Figure 5-1. Photo of core collection. 77

Figure 5-2. Photo of Gust Chambers (twin cylinders mounted in plate suspended on blue box) set up for measurements. 78

Figure 5-3. Conducting an erosion microcosm experiment in the field immediately after collecting the cores. 79

Figure 5-4. Time series of applied bed shear stress τ, SSC, and erosion rate E for WHR field cores. Data are provisional and subject to revision. 81

Figure 5-5. Time series of applied bed shear stress τ, SSC, and erosion rate E for WR field cores. Data are provisional and subject to revision. 82

Figure 5-6. Time series of applied bed shear stress τ, SSC, and erosion rate E for DSW cores. Data are provisional and subject to revision. 82

Figure 5-7. Time series of applied bed shear stress τ, SSC, and erosion rate E for un-disked UDSW cores. Data are provisional and subject to revision. 83

Figure 5-8. Critical shear stress as a function of eroded mass from 8 cores collected at 4 sites in 2015. Provisional data subject to revision. 84

Figure 5-9. Erosion constant M as a function of eroded mass from 8 cores collected at 4 sites in 2015. Provisional data subject to revision. 85

Figure 5-10. Mass eroded when the critical shear stress is 0.4 Pa. 86

Figure 5-11. Probabilities of initial critical shear stress τ_c and mass eroded when the critical shear stress is 0.4 Pa $m_{0.4}$ for the 8 Yolo Bypass cores analyzed in 2015 and 38 Delta subtidal cores analyzed 2011-2014 (Schoellhamer and Manning in press). 87

Figure 5-12. Critical shear stress as a function of solids volume fraction of the mud matrix. Dickhudt et al. (2011) provide 56 measurements. 88

Figure 5-13. Bottom shear stress as a function of mean current speed. 89

Figure 5-14. Bale and Gust Chamber results for wild rice. Two cores from the same site were tested with the Gust Chamber. MLML and USGS calculated eroded mass independently and got slightly different results. 92

Figure 5-15. Bale and Gust Chamber results for an un-disked wetland. 93

Figure 5-16. Photo of Gust Chamber with flow pattern represented by drawn lines and arrows (Green Eyes LLC, 2011). 94

Figure 5-17. Shear stress distribution in Gust and Bale Chambers for a mean shear stress of 0.1 Pa..... 95

Figure 6-1. a) Diagram of Bale Chamber from Bale and others, 2006. b) Partially fabricated Bale Chamber..... 99

Figure 6-2. a) Location of sample sites. b) Wild rice sediment. 100

Figure 6-3. Concentrations of TSS in particulate experiment. 115

Figure 6-4. Concentrations of pMeHg in particulate experiment. 115

Figure 6-5. TSS vs. pMeHg in particulate experiment..... 116

Figure 6-6. pMeHg vs. time in particulate experiment. 116

Figure 6-7. Particulate experiment. a) Concentrations of filtered and particulate MeHg in wild rice sample by velocity step. b) Concentrations of filtered and particulate MeHg in an un-disked seasonal wetland sample by velocity step. c) Concentration of filtered and particulate MeHg in wild rice sample vs. velocity. d) Concentration of filtered and particulate MeHg in un-disked seasonal wetland sample vs. velocity. e) Calculated Kd in wild rice sample vs. velocity. f) Calculated Kd in un-disked seasonal wetland sample vs. velocity. 117

Figure 6-8. pHg vs. time for WR and UDSW samples-particulate experiments. 118

Figure 6-9. TSS vs. pHg from wild rice sample-particulate experiment..... 119

Figure 6-10. TSS vs. pHg from un-disked seasonal wetland sample-particulate experiment. .. 119

Figure 6-11. Concentrations of dMeHg of WR and UDSW in diffusion experiment..... 120

Figure 6-12. Concentrations of TSS in diffusional experiment. 120

Figure 7-1. Photo of intact sediment cores collected from a wild rice (WR) field in the Yolo Bypass. 125

Figure 7-2. Photo showing aliquots for mercury analysis collected using 60 mL trace clean syringes five times over a 12 hour period. 126

Figure 7-3. Photo of pore water extraction from sectioned cores conducted in glove box under nitrogen..... 127

Figure 7-4. Photo of Unisense micro profiling system used for determination of fine scale depth profiles of oxygen, pH, and sulfide in sediment cores..... 128

Figure 7-5. Mean surficial (0-2 cm) sediment MeHg concentrations in wild rice (WR) and un-disked seasonal wetland (UDSW) fields having either Sacramento River or Cache Creek overlying water. Error bars are standard deviation of triplicate field replicates. 132

Figure 7-6. Mean surficial (0-2 cm) sediment THg concentrations in wild rice (WR) and un-disked seasonal wetland (UDSW) fields having either Sacramento River or Cache Creek overlying water. Error bars are standard deviation of triplicate field replicates. 133

Figure 7-7. Mean MeHg percentage of THg in surficial (0-2 cm) sediment in wild rice (WR) and un-disked seasonal wetland (UDSW) fields having either Sacramento River or Cache Creek overlying water. Error bars are standard deviation of triplicate field replicates. 133

Figure 7-8. Mean Pore water MeHg concentrations in surficial (0-2 cm) sediment of sectioned cores collected from wild rice (WR) and un-disked seasonal wetland (UDSW) fields having either Sacramento River or Cache Creek overlying water. Error bars are standard deviation of triplicate field replicates. 134

Figure 7-9. Mean Pore water THg concentrations in surficial (0-2 cm) sediment of sectioned cores collected from wild rice (WR) and un-disked seasonal wetland (UDSW) fields having either Sacramento River or Cache Creek overlying water. Error bars are standard deviation of triplicate field replicates. 134

Figure 7-10. Vertical microelectrode profiles of dissolved oxygen in interstitial water at WR and UDSW having Sacramento River or Cache Creek water. Note depth scale is in millimeters. 137

Figure 7-11. Vertical microelectrode profiles of hydrogen sulfide (H_2S), bisulfide (HS^-), and total sulfide (Stot) in interstitial water at WR and UDSW having Sacramento River or Cache Creek water. Note depth scale is in centimeters. 138

Figure 8-1. Approximate domains for the two mercury models being developed for the open water portion of the DMCP. 151

Figure 8-2. Model Domain and Boundary Data Locations for the Delta Simulation Model 2... 152

Figure 8-3. Delta methylmercury Budget with Largest Source and Sinks Highlighted (excerpted from Stephenson and others, 2008). 157

Figure 8-4. Expansion of the Delta Simulation Model 2 (DSM2) to represent Mercury Cycling and Transport. 158

Figure 8-5. Progress and Key Steps for Development of the Delta Mercury Model. 159

Figure 8-6. Progress on Development of the DSM2 General Transport Model (DSM2-GTM). . 162

Figure 8-7. Conceptual diagram of model approach for solids in the sediment bed in DSM2. 166

Figure 8-8. Progress and Key Steps for Development of the Yolo Bypass Mercury Model..... 170

Figure 8-9. Schematic showing key factors that influenced D-MCM grid development..... 176

Figure 8-10. . Land use datasets used to develop the D-MCM grid. (a) 2005-2009 survey by Howitt et al. (2013), (b) more recent data for the Yolo Bypass Wildlife Area from Jeff Stoddard, (c) land use represented in the final D-MCM grid. 178

Figure 8-11. Mercury sampling conducted by Heim et al. (2010) in June/December 2007. (a) Sample sites and concentrations (N=97, 84 within model boundary), (b) interpolation using inverse distance weighting. 179

Figure 8-12. THg and MeHg sampling conducted for this study in March-April 2015. Fully shaded panels illustrate interpolation using inverse distance weighting to better visualize the data. 180

Figure 8-13. Disking in the Yolo Bypass. (a) Original analysis conducted by D. Bosworth, (b) Disking represented in the final D-MCM grid. 181

Figure 8-14. Hydrological factors included in D-MCM grid development. (a) Wetting frequency calculated as the percentage of wet days in TUFLOW simulations for 1997-2012, (b) Average number of wet/dry cycles per year in TUFLOW simulations for 1997-2012. 182

Figure 8-15. GIS layers representing five general factors contributed to the final D-MCM grid. 183

Figure 8-16. Geographic overlap between the Yolo Bypass and Delta Mercury models. 187

Figure 8-17. How the Yolo Bypass and Delta Mercury models could be linked for Scenario Analysis. 188

Figure 9-1. Draft revised open water modeling and field/laboratory schedule. 203

List of Abbreviations

ADR Advection-Diffusion-Reaction

BC Boundary conditions

CCSB Cache Creek Settling Basin

CDEC California Data Exchange

CFL Courant–Friedrichs–Lewy numerical computation stability condition

cfs cubic feet per second

CSLC California State Lands Commission

CVFPB Central Valley Flood Protection Board

CVRWQCB Central Valley Regional Water Quality Control Board

DFW California Department of Fish and Wildlife

DICU Delta Island Consumptive Use

DMCP Delta Mercury Control Program

D-MCM Dynamic Mercury Cycling Model

DSM2 Delta Simulation Model 2

DSW Disked seasonal wetland

DWR California Dept. of Water Resources

EC Electrical Conductivity

ft/sec foot per second

GTM General Transport Model

g/day grams per day

HDF5 Hierarchical Data Format (HDF) output file format originally developed at the National Center for Supercomputing Applications

HEC-DSS output file format created by the US Army Corp of Engineers Hydrologic Engineering Center

Hg Generic term for the element mercury.

IC Initial conditions

Kd equilibrium dissociation constant

kg/day kilograms per day

KLRC Knights Landing Ridge Cut

L/kg liters per kilogram

MeHg Methylmercury

MLML Moss Landing Marine Laboratory

mm/day millimeter per day

MQO Method Quality Objectives

ng/L nanogram per liter

ORP Oxidative Reduction Potential

Pa Shear stress

QA/QC Quality Assurance/Quality Control

SCHISM Semi-implicit Cross-scale Hydroscience Integrated System Model

SSC Suspended Sediment Concentration

TAC Technical Advisory Committee

THg Total mercury

TSS Total Suspended Solids

TUFLOW Two dimensional Unsteady Flow

WHR White Rice

WR Wild Rice

UDSW Un-disked seasonal wetland

USACE United States Army Corps of Engineers

USBR United States Bureau of Reclamation

USGS United States Geological Survey

Executive Summary

Background

The Delta Mercury Control Program (DMCP) was adopted in October 2011 and includes the legal Delta and the full extent of the Yolo Bypass. It lays out an implementation strategy for the control of methylmercury (MeHg) and total mercury (THg) in the Delta and Yolo Bypass designed to reduce MeHg levels in Delta fish tissue. It is designed to protect people eating one meal per week of trophic levels 3 and 4 Delta fish, plus some non-Delta (commercial market fish).

For open waters, a combined modeling, field data and laboratory approach was approved by the Central Valley Regional Control Board (Regional Board) to evaluate the potential effects of operational changes on mercury cycling and methylmercury (MeHg supply). Additionally, for other open water activities, the Central Valley Flood Protection Board (CVFPB), and the United States Army Corps of Engineers (USACE) are ensuring that as new permits or leases are issued or renewed, provisions are incorporated into documentation to minimize MeHg open water discharges. The California State Lands Commission (CSLC) staff is currently discussing additional language that could be added as a condition(s) to further address how to avoid or minimize the re-introduction of existing mercury into open waters.

This Progress Report summarizes the progress of the open water workgroup (workgroup) from February 2014 through approximately June 2015.

Modeling

Two models are being modified for use in this study, one for the open waters of the Sacramento-San Joaquin Delta and one for the intermittently flooded Yolo Bypass in winter (Figure ES-1). The Department of Water Resources (DWR) Delta Simulation Model 2 (DSM2) was chosen to model Hg in the Delta, but its domain does not include most of the Yolo Bypass. The Dynamic Mercury Cycling model (D-MCM) (EPRI 2013) was chosen to model Hg in the Yolo Bypass.

Model-related tasks began in 2014. For the Delta modeling effort, DSM2 simulates hydrodynamics, water quality, and ecological conditions in riverine and estuarine systems; however, for Hg simulations, it requires replacing its water quality module (QUAL) and the addition of new modules for Hg, suspended sediments and bed sediments. The QUAL replacement is known as the General Transport Module (GTM). In 2014, DWR's, Bay Delta Office (BDO) continued GTM coding tasks, while Reed Harris Environmental Ltd. (RHE Ltd.) finished coding most of the Hg algorithms that will interact with GTM in DSM2. With respect to suspended and bed sediment additions, BDO staff have completed preliminary suspended

sediment equations, which next require coding and testing. RHE Ltd. has identified equations and begun coding the bed sediment module. However, DWR staff is investigating funding mechanisms to cover calibration of the bed sediment module. A summary of Delta and Yolo Bypass mercury modeling tasks, progress, and milestones are shown in Figures ES-2 and ES-3, respectively.

For the Yolo Bypass Modeling effort, D-MCM simulates Hg cycling and bioaccumulation in aquatic systems; however, it requires hydrodynamic inputs and estimates of resuspension rates for solids, among other inputs. In the case of the Yolo Bypass, hydrodynamics are complex and need to be estimated using a separate hydrodynamic model applied by DWR (TUFLOW). Solids resuspension rates are complex and are being estimated with a combination of field studies and TUFLOW estimates of velocities and associated shear stress acting on particles. The D-MCM also required the development of a modeling grid for the modeled area. Figure ES-4 summarizes the tasks, progress, and milestones associated with the D-MCM Yolo Bypass work.

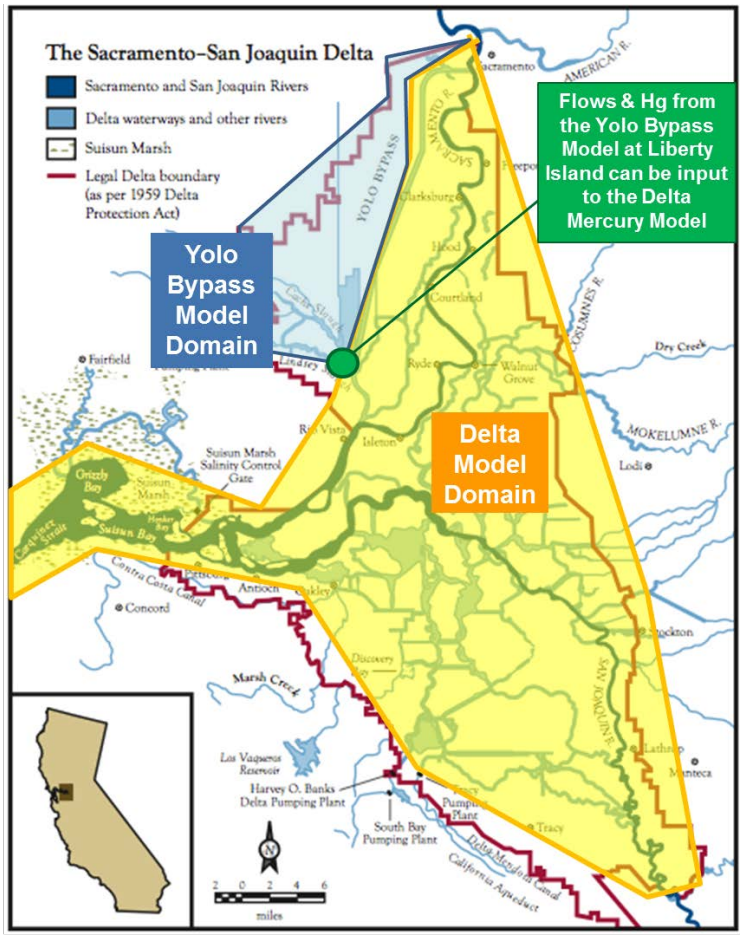

Figure ES- 1. Approximate domains for the two mercury models being developed for the open water portion of the DMCP.

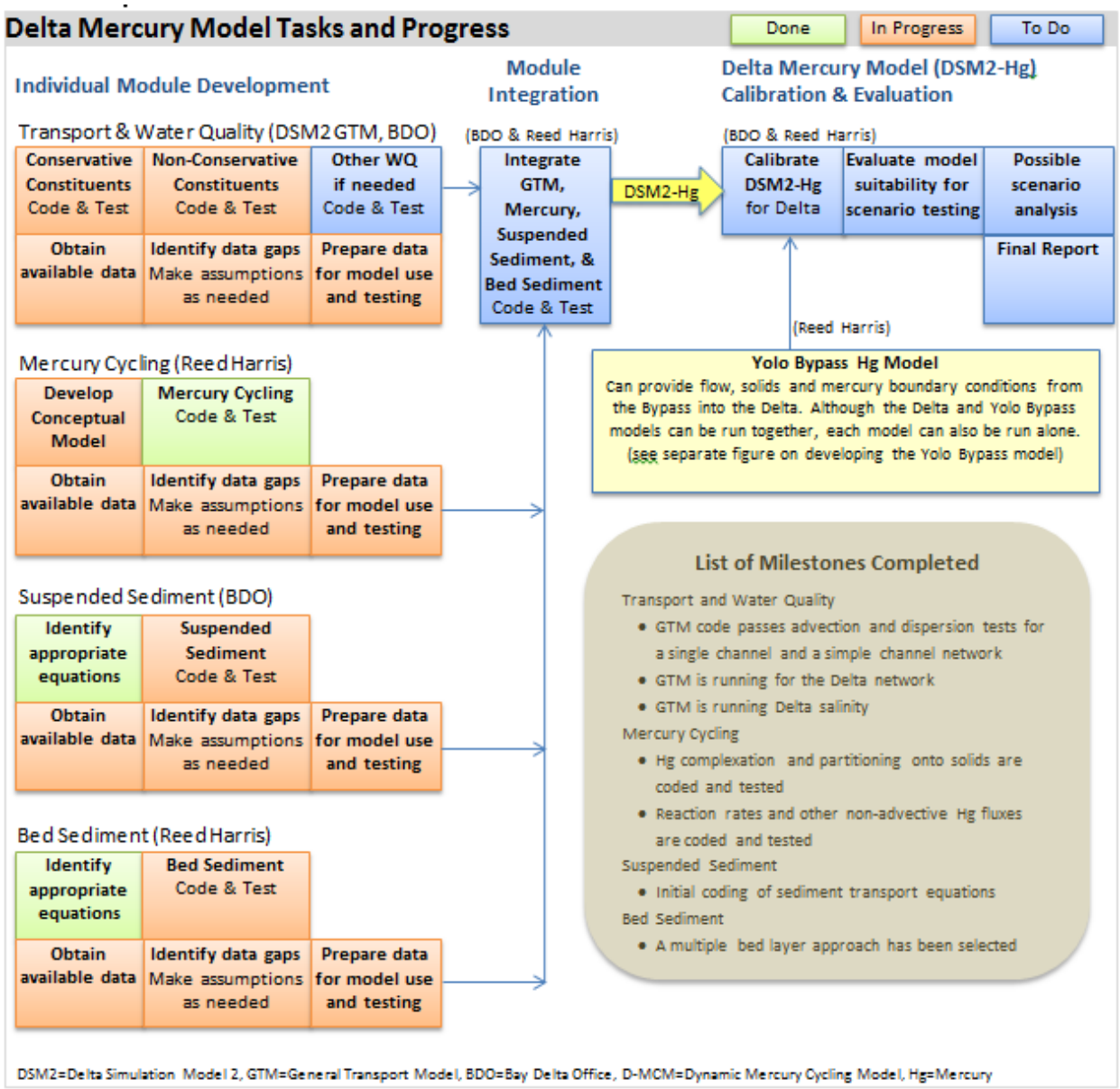

Figure ES- 2. Progress, key steps, and milestones associated with the development of the Delta DSM2-Hg model.

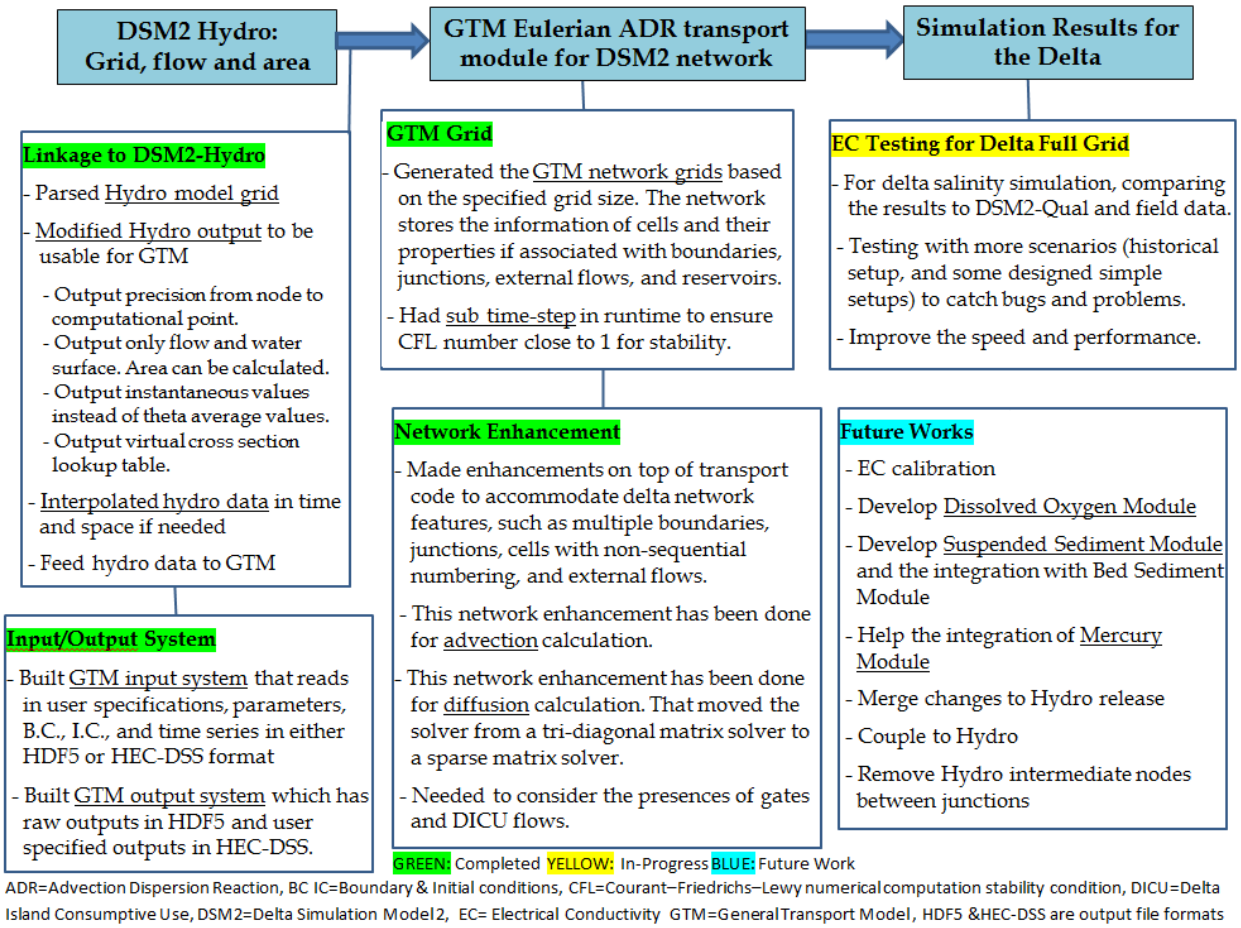

Figure ES- 3. Progress on development of the DSM2 General Transport Model (DSM2-GTM).

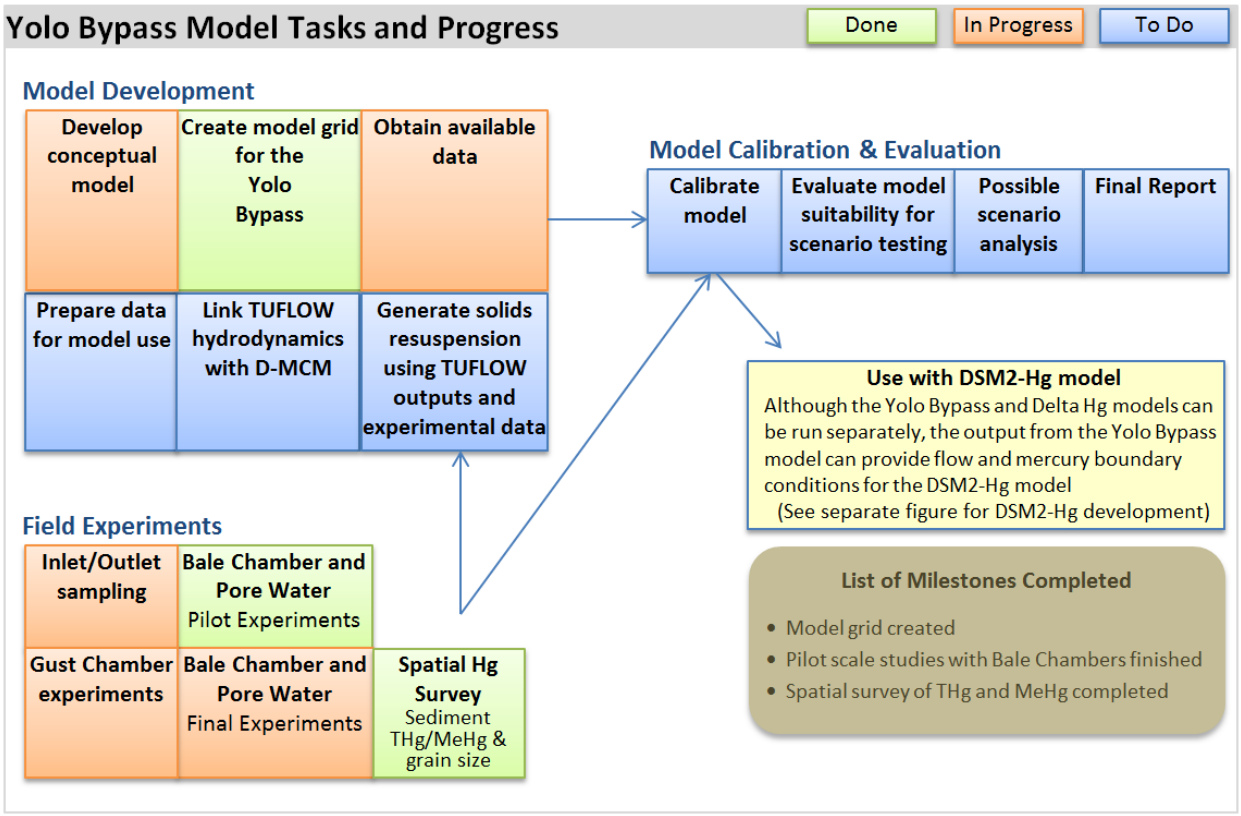

Figure ES- 4. Progress, key steps, and milestones associated with the development of the Yolo Bypass D-MCM.

Field and Laboratory Linkage and Studies

Since the original workplan was accepted in February 2014, the emphasis on field, mesocosm, and laboratory studies has evolved. The technical team of the workgroup evaluated the use of nine replicate, 75-foot (ft) x 300-ft experimental ponds, constructed by the Department of Fish and Wildlife (DFW) in the Yolo Wildlife Area of the Yolo Bypass. The goal was to use mesocosms to examine Hg and MeHg erosional and diffusional flux dynamics under different flood water velocities.

Subsequent calculations indicated that it was neither possible to study diffusion and erosion simultaneously in the same pond nor to use the ponds to isolate just erosion or just diffusion effects. These findings were presented to Regional Board staff in January 2015. Regional Board staff agreed that the ponds were not a practical approach and supported the updated workplan submitted to them, which returned to a laboratory based approach to provide some of the information required by the model.

The revised studies supported by the Regional Board are described below briefly and summarized in Table ES-1. Table ES-1 provides an overview of how field and laboratory efforts fit into the overall D-MCM modeling effort for the Yolo Bypass. The laboratory and field studies are stand-alone studies and are reported as such in the progress report. However, they also function as an integrated group providing additional insights when combined.

1) Inlet/Outlet Studies--these field experiments measure filtered and unfiltered THg and MeHg concentrations and fluxes associated with flow at the inlet, outlet, and intermediate locations in the Yolo Bypass. This information quantifies whether the Yolo Bypass, and reaches within it, are net sources or sinks of THg and MeHg. Measurements of filtered and unfiltered Hg phases help determine whether fluxes within the Yolo Bypass are primarily associated with particles (e.g., erosion) or dissolved transport (e.g., diffusion of MeHg from sediments) during flood conditions.
2) Bale Chamber flux studies—these field or laboratory studies quantify solids and MeHg loads from sediments to the water column, as a function of water velocity, using a mini-annular flume known as a Bale Chamber. Bale Chamber values will be compared to Gust Chamber values to determine its ability to quantify solids.
3) Pore Water flux studies—these laboratory experiments quantify chemical parameters in sediment and pore water which are useful to estimate and understand factors controlling MeHg production and MeHg and THg diffusional fluxes from sediment to overlying water.
4) Gust Chamber erosion studies—these laboratory studies are the accepted standard for quantifying erosion rates. These studies will help provide erosion metrics by land-use for the model.

In addition, in 2015, soil samples were collected in the Yolo Bypass to spatially map patterns of Hg and MeHg concentrations. This effort was not part of the updated workplan submitted to the Regional Board in January 2015. The results of these samples have been incorporated into the development of the model grid for the Yolo Bypass, but are not discussed separately in this document.

Table ES- 1. Linkage between D-MCM Yolo Bypass Model and Field and Laboratory Studies.

Information Source	Information	Intended use of information	
		Used as direct model input or to help develop model input	**Model calibration**
TUFLOW hydrodynamic model	Flows	Flows	
	Water velocities and shear stresses	Solids resuspension rates	
	Bathymetry	Bathymetry for model cells	
Inlet/Outlet Studies	THg, MeHg, TSS concentrations and fluxes at inlet, outlet and intermediate locations		Water column THg and MeHg concentrations in particulate and filtered phases, and solids/dissolved Hg partitioning.
	Net gain/loss of solids in Yolo Bypass		Mass sedimentation rate (burial)
Gust Chamber	Solids resuspension rates	Solids resuspension rates	
Bale Chamber	Solids resuspension rates	Effects of vegetation on solids resuspension rates	
Pore Water studies	THg and MeHg in pore water and sediment solids.		THg and MeHg concentrations in pore water, and partitioning in sediments, and diffusive fluxes.
	Pore water chemistry (DOC, pH, etc.)	Pore water chemistry	
Spatial mapping of surface soil Hg	THg and MeHg in different land uses and locations		THg and MeHg in surface soils
	Grain size distribution in soils	Initial conditions for grain size distribution	Grain size distribution vs. time
USGS studies in Yolo Bypass (published in 2014)	Effects of vegetation on methylation		Production of MeHg
	Role of water level fluctuations on methylation		Production of MeHg
Cache Creek Settling Basin studies (USGS, in preparation)	THg and MeHg loads to Yolo Bypass from CCSB	External loads of THg and MeHg from CCSB	

Progress and preliminary results associated with field and laboratory studies are provided below.

Inlet/Outlet

The occurrence of one flood event in December 2014 allowed the collection of field samples to examine loading of both particulate and filtered THg, MeHg and TSS. Progress and preliminary results include the following:

- Samples were collected from the only flooding event that occurred during the period covered by this Progress Report. The Fremont Weir did not overtop, which classified this as a mini-flooding event.
- Samples were collected at the top of the rising limb of the hydrograph at the Knights Landing Ridge Cut (KLRC), the Yolo Bypass near Woodland, and the Toe Drain at Lisbon Weir stations. Samples were collected on the falling limb of the hydrograph for the Cache Creek Settling Basin (CCSB), while flood flows had returned to baseline at the Putah Creek station.
- All of the flow in the Toe Drain at Woodland could be explained by flows from the KLRC and CCSB stations. The KLRC provided ~78% of the flow, while the CCSB contributed ~22%.
- Water masses balanced upstream; however, there was a 30% water loss between upstream tributary inputs and Lisbon Weir.
- Calculated water losses did not appear to be due to malfunctioning stage gages and may have been due to overland flow, groundwater seepage, or rerouting of water flows. Water losses were consistent with hydrology models already in development by DWR.
- With respect to THg concentrations, the CCSB had the highest filtered and unfiltered THg concentrations. From Road 22 to the export site at ½ Lisbon, there was a slight increase in THg concentrations.
- MeHg concentrations for particulate and filtered samples collected at the Toe Drain at Lisbon Weir increased by a factor of 2 -3 times over upstream sites. Both phases continued to increase downstream to the export site of ½ Lisbon.
- Increases in particulate MeHg in the lower Toe Drain were due to higher MeHg concentrations on solids, not more TSS.
- Calculated Kds for MeHg fell between upstream tributary locations and the Toe Drain at Lisbon Weir. This suggested that the direction of MeHg partitioning was from the particulate to the dissolved.
- With respect to external sources, the CCSB was the largest contributor to THg loads while the KLRC was the largest contributor to MeHg loads. Approximately 80% of the

CCSB's THg load occurred in the particulate fraction. In the case of the KLRC, its MeHg loads were evenly distributed between the particulate and filterable fractions.

- The greatest increase in total MeHg loads occurred between the Toe Drain at I-80 and the Toe Drain at Lisbon Weir. Total MeHg loads increased ~40% between these points.
- The source for the large increase in MeHg at the Toe Drain at Lisbon Weir was unknown; however, rough calculations suggested that resuspension of sediment could be a plausible explanation for the observed increase in MeHg mass. However, without further investigation, it may be the most realistic to assume that this increase is due to a combination of multiple processes with some being more important than others.
- Tributaries contributed ~ 48% of the MeHg exported load, while internal supply contributed ~52%.
- The Yolo Bypass was a net source for unfiltered THg, unfiltered and filtered MeHg, and TSS. For THg, it was a net source due entirely to increases in the particulate phase. The source for MeHg was distributed roughly equally between particulate and filtered fractions. The Yolo Bypass was a net sink for filtered THg.

Gust Chamber

Gust Chamber erosion characteristics were conducted on four land-use types used in the D-MCM Yolo Bypass model (wild rice [WR], white rice [WHR], disked seasonal wetland [DSW], and un-disked seasonal wetland [UDSW]) under a range of velocities to provide the D-MCM with erosion characteristics associated with different land-uses and floodwater velocities in the Yolo Bypass. Progress and preliminary results from the first set of Gust Chamber analyses include the following:

- Sediment cores collected at Yolo Bypass sites featuring four different land uses for assessment of erosion rates as a function of applied shear stress (two cores per site, for a total of eight cores). The different land-use types are represented in the D-MCM Yolo Bypass model.
- Completed testing of each core using a Gust Chamber to reveal eroded soil mass per unit area per unit time versus shear stress.
- Summarized and plotted mathematical relationships between flow speed and applied shear stress. This will allow hydrodynamic model output to be used to compute shear stress on the bed.
- Used the Gust Chamber data to develop mathematical relationships linking critical shear stress (required to initiate erosion) to eroded mass for each of the four land uses tested.
- Developed a methodology to use hydrodynamic model output (on a fine grid) to define sediment input to the D-MCM model (coarser grid).

- Developed a method to use Bale Chamber tests performed on vegetated patches to quantify the influence of vegetation on critical shear stress and erosion rates.
- Preliminary results suggest that for a given shear stress, white rice was the least erodible of the four land-use types, while disked and un-disked wetlands were most erodible. However, these results should be interpreted cautiously as only two cores/land uses were analyzed, so statistical tests of significance were not possible, and soil heterogeneity can cause significant spatial variability.

Bale Chamber

Since the Gust Chamber lacks the volume for collection of Hg or MeHg samples, two pilot experiments were conducted with an experimental Bale Chamber to determine if it could provide comparable Gust Chamber erosion information while also allowing for the collection of Hg and MeHg useful to D-MCM calibration. Pilot studies were conducted on sediment cores collected from a WR field and an UDSW in the Yolo Wildlife Area. Samples were analyzed for particulate and dissolved THg and MeHg, and TSS. Progress and preliminary results from the Bale Chamber pilot experiments showed the following:

- Bale Chamber erosion values appeared reasonable at velocities ≤ 1 ft/sec. Above this velocity, the relationship between velocity and erosion did not appear realistic to field conditions.
- Diffusive flux is minor compared to particulate flux at higher flood water velocities >1 ft/sec. As a result, the high velocity diffusive flux experiments should be eliminated. Future studies should concentrate on particulate flux as a function of velocity.
- Erosional fluxes of TSS, MeHg and Hg increased exponentially with velocity.
- Erosional fluxes of TSS are higher in the Bale Chamber than the Gust Chamber, therefore calibrations are necessary.
- The best use of the Bale Chamber may be for a relative comparison of erosional rates among the different land uses, as it can measure rates in soft as well as vegetated substrates.

Pore Water

This task was designed to (1) investigate the relationship between MeHg production and major biogeochemical processes in sediments, (2) measure dissolved fluxes of mercury and MeHg between sediment and overlying water, and (3) provide sediment concentrations of MeHg and THg in dissolved and particulate phases to help calibrate the D-MCM. Pilot experiments were carried out on two land-use types, a wild rice (WR) field and an un-disked seasonal wetland (UDSW) in the Yolo Wildlife Area. Progress and preliminary results from pore water pilot experiments included the following.

- Core incubation method appears to provide reasonable assessments of flux based on comparison to previous studies.
- Core Incubations were carried out over a 12 hour period with the cores remaining stable and providing reliable results for the duration. In fulfillment of the pilot study objective to determine optimal time for incubations, we recommend the next round of experiments be carried out for at least 12 hours. The possibility of increasing incubation times to 18-24 hours in measured flux experiments is an option given our ability to maintain stable cores during experiment. This option would allow for day/night incubations to investigate effect of benthic diatoms on mercury cycling.
- Given the pilot study results, our working hypothesis that there is no difference in sediment water mercury exchange fluxes using Sacramento River and Cache Creek waters was not supported. Therefore, it is important to continue work on additional habitat types using two sources of water (that is, low mercury concentration water from the Sacramento River, and high mercury concentration water from Cache Creek) in core incubation studies.
- Dissolved oxygen penetration into sediments was shallow (<3.5 mm).
- The absence of measureable sulfide species in WR fields and the presence of sulfide species in an UDSW, in combination with solid phase MeHg concentrations, MeHg percent of THg, and MeHg flux being higher in the UDSW than in the WR field, support a link between sulfate reduction and MeHg production.
- The working hypothesis that sediment water exchange flux of mercury can be modeled by pore water and sediment chemistry measurements of MeHg, THg, total organic carbon, and grainsize currently lacks sufficient data to be evaluated as only two land-use types have been sampled.
- The working hypothesis that mercury sediment water exchange fluxes differ among the two different land uses is supported by pilot study results.

Next Steps

Field and Laboratory

With respect to field studies, as weather and hydrology allow, DWR will continue to collect samples for inlet/outlet mass load estimates.

Results of the pilot pore water diffusion experiments successfully demonstrated their ability to provide the D-MCM Yolo Bypass model with sediment mercury concentration, partitioning and dissolved flux estimates. Final approaches will be determined by the technical team, but next steps potentially include conducting pore water diffusion experiments on the remaining land uses or important locations covered by the D-MCM Yolo Bypass Model: (1) white rice, (WHR),

(2) disked seasonal wetland (DSW), (3) below Putah Creek, (4) fallow or irrigated pasture, (5) below CCSB, (6) Liberty Island, (7) Toe Drain near Lisbon Weir, and (9) the Toe Drain near Little Holland tract (Liberty Cut). The pilot experiments suggest that we may wish to adapt our upcoming experiments to incorporate more replicates, a finer resolution of core sections for more accurate diffusive flux calculations, and potentially add a temporal component to a subset of sample stations to determine if results vary with time during the flood season.

Under certain conditions, the Gust Chamber can successfully provide erosion information for the D-MCM Yolo Bypass model. The technical team will evaluate final approaches; however, it is anticipated that Gust Chamber samples will be collected from the remaining land uses or important locations in the D-MCM Yolo Bypass model that were not tested in the winter of 2014. These land uses or locations potentially include (1) fallow or irrigated pasture, (2) below CCSB, (3) Liberty Island, (4) Toe Drain near Lisbon Weir, and (5) the Toe Drain near Little Holland tract (Liberty Cut). At higher velocities, and in vegetated areas, the Gust Chamber is not capable of providing erosion characteristics for the D-MCM Yolo Bypass model. The technical team is currently investigating approaches that could be used under these circumstances. Some of the approaches being evaluated include whether literature values can be used to extrapolate Gust Chamber erosion characteristics at higher velocities, or whether the Bale Chamber or a different apparatus could be used to provide a relative indicator of erosion characteristics between vegetated and non-vegetated sites.

Pilot experiments indicate that the Bale Chamber could not reliably provide erosion information at velocities > 1 ft/second (sec). The technical team is evaluating if the Bale Chamber can still provide the Gust Chamber with relative information on the erosion characteristics of vegetated and non-vegetated land uses. The technical team is also evaluating if the Bale Chamber can still provide useful Hg concentration information for the D-MCM Yolo Bypass calibration and validation runs.

Modeling

With respect to the Delta, the next steps for the DSM2-Hg modeling effort focus on completing the General Transport Model (GTM), the suspended and bed sediment modules, and completing the mercury cycling routines. This will be followed by testing these modules individually and then testing them as an integrated unit.

Once this has been successfully completed, the Delta model will be calibrated and validation runs will be evaluated to determine the robustness of the model. Tables 8-1 and 8-2 in Chapter 8 lists all the data sources, to date, that have been examined for possible data inputs and for use during calibration/validation runs. These calibration and validation runs will be used to determine if final Delta scenario runs are practical or if additional work is required. If final Delta

scenario simulations are practical and approved by a technical, management, and legal review committee, then modeling runs will continue forward and examine Delta MeHg production under current and selected operational scenarios. If they are not practical, then additional data needs will be identified so that future modeling and field efforts can be focused to address these data gaps.

Our next step for the D-MCM Yolo Bypass modeling is to set up the model for existing conditions. We will estimate some inputs using field data while, for other inputs, we will use outputs from other models. For example, for bathymetry, water flows, and surface elevations of model cells in the D-MCM grid, we will rely on outputs from the TUFLOW model. Then we will use TUFLOW outputs for velocity and shear stress to estimate solids erosion rates which, we will, in turn, use as inputs for model simulations. Subsequently, we will do trial model runs and compare them to existing Hg measurements in Yolo Bypass. For model calibration, we will optimize the fit to observations, based on data available at that time. Once inlet/outlet, pore water, and Gust Chamber field studies have been completed, we will carry out final calibration of the model to existing conditions, as well as validate the model. Similar to DSM2-Hg modeling, validation runs will help determine the robustness of the model and suitability for moving forward to scenarios vetted by a technical, management, and legal internal review team. While we have not finalized the approach to model validation, it may involve calibrating the models to data from one time period, and validating the model using data from another time period.

While the workgroup's modeling team is making every effort to create a modeling product within the DMCP's deadline, it has become apparent that the schedule provided in the original workplan did not fully represent the tasks or complexity associated with building a Delta Hg model. Therefore, a timeline extension will be required to complete modeling tasks. Additionally, obtaining funding for bed sediment work has also been challenging. As shown in Figure ES-5, the updated timeline reflects all the currently identified tasks. We are still refining scheduling timelines. However, we have currently identified the tentative report submittal date as December 2019.

Literature Cited

EPRI, 2013. Dynamic Mercury Cycling Model for Windows 7/Vista/XP, D-MCM Version 4.0, Product ID: 3002002518, User Guide and Technical Support, Electric Power Research Institute, December 2013.

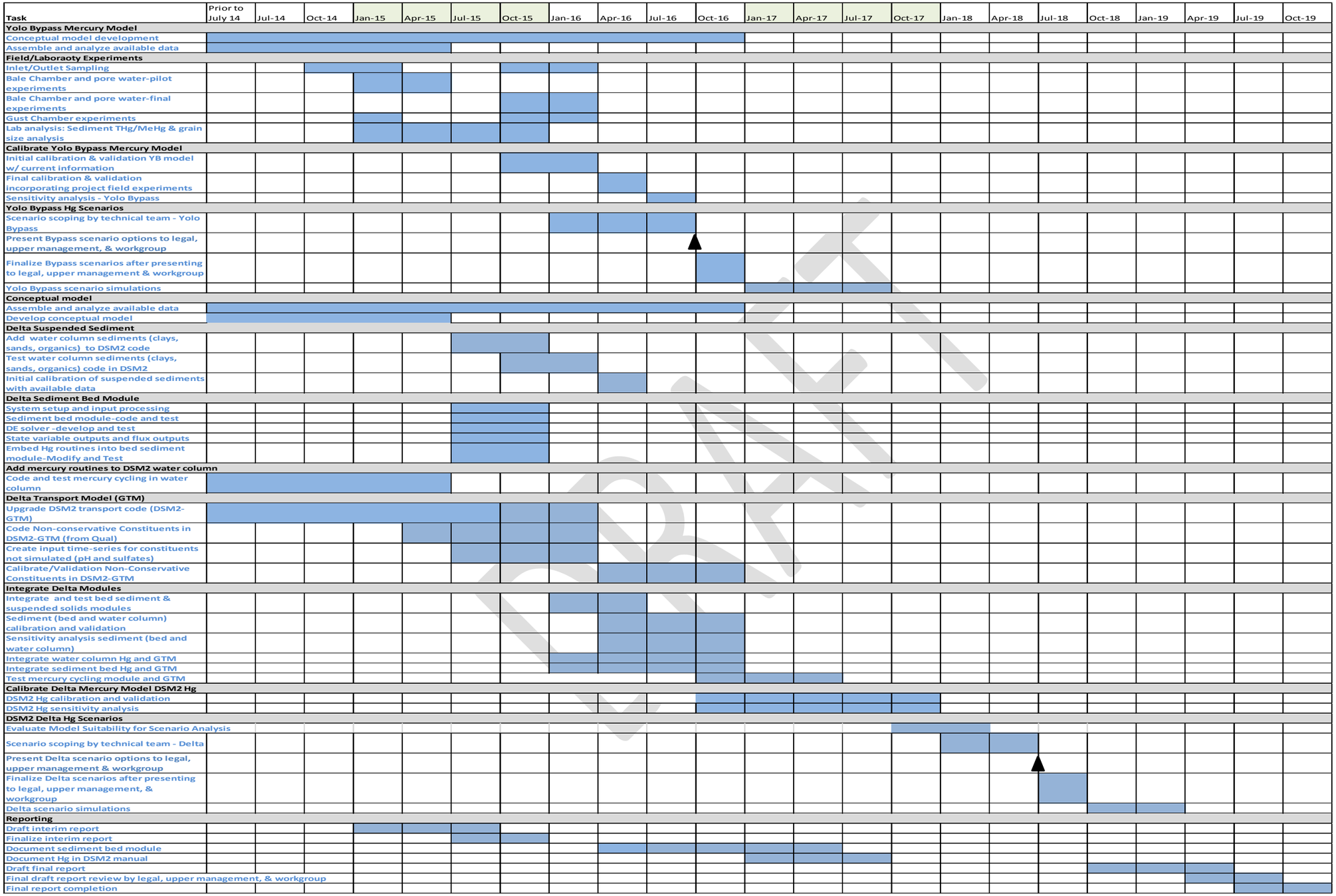

Figure ES- 5. Draft revised open water modeling and field/laboratory schedule.

1. Introduction

This progress report covers the period between February 2014, when the open water workplan was accepted by the Central Valley Regional Water Quality Control Board (Regional Board), and approximately June 2015.

The progress report is divided into nine chapters. To provide context for the report, this chapter provides background information, which sets the stage for the progress report on open water control studies.

The DWR is funding and leading the technical control studies associated with open water requirements of the DMCP. However, the open water portion of the DMCP also requires actions by other entities, such as the CSLC. Chapter 2 summarizes the non-technical actions taken by partner open water workgroup members.

The creation of an Hg model for two complex systems, the Sacramento-San Joaquin Delta and Yolo Bypass, has never been attempted. There are numerous interrelated tasks required in the creation of these models, including the development of the models themselves and obtaining field and laboratory information to help model refinement. In the case of the creation of the Yolo Bypass D-MCM model, it can be especially challenging to understand how each piece fits into the overall modeling process. Therefore, to provide the reader with a linkage between the different studies and how each will be incorporated and used by the D-MCM, Chapter 3 provides an overview of the different supporting field, laboratory, and modeling studies and where each will be used.

Chapters 4-7 provide results for the different supporting field and laboratory studies used by the model. Each of these studies contains results that may be of interest to researchers outside of model development. Therefore, study results present preliminary data analysis in addition to the data used specifically by the model.

Chapter 8 documents the progress to date on the different modeling components associated with the open water modeling framework. This includes an update on the GTM, the additional module development for the Delta DSM2-Hg model, and the refinement of the D-MCM model for the Yolo Bypass.

Finally, Chapter 9 provides information on the next steps required for each of the field, laboratory, and modeling components of the study. It also highlights potential uncertainties and how these could impact the current schedule.

1.1. Background

To address Hg contamination in the Delta and Yolo Bypass, the Central Valley Regional Water Quality Control Board (Regional Board) adopted the Methylmercury Total Maximum Daily Load and Basin Plan Amendment that established a DMCP (Wood and others 2010a, Wood and others 2010b). The DMCP includes the legal Delta and the full extent of the Yolo Bypass (Figure 1-1). It is designed to protect people eating one meal per week of trophic levels 3 and 4 Delta fish, plus some non-Delta (commercial market fish).

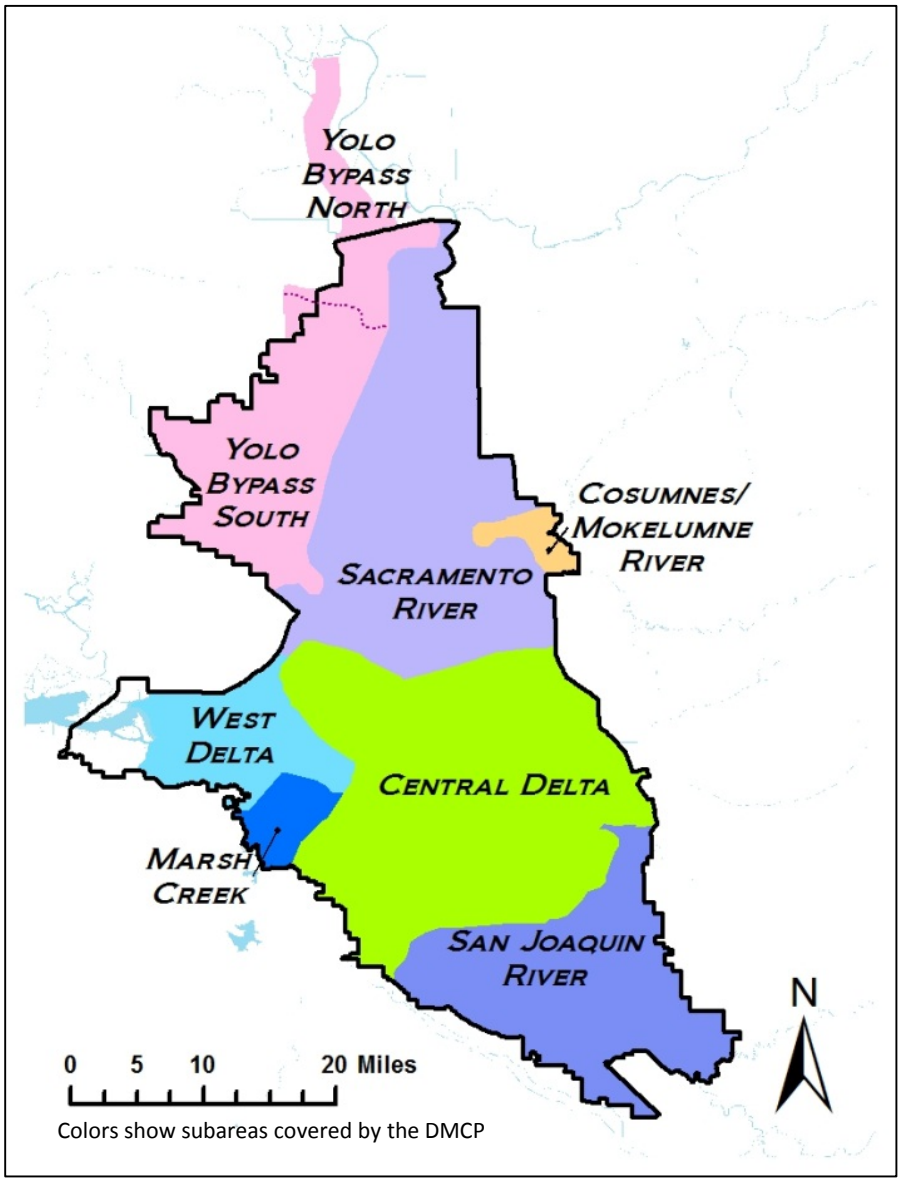

Figure 1-1. Geographical extent of the Delta Mercury Control Program.

The DMCP uses an adaptive management approach and is divided into phases. Phase 1 spans the period from October 20, 2011, to approximately October 20, 2020. During Phase I, stakeholders are required to conduct MeHg control studies to evaluate existing control methods and, as needed, develop additional control methods that could be implemented to achieve their MeHg load and waste load allocations. Stakeholders may conduct characterization studies to inform and prioritize the control studies. Following an approved workplan, stakeholders are required to submit a progress report of their control studies by October 20, 2015.

The DMCP contains load allocations and reductions for a number of activities within the DMCP geographic area; one of these is open water. As defined in the DMCP, open water allocations apply to the MeHg load that fluxes to the water column from sediments in open water habitats within channels and floodplain in the Delta and Yolo Bypass. In 2012, a workgroup was formed consisting of stakeholders identified in the open water section of the DMCP. The workgroup consists of the DWR, the CSLC, the CVFPB, the USACE, and the US Bureau of Reclamation (USBR). These agencies are required to *……"evaluate their activities to determine whether operational changes or other practices or strategies could be implemented to reduce ambient MeHg concentrations in Delta open water areas and floodplain areas inundated by managed floodplain flows"* (DMCP, 2011).

The open water workplan (workplan) submitted to the Regional Board by the workgroup uses a modeling approach to evaluate MeHg loads. We selected a modeling approach because, unlike other DMCP regulated activities, evaluating the impact of changes in water operations to MeHg loads cannot easily be addressed through conventional field and laboratory studies. By necessity, two separate MeHg models are being created: one for the Delta and a second for the Yolo Bypass. The nexus of the two is at Liberty Island in the Yolo Bypass.

The objectives of the workplan are to do the following:

1. Provide working models for Hg and MeHg supply, transport, and fate in the open waters of the Delta and Yolo Bypass;

2. Apply the models to identify processes governing open water MeHg supply to the Delta and Yolo Bypass;

3. Apply the models to examine the potential impacts of proposed operational changes in water management and flood conveyance in the Delta and Yolo Bypass on open water MeHg supply, and compare to TMDL allocations; and

4. Use existing data, supplemented as needed by field and laboratory studies, to elucidate fundamental MeHg processes under flooding events.

1.2. Field and Laboratory Study Background

As part of phase 1 requirements, the workgroup submitted a workplan in April 2013. Comments from the Technical Advisory Committee (TAC), convened by the Regional Board were received at the end of July 2013, with further clarification from the Board in September 2013. The original workplan relied primarily on a laboratory-based approach to address data gaps. The TAC's review of the workplan, expressed concern over the extrapolation of laboratory generated data to real world mercury processes to provide the necessary information to the Yolo Bypass D-MCM. To address these concerns, the final workplan included a technical memorandum that replaced laboratory experiments with field based mesocosms. In February 2014, the Regional Board approved the workplan and its accompanying technical memorandum. These documents have already been provided to the Board and are not included with this report.

For mesocosm work, the finalized workplan and technical memo proposed the use of DFW replicate, 75-ft x 300-ft constructed ponds. The mesocosm work was meant to provide realistic, field-based, experimental estimates of mercury dynamics associated with erosion and dissolved fluxes across the sediment-water interface under a range of conditions that included flow rate and velocity, land use, and time of year.

Following workplan acceptance, the workgroup's technical team further examined the feasibility of using the DFW ponds to provide Yolo Bypass floodwater erosional and diffusion dynamics. This included extensive outreach and discussions with experts in the field (Rocky Geyer, Woods Hole Oceanographic Institution, and the United States Geological Survey (USGS), including Charlie Alpers, Jacob Fleck, and David Krabbenhoft). Additionally, the technical team engaged engineers at California State University, Chico to examine the operational criteria necessary for the ponds to provide diffusion and erosion data under velocities observed with mini- and major flood-events[1] in the Yolo Bypass.

Calculations showed that using the ponds as raceways was not a practical approach to generate the required erosional and dissolved flux data. These findings were documented and presented to Regional Board staff in January 2015. As outlined in the document, the pond approach was not practical for the following reasons:

---

[1] A mini-flood event is defined as flooding due to overtopping of the banks of the westside tributaries into the Yolo Bypass, but no overtopping of the Fremont Weir. A major flooding event is defined as overtopping of the Fremont Weir. This range of velocities also encompassed the velocities that should be observed under gating of the Fremont Weir for fish passage improvement and floodplain habitat.

1. It was not possible to study diffusion and erosion in the same pond. During flood events, field velocities in the Yolo Bypass at Lisbon Weir can vary from 1-3 ft/sec. Velocities of approximately 1 ft/sec. can be obtained by creating a narrow channel through the pond (e.g. a few feet wide). This configuration would also likely induce erosion. However, calculations of the diffusion signal at the lowest velocity tested (1 ft/sec.) suggested that there would be insufficient time for diffusion to produce a measurable increase in water column MeHg (e.g. 0.04 ng MeHg/ L). This conclusion was based on assumed diffusion rates on the order of 2-20 $ng/m^2/day$[1], comparable to flux Chamber estimates in the Delta (Stephenson 2008).

2. It was not possible to use the ponds to isolate just erosion or just diffusion effects.
   a. At velocities > 1ft/sec., it became impractical to engineer the ponds to study just erosion. The head heights to create the desired velocities were too large, as was the variability in velocity between the inlet and the outlet. This approach suffered from a limited ability to test the effects of different land uses.

   b. Ponds could be used to investigate dissolved fluxes from sediments to the water column, but the slow velocities required to obtain a measurable increase were below most flood conditions in the Yolo Bypass, and this approach also suffered from a limited ability to test the effects of different land uses.

3. Finally, consideration was given to creating a long narrow channel, (e.g. a few feet wide), with sufficient velocity to induce erosion and sufficient water residence time to induce a measurable effect from dissolved fluxes. However, calculations showed that this was not practical. A channel length of several thousand feet would be required, the elevation drop would be too large to be practical (several feet deep at the upstream end), and velocities would change significantly along the length of the channel, making it more difficult to establish a relationship between velocity and erosion.

In a February 2015 meeting to review the open water technical team's conclusions, Regional Board staff agreed that the ponds were not a practical approach and supported the updated workplan also submitted to Regional Board staff in January 2015.

The January 2015 revised workplan used a combined field and laboratory approach to provide some of the information required by the model. Inlet/outlet sampling and loading calculations were still proposed to understand the partitioning of Hg between the dissolved and particulate phase under mini-flood and major flooding events in the Yolo Bypass. However, the updated workplan contained lab based experiments using Bale and Gust Chambers, as well as pore water diffusion experiments. In brief the data gaps and information provided by the four approaches are the following:

1) Inlet/Outlet Mass Balance—these field experiments quantify THg and MeHg increases by calculating loads and creating a mass balance for particulate and dissolved THg and MeHg in the Yolo Bypass during flood events;
2) Bale Chamber flux studies—these field or laboratory studies quantify MeHg particulate and dissolved erosion rates as a function of velocity from sediment to water using a mini-annular flume known as a Bale Chamber;
3) Pore Water flux studies—these laboratory experiments quantify chemical parameters in sediment and pore water to provide MeHg and THg diffusional fluxes from sediment to overlying water and parameters useful to the D-MCM to predict MeHg production;
4) Gust Chamber erosion studies—these laboratory studies quantify erosion rates and grain sizes of several representative sediments and land use types using a Gust Erosion Chamber.

Our overall objectives for the different field and laboratory studies is to provide rate constants or data to calibrate or validate the Dynamic Mercury Cycling Model (D-MCM) for sediment/water fluxes of mercury and methylmercury (MeHg) as a function of the following factors:

1) Flow;
2) Land use;
3) Phase (dissolved or particulate);
4) Time of year, and;
5) Type of flooding.

Since methodology or instrumentation for the Bale Chamber and pore water experiments required preliminary investigation, we conducted pilot experiments to assess their suitability for our experimental needs.

The objectives associated with the laboratory and field experiments are listed below.

1.2.1. Inlet/Outlet Mass Balance Study

1) Determine whether the Yolo Bypass and reaches within it are sources or sinks for THg and MeHg under different flow and flood conditions. This information will help calibrate sediment to water fluxes of MeHg under different conditions.
2) Provide data for water column concentrations of THg and MeHg in the particle and filtered phases. This information will help calibrate the model to existing mercury concentrations and to calibrate mercury partitioning between solid and dissolved phases.

1.2.2. Gust Chamber Study

1) Provide solids erosion rates of sediment under different velocities and land uses for use in the D-MCM.
2) Provide data to calibrate the velocity vs. erosion relationship developed by the Bale Chamber.

1.2.3. Bale Chamber Flux Study

Pilot Study

1) Determine if the Bale Chamber methodology can be used to estimate MeHg and THg sediment water fluxes in the particulate and dissolved phase.
2) Determine the optimal time of sampling the Bale Chamber at water velocities observed in the Yolo Bypass at Lisbon Weir under mini and major flooding events.

Final Study

1) Provide solids and MeHg and THg particulate and dissolved fluxes as a function of velocity, and land use.
2) Determine if dissolved flux for MeHg and THg are similar to values produced by the pore water experiments.

1.2.4. Pore Water Flux Study

Pilot Study

1) Provide pore water rate constants for dissolved MeHg and THg sediment water fluxes on 2 different land uses.
2) Provide important, non-mercury pore water chemistry information that could be used in the D-MCM for predicting MeHg production within sediments and MeHg and THg sediment to water fluxes.
3) Determine if the overlying water source affects sediment to water fluxes to understand which water source should be used in pore water and Bale Chamber tests.
4) Determine the optimal times of sampling overlying water, pore water and sediment.

Final Study

1) Provide rate constants for MeHg and THg sediment water fluxes at zero velocities for dissolved MeHg on different land uses and times of the year.
2) Provide ancillary data that could be used in the D-MCM for predicting MeHg production within sediments and MeHg and THg sediment to water fluxes.

In early 2015, proof of concept laboratory pilot experiments for the Bale Chamber and pore water experiments were conducted. Additionally, one mini-flood event allowed the collection of field samples so that loads could be calculated for particulate and dissolved THg, MeHg and TSS. Gust Chamber analyses of erosional characteristics of four land-use types in the Yolo Bypass were also completed. The Regional Board also provided funding to Moss Landing Marine Laboratory (MLML) to support the collection and analysis of sediment samples in the Yolo Bypass for THg, MeHg, Loss on Ignition (LOI), and grain size (spatial mapping). These analyses are used to generate values for model inputs or for model calibration and validation. Grain size analysis was funded by DWR, while other sediment analyses were funded by the Regional Board. Results of the spatial distribution of MeHg and THg on sediment were integrated into the final base-layer of the Yolo Bypass D-MCM and are not discussed separately in this document. Grain size analysis is ongoing and will also be incorporated directly into the model.

1.3. Delta and Yolo Bypass Modeling-Background

A calibrated and validated mercury model for the Delta and Yolo Bypass has never been created. The TAC assembled by the Regional Board, recognized the size and scope of the effort as large and ambitious. For this modeling effort, DWR has partnered with a number of different agencies and experts. DWR is updating and replacing the QUAL portion of the Delta Simulation Model 2 (DSM2). This upgrade, known as the GTM is already in progress within the Department. In addition to DSM2 upgrades, Department modelers, and consultants from Reed Harris, Environmental Ltd., are building the bed sediment, suspended sediment, and mercury modules necessary for a fully functional Delta Hg model. In the Yolo Bypass, a fully functioning Hg model, the Dynamic Mercury Cycling Model or D-MCM is being used and applied to the Yolo Bypass by Reed Harris Environmental Ltd. This requires the development of a geographic information system (GIS)-based grid based on several factors for the model to run, as well as the additional field and laboratory requirements described previously. The D-MCM is not a hydrodynamic model, and requires hydrodynamic inputs for its operation. For the D-MCM, hydrodynamics are being supplied from a separate, on-going DWR/USBR modeling project (TUFLOW model), spurred by fish passage improvement requirements associated with the Biological Opinions Reasonable and Prudent Action 1.6.1 and 1.7. Additionally, it is anticipated that boundary conditions associated with the Cache Creek Settling Basin (CCSB) will be supplied by yet another, DWR effort, associated with understanding the basin's settling capacity and its MeHg dynamics. This work is being conducted, by UC Davis and the USGS, under contract to DWR.

1.4. Literature Cited

Bosworth, D. H., S.J. Louie, M.L. Wood, D.J. Little, and H. Kulesza. 2010. A Review of Methylmercury and Inorganic Mercury Discharges from NPDES Facilities in California's Central Valley Staff Report. Final. March 2010. California Environmental Protection Agency. Regional Water Quality Control Board. Central Valley Region.

DMCP. 2011. Amendments to the Water Quality Control Plan for the Sacramento River and San Joaquin River Basins for the Control of Methylmercury and Total Mercury in the Sacramento-San Joquin River Delta Estuary (Attachment 1 to Resolution NO. R5-2010-0043).

Stephenson M., C. F., G. A. Gill, and K. H. Coale , C. Foe, G. A. Gill, and K. H. Coale. September 15, 2008. CALFED Mercury Project Final Report. California Department of Fish and Game, California Bay Delta Authority.

Wood, M. L., C. G. Foe, J. Cooke, and S. J. Louie. 2010a. Sacramento-San Joaquin Delta Estuary TMDL for Methylmercury, Staff Report. Regional Water Quality Control Board, California Environmental Protection Agency, Central Valley Region, April 2010.

Wood, M. L., P. W. Morris, J. Cooke, and S. J. Louie. 2010b. Amendments to the Water Quality Control Plan for the Sacramento River and San Joaquin Basins for the Control of Methylmercury and Total Mercury in the Sacramento-San Joaquin Delta Estuary, Staff Report. California Environmental Protection Agency, Regional Water Quality Control Board, Central Valley Region. April 2010.

2. Non-modeling Activities

In the workplan, the CVFPB, the CSLC and the USACE agreed that, as new permits are issued or come up for renewal, these permits will be examined to determine what modifications are necessary to address the mobilization and transport of sediment bound mercury. The progress with these activities is discussed below.

2.1. State Agencies

2.1.1. California State Lands Commission and Central Valley Flood Protection Board

As stated in the workplan, the CSLC leases sovereign land for various purposes that are consistent with the Public Trust Doctrine. Some of these leases may include activities (e.g., dredging, riprap installation, spur dike removal) that contribute to the disturbance of streambed sediments. To more effectively modify future leases to address the mobilization and transport of sediment-bound Hg, the CSLC will, as part of this workplan, conduct an examination of current effective methodologies to strengthen existing best management practices or develop new control measures aimed at reducing the concentration of Hg and/or MeHg released into the Delta due to sediment disturbance.

In 2014/2015, CSLC staff has examined the standard conditions specified in our leases and are currently discussing additional language that could be added as a condition(s) to further address how to avoid or minimize the re-introduction of existing mercury into open waters within the Delta. In addition, when reviewing projects provided to us by the State Clearinghouse that have the potential to result in sediment release within the Delta, CSLC staff has incorporated specific comments addressing the potential for mercury and methylmercury release to promote agency and public awareness. Examples of these projects include the following:

- Smith Canal Gate Project, San Joaquin County (SCH# 2014062079);
- Delta Levee Investment Strategy, Sacramento and San Joaquin Counties (SCH# 2015052070);
- North Sacramento Streams, Sacramento River East Levee, and Related Flood Improvements Project, Sacramento, Yolo, Sutter & Solano Counties (SCH# 2014052038);
- San Joaquin River Parkway Sycamore Island Pond Isolation Project, Fresno and Madera Counties (SCH# 2015011041);
- Emergency Drought Barriers Project, Yolo, Sacramento, and Contra Costa Counties (SCH #2015012048);

- Delta Emergency Facilities Improvement Project Refinements, San Joaquin and Solano Counties (SCH #2014112056);
- I Street Bridge Replacement Project, Sacramento and Yolo County (SCH #2014092069);
- Butte Slough Outfall Gates Rehabilitation Project, Sutter and Colusa Counties (SCH #2014082018);
- Sherman Island "Little Baja and Manzo Ranch" Fish Release Sites Project, Sacramento County (SCH #2014052035);
- Decker Island Electrical Crossing Project, Sacramento and Solano Counties (SCH #2014032039); and
- Raley's Dock Replacement and Rice Mill Pier Rehabilitation Project, Yolo County (SCH #2014022054).

CSLC staff will continue to look for ways to further emphasize the need to reduce sediment disturbance and subsequent methylmercury release in the Delta by incorporating adequate best management practices.

2.2. Federal Agencies

2.2.1. US Army Corps of Engineers and US Bureau of Reclamation

Both the U.S. Army Corps of Engineers and the U.S. Bureau of Reclamation (USBR) participate in the open water Delta mercury TMDL process in accordance with the workgroup's methylmercury control study workplan and its own authorizations. The USACE and USBR are currently authorized to provide technical support to the effort, which it has provided when necessary or requested. Both agencies have attended scheduled meetings and are also continuing to review authorizations to determine if funding can be made available in the future to support workgroup efforts. Both the USACE and USBR will continue to provide technical support for the duration of the activity.

3. Model and Field Data Linkages

A MeHg model for the Delta and Yolo Bypass has never been created, therefore, to achieve its goal, two approaches are being followed simultaneously. The first approach focuses on the mechanics associated with developing and running the model. This includes the development of the necessary code and algorithms, model grid development, data assembly, calibration, validation, etc. The second approach focuses on field and laboratory work to fill key data gaps necessary for model development. In some cases experimental results may also suggest management strategies to reduce MeHg production.

The recognition that data gaps existed and needed to be addressed were recognized early in the modeling process. In the case of the Yolo Bypass, this was especially true. Due to the highly variable nature of the Yolo Bypass, additional data needs included the following:

- Particle fluxes (settling, resuspension, lateral transport) in the Delta and Bypass, including the role of vegetation. This information is needed to better estimate particle-based fluxes of total mercury and MeHg.
- Particle-based mercury fluxes. This information is needed to calibrate the models to realistically represent particle-based mercury fluxes in the Delta and Yolo Bypass.
- Sediment-water fluxes of total mercury and MeHg via diffusion. This information is needed to understand and simulate conditions leading to greater or smaller MeHg supply rates from sediments in open waters, for a range of flow conditions.
- Effects of water level fluctuations on MeHg production rates. This is particularly important in the Yolo Bypass, where water level changes may significantly influence methylmercury production and supply to open waters.
- Hydrodynamics. Water flows are needed among cells in the Yolo Bypass.

A number of standalone, but interrelated, experiments are required to fill identified data gaps. Based on input from the Regional Board and the TAC, the workplan approved in February 2014 included a technical memo which proposed the use of DFW ponds to provide much of the information needed by the model. Since this mesocosm approach proved impractical (see discussion in Chapter 1), the workgroup returned to a combination of standalone laboratory and field experiments to fill some of the data gaps for the model. This approach was summarized, presented, and approved by Regional Board staff in February 2015

The suite of ongoing and planned field and laboratory studies to address data gaps for Yolo Bypass mercury modeling include the following:

i. Inlet/Outlet Hg fluxes: These field measurements will quantify THg and MeHg fluxes at the inlet, outlet and intermediate reaches in the Yolo Bypass during flood events. Particulate and filtered mercury fluxes will be estimated. This will allow the determination of whether

the Yolo Bypass, and reaches within it, are sources or sinks of THg and MeHg, and will help to determine whether sediment Hg loads are primarily via the dissolved or particulate phase.

ii. Bale Chamber and Gust Chamber flux studies: These mini-annular flume studies will quantify fluxes of solids and mercury (THg, MeHg) from sediments to overlying waters for a range of land use types and velocities. This information will be used in conjunction with hydrodynamic model outputs to predict erosion rates at different locations and times in the Yolo Bypass.

iii. Sediment pore water studies**:** These laboratory experiments will quantify mercury concentrations and water chemistry in pore waters at the same locations as the Bale and Gust Chamber studies. This information will help estimate diffusional fluxes of THg and MeHg between sediments and the water column. It will also help to calibrate MeHg production rates (that produce observed MeHg concentrations).

iv. Spatial soil sampling**:** Samples were collected in the Yolo Bypass (69 locations) to measure THg and MeHg concentrations in surface soils, grain size, and loss on ignition, for different land use types. This information will help identify areas of the Yolo Bypass with elevated concentrations of THg and MeHg, which will be used when calibrating the model.

v. Hydrodynamics**:** The mercury model requires estimates of water flowrates in and out of the Yolo Bypass, as well as among model cells in the Yolo Bypass. This information is being provided from a hydrodynamic model (TUFLOW) previously applied by Bahia and others to the Yolo Bypass (2014 BiOP Yolo Bypass TUFLOW Hydraulic Model)

In addition to the above studies, several other studies have recently been completed that provide information to address data gaps. These include:

a. CCSB Hg loads**.** Hg inputs to the Yolo Bypass from the CCSB are also needed for D-MCM simulations in Yolo Bypass. These loads have been estimated by a USGS-led team studying Hg in the CCSB, and will be available shortly when a report is issued (C. Alpers, pers. comm.).

b. Effects of vegetation and wetting/drying**.** The USGS recently published several articles on Hg cycling in Yolo Bypass, discussing the effects of vegetation and seasonal/wetting and drying on methylmercury production and transport (Windham-Myers 2014, Windham-Myers and others, (2014a,b.c), Alpers and others. (2014), Marvin-DiPasquale and others. (2014), Bachand and others. (2014).

Since field and laboratory results may go beyond the data needs of the model, understanding how each of these standalone studies address the data needs of the model can be confusing. Therefore, Table 3-1 provides the reader with a linkage between the different studies and how information from each will be incorporated and used by the D-MCM.

Table 3-1. Linkage between D-MCM Yolo Bypass Model and Field and Laboratory Studies.

Information Source	**Information**	**Intended use of information**	
		Used as direct model input or to help develop model input	**Model calibration**
TUFLOW hydrodynamic model	Flows	Flows	
	Water velocities and shear stresses	Solids resuspension rates	
	Bathymetry	Bathymetry for model cells	
Inlet/Outlet Studies	THg, MeHg, TSS concentrations and fluxes at inlet, outlet and intermediate locations		Water column THg and MeHg concentrations in particulate and filtered phases, and solids/dissolved Hg partitioning.
	Net gain/loss of solids in Yolo Bypass		Mass sedimentation rate (burial)
Gust Chamber	Solids resuspension rates	Solids resuspension rates	
Bale Chamber	Solids resuspension rates	Effects of vegetation on solids resuspension rates	
Pore Water studies	THg and MeHg in pore water and sediment solids.		THg and MeHg concentrations in pore water, and partitioning in sediments, and diffusive fluxes.
	Pore water chemistry (DOC, pH, etc.)	Pore water chemistry	
Spatial mapping of surface soil Hg	THg and MeHg in different land uses and locations		THg and MeHg in surface soils
	Grain size distribution in soils	Initial conditions for grain size distribution	Grain size distribution vs time
USGS studies in Yolo Bypass (published in 2014)	Effects of vegetation on methylation		Production of MeHg
	Role of water level fluctuations on methylation		Production of MeHg
Cache Creek Settling Basin studies (USGS, in preparation)	THg and MeHg loads to Yolo Bypass from CCSB	External loads of THg and MeHg from CCSB	

3.1. Literature Cited

Alpers, C.N., Fleck, J.A., Marvin-DiPasquale, M., Stricker, C.A., Stephenson, M., Taylor, H.E., 2014, Mercury cycling in agricultural and managed wetlands, Yolo Bypass, California: spatial and seasonal variations in water quality. Sci Total Environ 484, 276-287.

Marvin-DiPasquale, M., Windham-Myers, L., Agee, J.L., Kakouros, E., Kieu, L.H., Fleck, J.A., Alpers, C.N., Stricker, C.A., 2014, Methylmercury production in sediment from agricultural and non-agricultural wetlands in the Yolo Bypass, California, USA. Science of The Total Environment 484, 288-299.

Windham-Myers, L., 2014, Methylmercury cycling in wetlands managed for rice agriculture and wildlife: Implications for methylmercury production, transport, and bioaccumulation Preface. Science of The Total Environment 484, 219-220.

Windham-Myers, L., Fleck, J.A., Ackerman, J.T., Marvin-DiPasquale, M., Stricker, C.A., Heim, W.A., Bachand, P.A., Eagles-Smith, C.A., Gill, G., Stephenson, M., Alpers, C.N., 2014a, Mercury cycling in agricultural and managed wetlands: a synthesis of methylmercury production, hydrologic export, and bioaccumulation from an integrated field study. Sci Total Environ 484, 221-231.

Windham-Myers, L., Marvin-DiPasquale, M., A. Stricker, C., Agee, J.L., H. Kieu, L., Kakouros, E., 2014b, Mercury cycling in agricultural and managed wetlands of California, USA: Experimental evidence of vegetation-driven changes in sediment biogeochemistry and methylmercury production. Science of The Total Environment 484, 300-307.

Windham-Myers, L., Marvin-DiPasquale, M., Kakouros, E., Agee, J.L., Kieu le, H., Stricker, C.A., Fleck, J.A., Ackerman, J.T., 2014c, Mercury cycling in agricultural and managed wetlands of California, USA: seasonal influences of vegetation on mercury methylation, storage, and transport. Sci Total Environ 484, 308-318.

4. Inlet/Outlet Mass Balance Field Study

Prepared by David Bosworth and Carol DiGiorgio, Department of Water Resources.

4.1. Introduction

This section provides preliminary loading results and analyses for filtered and unfiltered THg, MeHg, and TSS samples collected during the only flooding event covered to-date. Because only one event could be sampled, it was not possible to test hypotheses comparing mini-flood and major flooding events, or differences between reaches of the Yolo Bypass. However, in terms of meeting study objectives to provide loads and mass balances, the capture of this single flooding event was successful. The objectives and hypotheses associated with this study are provided below.

Objectives

1) Provide rate constants to the D-MCM for sediment to water fluxes of dissolved and particulate MeHg and THg as a function of 1) flow, 2) type of flood, and 3) reach in the Yolo Bypass.
2) Quantify loads for particulate and dissolved fractions of MeHg and THg.
3) Provide field data for D-MCM validation or calibration.

Hypotheses

1) MeHg and THg sediment to water flux during flooding increases with increasing water velocity.
2) At higher velocities, the majority of MeHg and THg flux is in the particulate phase, not the dissolved phase.
3) MeHg and THg sediment to water flux in both the particulate and dissolved phases differs under mini-flood or major flooding events.
4) MeHg and THg sediment to water flux in both particulate and dissolved phases differs among reaches of the Yolo Bypass.

Most of water years 2014 and 2015 have been extremely dry in California. As a result, inundation of the Yolo Bypass due to flood flows has only occurred once during the reporting period. From December 11-19, 2014, a series of very wet winter storms struck Northern California resulting in high rainfall amounts across much of the north state. On December 20, the stage height at the Toe Drain at Lisbon gage exceeded our pre-determined value of 10.5

feet[2], which triggered a flood sampling event in the Yolo Bypass (Figure 4-1). On December 22-23, DWR staff collected water samples from the major inputs and outputs of the Bypass (see Figures 4-2-3 for pictures of the Toe Drain during the event). Since the Sacramento River did not overtop the Fremont Weir during this flood event, we classified this sampling event as a "mini-flood" event as defined in the Open Water Monitoring Plan for our inlet/outlet water sampling effort.

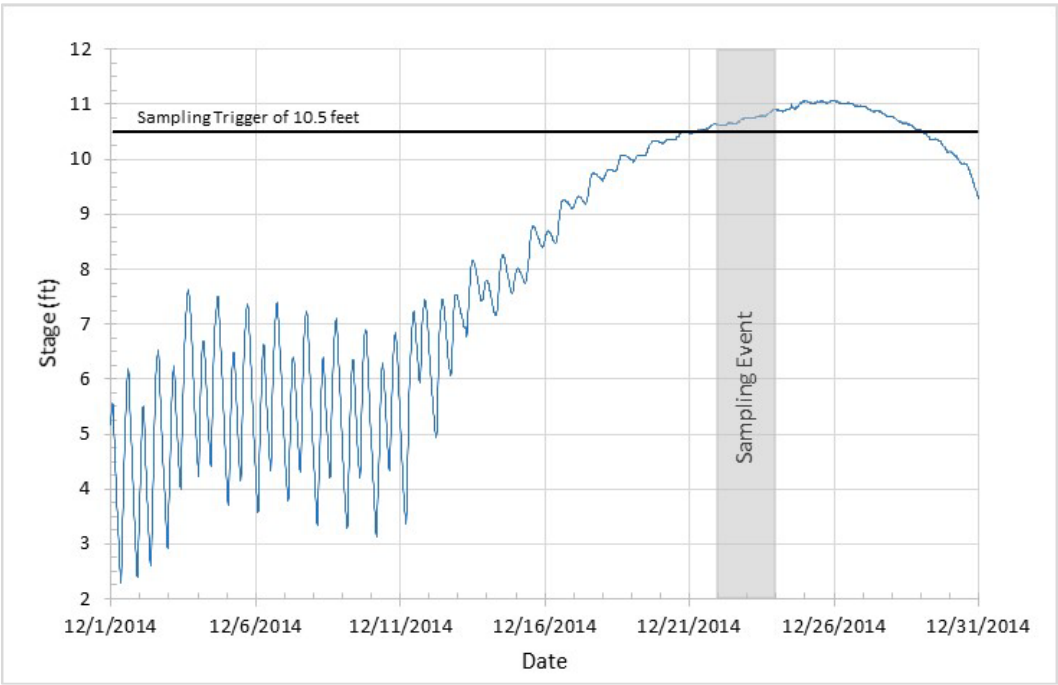

Figure 4-1. Stage at the Toe Drain at Lisbon gage during the month of December 2014.

[2] Water begins to overtop the Toe Drain and flow into the floodplain of the Yolo Bypass at a stage of 9.5 feet. The extra foot in stage height is necessary to ensure that there is adequate inundation of the floodplain.

Upstream of the Lisbon gage

At the Lisbon gage

Downstream of the Lisbon gage

(Photos taken at the Lisbon Weir sampling location on December 23, 2014.)

Figure 4-2. Pictures showing the inundation of the Yolo Bypass along the Toe Drain.

(Note that the water is contained within the banks of the channel)

Figure 4-3. Photo of the Toe Drain at ½ Lisbon sampling location on December 23, 2014.

4.2. Methods

4.2.1. Sampling Locations and Analytes

Figure 4-4 shows the locations where water samples were collected during this sampling event. At each sampling location, water samples were collected in one double-bagged 4-liter glass amber bottle that was cleaned according to EPA 1631 standards by the supplier (USEPA, 2002). DWR field staff used EPA Method 1669 "clean hands-dirty hands" methods when collecting samples at each site (USEPA, 1996). Once filled, the 4-liter bottles were immediately stored on wet ice and transported to our clean laboratory.

Water samples were processed in the laboratory within 24 hours of sample collection. Aliquots from each 4-liter bottle were poured into EPA 1631 pre-cleaned bottles and submitted to either Bryte or MLML for analysis. Dissolved analytes were filtered using a peristaltic pump, acid-rinsed Teflon and peristaltic pump tubing, and pre-rinsed 0.45-µm capsule filters. A number of analytes were measured for this project, however, this progress report provides data for only the following analytes:

1) Total Mercury (unfiltered)
2) Total Mercury (filtered)
3) Methylmercury (unfiltered)

4) Methylmercury (filtered)
5) Total Suspended Solids

MeHg was analyzed by MLML. Total mercury and all other analytes were analyzed by DWR's Bryte Laboratory. All sample preservation, analysis, and quality assurance and quality control (QA/QC) followed the methods and procedures documented in the inlet/outlet open water monitoring plan.

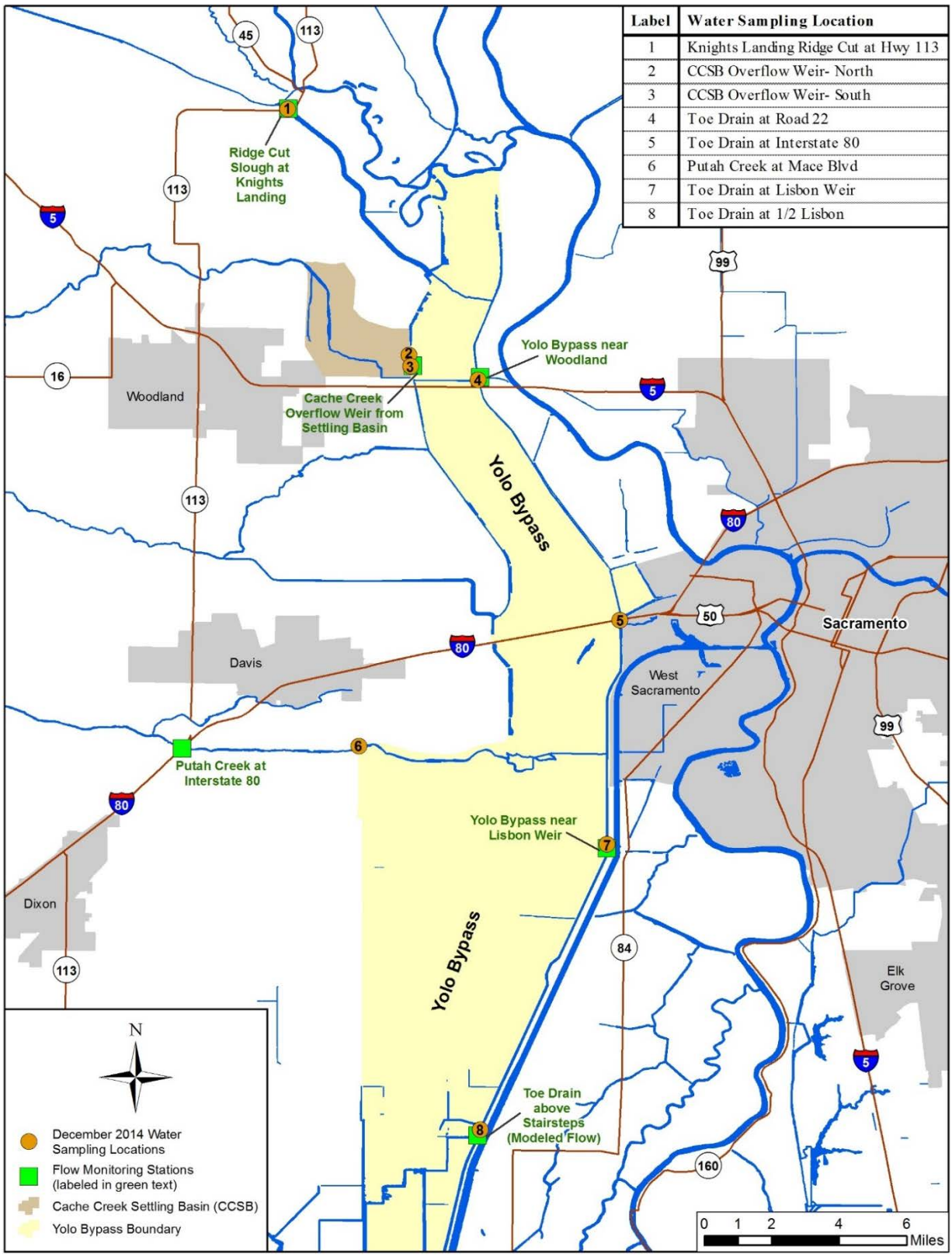

Figure 4-4. Water sampling locations and flow monitoring stations for the December 2014 event.

4.2.2. Water Flow Calculations-

In order to calculate mass loads, measurements of water flow rate are required at each sampling location. For a majority of the sampling locations, we used a nearby flow monitoring station to estimate flows. Flow gages are available for the KLRC, CCSB, Toe Drain at Road 22, and Toe Drain at Lisbon Weir locations. There are no flow monitoring stations immediately near the Putah Creek at Mace Boulevard and Toe Drain at Interstate 80 sampling locations; therefore, we used flow data from monitoring stations that were 4.2 and 8.0 miles upstream of these sampling locations, respectively. The Toe Drain at ½ Lisbon sampling location does not have a nearby flow station either, so we used calculated flows from the DWR's recently calibrated SCHISM model for this site (DWR Appendix A) (http://baydeltaoffice.water.ca.gov/modeling/deltamodeling/models/bay_delta_schism/, http://ccrm.vims.edu/schism/). Table 4-1 provides the flow monitoring stations and calculation methods that we used to estimate flows, and Figure 4-4 shows a map of their locations in relation to the water sampling sites.

Table 4-1. Flow Estimation Methods for Each Sampling Location.

Sampling Location	Flow Calculation Method	Name of Flow Monitoring Station used for the Calculation	CDEC, WDL or USGS Code
KLRC at Hwy 113	Directly from flow gage	Ridge Cut Slough at Knights Landing	CDEC- RCS WDL- A02939
CCSB Overflow Weir- both North and South stations	Directly from flow gage	Cache Creek Overflow Weir from Settling Basin	USGS- 11452800
Putah Creek at Mace Blvd	Estimated from upstream flow gage	Putah Creek at Interstate 80	[a]
Toe Drain at Road 22	Directly from flow gage	Yolo Bypass near Woodland, CA	USGS- 11453000
Toe Drain at Interstate 80	Estimated from upstream flow gage	Yolo Bypass near Woodland, CA	USGS- 11453000
Toe Drain at Lisbon Weir	Directly from flow gage	Yolo Bypass near Lisbon Weir	CDEC- LIS WDL- B91560Q
Toe Drain at ½ Lisbon	SCHISM model output	Modeled flow for Toe Drain above the Stairsteps	N/A

[a] Flow data for the Putah Creek at Interstate 80 station was provided by Jay Cuetara, Senior Water Resources Engineer at the Solano County Water Agency.

4.2.3. Load Calculations

We used the following equation to calculate daily mass loads of methylmercury, total mercury, and total suspended solids at each sampling location:

$$M = C \times Q \times 28.317\ (\frac{L}{ft3}) \times 86400\ (\frac{seconds}{day})$$

Where: M = daily mass load in either ng/day or mg/day depending upon the analyte
C = concentration of analyte in either ng/L or mg/L depending upon the analyte
Q = daily average flow in cfs

The flow data from the monitoring stations listed in Table 4-1 was collected in 15-minute intervals. We calculated the daily average flows for each sampling location by taking the average of the 15-minute flow data on the day when water samples were collected.

For the CCSB Overflow Weir, we collected samples on the north and south ends of the weir due to the long length of the weir. For the load calculations, we averaged the concentration data of the two sampling locations to provide an overall concentration for the Overflow Weir.

4.3. Results and Discussion

4.3.1. QA/QC Samples

All of the water samples were preserved, received, and analyzed within their respective holding times. In addition, all of the samples arrived at Bryte Lab and MLML within the proper temperature range of 2-6°C.

Tables 4-2 and 4-3 show the results for the field QA/QC samples collected during this sampling event including field blanks, filter blanks, and field duplicates. All of these samples met the Measurement Quality Objectives (MQO's) for this study, with one exception. One of the filter blanks had a MeHg concentration greater than its method detection limit of 0.011 nanogram per liter (ng/L) and a THg concentration that exceeded its reporting limit of 0.5 ng/L. This is the only occurrence of a filter blank exceedance among a total of approximately 14 filter blanks that we have processed so far, including blanks for our tidal wetland studies; therefore, the dissolved MeHg and dissolved THg data is included in this report.

DWR Appendix B provides laboratory results for QA/QC samples associated with this sampling event including lab method blanks, lab replicates, lab control standards, and matrix spikes and duplicates. All of these samples met the MQO's for this study.

Table 4-2. Field and Filter Blanks.

Analyte	Collection Date/Time	Sample Type	Result	Units	Meets QA Standards?
Methylmercury (total)	12/22/2014 14:35	Field Blank	< 0.011	ng/L	Yes
Total Mercury (total)		Field Blank	< 0.5	ng/L	Yes
Total Suspended Solids		Field Blank	< 1.0	mg/L	Yes
Methylmercury (total)	12/23/2014 10:55	Field Blank	< 0.011	ng/L	Yes
Total Mercury (total)		Field Blank	< 0.5	ng/L	Yes
Total Suspended Solids		Field Blank	< 1.0	mg/L	Yes
Methylmercury (dissolved)	12/23/2014 12:00	Filter Blank	**0.016**	ng/L	**No**
Total Mercury (dissolved)		Filter Blank	**0.6**	ng/L	**No**
Methylmercury (dissolved)	12/23/2014 16:00	Filter Blank	< 0.011	ng/L	Yes
Total Mercury (dissolved)		Filter Blank	< 0.5	ng/L	Yes

Table 4-3. Field Duplicates.

Sampling Location	Collection Date/Time	Analyte	Result	Duplicate Result	Units	RPD	Measurement Quality Objective	Meets QA Standards?
Toe Drain at Road 22	12/22/2014 13:30	Methylmercury (dissolved)	0.073	0.077	ng/L	5.3%	≤ 25%	Yes
		Methylmercury (total)	0.198	0.201	ng/L	1.5%	≤ 25%	Yes
		Total Mercury (dissolved)	2.6	3.1	ng/L	17.5%	≤ 25%	Yes
		Total Mercury (total)	14.5	13.9	ng/L	4.2%	≤ 25%	Yes
		Total Suspended Solids	83	84	mg/L	1.2%	≤ 25%	Yes
Toe Drain at Lisbon Weir	12/23/2014 11:35	Methylmercury (dissolved)	0.257	0.232	ng/L	10.2%	≤ 25%	Yes
		Methylmercury (total)	0.448	0.428	ng/L	4.6%	≤ 25%	Yes
		Total Mercury (dissolved)	3.7	3.6	ng/L	2.7%	≤ 25%	Yes
		Total Mercury (total)	16.6	16.4	ng/L	1.2%	≤ 25%	Yes
		Total Suspended Solids	60.5	59	mg/L	2.5%	≤ 25%	Yes

4.3.2. Yolo Bypass Flows and Water Balance

Hydrographs for the December sampling event are shown in Figure 4-5. Samples were collected at the top of the rising limb of the hydrograph at the KLRC, the Yolo Bypass near Woodland, and the Toe Drain at Lisbon Weir stations. In the case of the CCSB station, samples were collected during the falling limb of the hydrograph, while flood flows had returned to baseline at the Putah Creek station. The majority of tributary inputs into the Toe Drain came from the KLRC. As shown in Table 4-4, the KLRC provided 78% of the water volume contributed by the three tributaries into the Toe Drain.

Table 4-4 provides total water volumes during the two-day sampling period (December 22-23) for the Yolo Bypass flow monitoring stations. Water balance calculations demonstrated that 99.6% of the water volume at the Yolo Bypass at Woodland station could be explained by water volumes from the KLRC and the CCSB stations.

While water masses balanced upstream, there was a 30% water loss between the upstream inputs and downstream at Lisbon Weir. If there were no losses in the system, then the sum of the water volumes from the input stations (KLRC, CCSB, and Putah Creek) should roughly equal the water volumes downstream at the Toe Drain at Lisbon Weir and Toe Drain above the Stairsteps. However, water volumes for the Toe Drain at Lisbon Weir and the Toe Drain above the Stairsteps stations were both lower (approximately 6,000 acre-feet over the two-day period) than the sum of the three input stations. The water volumes at these stations accounted for 69.6% (Lisbon) and 67.6% (Stairsteps) of the total volume of the three inputs.

One explanation of water balance loss could come from a malfunctioning stage gage; however, as shown in Figure 4-6, flow patterns between upstream and downstream sites followed a consistent pattern. This suggests that the import and export flow gages were recording correctly and that the observed water losses were real and could be due to other causes such as overland flow, groundwater seepage, or rerouting of water flows. The observed water losses were also consistent with observations by DWR staff working on a hydrology model for the Yolo Bypass. As part of the Department's SCHISM model development, DWR staff has noticed a loss in water volume between the input stations and the Lisbon Weir station during the summer months (E. Ateljevich, pers. comm., 7/2015).

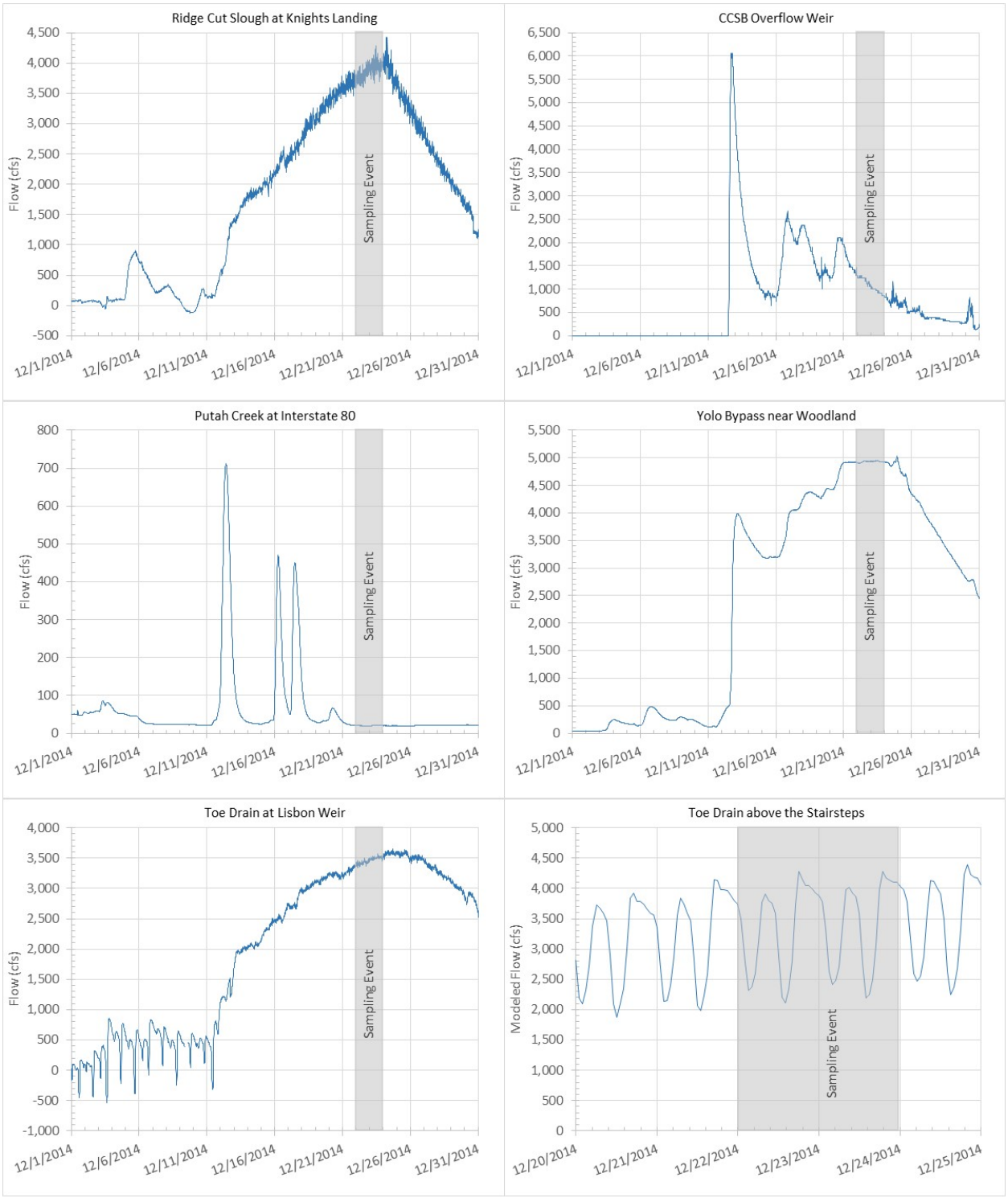

Figure 4-5. Hydrographs for the flow monitoring stations used to calculate loads.

Table 4-4. Yolo Bypass Water Volume and Balance for December 22-23, 2014.

Flow Monitoring Station	Total Acre-ft for Dec 22-23
Ridge Cut Slough at Knights Landing (KLRC)	15,388
CCSB Overflow Weir (CCSB)	4,260
KLRC + CCSB	*19,648*
Yolo Bypass near Woodland	19,575
% of KLRC + CCSB	**99.6%**
Putah Creek at Interstate 80 (PC)	79
KLRC + CCSB + PC	*19,727*
Toe Drain at Lisbon Weir	13,731
% of KLRC + CCSB + PC	**69.6%**
Toe Drain above the Stairsteps	13,328
% of KLRC + CCSB + PC	**67.6%**
% of Lisbon	**97.1%**

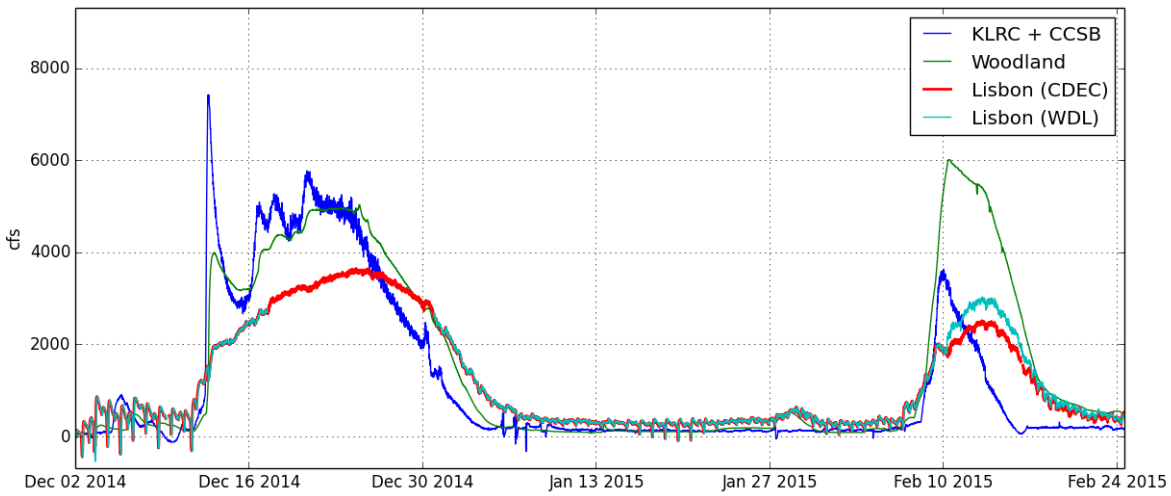

Note: Yolo Bypass at Hwy 5 (Woodland), and uncorrected (CDEC) and recalibrated (WDL) flow for Lisbon Weir (graphic courtesy of Eli Ateljevich, DWR).

Figure 4-6. Flow data for the sum of Knight's Landing Ridge Cut and Cache Creek Settling Basin

4.3.3. Total Mercury, Methylmercury, and TSS Concentrations, Loads, and Mass Balance

Concentrations

Because we only sampled one event in the period covered by this Progress Report, statistical analyses were not possible; however, there were spatial patterns to the THg, MeHg, and TSS data. With respect to THg concentrations, the CCSB Overflow Weir had much higher unfiltered (34.3 ng/L) and filtered (8.4 ng/L) concentrations than other sampling locations (Figure 4-7a). In contrast, unfiltered MeHg concentrations at the CCSB overflow were not higher than other locations (Figure 4-7b).

Along the Toe Drain from Road 22 to ½ Lisbon, unfiltered MeHg concentrations increased nearly three-fold, with much of the increase occurring between I-80 and Lisbon Weir (Figure 4-7b). Unfiltered MeHg concentrations for this event were similar to mini-flood concentrations sampled in 2005 (Stephenson and others, 2008). The increase in MeHg concentrations between Road 22 and ½ Lisbon occurred in both the filtered and particulate phases. Filtered MeHg concentrations increased by approximately a factor of 3.5 from Road 22 to ½ Lisbon while particulate MeHg concentrations increased by approximately 2X between these two stations. This increase in particulate MeHg concentrations was not due to an increase in TSS since TSS concentrations were similar between Road 22 and at ½ Lisbon (Figure 4-8), but rather because concentrations on individual particles were 2X higher (ng/g) (Figure 4-9). Total mercury concentrations also increased along the Toe Drain in the unfiltered, filtered, and particle (ng/g) phases by factors of approximately 1.5, 1.25, and 1.6 respectively, which were less than the increases in MeHg concentrations (Figures 4-7a and 4-9).

The apparent partitioning ("Kd", ratio of particulate concentration in ng/g divided by filtered concentration) declined for MeHg in the Toe Drain in the direction of flow (Figure 4-10a), while the Kd for total mercury increased slightly. The decline in partitioning of MeHg along the toe drain occurred because of greater partioning of MeHg into the filtered phase (3.7X) as opposed onto the solid phase (2.1X). The Kd data along the Toe Drain are also presented in Figure 4-10b in units commonly used in mercury studies (log10 [liters per kilogram (L/kg)]).

Table 4-5 provides concentration data for THg, MeHg and TSS as well as daily average flows for this sampling event.

Loads and Mass Balance

The greatest tributary load of THg to the Toe Drain was the CCSB (Figure 4-11a). Approximately 80% of the CCSB THg load was in the particulate form (Table 4-6). Because MeHg concentrations were similar among the tributary inputs, flow was the governing factor for the

relative importance of tributary MeHg loads. Greater flow at KLRC contributed to greater MeHg loading from that source (Figure 4-11b). MeHg loads contributed by all of the tributary inputs were equally distributed between the particulate and the filterable fractions (Table 4-6).

Table 4-7 and Figures 4-12 and 4-13 show the THg, MeHg, and TSS mass balance calculations and conceptual model for the December 2014 sampling event. Note that the loss in water volume between Road 22 and ½ Lisbon was included as an export in the mass balance calculations. During this sampling event, the Yolo Bypass at ½ Lisbon was a net source of THg, MeHg, and TSS. The Yolo Bypass was a net source of THg entirely due to its particulate fraction, while it was a net source of MeHg due to relatively equal contributions from the particulate and filtered phases. Differences between the sum of the export loads and the sum of the input loads were 44.6 grams per day (g/day) for THg, 2.7 g/day for MeHg, and 115,000 kilograms per day (kg/day) for TSS (Table 4-7).

The greatest increase in total MeHg loads occurred between I-80 and Lisbon. As shown in Table 4-6 and Figure 4-11b, there was little change in total MeHg loads between the tributaries (2.52 g/day) and further downstream along the Toe Drain at I-80 (2.30 g/day). However, total MeHg loads increased by ~40% between I-80 (2.30 g/day) and Lisbon (3.75 g/day). Loads increased another 15 % between Lisbon (3.75 g/day) and the outlet point at ½ Lisbon (4.45 g/day).

4.3.4. Mercury Sources and Sinks

The largest sources of MeHg to the Toe Drain were tributary inputs at KLRC and internal supply (Figure 4-12). Of the total MeHg loads exported from the Yolo Bypass, the tributaries contributed ~48% of the total exported load, while internal supply contributed ~52% (Table 4-7). These percentages were greater than those calculated by Foe and others (2008) who captured two mini-flood events and calculated that in-situ production comprised 36 and 39 percent of the total MeHg load exiting at Prospect Slough.

Per mass balance calculations, the Yolo Bypass was a net source for THg, MeHg, and TSS (Table 4-7). For THg, it was a net source due entirely to its particulate fraction. The source for MeHg was distributed roughly equally between particulate and filtered fractions. While a net source for THg, per mass balance calculations, the Yolo Bypass was a net sink for filtered THg.
The internal source of MeHg in the Toe Drain is unknown but could include one or more of the following:

1) Diffusion from sediments
2) Sediment resuspension
3) Inputs from agricultural drains

In order for sediment diffusion to play a major role in internal Yolo Bypass production, rough calculations suggested that pore-water MeHg concentrations would have to be very high (on the order of 50-100 ng/L) to produce diffusion rates that would supply the observed increase in the water column from Road 22 to ½ Lisbon in either the dissolved phase or the unfiltered phase (if some MeHg loaded by diffusion then sorbed to solids). The magnitude of these concentrations makes this production scenario unlikely.

Rough calculations to quantify the mass of required re-suspended sediment to explain the observed increase in MeHg mass in the water column seemed more plausible. Assuming a sediment bed MeHg concentration of 3 ng/g (similar to the dry weight concentration of MeHg on suspended particles at ½ Lisbon), a mass suspension rate of about 2 millimeters per day (mm/d) would be needed during the event to account for the increase in particulate MeHg. About 4 mm/day of erosion would be required to support the observed increase in unfiltered MeHg from Road 22 to ½ Lisbon (i.e., if MeHg desorbed from resuspended solids and produced the observed increase in filtered MeHg as well as particulate MeHg). Other assumptions/inputs included a flow of 4000 cubic feet per second (cfs), Toe Drain distance of 24 kilometers (km) and width of 30 m, solids density of 2.5 g/mL and porosity of 0.85. These erosion rates (average for the entire Toe Drain from Road 22 to ½ Lisbon) seem plausible in the short term.

Finally, the potential for MeHg inputs from agricultural inputs also exists, as there are several drains between Road 22 and ½ Lisbon (Chris Foe, CVRWQCB, pers. comm.). No flow or MeHg concentration data were available for the agricultural drains for the sample period, however, some insights can be gained by the fact the flows did not increase from Road 22 to ½ Lisbon. For example, if flows from the drains were small (e.g., 10% or less, of the overall Toe Drain flow), simple mixing calculations would require MeHg concentrations in the agricultural drains to be about 30X greater (or more) than the MeHg concentration at Road 22 (i.e., 6 ng/L of MeHg or more). This is possible but represents a highly elevated MeHg concentration. Field data are required to properly assess the importance of MeHg inputs from agricultural drains.

Overall the above rough calculations suggest that it is unlikely that diffusion alone would explain most of the observed increase in MeHg mass in the Toe Drain from Rd 22 to ½ Lisbon. If only one process were responsible for the MeHg increase in the Toe Drain, resuspension of bottom sediments may be the more plausible. However, without further investigation, it may be the most realistic to assume that this increase is due to a combination of multiple processes with some being more important than others.

4.3.5. Next Steps-Inlet/Outlet Study

Samples will again be collected in the Yolo Bypass in the winter of 2015/16, weather permitting.

4.4. Literature Cited

Stephenson M., C. Foe., G. A. Gill, and K. H. Coale. September 15, 2008. CALFED Mercury Project Final Report. California Department of Fish and Game, California Bay Delta Authority.

USEPA, July 1996. Method 1669, Sampling Ambient Water for Trace Metals at EPA Water Quality Criteria Levels. Pages 39. United States Environmental Protection Agency Office of Water (4303), Washington D.C.

USEPA, August 2002. Method 1631, Revision E: Mercury in Water by Oxidation, Purge and Trap, and Cold Vapor Atomic Fluorescenc Spectrometry. Pages 46. United States Environmental Protection Agency, Washington, DC.

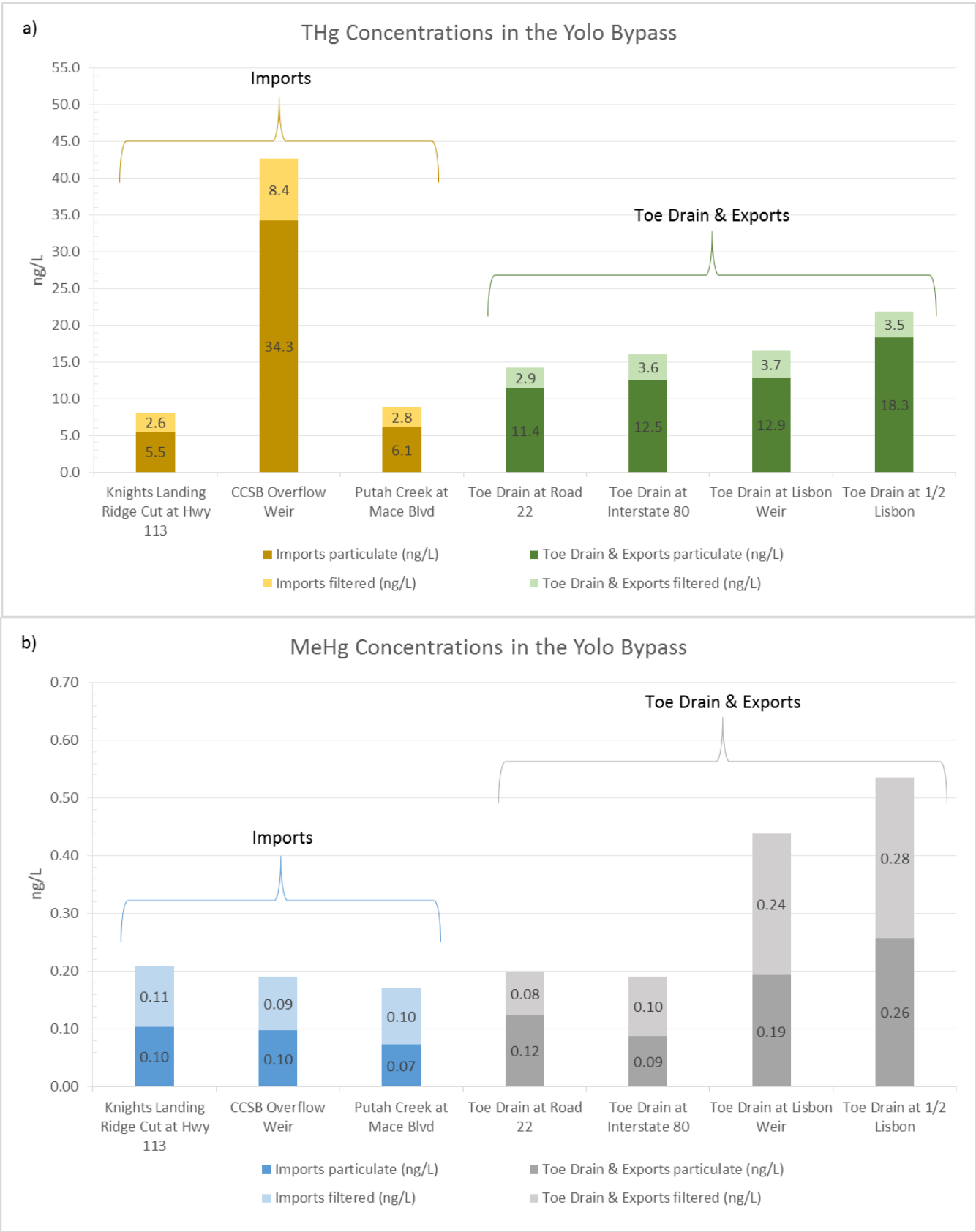

Figure 4-7. a) Hg, and b) MeHg concentrations for samples collected in the Yolo Bypass, December 22-23, 2014.

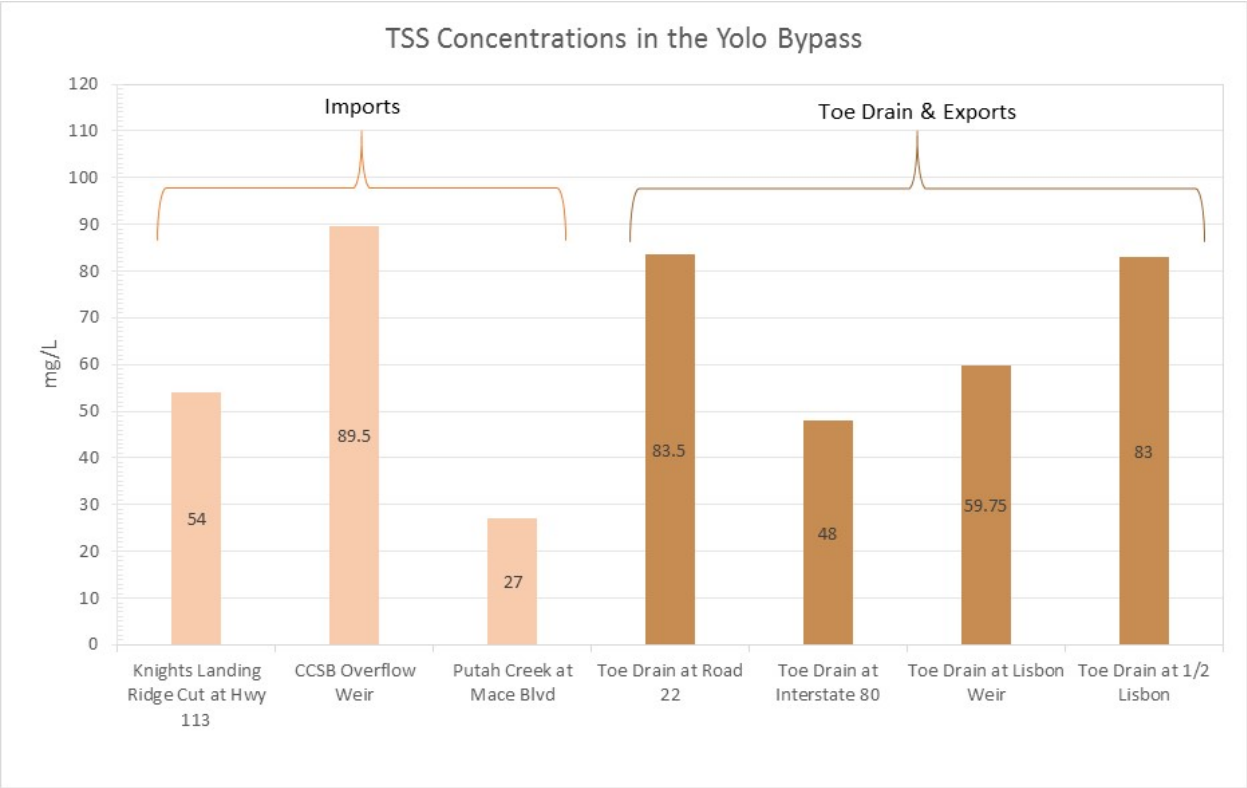

Figure 4-8. Total suspended solids concentrations for samples collected in the Yolo Bypass

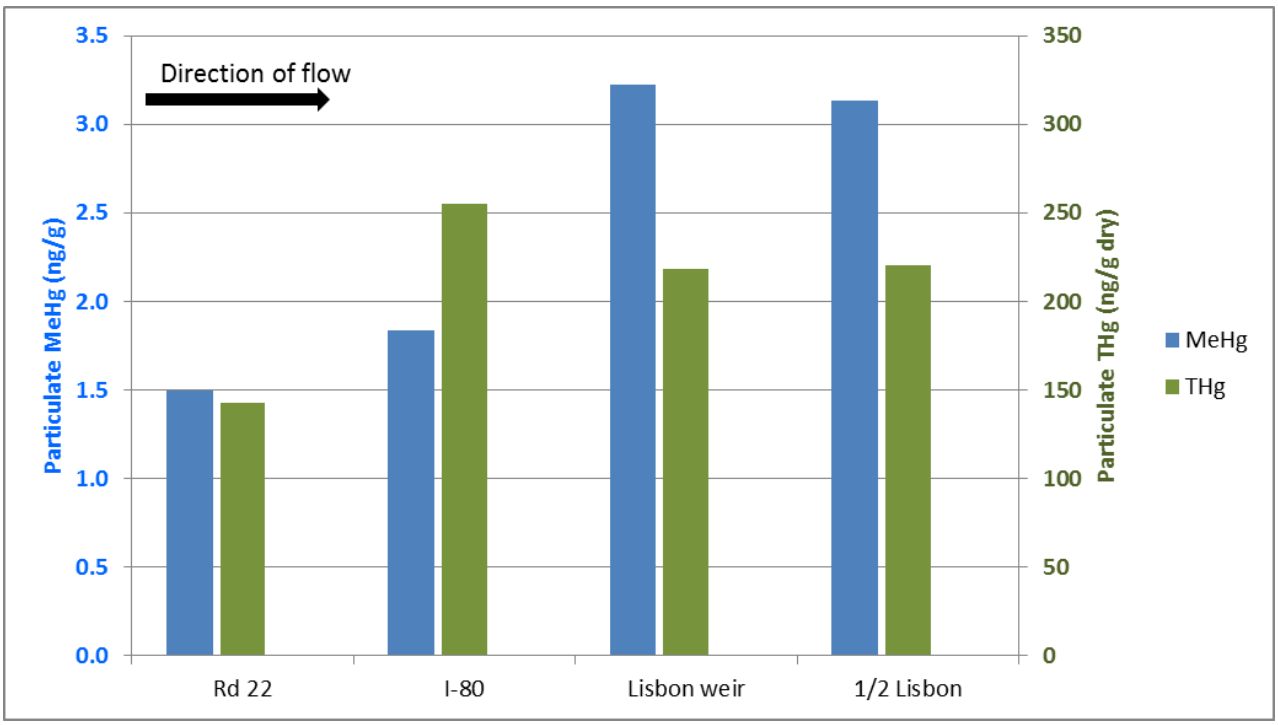

Figure 4-9. Particulate THg and MeHg concentrations (ng/g) for selected Toe Drain sites. Note: Dry weight concentrations were calculated by dividing the particle phase concentration (ng L^{-1}) by TSS (g/L).

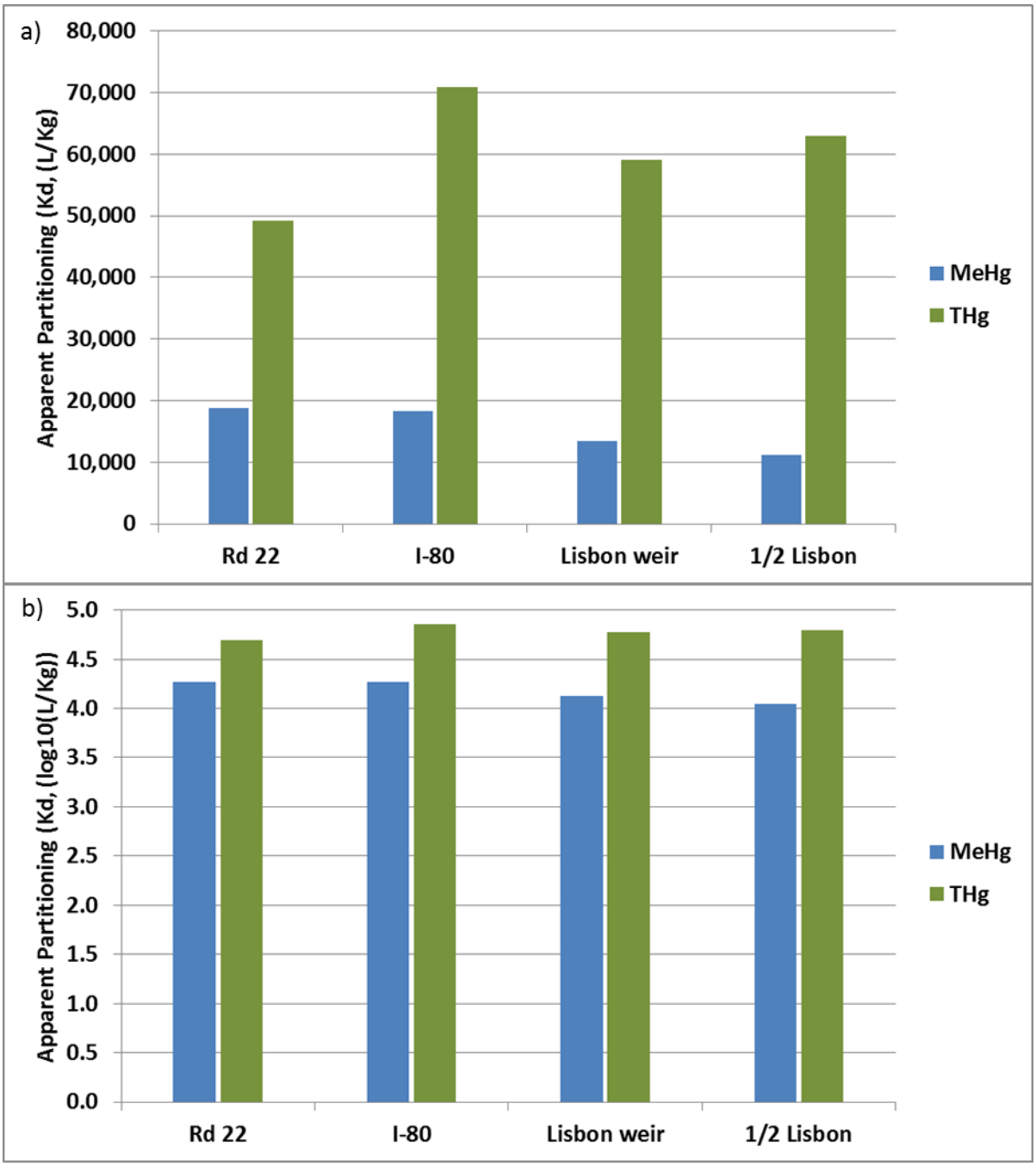

Note: The underlying data in the two panels are the same. The upper panel presents partitioning in units of L/Kg. The lower panel presents the log10 value (L/Kg).

Figure 4-10. Apparent partitioning of MeHg and THg at selected Toe Drain sites.

Table 4-5. THg, MeHg, and TSS Concentration Data and Daily Average Flow Data for the December 2014 Sampling Event.

Sampling Location	Sample Date	Sample Time (PST)	Daily Average Flow (cfs)	THg (total) Conc (ng/L)	THg (filtered) Conc (ng/L)	MeHg (total) Conc (ng/L)	MeHg (filtered) Conc (ng/L)	TSS Conc (mg/L)
Knights Landing Ridge Cut at Hwy 113	12/22/2014	12:10	3,808	8.1	2.6	0.210	0.105	54.0
CCSB Overflow Weir- South	12/22/2014	9:45	1,196	39.0	8.0	0.177	0.089	79.0
CCSB Overflow Weir- North	12/22/2014	11:00		46.3	8.8	0.206	0.099	100.0
Putah Creek at Mace Blvd	12/22/2014	15:00	20	8.9	2.8	0.171	0.097	27.0
Toe Drain at Road 22	12/22/2014	13:30	4,928	13.9	3.1	0.201	0.077	84.0
Toe Drain at Road 22- Field Duplicate	12/22/2014	13:30		14.5	2.6	0.198	0.073	83.0
Toe Drain at Interstate 80	12/22/2014	16:00	4,928	16.1	3.6	0.191	0.103	48.0
Toe Drain at Lisbon Weir	12/23/2014	11:35	3,501	16.4	3.6	0.428	0.232	59.0
Toe Drain at Lisbon Weir- Field Duplicate	12/23/2014	11:35		16.6	3.7	0.448	0.257	60.5
Toe Drain at 1/2 Lisbon	12/23/2014	13:00	3,396	21.8	3.5	0.535	0.277	83.0

Table 4-6. Total Mercury, Methylmercury, and Total Suspended Sediment Loads for the December 22-23, 2014 Sampling Events.

Sampling Location	Total Mercury					Methylmercury					Total Suspended Solids (kg/day)
	Total fraction (g/day)	Filtered fraction (g/day)	Filtered/ Total as a %	Particulate fraction (g/day) [a]	Particulate/ Total as a %	Total fraction (g/day)	Filtered fraction (g/day)	Filtered/ Total as a %	Particulate fraction (g/day) [a]	Particulate/ Total as a %	
Input Loads:											
Knights Landing Ridge Cut at Hwy 113	75.5	24.2	32.1%	51.2	67.9%	1.95	0.98	50.1%	0.97	49.9%	503,000
CCSB Overflow Weir	124.8	24.6	19.7%	100.2	80.3%	0.56	0.28	49.1%	0.29	50.9%	262,000
Putah Creek at Mace Blvd	0.4	0.1	31.5%	0.3	68.5%	0.008	0.005	56.7%	0.004	43.3%	1,310
Intermediate Toe Drain Loads:											
Toe Drain at Road 22	171.2	34.4	20.1%	136.8	79.9%	2.41	0.90	37.6%	1.50	62.4%	1,007,000
Toe Drain at Interstate 80	194.1	43.4	22.4%	150.7	77.6%	2.30	1.24	53.9%	1.06	46.1%	579,000
Toe Drain at Lisbon Weir	141.3	31.3	22.1%	110.1	77.9%	3.75	2.09	55.8%	1.66	44.2%	512,000
Export Loads:											
Toe Drain at 1/2 Lisbon	181.1	29.1	16.1%	152.1	83.9%	4.45	2.30	51.8%	2.14	48.2%	690,000

[a] The particulate fraction was calculated by subtracting the dissolved fraction from the total.

.

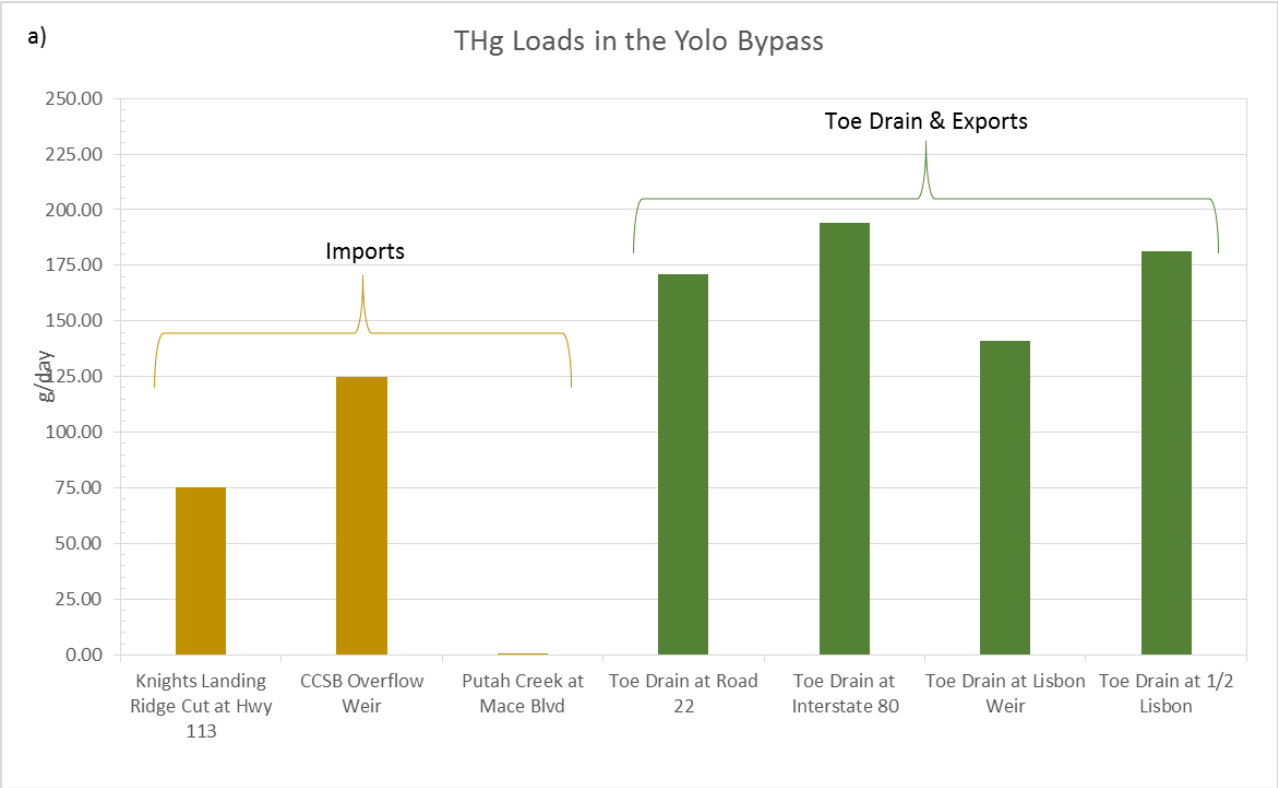

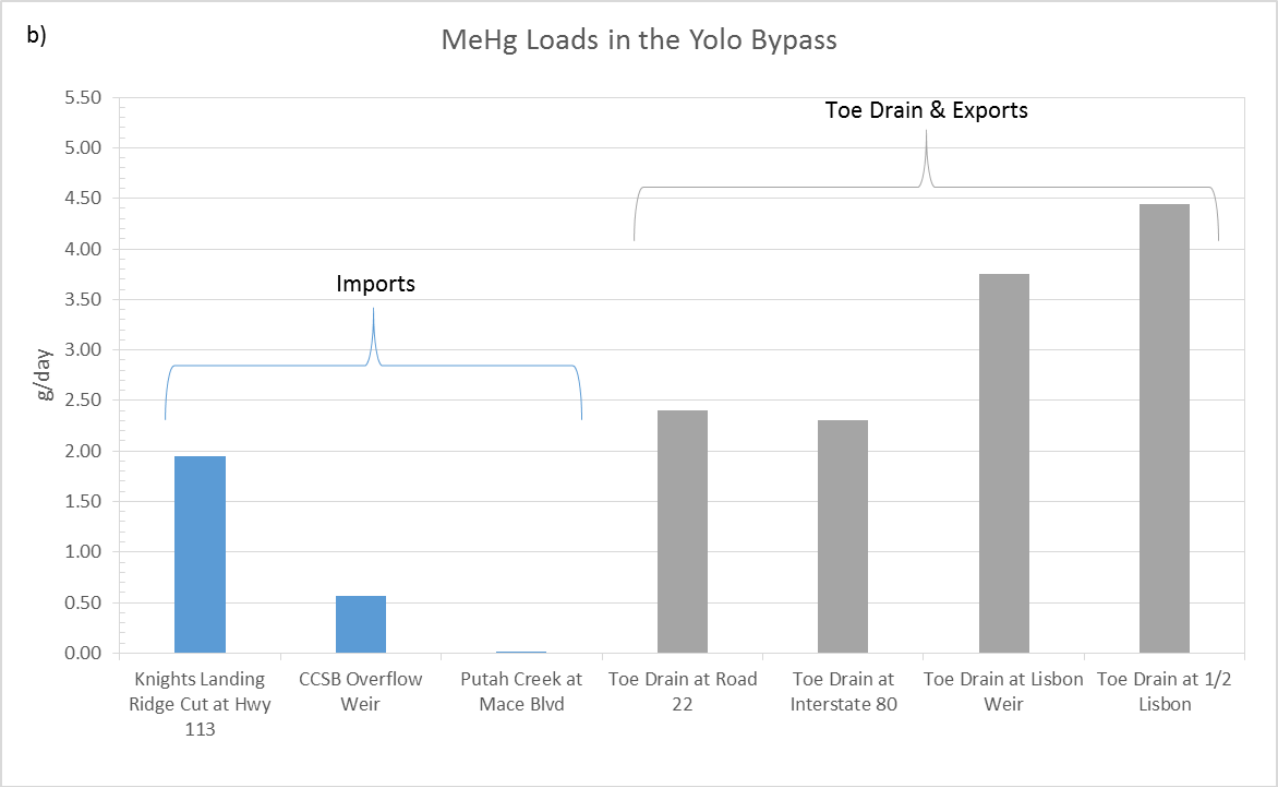

Figure 4-11. a) Hg, and b) MeHg loads in the Yolo Bypass, December 22-23, 2014.

Table 4-7. Total Hg, MeHg, and TSS Mass Balance for the December 22-23, 2014 Sampling Event.

	Total Mercury			Methylmercury			Total Suspended Solids (kg/day)
	Unfiltered THg (g/day)	**Filtered THg (g/day)**	**Particulate THg (g/day)**	**Unfiltered MeHg (g/day)**	**Filtered MeHg (g/day)**	**Particulate MeHg (g/day)**	
Sum of Input Loads	200.7	48.9	151.8	2.52	1.26	1.26	766,000
Export Loads:							
Toe Drain at 1/2 Lisbon	181.1	29.1	152.1	4.45	2.30	2.14	690,000
Exported water due to overland flow, etc. [(a)]	64.1	14.3	49.8	0.76	0.41	0.35	191,000
Sum of Export Loads	245.3	43.4	201.8	5.21	2.71	2.49	881,000
Exports - Inputs	**44.6**	**-5.5**	**50.1**	**2.69**	**1.45**	**1.23**	**115,000**

[(a)] This load was calculated by using the concentration data from the Toe Drain at I-80 station and the difference in daily average flow data between the Yolo Bypass near Woodland and the Toe Drain above the Stairsteps stations.

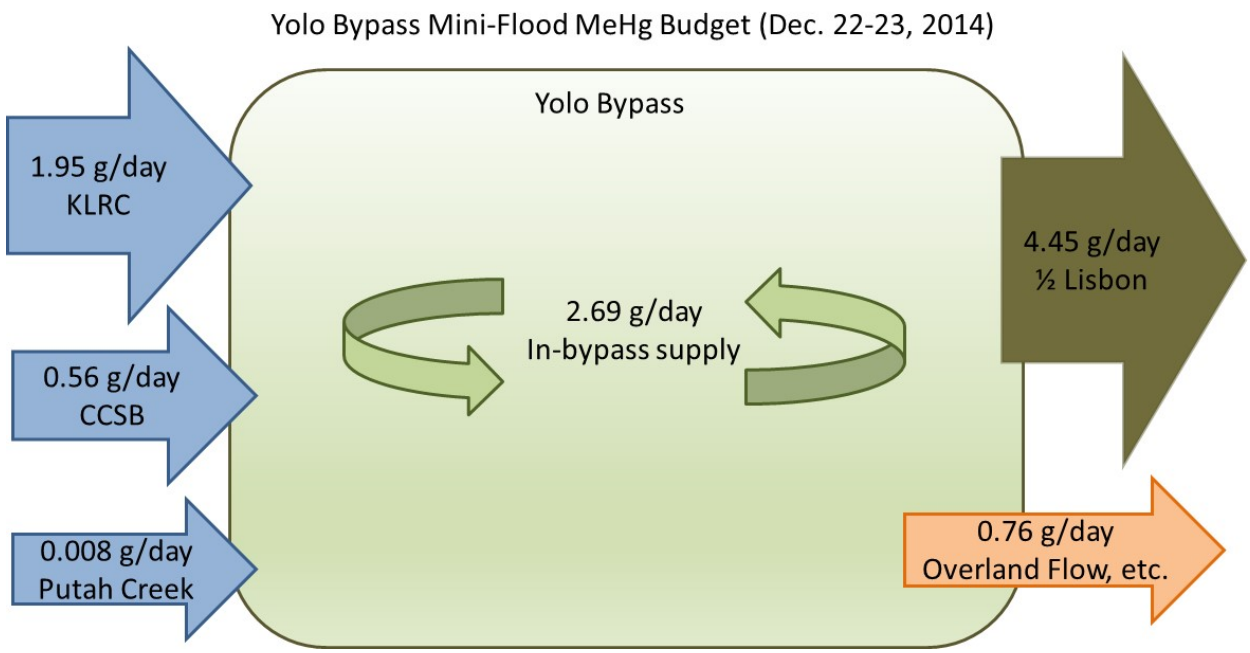

Figure 4-12. Conceptual model of MeHg imports and exports from the Yolo Bypass mini-flood sampling event, December 22-23, 2014.

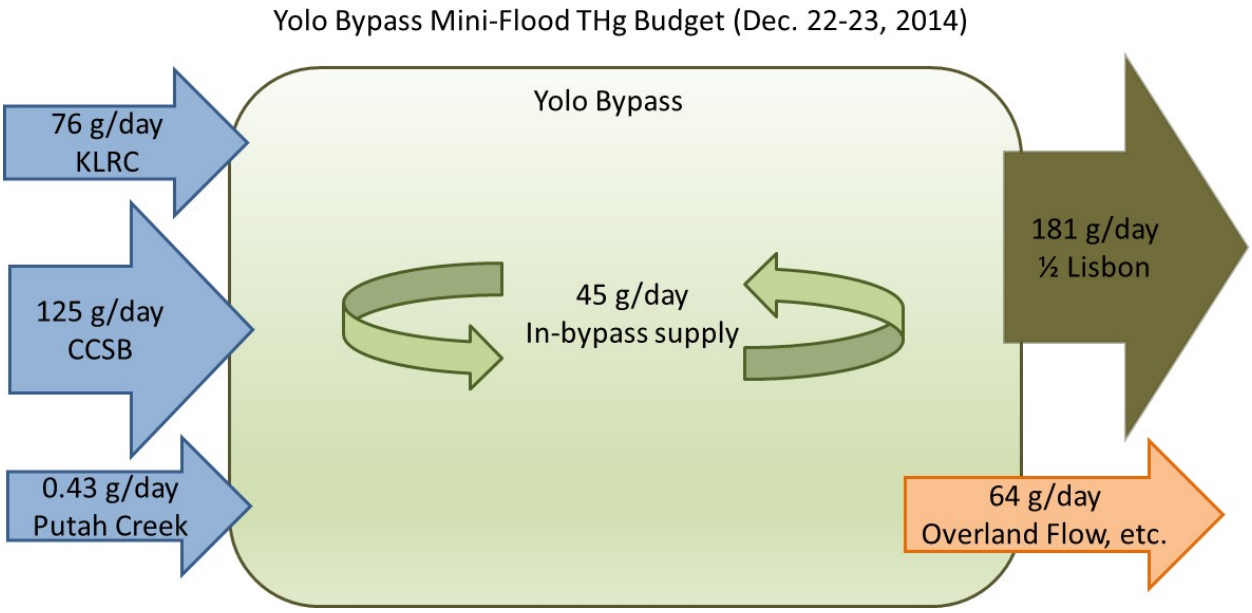

Figure 4-13. Conceptual model of THg imports and exports from the Yolo Bypass mini-flood sampling event, December 22-23, 2014.

4.5. Appendix A Computation of Stairstep's Modeled Flows for December Inlet/Outlet Sampling Event

Flows near the stairstep and Toe Drain is not completely monitored. The dominant patterns were obtained by means of hydrodynamic simulation using the Bay-Delta SCHISM model (http://baydeltaoffice.water.ca.gov/modeling/deltamodeling/models/bay_delta_schism/). Bay-Delta SCHISM is a 3D baroclinic model application of the entire Bay-Delta estuary that was specifically refined for this study in the region of collection. The assumptions of this modeling application are described in Ateljevich and others. (2014), including peer-reviewed references of the underlying software. Bathymetry for the region comes from an updated version of the map described in Wang and Ateljevich (2012, http://baydeltaoffice.water.ca.gov/modeling/deltamodeling/modelingdata/DEM.cfm), with the notable addition of new multi-beam soundings in the Stairstep region. A multi-dimensional model was used for this application because of the proximity of the flow of interest to open water and because such a model was already under development to describe fluxes in the Stairstep region; local flow is predominantly two dimensional.

The most sensitive modeling input for this application is the boundary inflow from the Yolo Bypass through the Toe Drain. The Toe Drain is only weakly tidal during mini-events similar to the December 2014 event, and the flow past Lisbon to the south "splits" at the junction -- if the boundary flux is wrong, so will be the two partitioned fluxes. While the boundary condition is a sensitive input, there is no clear preferred source of data during small floods. For the event of December 2014, we used flows from the DWR-NCRO station just below Lisbon Weir (Water Data Library B91560Q, CDEC LIS). This station is considered reliable until the free surface reaches roughly 10 ft, at which point the Toe Drain overtops its banks and the relationship between stage, velocity, and flow becomes more complex. The event of December 2014 does exceed this limit by up to 1 ft (comparatively small), and some overtopping was observed with an unknown effect on the quality of the flow rating. The best alternative source of data, includes the USGS station at Woodland, which is considerably farther upstream and was originally designed for larger flows. The two stations were in good agreement in years prior to 2012, as would have been the case during our validation described below. However, in 2014 the stations disagree by 30% or more in the 2,000 cfs range even on flows when both stations are nominally "in-bounds." Subsequent inspection revealed that the Lisbon station seemed closer to its historical relationship of stage and flow; Woodland station had been recently re-rated to include lower flows, with an unknown effect on data quality.

Local validation of the model was accomplished by simulating a February 2009 event of roughly similar magnitude, during a period when additional instrumentation was deployed by the USGS as part of a special study and when some of the data quality discrepancies noted above did not

seem to be important. Figure 4-14 compares simulated and observed flow for a station at the Toe Drain just below the junction with the Stairstep (USGS 11455140) and Figure 4-15 compares simulated and observed flows at Liberty Cut (USGS 11455147). Note the units – the plot has cfs on the right axis. The top panel is a time series showing one spring-neap cycle of tidal behavior. The bottom left panel shows net (tidally filtered) results. Various metrics can be found at the bottom of the figure, including raw root mean square error, bias and Nash Skill index. Metrics subscripted with a ϕ are calculated after first correcting for phase differences. Tidal and net flow responses are captured well by the model at both sites particularly in the Toe Drain right at the location of interest; there is some tidal attenuation at Liberty Cut, which subsequent simulations have demonstrated may be due to local bathymetry and mesh choices. While we found the Stairstep to be a challenging location to model, particularly around breaches, a lot of the difficulty is associated with more delicate aspects of the local mean flow. At the junction, upstream flow described above is the main source of uncertainty.

The main result of the simulations is simple -- dynamics near the junction are dominated by flow along the Toe Drain itself. This is true both in general tidal circumstances (when net flow is south-to-north until October) and mild flooding, which is entirely north-to-south. For the 2014 event, the flow split is shown in Figure 4-16, which indicates a flow of roughly 2500 cfs down the Toe Drain compared to 500 cfs along the Stairstep. During a flood event, net flow dominates over tidal at the junction and the direction of flow does not change over the tide cycle. Under such a flow regime, contaminants would be expected to travel some distance along the Toe Drain before tidal dispersion could take over as the main mechanism of mixing. In contrast, summer flow is bidirectional and net flow is actually directed northward; under these circumstances tidal dispersion is the only mechanism that can bring mercury into the Delta from the north (on ebb tides).

4.6. Literature Cited

Ateljevich, E., Nam, K., Zhang, H., R., W., Shu, Q. 2014. Bay-Delta SELFE Calibration Overview. In Methodology for Flow and Salinity Estimates in the Sacramento-San Joaquin Delta and Suisun Marsh 35th Annual Progress Report, 2014.

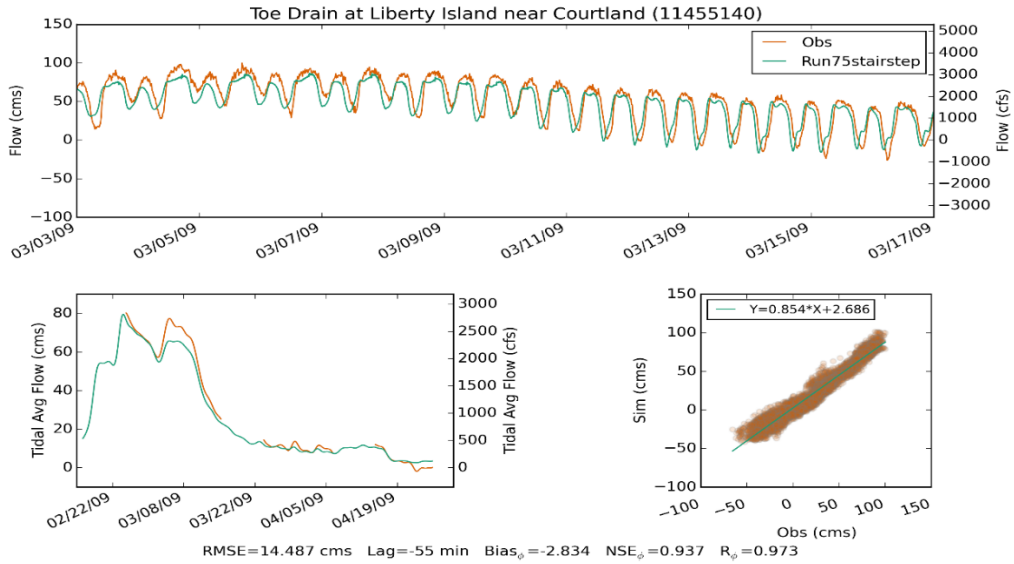

Figure 4-14. Comparison between SCHISM modeled and observed flows in 2009 for the Toe Drain below the junction.

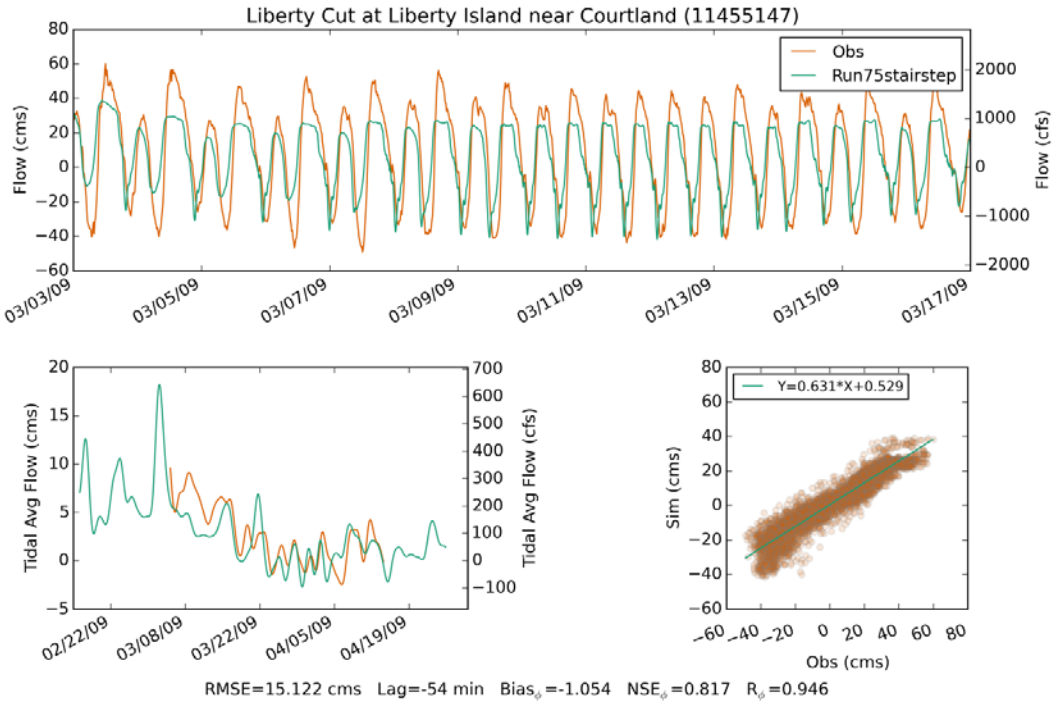

Figure 4-15. Comparison between SCHISM modeled and observed flows in 2009 for the Toe Drain at Liberty Cut.

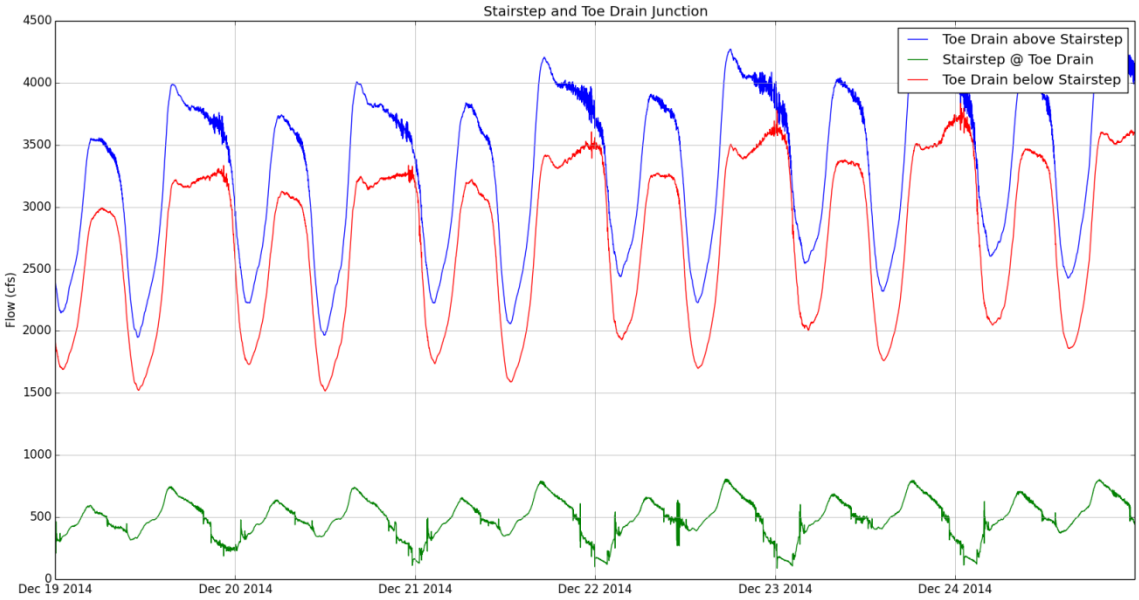

Figure 4-16. Modeled flow on the upper Toe Drain above the Stairstep, below the Stairstep, and entering the Stairstep during the December 2014 Event.

4.7. Appendix B Laboratory QA/QC for Inlet/Outlet Samples Collected December 22-23, 2014

Table 4-8. Laboratory Method Blanks.

Analyte	Analysis Date	Result	Units	Meets QA Standards?
Methylmercury	1/14/2015 -1/16/2015	< 0.011	ng/L	Yes
Methylmercury	1/14/2015 -1/16/2015	< 0.011	ng/L	Yes
Methylmercury	1/14/2015 -1/16/2015	< 0.011	ng/L	Yes
Methylmercury	1/14/2015 -1/16/2015	< 0.011	ng/L	Yes
Methylmercury	1/14/2015 -1/16/2015	< 0.011	ng/L	Yes
Methylmercury	1/14/2015 -1/16/2015	< 0.011	ng/L	Yes
Total Mercury	1/5/2015	< 0.5	ng/L	Yes
Total Mercury	1/5/2015	< 0.5	ng/L	Yes
Total Mercury	1/5/2015	< 0.5	ng/L	Yes
Total Mercury	1/5/2015	< 0.5	ng/L	Yes
Total Suspended Solids	12/29/2014	< 1.0	mg/L	Yes
Total Suspended Solids	12/29/2014	< 1.0	mg/L	Yes

Table 4-9. Laboratory Replicates.

Sampling Location	Analyte	Result	Replicate Result	Units	RPD	Measurement Quality Objective	Meets QA Standards?
Knights Landing Ridge Cut at Hwy 113	Methylmercury (total)	0.212	0.207	ng/L	2.4%	≤ 25%	Yes
From another project	Methylmercury	0.365	0.364	ng/L	0.3%	≤ 25%	Yes
From another project	Total Suspended Solids	57	60	mg/L	5.1%	≤ 25%	Yes
Toe Drain at Lisbon Weir	Total Suspended Solids	58	60	mg/L	3.4%	≤ 25%	Yes
Toe Drain at Lisbon Weir Field Duplicate	Total Suspended Solids	60	61	mg/L	1.7%	≤ 25%	Yes

Table 4-10. Lab Control Standards and Duplicates.

Analyte	Standard Conc	Result 1	% Recovery for Result 1	Result 2	% Recovery for Result 2	Units	RPD	Measurement Quality Objectives	Meets QA Standards?
Methylmercury	1	1.121	112.1%			mg/L		75-125%	Yes
Methylmercury	1	0.954	95.4%			mg/L		75-125%	Yes
Total Mercury	5	4.64	92.8%	4.65	93.0%	ng/L	0.2%	Recovery: 75-125% RPD: ≤ 25%	Yes
Total Mercury	5	4.84	96.8%	4.43	88.6%	ng/L	8.8%	Recovery: 75-125% RPD: ≤ 25%	Yes
Total Mercury	5	5.12	102.4%	5.07	101.4%	ng/L	1.0%	Recovery: 75-125% RPD: ≤ 25%	Yes
Total Mercury	5	5.20	104.0%	4.76	95.2%	ng/L	8.8%	Recovery: 75-125% RPD: ≤ 25%	Yes

Table 4-11. Matrix Spikes and Duplicates.

Analyte	Sample Conc	Spike Conc 1	Matrix Spike Result 1	% Recovery for Spike 1	Spike Conc 2	Matrix Spike Result 2	% Recovery for Spike 2	Units	RPD	Measurement Quality Objectives	Meets QA Standards?
Methylmercury	0.34	1.94	2.32	97.3%	1.95	2.23	101%	ng/L	4.0%	Recovery: 70-130% RPD: ≤ 25%	Yes
Methylmercury (dissolved)	0.11	1.97	2.06	99.4%	1.97	2.07	99.9%	ng/L	0.5%	Recovery: 70-130% RPD: ≤ 25%	Yes
Methylmercury (total)	0.12	1.98	2.22	106.0%	1.98	2.16	103.0%	ng/L	2.7%	Recovery: 70-130% RPD: ≤ 25%	Yes
Methylmercury (total)	0.21	2.00	2.22	101.0%	1.99	2.24	102.0%	ng/L	0.9%	Recovery: 70-130% RPD: ≤ 25%	Yes
Total Mercury (dissolved)	2.76	5.00	7.19	88.7%	5.00	7.08	86.5%	ng/L	1.5%	Recovery: 75-125% RPD: ≤ 25%	Yes
Total Mercury (dissolved)	3.60	5.00	8.75	103.0%	5.00	8.75	103.0%	ng/L	0.0%	Recovery: 75-125% RPD: ≤ 25%	Yes
Total Mercury (total)	8.86	5.00	13.40	90.9%	5.00	13.64	95.7%	ng/L	1.8%	Recovery: 75-125% RPD: ≤ 25%	Yes
Total Mercury (total)	16.29	5.00	21.42	102.6%	5.00	21.32	100.6%	ng/L	0.5%	Recovery: 75-125% RPD: ≤ 25%	Yes

5. Gust Chamber Erosion Experiments

Prepared by David Schoellhamer and Paul Work, USGS.

5.1. Introduction

Mercury adsorbs to sediment, especially fine sediment, and there are deposits of Hg-enriched sediment in the Yolo Bypass. The realism of the mercury transport model depends on the realism with which the initial Hg levels are quantified and with which erosion is simulated. The results described here, and the work remaining to be done in the coming year of the project, provide information on erosion characteristics of selected Yolo Bypass soils for the Hg transport model. This work does not represent a definitive erosion study, but provides guidance and constraints for the modeling which do not presently exist. A definitive erosion study would require more resources and multiple methods, and may be infeasible in a complex setting like the Yolo Bypass.

The objectives of the Gust Chamber Erosion Experiments are to:

1) Provide erosional rates of sediment under different velocities and land uses for use in the D-MCM.
2) Provide data to calibrate the velocity vs. erosion relationship developed by the Bale Chamber.

The following write-up provides an update on the progress of these experiments and provides provisional data that are subject to revision.

5.2. Field Methods

Field methods are similar to those described by Dickhudt and others. (2011) and used previously in the Delta (Schoellhamer and Manning, in press). Two sediment cores are collected from a study site using 10-centimeter (cm)-diameter cylinders (Figure 5-1). The sample locations usually had 5-30 cm of standing water overlying the sampled soil. Samples are disturbed as little as possible while coring. The top 1 cm of soil adjacent to the core is also sampled for grain size and water content analysis. A piston inserted into the bottom of the cylinder is used to push the sediment surface up to 10 cm from the top of the cylinder. This piston is sealed to prevent loss of water or sediment from the bottom of the chamber.

Figure 5-1. Photo of core collection.

The piston is being placed under the soil in the bottom of the cylinder. The piston is pushed up into the cylinder until the soil surface is 10 cm below the top of the cylinder. An erosion head is then placed on top of the cylinder that contains a motor that spins a disc to move water in the chamber and ports from which water is pumped into and out of the chamber.

The core is eroded using a dual core University of Maryland Center for Environmental Science - Gust Erosion Microcosm System (Figure 5-2). A disk rotates at the water surface at the top of the chamber and water is pumped through the water column in the chamber at predetermined rates that result in nearly uniform and known shear stresses at the sediment/water interface. The relation between rotation speed, pumping rate, and shear stress was determined empirically by the manufacturer (Suttles and others, 2011). Turbidimeters continuously monitor

the effluent. A 0.01 pascal (Pa) shear stress is initially applied to flush and stabilize the system. An applied bed shear stress (denoted as τ_b,) is increased stepwise to 0.05, 0.10, 0.15, 0.20, 0.30, 0.45, and 0.60 Pa over a period of about 3 hours. Water samples are collected during each step that are later analyzed for suspended-sediment concentration (SSC) to allow calibration of measured turbidity to SSC. The end result is a relationship between applied bed shear stress (force per unit area) and erosion rate (eroded mass per unit area per unit time).

For the Yolo Bypass sites, two cores were taken per site, to help assess variability, with attempts being made to avoid heavy vegetation which can make both sample acquisition and testing difficult. Testing was done immediately after sample collection in the field (Figure 5-3).

Figure 5-2. Photo of Gust Chambers (twin cylinders mounted in plate suspended on blue box) set up for measurements.

On the back of the van are two turbidimeters to measure effluent from the erosion chambers. The erosion heads are on top of the cylinders.

Figure 5-3. Conducting an erosion microcosm experiment in the field immediately after collecting the cores.

On top of the table are a computer that collects data and controls the experiment and the pump. On the ground are the two cores being eroded (the erosion chambers) and a cooler with the ambient water being pumped through the erosion chambers.

Erosion rates for cores taken at 5-6 additional sites in the Yolo Bypass will be measured in winter 2016. This area features a variety of land uses, many of them related to rice production. Sites were selected in collaboration with DWR and the project team, attempting to span the range of land uses. Factors influencing site selection included spatial variability in hydrology, land use, mercury content, particle size, and accessibility.

Sites were sampled when the soil was saturated and had standing water to approximate conditions present when the Yolo Bypass floods. The sites are summarized in Table 5-1. One additional erosion experiment will be performed in 2016, if needed, to fill any data gaps, collect a replicate core, and (or) redo an experiment that yields unexpected results. The erosion microcosm method is most effective on fine-grained soil which is suspended when it moves and

thus is easy to measure as opposed to sand which initially moves as bed load and is more difficult to measure. It is not possible to include all of the soil heterogeneity in the Yolo Bypass, so sites with the most common land uses, high Hg content, and fine particle size were selected. The microcosm cannot measure the effect of large vegetation which likely limits or prevents erosion. In this sense the microcosm results are conservative in that they represent the upper bound on erosion rate for a given shear stress. It should be remembered that both the fluid-induced shear stress in the field, and the soil's resistance to erosion, can display significant spatial variability. Crop furrows, for example, will lead to spatial variations in turbulence and shear stress on the bed.

Table 5-1. Sites for Erosion Experiments in Yolo Bypass, Dates, and Initial Critical Shear Stress.

Land Use	Date Sampled	Core	Latitude	Longitude	$\tau_c(0)$, Pa
Wild Rice (WR)	1/30/2015	1	38˚ 32.864'	121˚ 37.173'	0.25
		2	38˚ 32.862'	121˚ 37.173'	0.25
Un-disked Seasonal Wetland (UDSW)	2/4/2015	1	38˚ 32.472'	121˚ 37.237'	0.075
		2	38˚ 32.472'	121˚ 37.236'	0.25
White Rice (WHR)	2/27/2015	1	38˚ 33.149'	121˚ 37.220'	0.25
		2	38˚ 33.148'	121˚ 37.219'	0.25
Disked Seasonal Wetland (DSW)	3/5/2015	1	38˚ 32.234'	121˚ 37.472'	0.25
		2	38˚ 32.235'	121˚ 37.474'	0.25

Data are provisional and subject to revision. Position data are in WGS datum. In winter 2016, the following additional sites will be sampled: Liberty Island, Toe Drain near Lisbon Weir, Stairsteps near Liberty Cut, a fallow field, and a site below Cache Creek Settling Basin.

Example time series of erosion rate E (kg/m^2/s) for the white rice (WHR) field cores is shown in Figure 5-4. The top panel shows the stepwise increase in shear stress during the erosion experiment. The mean value is shown but the standard deviation of the shear stress in the microcosm is about 11% of the mean (Gust and Muller, 1997). The middle panel shows SSC which decreases to a background level then increases when shear stress is increased from 0.2

to 0.3 Pa and erosion in both cores begins. The initial critical shear stress for erosion is taken as the midpoint, 0.25 Pa. The mean error of the turbidity to SSC calibration was 13% for the white rice cores and all eight cores eroded in 2015. The bottom panel shows the time series of erosion rate E calculated from SSC, flow rate through the chamber, and the geometry of the chamber. Erosion rate increases rapidly at the beginning of each shear stress step greater than the initial critical shear stress and then decreases until the next increase in shear stress. This behavior indicates depth-limited erosion for which only a limited amount of mass can be eroded for each shear stress. The SSC calibration error and typical flowrate error (difference between desired flow for a given shear stress and measured) of about 1-4% contribute to the error in erosion rate E.

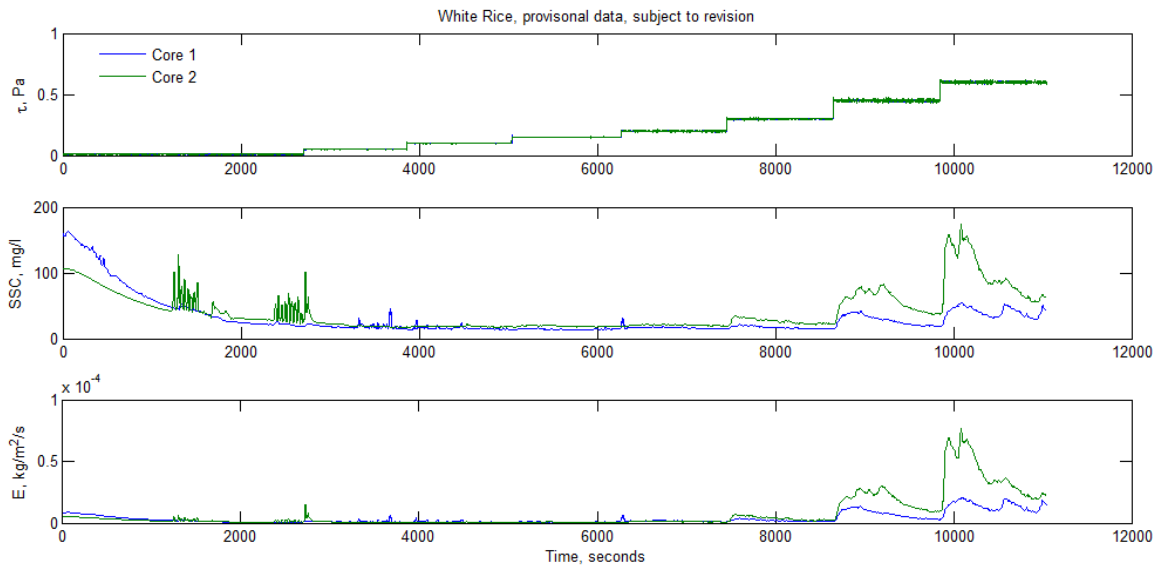

Figure 5-4. Time series of applied bed shear stress τ, SSC, and erosion rate E for WHR field cores. Data are provisional and subject to revision.

Experimental results for wild rice (WR), disked wetland (DSW), and un-disked seasonal wetland (UDSW) are shown in Figures 5-5 to 5-7.

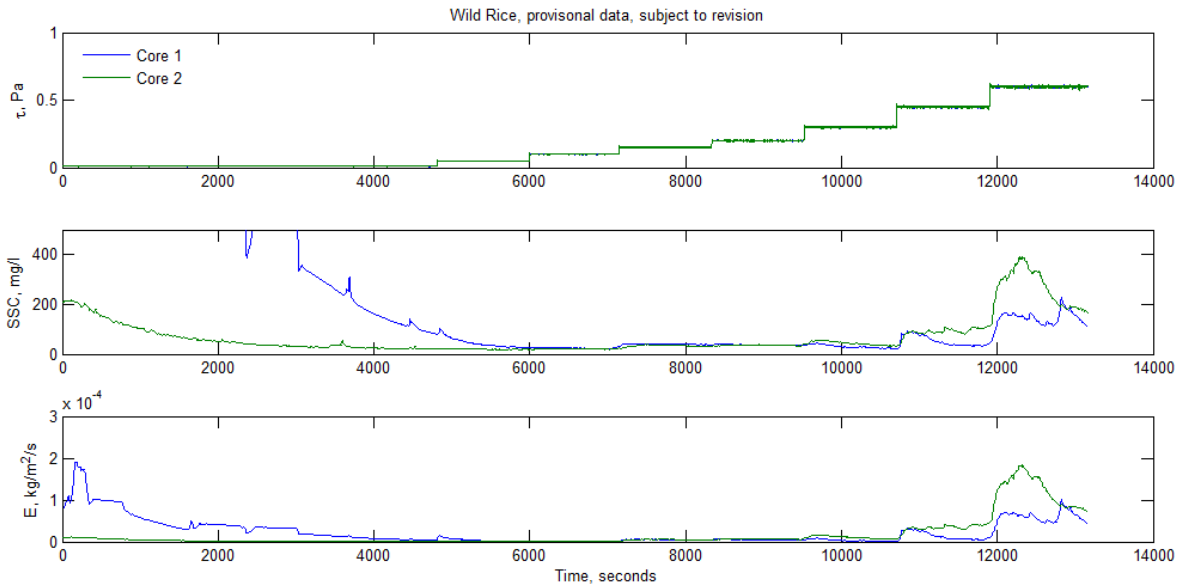

Figure 5-5. Time series of applied bed shear stress τ, SSC, and erosion rate E for WR field cores. Data are provisional and subject to revision.

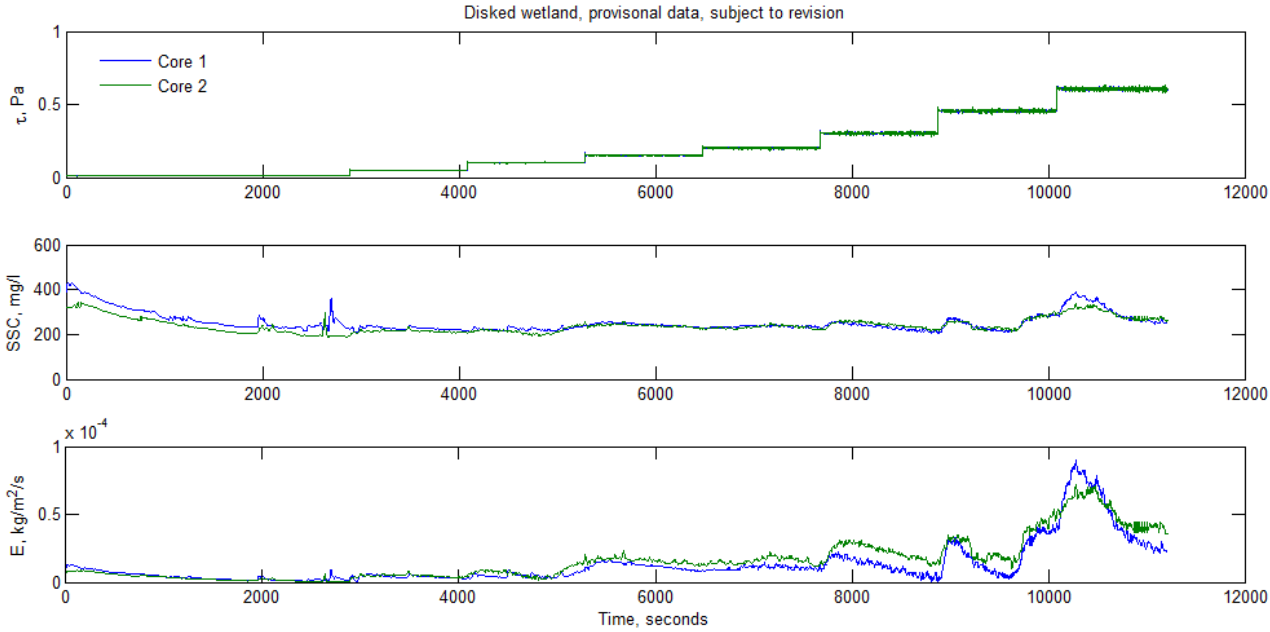

Figure 5-6. Time series of applied bed shear stress τ, SSC, and erosion rate E for DSW cores. Data are provisional and subject to revision.

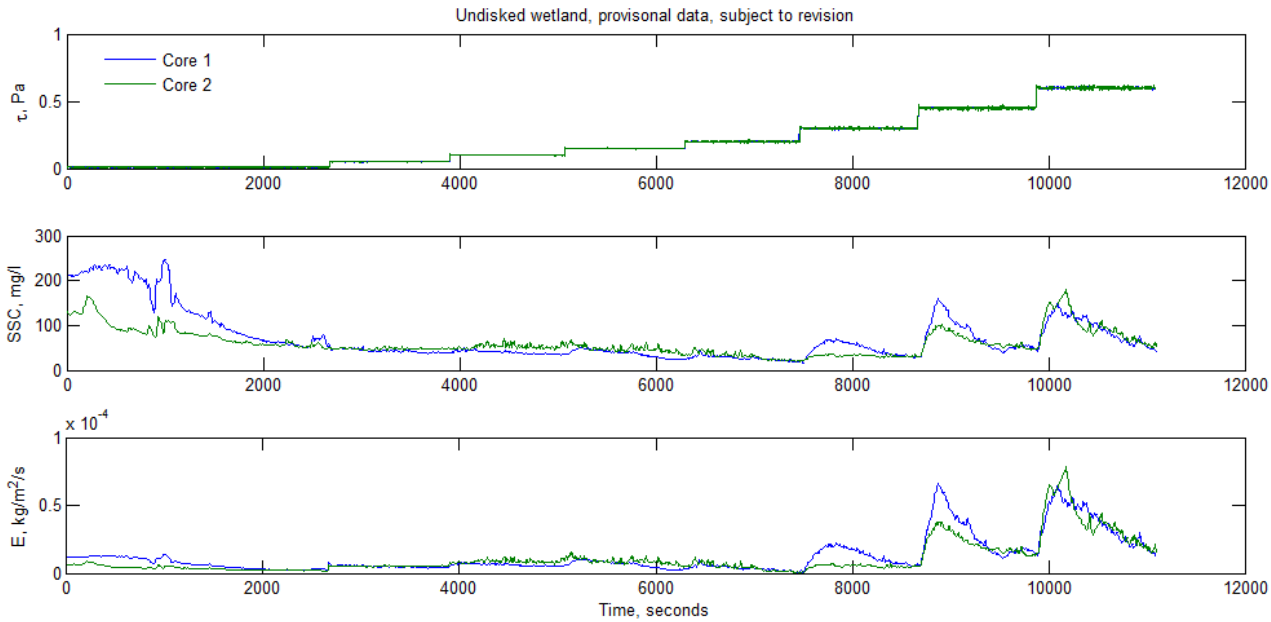

Figure 5-7. Time series of applied bed shear stress τ, SSC, and erosion rate E for un-disked UDSW cores. Data are provisional and subject to revision.

5.3. Data analysis

The erosion model of Sanford and Maa (2001) is used to calculate erosion parameters. The erosion rate E for an experiment as a function of mass eroded (m) and time (t) is

$$E(m,t) = M(m)\ [\ \tau_b(t) - \tau_c(m)\ ] \qquad (1)$$

Critical shear stress (τ_c) is calculated at the end of each step of applied bed shear stress ($\tau_{b,}$) and is assumed to increase with eroded mass (m), which in turn increases with erosion depth. The erosion rate M (m) is assumed to be a constant for each step.

With this information, the erodibility (τ_c and M) of the study sites relative to one another can be determined. Critical shear stress increases as the eroded mass increases (Figure 5-8). Eroded mass is proportional to the mean erosion depth, so Figure 5-8 shows that critical shear stress increases as erosion depth increases. The erosion constant M also generally increases with eroded mass or erosion depth (Figure 5-9). Typically M has more variability than τ_c as seen in Figures 8 and 9. The general increase in M with eroded mass may be due to small erosion depths and horizontal variability of critical shear stress (Schoellhamer and Manning in press). These parameters constrain erosion rates because the erodibility of each model box relative to the others is known. Thus, the erosion time series can be multiplied by a single calibration factor to achieve model calibration.

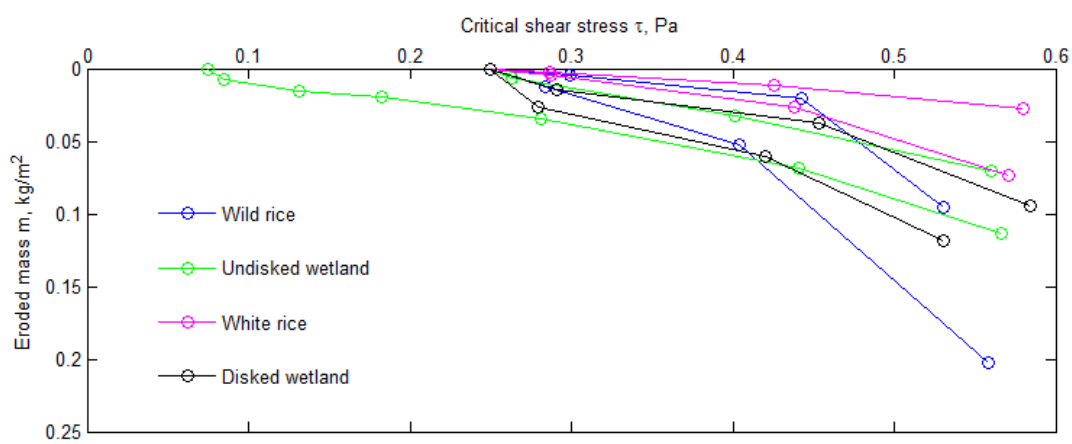

Figure 5-8. Critical shear stress as a function of eroded mass from 8 cores collected at 4 sites in 2015. Provisional data subject to revision.

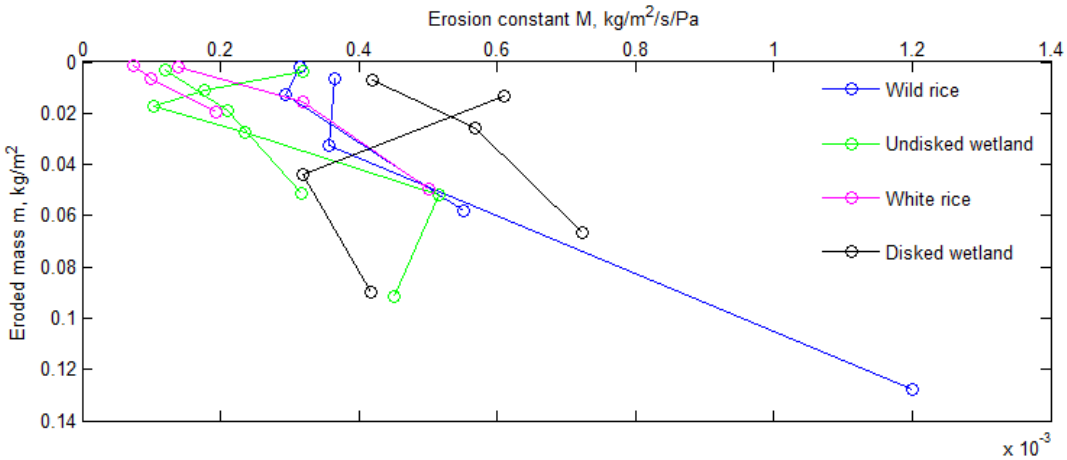

Figure 5-9. Erosion constant M as a function of eroded mass from 8 cores collected at 4 sites in 2015. Provisional data subject to revision.

A simple way to compare the relative erodibility of the land use types is to compare the mass eroded when the critical shear stress reaches 0.4 Pa ($m_{0.4}$, fig. 10, Dickhudt and others, 2011). The variability between replicate cores for a given land use type and between land use types are similar. Each land use type has only two replicate cores, so statistical tests of significance are not possible. The data graphically indicate that white rice is less erodible than the other land use types and perhaps that WR is less erodible than un-disked DSW and UDSW.

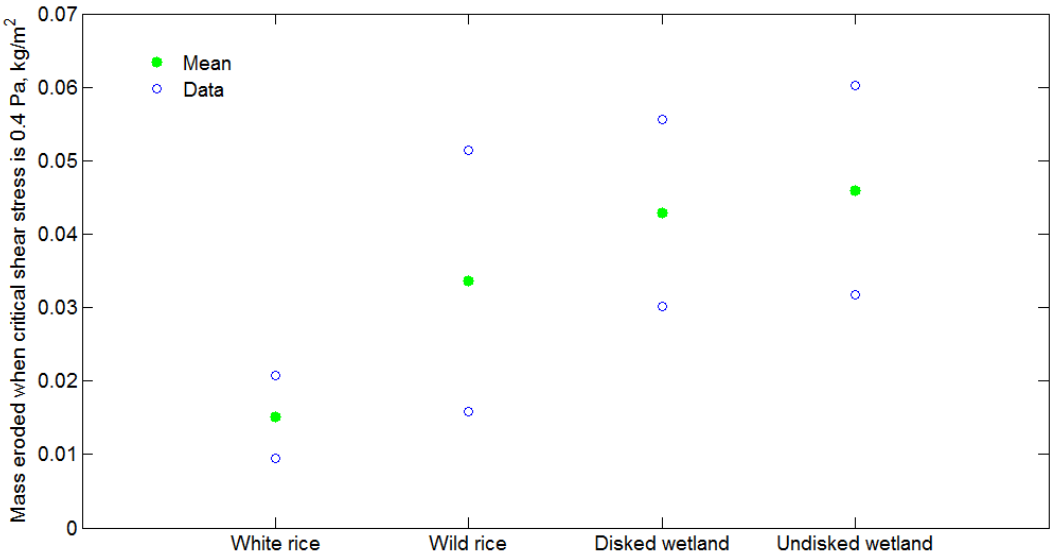

Figure 5-10. Mass eroded when the critical shear stress is 0.4 Pa.

Blue circles are data for the individual cores and green filled circles are the mean of the two values for each land use type. Land use types are ordered by increasing erodibility.

Erosion parameters from the Yolo Bypass can be compared to those found for 38 subtidal cores from the Delta (Schoellhamer and Manning in press). Seven of the eight Yolo Bypass cores tested in 2015 had an initial critical shear stress of 0.25 Pa which is larger than typically found in the subtidal Delta (Figure 5-11, left panels). The mass eroded when the critical shear stress is equal to 0.4 Pa is comparable between the Yolo Bypass and Delta (Figure 5-11, right panels). Thus, the Yolo Bypass cores generally had a greater erosion threshold, but would erode a similar quantity of mass if the applied shear stress were a constant 0.4 Pa. Tillage, greater sunlight, and ponded water rather than tidally flowing water, may account for these differences.

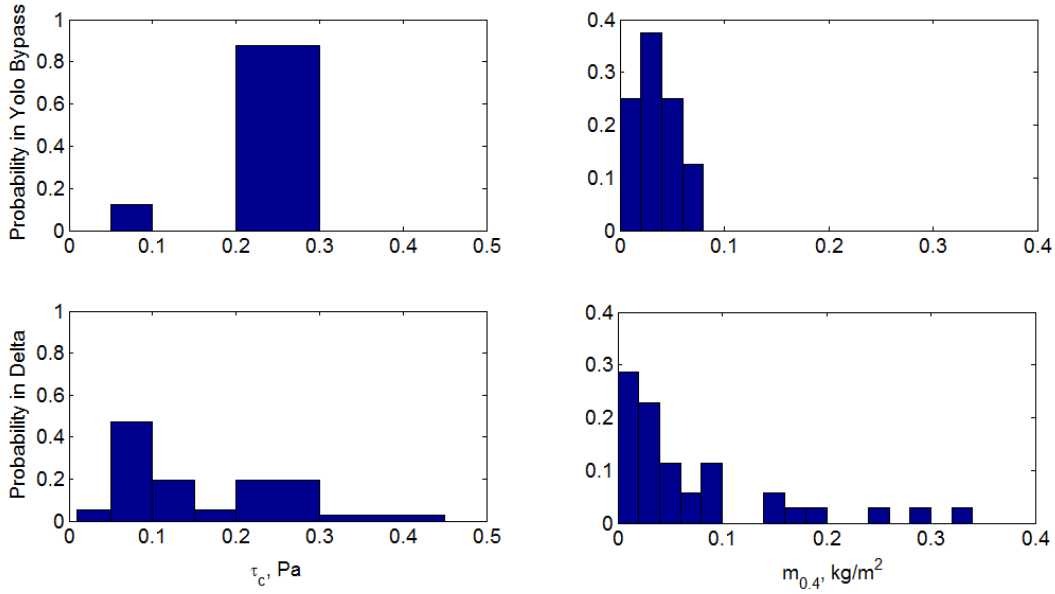

Figure 5-11. Probabilities of initial critical shear stress τ_c and mass eroded when the critical shear stress is 0.4 Pa $m_{0.4}$ for the 8 Yolo Bypass cores analyzed in 2015 and 38 Delta subtidal cores analyzed 2011-2014 (Schoellhamer and Manning in press).

Dickhudt and others (2011) compared their erosion data from Chesapeake Bay to several other lab and field measurements by others and found a weak relation between the initial critical shear stress and the solids volume fraction of the mud matrix (φ_{sm}). Data from these eight cores generally are at the outskirts of the envelope of Dickhudt and others (2011) data (Figure 5-12). Seven of the eight Yolo Bypass cores had a critical shear stress of 0.25 Pa, so they form a line on this figure. Most of the Dickhudt and others 2011 data are for estuarine, not terrestrial, sediment, so the agreement is probably reasonable.

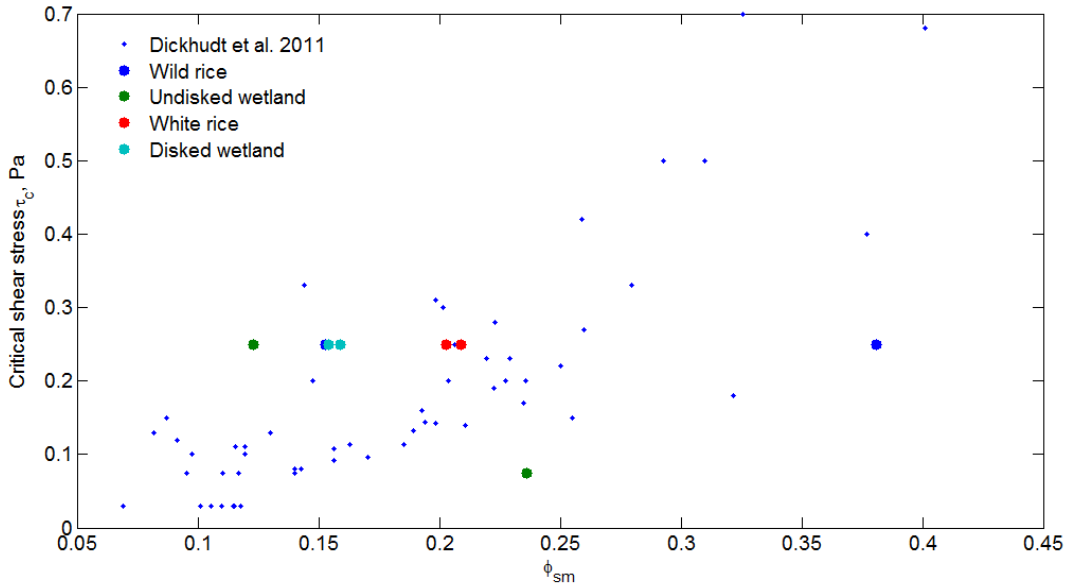

Figure 5-12. Critical shear stress as a function of solids volume fraction of the mud matrix. Dickhudt et al. (2011) provide 56 measurements.

An erosion rate time series can be calculated given depth-averaged velocities U from the DWR hydrodynamic model of the Yolo Bypass. Depth-averaged velocity U is related to shear stress by

$$U/u^* = 1/\kappa \ln(11H/k_s) \quad (2)$$

$$u^* = (\tau_b/\rho)^{1/2} \quad (3)$$

$$k_s = 3\, D_{90} \quad (4)$$

in which u* is the shear velocity, κ is the von Karman constant equal to 0.4, H is the water depth, k_s is the bottom roughness, □ is the density of water (1000 kg/m^2), and D_{90} is the 90th percentile by mass of particle size (American Society of Civil Engineers, 2008). These equations relate depth-averaged velocity U and shear stress τ_b (Figure 5 13). For a given time series of velocity from the hydrodynamic model, equations 1-4 can be used to estimate a time series of erosion. It is unlikely that the erosion time series will provide the best fit to measured SSC because the depth-averaged velocity varies within the model computational cell, the models assume a well-mixed water column that features unrealistic instantaneous mixing of eroded sediment, and the model calibration will also be dependent on uncertain settling parameters.

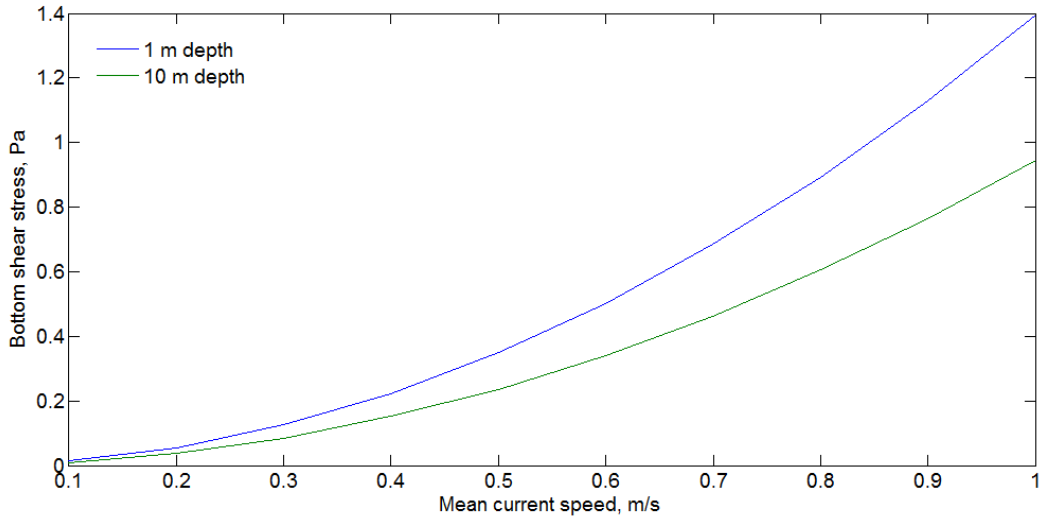

Figure 5-13. Bottom shear stress as a function of mean current speed.

This figure is derived from equations 2-4 using a D_{90} of 82 microns from a handful of completed bed particle size distributions and for water depths of 1 and 10 m.

Bed roughness is an input parameter for hydrodynamic models. It is used to compute bed shear stress, which serves as a boundary condition on the flow. So it should be possible to output the computed bed shear stress, or at least the depth-averaged flow speed, from which the bed shear stress could be computed using Equation 2. With the bed shear stress known, and the local critical shear stress and erosion rate constants known, the erosion rate can then be computed using equation 1.

The mercury model includes four sediment size classes: sand, fines, and two organic classes (easily degraded, and refractory). The experiments will determine erosion coefficients for fine sediment only. Sand is a small component of most Yolo Bypass soils and has much smaller surface area and less adsorbed mercury than fine sediment; thus, sand erosion will be estimated with a published formula (American Society of Civil Engineers, 2008). The organic components are generally fine and are a small fraction of the bed mass, so erosion will be estimated as being equal to the erosion rate for fine sediment multiplied by the proportion of bed sediment that is organic.

In addition to the erosion experiments, 69 soil samples collected by DWR and Dr. Mark Stephenson were analyzed for particle size during summer 2015.

5.4. Next Steps

In winter 2015/16, erosion experiments will be performed at 5-6 additional sites and the data analysis will be completed. Most of the sites are continuously submerged and will be sampled from a boat, helping reduce any dependency on weather conditions.

5.5. Literature Cited

American Society of Civil Engineers (2008). Sedimentation Engineering: Manual of Practice 110, 1132 p.

Dickhudt, P.J., Friedrichs, C.T., Sanford, L.P. (2011). Mud matrix solids fraction and bed erodibility in the York River estuary, USA, and other muddy environments: Continental Shelf Research 31:S3-S13.

Gust, G. and Muller, V., 1997, Interfacial hydrodynamics and entrainment functions of currently used erosion devices. Cohesive Sediments. N. Burt, W. R. Parker and J. Watts. New York, John Wiley and Sons: 149-174.

Sanford, L.P., Maa, J.P.-Y. (2001). A unified erosion formulation for fine sediments. Marine Geology 179:9–23.

Schoellhamer, D.H., and Manning, A.J., in press, Erosion characteristics and horizontal variability for small erosion depths in the Sacramento – San Joaquin River Delta, California, USA. Proceedings of the 13th International Conference on Cohesive Sediment Transport Processes, Leuven, Belgium, September 9-13, 2015.

Suttles, S., Sanford, L., and Dickhudt, P., 2011, Review, analysis, and recommendations for application of operation calibrations for UMCES-Gust erosion microcosm systems (U-GEMS), Green Eyes Environmental Observing Systems technical report, 5 p.

5.6. Appendix A Comparison of Gust and Bale Erosion Chamber Results

A fine sediment bed consolidates with time such that older, deeper sediment with more weight above will have a greater shear strength and be less erodible than sediment closer to the surface. The critical shear stress for erosion is the minimum shear stress that must be applied to the bed surface to have erosion. As sediment is eroded during an erosion chamber experiment, the critical shear stress increases.

For a Gust Chamber experiment, the time series of effluent suspended sediment concentration is used to calculate the critical shear stress as a function of mass eroded (figs. 1 and 2, see Dickhudt and others, 2011 for details).

For the Bale Chamber, a shear stress is applied for 20 minutes, then the shear stress is stepped up, and, unlike in the case of the Gust Chamber, there is no effluent, so suspended sediment concentration continues to increase even if erosion reaches steady state. The total mass eroded per unit bed surface area at the end of a step is the product of SSC (assumed uniform) and water depth (11 cm, Bale and others, 2006). This also assumes the initial still water SSC was zero. If SSC is not increasing at the end of a 20 minutes step, erosion is negligible and the critical shear stress of the bed equals the applied shear stress. Bale and others (2006) provide calibration equations to relate paddle velocity in revolutions per minute, mean water velocity, and shear stress. Thus, assuming negligible erosion at the end of a 20 minute long application of a shear stress, Bale Chamber eroded mass and critical shear stress can be compared to Gust chamber results (Figures 5- 14 and 5-15). Eroded mass calculated by USGS differs from the MLML result, possibly in part because the MLML Bale Chamber dimensions differ from those given by Bale and others (2006).

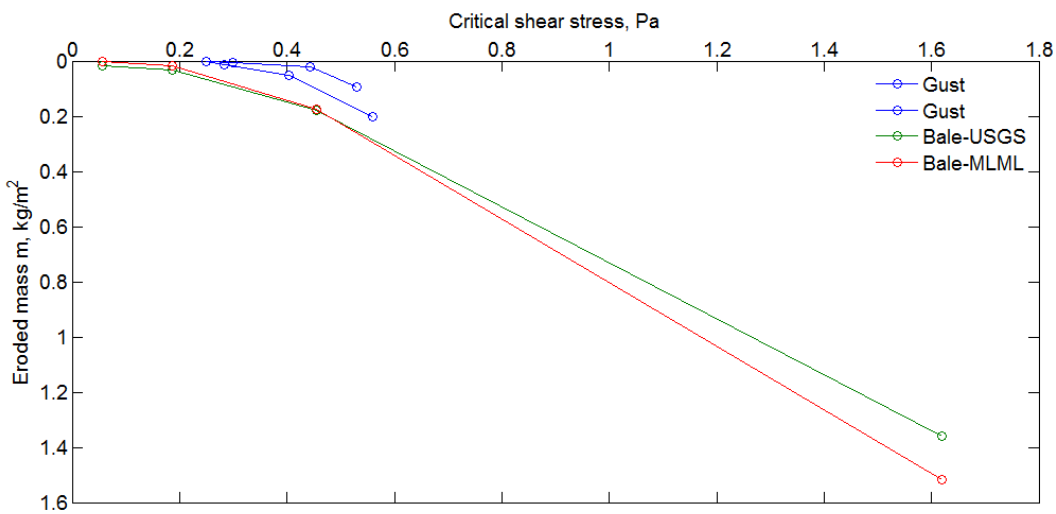

Figure 5-14. Bale and Gust Chamber results for wild rice. Two cores from the same site were tested with the Gust Chamber. MLML and USGS calculated eroded mass independently and got slightly different results.

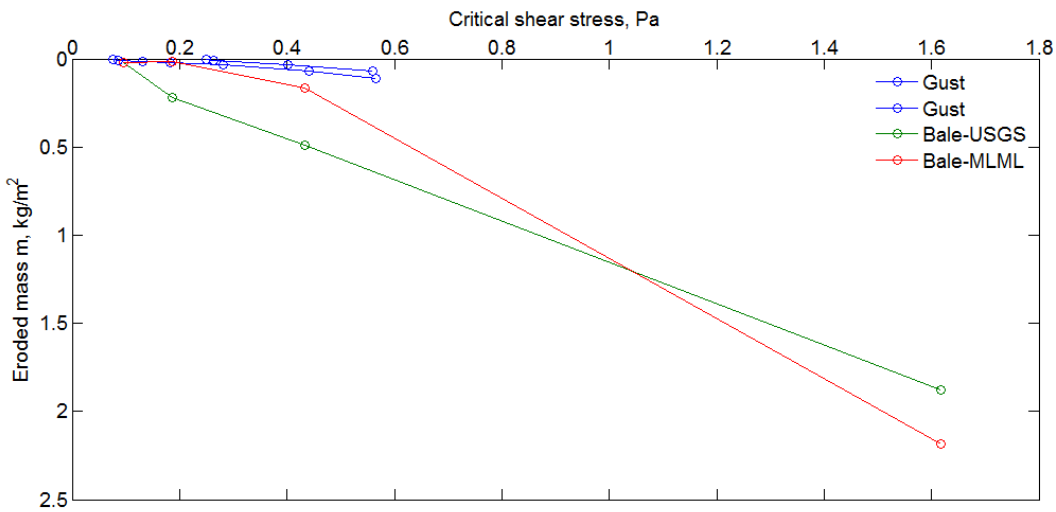

Two cores were tested with the Gust Chamber. MLML and USGS calculated eroded mass independently and got slightly different results

Figure 5-15. Bale and Gust Chamber results for an un-disked wetland.

The Bale Chamber erodes more sediment than the Gust Chamber. Possible reasons identified for the differences are that a) the Bale Chamber shear stress has more spatial variation than the Gust Chamber, b) the elevation and location of the port from which the water-sediment suspension is taken from the Bale Chamber may not be representative of the mean concentration, and c) the velocities at which some of the data have been collected with the Bale Chamber go outside of the calibration range. These possibilities are explored further below.

Bale Chamber shear stress varies more than the Gust Chamber: Both chambers use a rotating surface (disk for Gust, paddles for Bale) at the top of a cylindrical chamber to move water in the chamber. The rotational speed at the outside of the cylindrical chamber will be greater than inside. Shear stress is proportional to velocity squared and velocity is proportional to the radius so shear stress is proportional to the radius squared. Thus, shear stress is greater on the outside of the chambers. To correct this, the Gust Chamber pumps water in at the top outside of the chamber and out at the top center of the chamber. This creates a radial flow from the outside to the inside along the bed. This radial flow transports high velocity water from the outside to the inside, which reduces the variability of shear stress on the bed (Figure 5-16). The radial component of the velocity also increases with decreasing radius. Together these two effects combine to help reduce the radial variability in bed shear stress that would otherwise result. Gust and Muller (1997) made detailed measurements of shear stress to determine that the standard deviation of shear stress was 11% of the mean.

The Bale Chamber paddles extend from about 3 to 9 cm from the center of the cylinder. Thus the radius increases by a factor of 3 and shear stress would increase by a factor of 9. Radial mixing in the absence of net radial flow will reduce the shear difference somewhat. Assume

the worst case that the shear stress in the Bale Chamber is proportional to the square of the radius r, $\tau(r) = \alpha r^2$. Apply the mean value theorem of calculus in cylindrical coordinates for r = 3 to 9 cm to get that the mean shear stress τ_m=45α. For τ_m =0.1 Pa, α=1/450. The shear stress distributions for the chambers for a mean shear stress of 0.1 Pa are plotted in Figure 5-17. In this case, the outside of the Bale Chamber would have a shear stress of 0.18 Pa and the inside 0.02 Pa. If the critical shear stress of the bed were 0.1 Pa, half the bed would erode, half would not. This would lead to an overestimation of erosion.

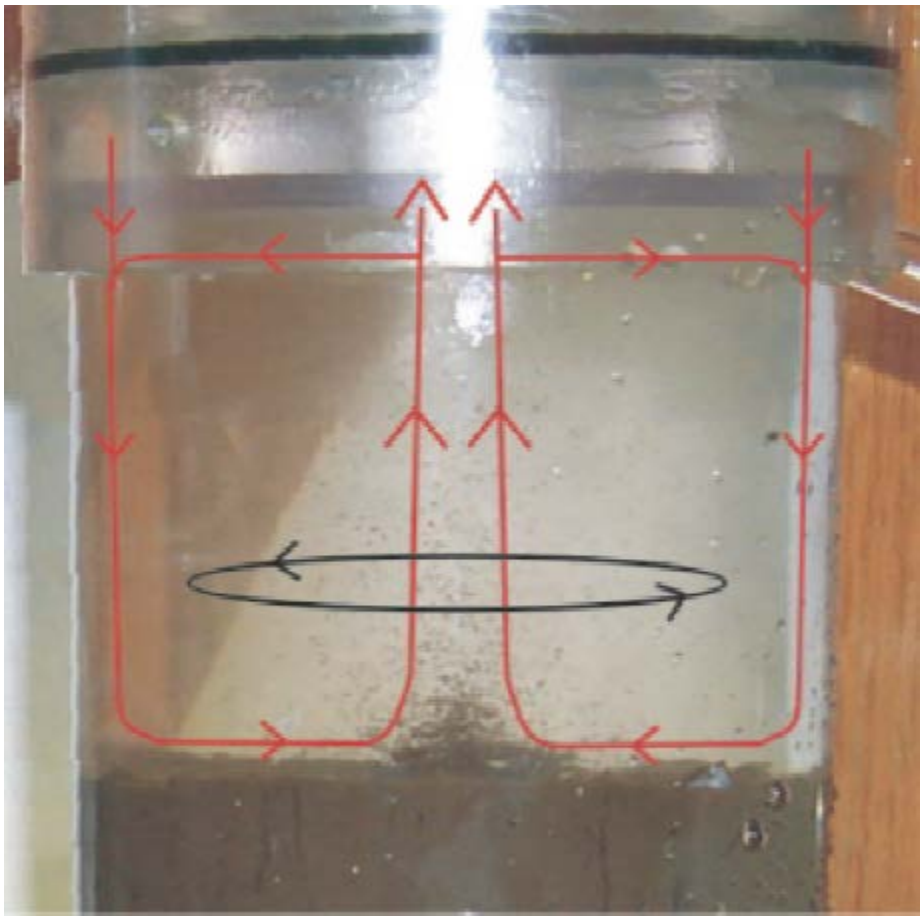

Figure 5-16. Photo of Gust Chamber with flow pattern represented by drawn lines and arrows (Green Eyes LLC, 2011).

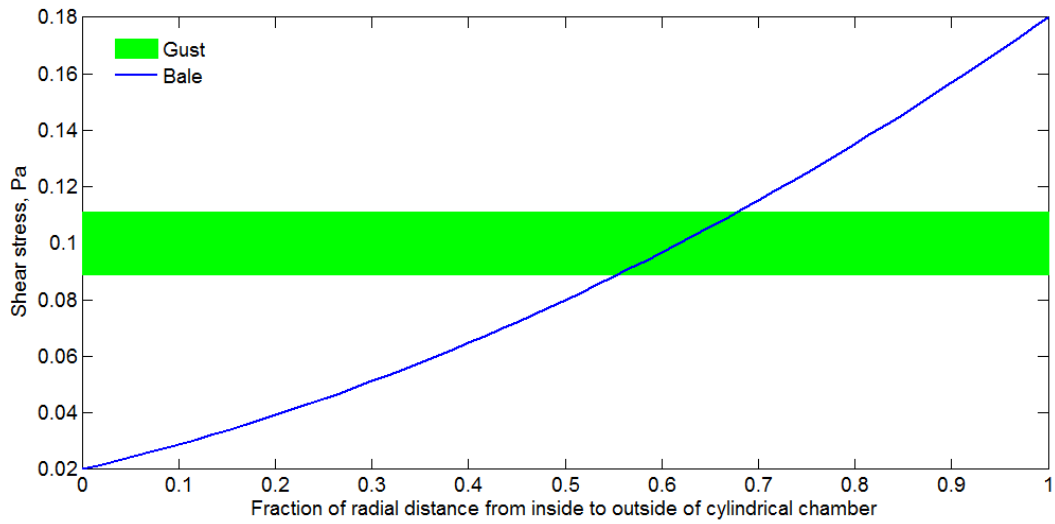

Figure 5-17. Shear stress distribution in Gust and Bale Chambers for a mean shear stress of 0.1 Pa.

The fraction of radial distance from inside to outside of cylindrical chamber equals 0 at the inside wall for the Bale Chamber, 0 at the center of the Gust Chamber, and 1 at the outside wall of both chambers. The chambers have different dimensions, so this scale is used to normalize them.

There are two ways fine sediments can erode given a shear stress applied to the sediment bed by flowing water. Type I erosion is where a certain amount of sediment erodes, but then erosion is negligible. Essentially the sediment that can erode is winnowed (removed) from the bed surface and an increase in shear stress is needed to get more erosion. The applied shear stress and the critical shear stress needed to erode sediment are the same. At greater shear stresses, type II erosion is where there is a mass failure of the bed and erosion removes up to inches or feet of material. Depending on the variability of shear stress in the Bale Chamber and the shear stress at which type I erosion becomes type II, both types of erosion could occur in the Bale Chamber, which would appear to be type II erosion.

Bale port height and location: The port height for the Bale Chamber is close to the sediment bed. This could make the SSC of withdrawn samples greater than the mean SSC. Fine sediment, however, typically has a low settling velocity and is nearly uniformly distributed in the water column. This would be especially likely in the Bale Chamber where the 4 paddles would generate large eddies that vertically mix the water column.

Calibration ranges: According to Bale and others (2006), their experiments and calibration measurements were conducted for mean velocities up to 0.5 m/s which according to their equation 2 corresponds to a shear stress of 0.56 Pa. The Gust Chamber was calibrated up to 0.45 Pa and its useful range is commonly extended up to 0.60 Pa by extrapolation. For both chambers, results at shear stresses greater than their calibration range are more uncertain. This could account for some of the difference at shears greater than about 0.5 Pa. The methodology to utilize both the Bale and Gust Chamber results is outlined in Appendix B.

5.7. Literature Cited

Bale, A.J., Widdows, J., Harris, C.B., and Stephens, J.A., 2006, Measurements of the critical erosion threshold of surface sediments along the Tamar Estuary using a mini-annular flume: Continental Shelf Research, v. 26, p. 1206-1216.

Dickhudt, P.J., Friedrichs, C.T., Sanford, L.P. (2011). Mud matrix solids fraction and bed erodibility in the York River estuary, USA, and other muddy environments: Continental Shelf Research 31:S3-S13.

Gust, G. and Muller, V., 1997, Interfacial hydrodynamics and entrainment functions of currently used erosion devices. Cohesive Sediments. N. Burt, W. R. Parker and J. Watts. New York, John Wiley and Sons: 149-174.

5.8. Appendix B Utilization of both Gust and Bale Chamber Results for Sediment and Mercury Mobilization, Respectively

Issues and proposed solutions:

1) Gust Chamber and Bale Chamber erosion rates differ.
   There are numerous potential reasons for this, including the theorized greater horizontal variations in shear stress in the Bale Chamber that are not resolved, as shear stress is estimated at a single value.

2) Vegetation is likely to reduce erosion rates significantly, but we don't know how much.

   Solution:
   1) Rely on Gust Chamber for absolute erosion rates.
   2) Use Bale Chamber to provide a relative scaling factor and use for vegetated locations not suitable for Gust Chamber analysis.
      Take Bale Chamber in the field and test adjacent sites that feature same land use but are vegetated differently. Determine the ratio of erosion rate for vegetated site to unvegetated. Use this dimensionless ratio to scale down the Gust Chamber results to determine erosion rates for vegetated sites.

3) We suspect that flows will be found in the model results that feature velocities that take us out of the calibration range for both chambers.

   Solution:
   1) Inspect a map of the square of the velocity, for a high-flow event, based on model results. Or even better, a map like this superimposed on a classified map that reveals degree of vegetation. This will help us see how big a problem the high flow speeds might be.

   2) Extrapolate Gust Chamber results to higher shear stresses, as need be. Do we get to Type II erosion, where behavior changes? Uncertain.

6. Bale Chamber-Particulate and Dissolved Flux Rates-Pilot Study

Prepared by Mark Stephenson and Wesley Heim, Moss Landing Marine Labs

6.1. Introduction

In this set of pilot studies, a mini-annular flume, known as a Bale Chamber, was tested to determine if it could provide erosion values comparable to the Gust Chamber and provide measurements of Hg and MeHg concentrations on eroding particles. Erosion information associated with different land uses is already being obtained using a Gust Chamber (Chapter 5), however, the water volume in a Gust Chamber is only 0.75 L. With a water volume of less than a liter, the Gust Chamber lacks sufficient capacity for multiple samples to be collected for Hg and MeHg. The Bale Chamber has a capacity of 2.9 L. This allows for multiple aliquots to be removed for Hg and MeHg analyses. The D-MCM does not directly require Hg or MeHg resuspension rates from the Bale Chamber, however, Bale Chamber Hg and MeHg measurements could be used for model calibration. Two Bale Chamber pilot experiments were conducted to provide information for the model and to determine if the methodologies employed would provide useful information on how to minimize production of MeHg in different land uses. The Bale Chamber particulate experiment simulated flood flows over a short period of time. Fluxes of TSS, particulate bound MeHg and THg were measured. The second Bale Chamber pilot study was a diffusional experiment. This experiment examined fluxes of the same parameters but over a longer period of time so as to simulate slow moving flood waters.

The objective of the Bale Chamber pilot study was to:

1. Determine if the Bale Chamber will give accurate MeHg flux and TSS erosion information for the D-MCM as well as provide information helpful to the development of best management practices to reduce MeHg production in the Yolo Bypass.

The hypotheses of the Bale Chamber pilot study were:

1. The Bale Chamber produces accurate erosion rate data that is comparable to the Gust Chamber;

2. At higher velocities, the majority of MeHg and THg flux is from the particulate phase, not the dissolved phase;

3. In Bale Chamber experiments 4 hours is enough time to obtain measureable concentrations of dissolved phases of MeHg and THg and 20 minutes is enough time to obtain measureable concentrations in particulate phases of MeHg.

6.2. Methods

Erosion threshold measurements were made using a mini-annular flume apparatus described in Bale and others, 2006. According to Bale, the design of the flume was based on a number of well-defined and calibrated laboratory flumes (Fukada and Lick, 1980; Amos and others, 1992; Widdows and others, 1998) but scaled so that the device was sufficiently small to be portable and used either in the laboratory or in the field.

The chamber was constructed with a 200 mm (o.d.) and 180 mm high acrylic tube (3mm wall thickness) that was inserted 70 mm into the sediment inside of a larger 254 mm diameter core tube, so that a 101 mm depth of water could be retained above the sediment. The lower edge of the chamber/core tube was beveled to aid insertion in the sediment and the upper edge was cemented to an acrylic plate. To form the annular flume track, a short length of acrylic rod (50 mm o.d., 70 mm long) was cemented to the center of the rotor plate. The lower end of the rod was pushed down to the surface of the mud when operating. The resultant annular track was 70 mm wide and 101 mm deep. (Figure 1).

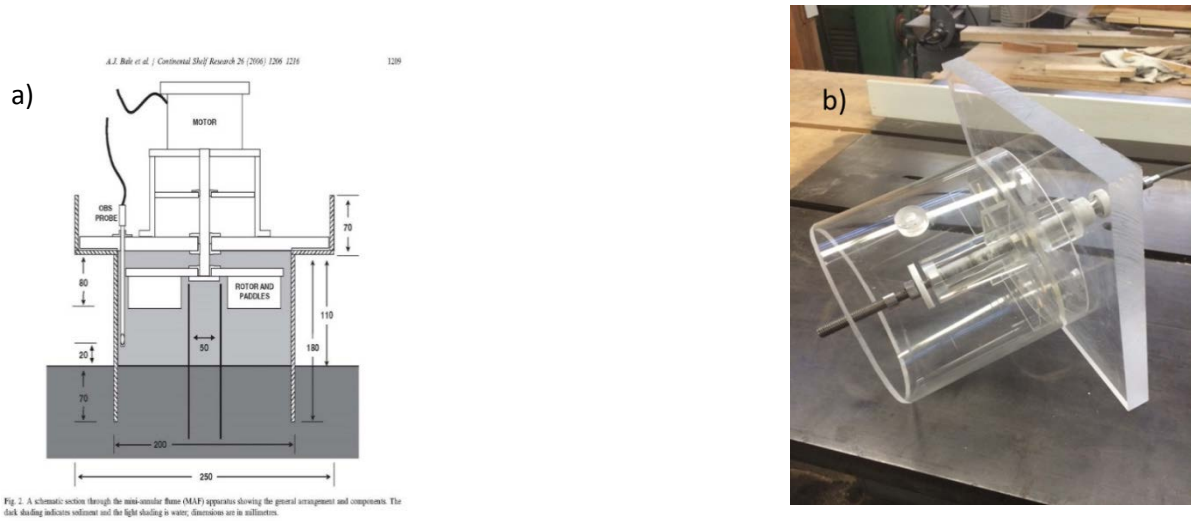

Figure 6-1. a) Diagram of Bale Chamber from Bale and others, 2006. b) Partially fabricated Bale Chamber.

A variable speed motor was attached to a plate above the chamber and connected to the rotor within the chamber with a flexible shaft. The rotor was 165 mm in diameter and carried four, 52 mm x 20 mm paddles. The drive speed of the rotor and paddles could be adjusted continuously from 0.5 to a maximum linear velocity of 3 ft/sec. The footprint of the chamber was 0.0264 m^2. The volume of water contained within the annular track was 2.9 L. The linear water velocity within the chamber was estimated by placing a neutral density particle in the chamber and measuring the revolutions per minute of the rotor and particle. The neutral particle traveled near the outside of the chamber about 7 inches from the center and traveled at 70% of the speed of the rotor at the outside diameter (8 inches) of the chamber. The speed of the water in the chamber was estimated at 70% of the speed of the rotor from the results of the neutral particle experiment. Water velocities, however, varied across the chamber. For example at a 20 RPM rotor speed, the water velocity was 0.15 ft/sec at 2 inches from the center and 0.5 ft/sec at 7 inches from the center. Because of these differences, Bale Chamber values required calibration against the Gust Chamber under the same land-uses and velocities.

Two sediment cores (10 inch diameter) from two different land uses were collected in the Yolo Wildlife area (Figure 2a). Samples were collected from a wild rice field (WR) on 3/11/15 and from an un-disked seasonal wetland (UDSW) on 3/23/15. Samples collected from the WR field had approximately 4-6 inches of standing water on the site since approximately October of the previous year (Figure 2b). On the UDSW, standing water had also been present since approximately October 2014, however the depth of the water was between 18-24 inches. Following sample collection, the 10 inch cores were transported back to the laboratory on ice.

Figure 6-2. a) Location of sample sites. b) Wild rice sediment.

At the laboratory the cores were kept at 14°C before and during the flux experiments. One core was used for particulate experiments and one for diffusional experiments. The diffusional experiment was conducted the day after sample collection. Particulate experiments were conducted two days after sample collection. The overlying water used for both experiments was collected from the Sacramento River at Discovery Park and was filtered through a 0.45 µm filter. As defined by Bale and others, 2006, the relationship between current velocity and bed shear stress is defined as:

$$T_0 = 2.6038U^3 + 0.5562U^2 + 0.1759U + 0.008.$$

Where T_0 is bed shear stress (Pa) and U is current velocity in units of m/sec.

The primary objective of the particulate experiment, was to estimate the flux of TSS, particulate Hg (pHg) and particulate methyl mercury (pMeHg) over periods of 20 minutes at each water velocity. The chamber was operated at 5 different velocities (0.5, 1.0, 1.5, 2.0 and 3.0 ft/sec.). Water in the chamber was sampled at times 0, 10 and 20 minutes at each velocity. In the particulate study a limited number of water samples were also collected to estimate diffusional flux by analyzing the samples for dissolved MeHg (dMeHg) and dissolved Hg (dHg).

The first objective of the diffusional experiment was to estimate the sediment to water flux of dissolved Hg and dissolved MeHg mercury over periods of 4 hours at 3 velocities (0.5, 1.0 and 2.5 ft/sec). The dissolved fraction was defined as the amount passing through a 0.45 µm filter. The second objective of this experiment was to determine the erosion rate of TSS at each velocity. Water in the chamber was sampled at times 0, 1, 2, 3, and 4 hours at each velocity. In previous experiments, with flux chambers under low water velocities, it was determined that 4 hours was enough time to ensure there would be a measureable signal of dMeHg from the sediment to the water (Choe and others 2004).

For the analysis of filtered and particulate mercury species, 40 mL of sample were collected at each collection time. For TSS, between 4 and 40 mLs of sample were collected at each collection time. To maintain the same volume of water in the chamber throughout the experiment, an equal volume of filtered water from the Sacramento River was used to replace water that had been collected for analyses. Sample concentrations were corrected for the amount of water added to the flux chamber to equal that extracted from the flux chamber. Over the course of the particulate and dissolved experiments, approximately 37% and 31%, respectively, of the water extracted for analysis was replaced with filtered Sacramento River water.

6.3. Results

Over the course of the first experiment, (WR, diffusional), it was determined that the water sampling port was located at the sediment-water interface. This location could potentially result in a bias towards high TSS results. Therefore, the following day, at the start of the particulate WR experiment, the port was raised 0.25" above the sediment-water interface to try to avoid a high TSS sampling bias. During UDSW testing, the port was again adjusted so that it was an inch above the sediment. As these experiments progressed, these changes in the location of the sampling port should be considered when evaluating results. Details on quality control results are provided in Chapter 7, Table 7-2. Quality control samples were only analyzed for the water matrix.

6.3.1. Particulate Experiment--Concentration Data

6.3.1.1. TSS and MeHg

Concentrations of TSS and pMeHg increased as velocity increased (Table 1 and Figures 3, and 4, TSS and pMeHg, respectively). Regardless of the land use, TSS concentrations increased dramatically above 1 ft/sec. TSS concentrations ranged from 144 to 36,804 mg/L in WR and from 32 to 81,224 mg/L in the UDSW (Table1). There was a strong linear relationship between pMeHg concentrations and TSS (r^2=0.972) (Figure 5). With one exception, 80-99% of the MeHg was associated with particles (Table1). These results suggested that under high velocity conditions, such as those associated with large flood events, MeHg was primarily associated with particulates and erosion. Because of the strong relationship between TSS and pMeHg, TSS (and potentially turbidity) may be a less expensive proxy for modeling MeHg transport in the Yolo Bypass, with the caveat that the ratio of MeHg to TSS may vary depending on the season, site, and other factors that affect MeHg production.

While there was a strong relationship between velocity, TSS, and pMeHg, WR and UDSW MeHg concentrations per particle decreased (Figure 6) while filtered concentrations roughly doubled (Figures 7 c & d). As a result, the apparent partitioning "Kd" between solids and the filtered phase decreased at higher velocities (Table 1, Figure 7, e & f). Kd is defined as the ratio of the concentration on the particles (dry weight basis) to the concentration in water of the dissolved phase. These results could occur if higher velocities re suspended large inorganic particles, with lower MeHg concentrations, resulting in an average decrease in MeHg per particle. This explanation was supported by visual inspection of the suspended sediment samples. At higher velocities, some sand was observed in the suspended sediment samples. Similarly, these same results could also occur if the top few mm of sediment were higher in MeHg than the sediment below. Under this scenario, the top few mm would be resuspended first, while deeper

sediments, with potentially lower MeHg concentrations, would become suspended later, resulting in a decrease in the average concentration on the particles over time. This phenomenon may also have occurred in our experiments. In our experiments, only the first 0.3 mm of material was suspended in the first few velocity steps. Conceivably, this top layer of sediment could be comprised of benthic algae, fecal pellets or vegetative detritus as well as sediment. This biogenic material could conceivably have higher MeHg concentrations than the sediment below it. Finally, increases in filtered MeHg could occur either due to very rapid desorption from re suspended particles into the water column, or due to increased diffusion from sediments at higher velocities.

At lower velocities, MeHg diffusional fluxes became important in the UDSW, but not WR. As shown in Table 1, at t=0 and a velocity of 0.7 ft/sec., UDSW MeHg concentrations were distributed roughly equally between the filtered and particulate fractions. This was not the case for WR where approximately 80% of the MeHg was associated with the particulate fraction.

6.3.1.2. Hg

Like pMeHg, particulate mercury (pHg) increased with velocity (Table 2, Figure 8). Similarly, there was a strong relationship between pHg and TSS (Figures 9 and 10), however unlike MeHg, essentially all of the Hg at t=0 was associated with the particles regardless of land use (96% and 77% for WR and UDSW, respectively). This suggested that there was little diffusional flux of THg at either low or high floodwater velocities.

6.3.2. Diffusion Experiment--Concentration Data

6.3.2.1. TSS and MeHg

Diffusion experiments were designed to quantify dissolved fluxes of MeHg and Hg under different velocities over longer time periods (12 hrs.). Previous experiments with intact cores and in situ benthic flux chambers suggested that diffusion could be a fairly slow process (Choe and others, 2004).

Diffusional flux rates varied between the two land uses. As shown in Table 3 and Figure 11, diffusional flux of dMeHg from UDSW sediments increased over the 12 hour duration of the experiment while this was not the case for the WR site. In the WR field, dissolved MeHg concentrations appeared consistent regardless of time or velocity.

The flux of dMeHg from these experiments was comparable to the dMeHg flux from the pore water experiments (see Chapter 7) which were conducted in cores with no stirring. This

suggested that water velocity either did not greatly affect dMeHg flux or that dMeHg rapidly partitioned onto particles.

Like the particulate experiment, TSS concentrations also increased over time (Figures 3 and 12), however, unlike the particulate experiments, the greatest increases in TSS were associated with WR.

6.3.2.2. Hg

Dissolved Hg flux rates approximately doubled with velocity (Table 4). These results were similar to dMeHg and dHg results from the particulate experiment (Tables 1 and 2). Linear increases of the dissolved phase contrasted with the exponential increases of the particulate phases for Hg and MeHg (see particulate experiment, Table 2).

6.3.3. Erosion Rates

In both the particulate and diffusion experiments, erosion rates of TSS and flux of pMeHg increased with velocity (Tables 1-4). Between 0.5 and 1.5 ft/sec., Bale Chamber erosion yields of TSS were 3.4 to 11.6 times higher than erosion yields obtained using the Gust Chamber (Table 5). The higher erosion yields observed in the Bale Chamber could be due to (1) the sampling port being too low in the Bale Chamber, (2) Unlike the Gust Chamber, the Bale Chamber does not use a flow through design, (3) the use of different methods to determine erosion rates in the Bale and Gust Chambers, (4) the larger surface area sampled in the Bale Chamber, or (5) the uneven surface area of the sediment within the Bale Chamber cores.

6.4. Discussion

One of the main goals of this pilot experiment was to determine if the Bale Chamber could provide erosion and mercury data for different land uses. At high velocities, Bale Chamber comparisons to Gust Chamber erosion results and real-world estimates of erosion provided strong evidence that the Bale Chamber could not be used directly to estimate erosion values. However, at velocities < 1ft/sec, Bale Chamber and Gust Chamber values only differed by a factor of 3.4. This suggests that the Bale Chamber could still provide useful information. One possibility is to use the Bale Chamber to provide erosional information in situations that are not well suited for Gust Chamber work (for example vegetated plots).

The Bale Chamber results supported our hypothesis that under high velocity floodwaters, increases in MeHg production are due to particulate erosion and not an enhancement to diffusional flux. At water velocities > .7 ft/sec., MeHg particulate flux rates were much greater than diffusional fluxes. These results appeared consistent with Toe Drain Inlet/Outlet field results. As explained in Chapter 4, rough calculations suggested that the most likely

explanation behind increasing particulate and dissolved water column MeHg concentrations was potentially from particle-based fluxes, however this would require verification.

At velocities below 1 ft/sec., particle based loads from sediments still exceeded dissolved fluxes, but the two pathways were comparable in terms of order of magnitude. Diffusional flux was an important but minor factor for UDSW samples but did not appear as important in WR Bale Chamber studies. Bale Chamber results for the UDSW land use were also consistent with pore water results (see Chapter 6) which also found that the WR site did not produce significant flux of MeHg. These results suggested that diffusional flux may play a larger role for some land uses during flood events where water velocities slow and/or water becomes pooled for long periods of time over parts of the Yolo Bypass (Yolo Wildlife Area Manager, personnel communication). This situation can occur under both mini-flood events and following a major flooding event. The increases in filtered MeHg in most treatments could occur due to diffusion, desorption from re suspended solids, or the resuspension of fine material that passes through a 0.45 micron filter.

Observed decreases in solid phase concentrations of MeHg and Hg over time could be due to different types of particles being re suspended at different velocities. At lower velocities, potentially finer grained, or biogenic material (such as diatoms or detritus), with higher Hg concentrations, would be re suspended first. At higher velocities, larger particles, (such as sand), with lower concentrations of mercury would become re-suspended. The overall result would be a lower Hg concentration per particle.

These experiments provided preliminary data to help design experiments for the upcoming year and highlighted areas that require further investigation. There are 4 issues with the Bale Chamber that need to be addressed:

1. Erosion rates are about 3-11 times higher from the Bale Chamber than the Gust Chamber at velocities of 0.5 to 1.5 ft/sec. This could be due to the sampling port being too low in the Bale Chamber, the chamber being circular instead of straight (velocities vary from the inner to the outer diameter of the chamber in a circular chamber), the methods for determining erosion rates being different, the larger surface area sampled, and the presence of several small mounds and depressions in the Bale Chamber cores which could change erosion and velocity characteristics.

2. The second issue is the Bale Chamber may not work well at higher velocities. The Bale Chamber is a circular flume and circular flumes are not usually used for determining erosion rates at high velocities (Schoellhamer, personal communication). The circular nature of the chamber may have caused the order of magnitude increases in erosion

rates at velocities of 2.0 ft/sec and higher. Therefore the results at velocities of 1.5 or greater should be considered qualitative.

3. The third issue is that the erosion rates were dependent on the length of experiment. For example, using UDSW data, which potentially had the least sampling bias of the two land uses (see methods), the erosion rates of TSS at 2.5 ft/sec. were 2.12 and 42.5 $g/m^2/min$ in the diffusional and particulate studies, respectively. These differences were large even though the TSS values differed by less than a factor of two. The ten-fold increase in erosion rates between the two experiments differ because the increase in TSS per m^2 is divided by time. In the diffusional experiment this is 12 hours, while in the particulate experiment the time is 1.6 hours. Another explanation for these results could be that the 20 minute experiment reflects an initial pulse of erosion that is not sustained over a longer, 4 hour, time period basis. Because of the dependence on time the erosion rates can differ considerably depending on the length of the experiment.

4. The fourth issue is that the Bale Chamber may be unable to resolve partitioning from pMeHg to dMeHg because of the extraordinarily high TSS concentrations in the chamber. For example, at the highest velocities tested, concentrations of TSS in the chamber at times were > 10,000 mg/L. In contrast, the typical concentrations in the field is < 300 mg/L.

The solution to these 4 issues are:

1. Rely on Gust Chamber for quantitative erosion rates and use the Bale Chamber to provide relative erosion and flux rates in situations where the Gust Chamber cannot be used (for example vegetated soils). Since a particular land use type may contain both vegetated and non-vegetated soils, the Gust Chamber erosion coefficient measured from a non-vegetated land use sample would be adjusted based on the relative erosion changes measured by the Bale Chamber from a vegetated and non-vegetated identical land-use.

2. Operate the Bale Chamber at lower velocities < 2 ft/sec.

6.5. Summary

1. The working hypothesis that the Bale Chamber produces accurate erosion rate data comparable to the Gust Chamber was rejected. The Bale Chamber overestimates erosion by a factor of 3-11. However, we believe that the Bale Chamber can be used to expand the range of the Gust Chamber by using it to provide a scaling factor for erosion rates measured by the Gust Chamber. The ratios of erosion rates for un-vegetated sites

to several types of vegetated substrates can be determined with the Bale Chamber and this ratio can be used to scale down the Gust Chamber results to determine accurate erosion rates for vegetated sites.

2. The working hypothesis that that at higher velocities, the majority of MeHg and THg flux is from the particulate phase, not the dissolved phase was supported. In all but one case, 90-95% of the MeHg was on particles. Future studies should focus on particulate phases of MeHg.

3. The working hypothesis that in Bale Chamber experiments 4 hours is enough time to obtain measureable concentrations of dissolved phases of MeHg and THg and 20 minutes is enough time to obtain measureable concentrations in particulate phases of MeHg was supported. Measurable concentrations were found in every experiment.

6.6. Next Steps

Several findings from this pilot study will contribute to next year's experimental design. The most important things learned were: 1) particulate erosion is much greater than diffusional erosion at higher water velocities, 2) erosion rates are dependent on length of experiment, 3) the Bale Chamber should be used at water velocities <1.5 ft/sec., 4) the sampling port on the Bale Chamber is probably too low, and 5) there are higher erosion rates in the Bale Chamber than the Gust Chambers. The Gust Chamber is more reliable for determining accurate erosion rates because of constant velocities within the chamber. Given these findings the following steps are proposed:

1. Rely on Gust Chamber for accurate erosion rates, and Bale Chamber results for relative erosion rates among vegetation types and MeHg concentration data on suspended particles. Even though the Bale Chamber does not produce accurate erosion rates it has utility in this study. The Bale Chamber is necessary because it has three attributes the Gust Chamber does not have; 1) it was designed to be mercury free, 2) the Bale Chamber has more volume which is necessary if multiple Hg and MeHg samples are withdrawn, and the Bale Chamber can be used on vegetated substrates.

2. Conduct a study to estimate relative erosion rates among land use types using the Bale Chamber. Sample at least 3 replicates per land use. Some land uses may require more replicates because of vegetation, crop type, soil preparation, and soil type. Conduct a study to determine erosion rates with differing vegetation types. Determine the ratios of erosion rates for un-vegetated sites to several types of vegetated substrates and use

this ratio to scale down the Gust Chamber results to determine accurate erosion rates for vegetated sites.

3. The diffusional studies using the Bale Chamber should be eliminated as the diffusional flux of MeHg is much less than the particulate flux of MeHg at high velocities. The flux at low velocities can be estimated using the static diffusional core methodology described in Chapter 7.

6.7. Literature Cited

Amos, C.L., Grant, J., Daborn, G.R., Black, K., 1992. Seacarousel—a benthic, annular flume. Estuarine, Coastal and Shelf Science 34, 557–577.

Bale, A.J. , J. Widdows, C.B. Harris, and J.A. Stephens. 2006. Measurements of the critical erosion threshold of surface sediments along the Tamar Estuary using a mini-annular flume. Continental Shelf Research 26 (2006) 1206–1216.

Choe KY, Gill GA, Lehman RD, Han S, Heim WA, Coale KH. 2004. Sediment-water exchange of total mercury and monomethyl mercury in the San Francisco Bay-Delta. Limnol. Oceanogr. 2004; 49: 1512-1527.

Foe, C., S. Louie, and D. Bosworth. 2008. Task 2. Methyl mercury Concentrations and Loads in the Central Valley and Freshwater Delta. https://mercury.mlml.calstate.edu/wp-content/uploads/2008/10/04_task2mmhg_final.pdf

Fukada, M.K., Lick, W., 1980. The entrainment of cohesive sediment in freshwater. Journal of Geophysical Research 85, 2813–2824.

Widdows, J., Brinsley, M.D., Bowley, N., Barrett, C., 1998. A benthic annular flume for in situ measurement of suspension feeding/biodeposition rates and erosion potential of intertidal cohesive sediments. Estuarine, Coastal and Shelf Science 46, 27–38.

Table 6-1. Bale Chamber Particulate Study. MeHg concentration vs. velocity for cores collected from Wild Rice and Un-disked Seasonal Wetland Soils. Kd = 1000 * dry weight pMeHg concentration (ng/g)/dMeHg (ng/L).

Land Use	Velocity	Time	dMeHg	pMeHg	TSS	Fraction associated with particles	pMeHg (dry)	Kd	log10 (Kd)
	ft/s	min	ng/L	ng/L	mg/L	fraction	ng/g	L/Kg	L/Kg
Wild Rice	0.5	0	0.15	0.58	169	0.795	3.4	22880	4.4
	0.5	10		0.6	144		4.2		
	0.5	20	0.14	0.62	175	0.816	3.5	25306	4.4
	1	0		1.07	363		2.9		
	1	10		0.97	341		2.8		
	1	20	0.15	1.11	345	0.881	3.2	21449	4.3
	1.5	0		3.6	1573		2.3		
	1.5	10		4.37	1674		2.6		
	1.5	20	0.18	6.65	2140	0.974	3.1	17264	4.2
	2.5	0		9.87	4557		2.2		
	2.5	10		35.14	12252		2.9		
	2.5	20	0.24	36.37	17727	0.993	2.1	8549	3.9
	3	0		45.05	17794		2.5		
	3	10		73.02	23706		3.1		
	3	20	0.27	101.79	36804	0.997	2.8	10243	4.0
Un-disked Seasonal Wetland	0.7	0	0.29	0.27	32	0.482	8.4	29095	4.5
	0.7	10		1.62	250		6.5		
	0.7	20		1.82	233		7.8		
	1	0		3.12	442		7.1		
	1	10		2.8	379		7.4		
	1	20	0.22	2.75	392	0.926	7.0	31888	4.5
	1.5	0		13.19	2466		5.3		
	1.5	10		11.73	2025		5.8		
	1.5	20	0.42	14.45	2105	0.972	6.9	16344	4.2
	2.5	0		23.81	6073		3.9		
	2.5	10		56.61	15140		3.7		
	2.5	20	0.44	75.35	24545	0.994	3.1	6977	3.8
	3	0		119.25	36225		3.3		
	3	10		154.81	59020		2.6		
	3	20	0.5	185.07	81224	0.997	2.3	4557	3.7

Table 6-2. Hg and TSS results-Particulate experiments.

Land Use	velocity ft/sec	time min.	dHg ng/L	pHg ng/L	TSS mg/L	Fraction associated with particles
Wild Rice	0.5	0	2.4	62	169	0.96
	0.5	10		85	144	
	0.5	20	1.9	58	175	0.97
	1	0		118	363	
	1	10		108	341	
	1	20	2.2	113	345	0.98
	1.5	0		510	1,573	
	1.5	10		588	1,674	
	1.5	20	3.3	838	2,140	0.99
	2.5	0		1,254	4,557	
	2.5	10		4,548	12,252	
	2.5	20	4.8	7,794	17,727	0.99
	3	0		9,217	17,794	
	3	10		15,158	23,706	
	3	20	7.1	20,294	36,804	0.99
Un-disked Seasonal Wetland	0.5	0	2.4	8	32	0.77
	0.5	10		53	250	
	0.5	20	3.3	62	233	0.94
	1	0		108	442	
	1	10		211	379	
	1	20	2.7	97	392	0.97
	1.5	0		581	2,466	
	1.5	10		545	2,025	
	1.5	20	3.5	520	2,105	0.99
	2.5	0		1,072	6,073	
	2.5	10		5,681	15,140	
	2.5	20	6.0	8,579	245,45	0.99
	3	0		8,967	36,225	
	3	10		9,894	59,020	
	3	20	8.6		81,224	

Table 6-3. MeHg and TSS concentrations--Diffusion experiments.

Land Use	Velocity	Time	dMeHg	TSS
	ft/sec	hours	ng/L	mg/L
Wild Rice	0.5	0	0.20	159
		1	0.16	282
		2	0.18	370
		3	0.19	312
		4	0.20	307
	1.0	0	0.20	1,029
		1	0.28	15,703
		2	0.18	9,621
		3	0.21	14,719
		4	0.18	13,117
	2.5	0	0.20	27,359
		1	0.22	45,633
		2	0.20	106,568
		3	0.17	150,663
		4	0.19	157,964
Un-disked Seasonal Wetland	0.7	0	0.17	421
		1	0.15	162
		2	0.21	83
		3	0.19	51
		4	0.20	54
	1.0	0	0.18	959
		1	0.31	1,629
		2	0.42	3,286
		3	0.31	3,479
		4	0.34	2,915
	2.5	0	0.42	5,043
		1	0.44	6,000
		2	0.46	10,659
		3	0.37	17,930
		4	0.38	18,452

Table 6-4. dHg and TSS data--Diffusion experiments.

Field	velocity ft/sec	Time hour	dHg ng/L	TSS mg/L
Wild Rice	0.5	0	2.2	282
		1	2.2	370
		2	2.3	312
		3	2.6	307
		4	2.8	1,029
	1.0	0	2.8	15,703
		1	19.9	9,621
		2	4.3	14,719
		3	4.8	13,117
		4	4.0	27,359
	2.5	0	4.9	45,633
		1	5.0	106,568
		2	6.1	150,663
		3	4.1	157,964
		4	4.2	421
Un-disked Seasonal Wetland	0.5	0	1.7	421
		1	16.7	162
		2	26.3	83
		3	31.6	51
		4	2.1	54
	1.0	4	2.0	959
		5	2.5	1,629
		6	3.0	3,286
		7	3.1	3,479
		8	2.9	2,915
	2.5	8	3.3	5,043
		9	3.8	6,000
		10	4.6	10,659
		11	5.1	17,930
		12	5.7	18,452

Table 6-5. Comparison of erosion results from Gust and Bale Chambers.

Approximate Velocity (ft/sec)	Critical Shear Stress Pa	Bale Eroded Mass kg/m2	Gust Eroded Mass kg/m2	factor difference
0.5	.08-.09	0.024	0.007	3.4
1	0.18	0.220	0.019	11.6
1.5	.43-.44	0.480	0.068	7.1

(Critical shear stress and Gust Chamber values from Schoellhamer, this report)

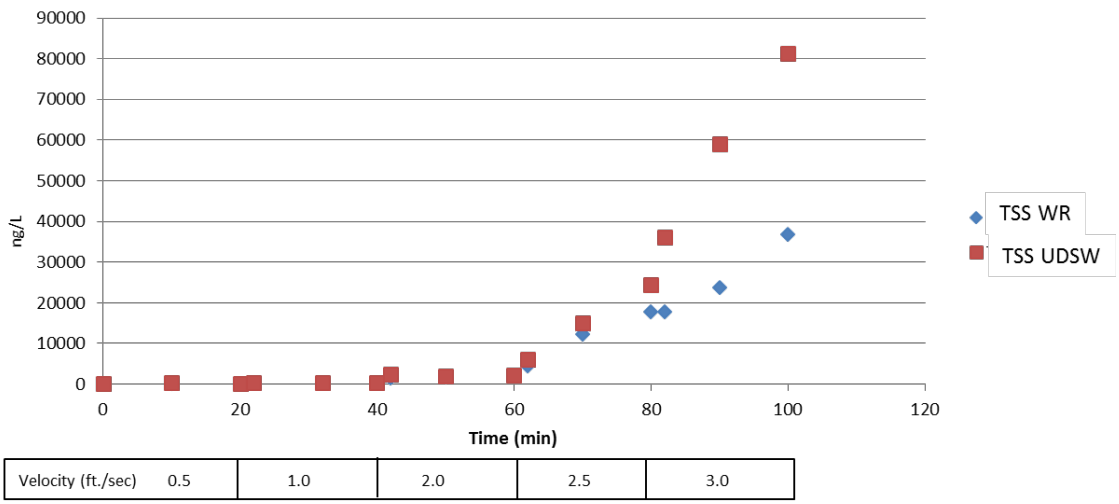

Figure 6-3. Concentrations of TSS in particulate experiment.

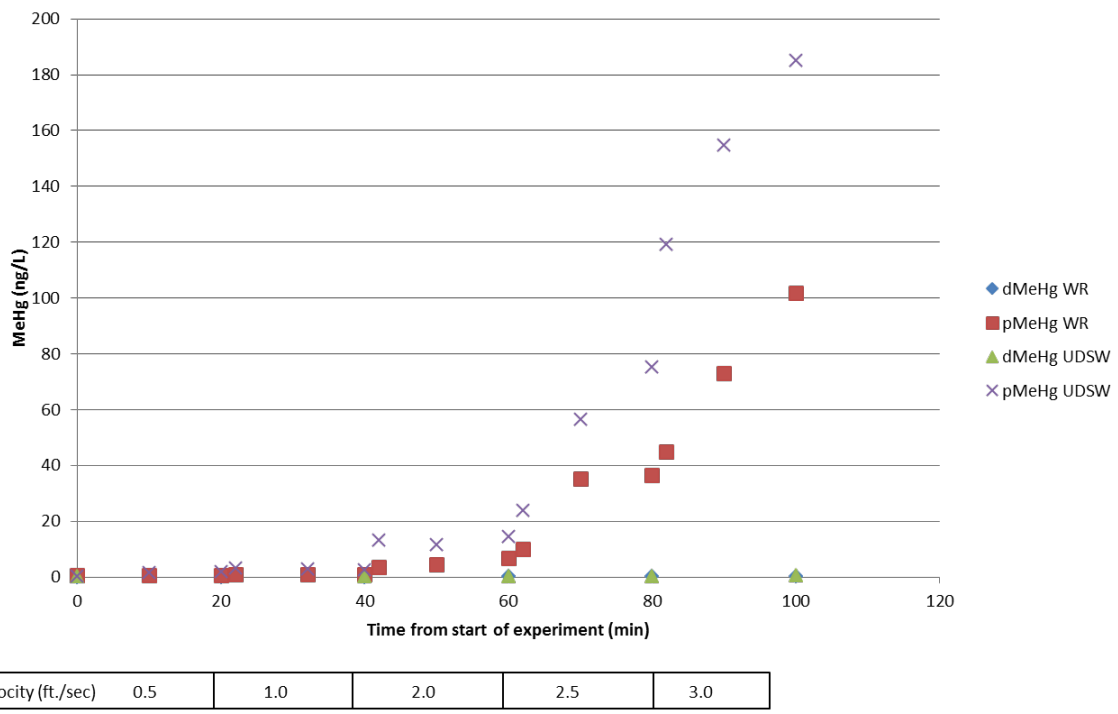

Figure 6-4. Concentrations of pMeHg in particulate experiment.

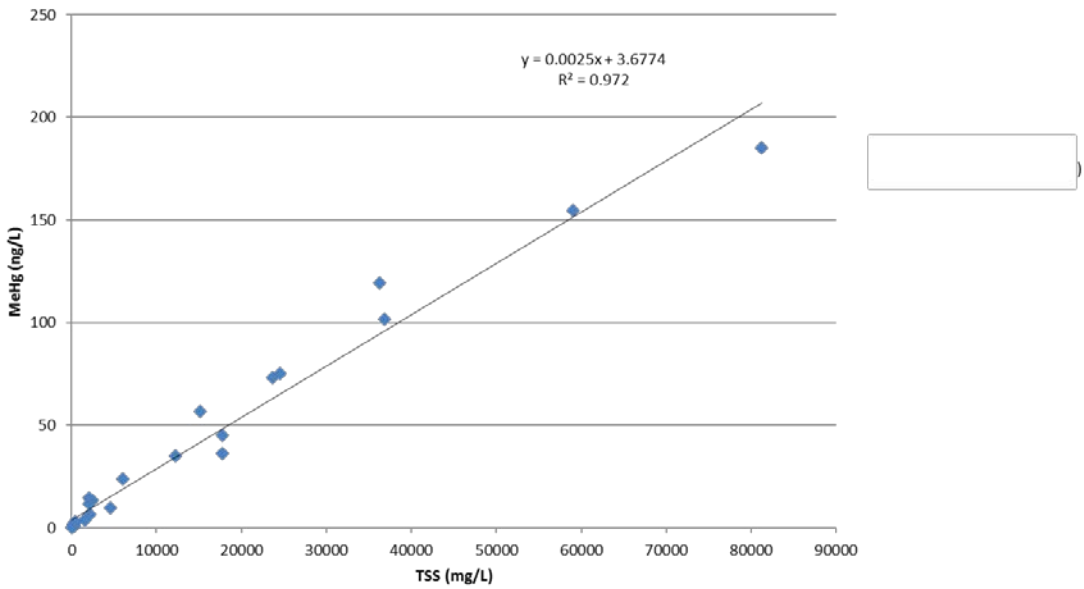

Figure 6-5. TSS vs. pMeHg in particulate experiment.

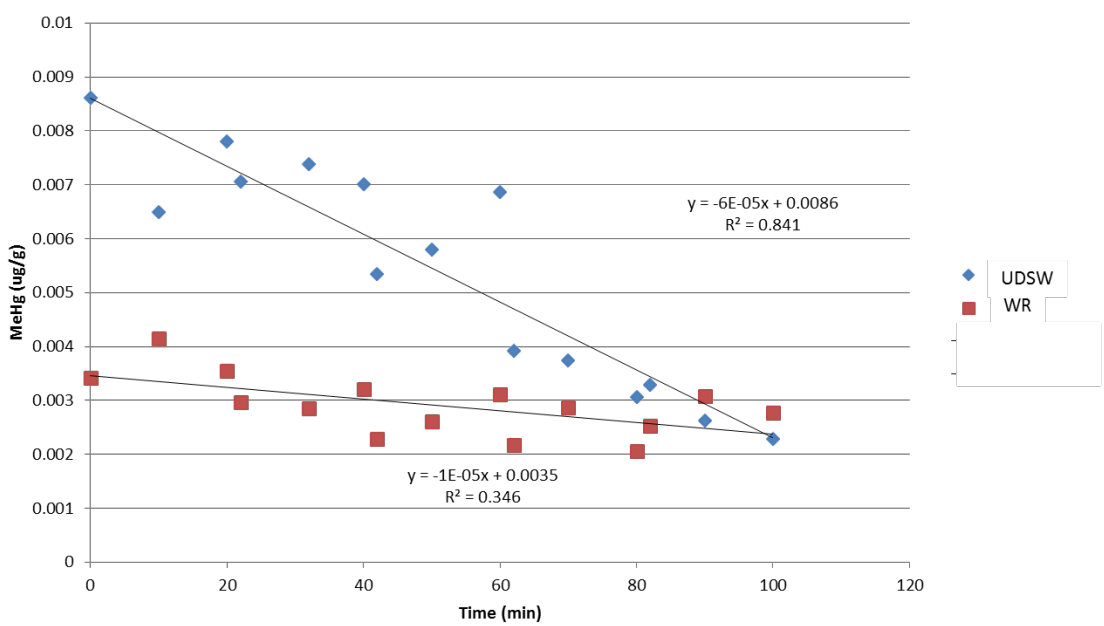

Velocity (ft./sec)	0.5	1.0	2.0	2.5	3.0

Figure 6-6. pMeHg vs. time in particulate experiment.

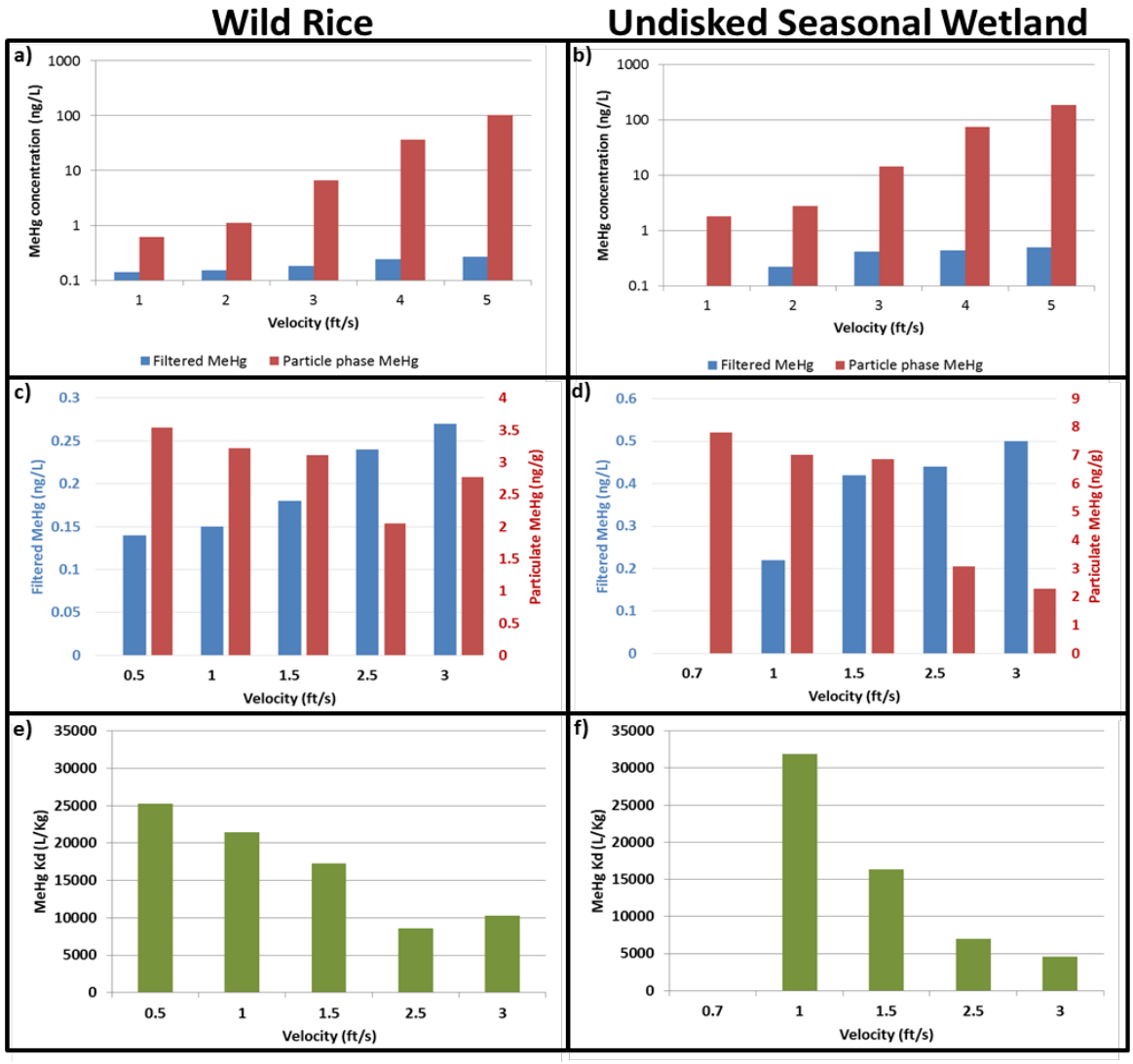

Figure 6-7. Particulate experiment. a) Concentrations of filtered and particulate MeHg in wild rice sample by velocity step. b) Concentrations of filtered and particulate MeHg in an un-disked seasonal wetland sample by velocity step. c) Concentration of filtered and particulate MeHg in wild rice sample vs. velocity. d) Concentration of filtered and particulate MeHg in un-disked seasonal wetland sample vs. velocity. e) Calculated Kd in wild rice sample vs. velocity. f) Calculated Kd in un-disked seasonal wetland sample vs. velocity.

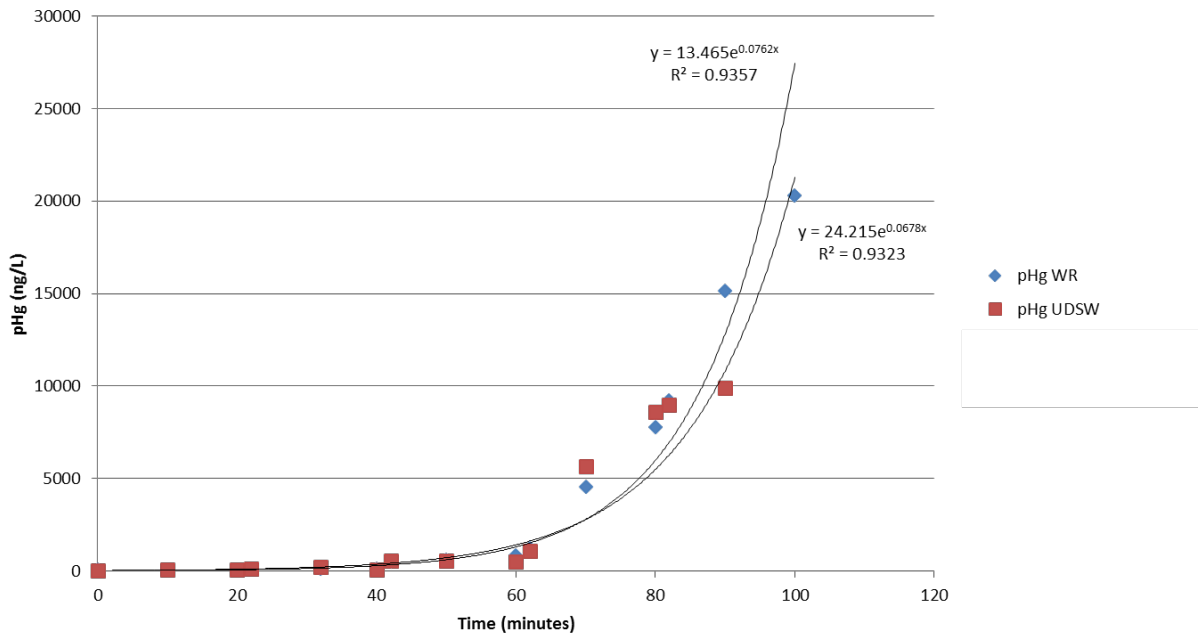

Velocity (ft./sec)	0.5	1.0	2.0	2.5	3.0

Figure 6-8. pHg vs. time for WR and UDSW samples-particulate experiments.

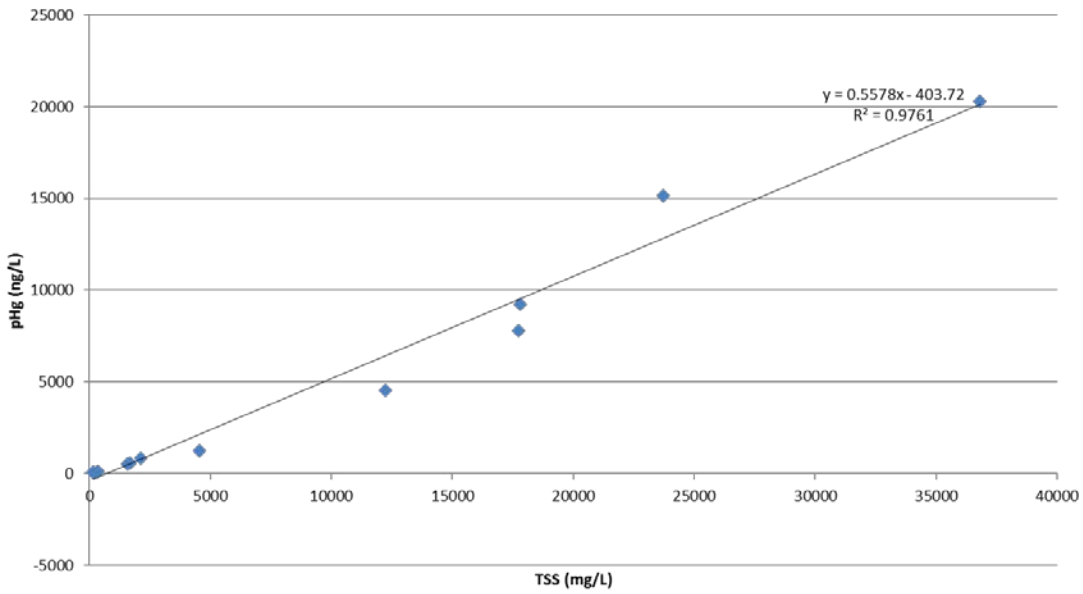

Figure 6-9. TSS vs. pHg from wild rice sample-particulate experiment.

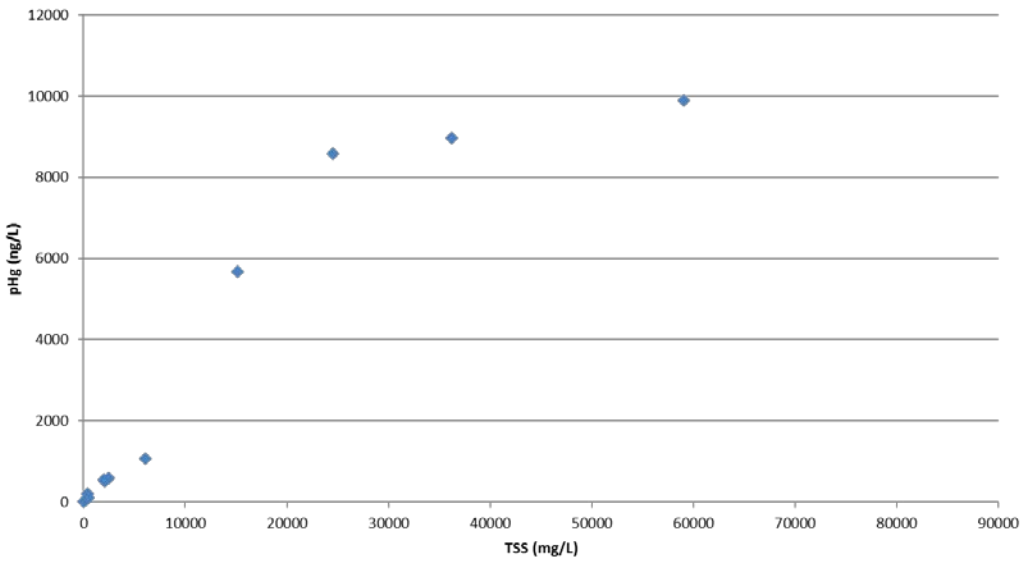

Figure 6-10. TSS vs. pHg from un-disked seasonal wetland sample-particulate experiment.

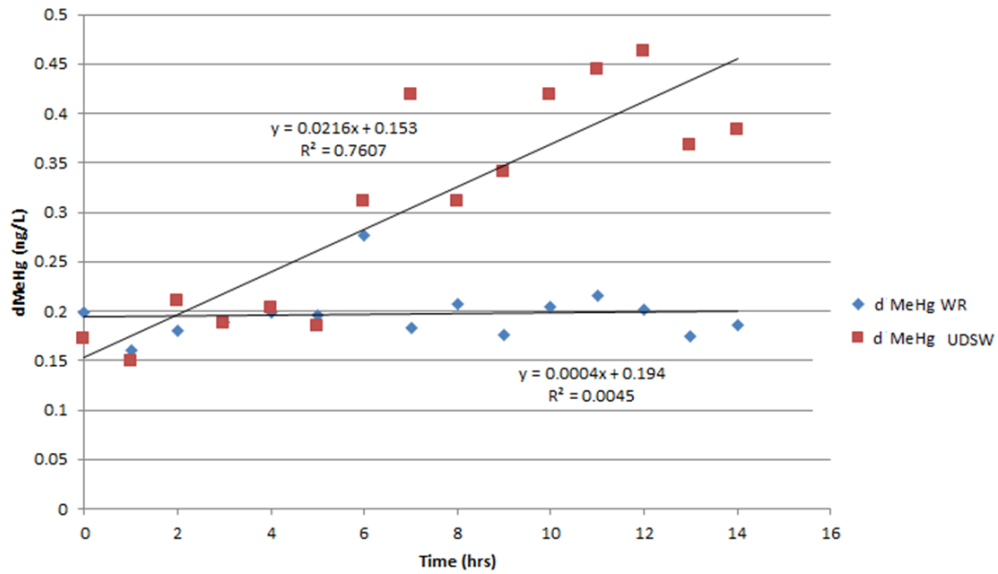

Velocity (ft./sec)	0.5	1.0	2.5

Figure 6-11. Concentrations of dMeHg of WR and UDSW in diffusion experiment.

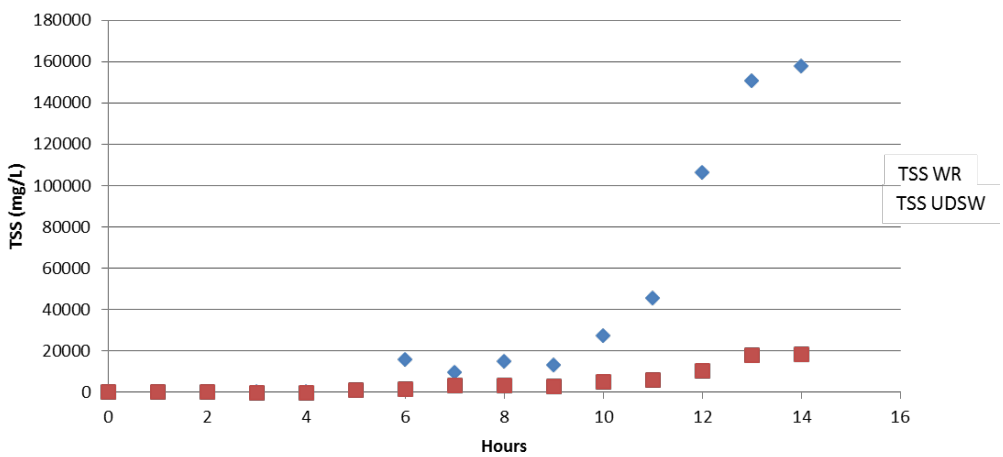

Velocity (ft./sec)	0.5	1.0	2.5

Figure 6-12. Concentrations of TSS in diffusional experiment.

7. Sediment-water Exchange of Total Mercury and Methylmercury in the Yolo Bypass Pilot Study (Pore Water Flux)

Prepared by Wesley Heim and Mark Stephenson, Moss Landing Marine Laboratories

7.1. Introduction

In aquatic ecosystems the primary site of monomethylmercury (MeHg) production is typically within surficial anoxic sediments (Compeau and Bartha 1985; Gilmour and others. 1998). Production of MeHg is generally accepted to be mediated by sulfate-reducing bacteria, hence, there are a number of environmental variables (organic carbon, sulfate, oxygen) and conditions (temperature, porosity, soil type) that could influence the net production of MeHg and its ultimate release into the water column of the Yolo Bypass floodplain (Compeau and Bartha 1985; Gilmour and others, 1998; Heim and others, 2007; Choe and others, 2004; St. Pierre and others, 2014; Kim and others, 2011).

This task is designed to investigate the relationship between major biogeochemical processes in sediments and MeHg production and to measure both advective and diffusive fluxes of mercury and MeHg between sediment and overlying water to assess the significance of sediment-water exchange in comparison to other sources of mercury to Yolo Bypass waters. The design of these experiments was aimed at providing calibration data to the Dynamic Mercury Cycling Model (D-MCM) which will be used to improve our understanding of factors controlling production and transport of Hg and MeHg in the Yolo Bypass.

The four objectives of this study were to: 1) determine if source water had an effect on mercury flux by using high and lower mercury concentration waters in incubations; 2) determine the optimal length of time for incubation experiments; 3) provide rate constants for dissolved MeHg and THg sediment water fluxes at zero velocity on two different land uses; and 4) provide ancillary data that could be used in the D-MCM for predicting MeHg production within the sediments and mercury sediment water exchange flux. Two basic methods were used to determine sediment-water exchange; first a direct assessment using incubated cores and second, modeling the sediment-water exchange from measurements of interstitial pore water concentration gradients. The work was framed by the following working hypotheses: 1) There is no difference in sediment water mercury exchange fluxes using Sacramento River and Cache Creek waters; 2) Mercury sediment water exchange fluxes differs among two different land use types; and 3) Sediment water exchange flux of mercury can be modeled by pore water and

sediment chemistry measurements of MeHg, THg, total organic carbon, and grainsize. *This progress report provides provisional data that are subject to revision.*

7.2. Methods

The field work for this task involved: (1) measurements of mercury and MeHg in interstitial pore waters by separating pore water from sediment of sectioned cores in an oxygen free environment; (2) measurements of high resolution near-surface profiles of pH, oxygen and sulfide in interstitial pore waters using a microelectrode profiler system (Unisense); (3) measurements of solid-phase mercury and MeHg in sediments; and (4) measurements of mercury, MeHg, and ancillary parameters (e.g. ORP, dissolved oxygen, temperature, and conductivity) in incubated cores to determine advective and diffusive fluxes.

Four inch diameter polycarbonate core tubes were used to collect cores from a wild rice field (WR) and an un-disked seasonal wetland (UDSW) field, which was wet but not flooded (Table 7-1, Figure 7-1). A total of 12 cores containing approximately 15 cm of sediment were hand collected from each field and transported on ice to Moss Landing Marine Laboratories (MLML). There was no visual evidence that cores lost their integrity or became stirred. Upon arrival at MLML, cores were transferred to a trace clean climate controlled laboratory and kept at 14°C (average March temperature) overnight until experiments were started the following morning. Experiments were conducted under fluorescent light with no day night cycle and no external ambient light.

The Yolo Bypass receives waters from many sources of varying mercury concentrations. For example, the Sacramento River and Cache Creek both flow into the Yolo Bypass but the former generally has much lower mercury concentrations than the latter. This brings up the question of whether the type of overlying flood water impacts sediment water exchange and biogeochemical conditions in surficial sediments. Ambient waters, with high concentrations of MeHg, could result in a flux from the overlying water into the sediment. Therefore fluxes associated with waters that have high (Cache Creek) or low (Sacramento River) ambient MeHg concentration were used to determine if the amount of MeHg in overlying water makes a difference in fluxes out of the sediment. Ambient unfiltered water from Cache Creek and Sacramento River (Table 7-1) were collected in large carboys and transported back to MLML on ice and in the dark for use as overlying water in the incubated core flux study. Carboys were stored overnight alongside cores. Ambient water was filtered (0.45 µm), using an inline trace metal clean filter cartridge connected to acid cleaned Teflon and Masterflex C-flex tubing, immediately prior to use as core overlying water.

Table 7-1. Sampling Dates and Locations.

Site	Type	Collection Date	Latitude	Longitude
Wild Rice	Sediment Cores	March 11, 2015	38° 32.864'	121° 37.180'
Un-disked Seasonal Wetland	Sediment Cores	March 25, 2015	38° 32.472'	121° 37.237'
Cache Creek	Overlying Water	Mar 11 & 25, 2015	38° 40.707’	121° 40.351’
Sacramento River	Overlying Water	Mar 11 & 25, 2015	38° 36.035’	121° 30.582’

Incubated core flux studies were conducted on March 12, 2015 (WR cores) and March 26, 2015 (UDSW). We adopted methods previously used to determine measured mercury flux in reservoirs with some minor modifications (Kuwabara and others, 2002). Cores were incubated at 14.0 ± 0.7 °C over a 12 h period and sample aliquots were taken at 3 h intervals. To start the experiment six cores had 0.45µm filtered Sacramento River water added (THg: 1.73 ± 0.17 ng/L, MeHg: 0.157 ± 0.49 ng/L) slowly in a way that minimized disturbance of surface sediment and this was repeated for remaining six cores using Cache Creek water (THg: 2.92 ± 0.09 ng/L, MeHg: 0.439 ± 0.027 ng/L). Three cores having each type of source water were designated for mercury sampling. One core with each source water was designated for ancillary measurements using a YSI and readings were taken at same time as mercury sampling. Two cores for each type of source water were designated for micro electrode profiling. Overlying water column heights in cores and volumes of samples drawn from cores were carefully recorded to enable correction of mass flux due to removal of mercury in aliquots over time. In addition, a control of ultra-pure (18 ohm) water in a 4” core was set up adjacent to incubated cores and sampled on same schedule as described previously. All control samples were ≤ 0.015 ng/L MeHg and ≤ 0.28 ng/L THg indicating results were not biased by laboratory conditions.

Figure 7-1. Photo of intact sediment cores collected from a wild rice (WR) field in the Yolo Bypass.

Mercury sample aliquots were taken from cores using 60 mL trace clean syringes (Figure 7-2). Water was stirred manually with a syringe without disturbing the sediment immediately prior to sampling. Samples were filtered in line using 0.45 µm disk filters and transferred to 40 mL trace clean borosilicate vials with Teflon lined lids. Samples were preserved to 0.5 % HCl and kept cool and in the dark prior to analysis. Samples were analyzed first for MeHg using a Tekran 2700 following standard methods (USEPA, 2001). The method detection level (MDL) for MeHg in water was 0.011 ng/L. Remaining sample was then analyzed for total mercury (THg) using standard methods (USEPA, 2002). The MDL for THg in water was 0.200 ng/L.

Figure 7-2. Photo showing aliquots for mercury analysis collected using 60 mL trace clean syringes five times over a 12 hour period.

At termination of incubated core flux study all cores used for mercury sampling were sectioned (0-2 cm) and a centrifuge was used to separate pore water from sediment. Pore water was extracted from sediment, under nitrogen in a glove box, for the determination of MeHg and THg (Figure 7-3). Pore water aliquots were collected using 12 mL trace metal clean syringes and filtering in line with trace metal clean 0.45 µm disk filters. Samples were transferred into 40 mL trace clean borosilicate vials with Teflon lined lids and preservation and analysis for mercury species followed procedures described previously for aqueous samples.

Sediment from sectioned cores were collected in trace metal clean 50 mL centrifuge tubes and kept frozen prior to analysis for MeHg and THg. Sediment was analyzed for THg using a Milestone DMA-80 following standard methods (USEPA, 1998). The MDL for THg in sediment was 4.0 ng g^{-1} dry weight sediment. Sediment was analyzed for MeHg by first extracting with acidic potassium bromine and copper sulfate into methylene chloride and then analysis of aqueous phase using a Tekran 2700 following standard methods (USEPA, 2001). The MDL for MeHg in sediment was 0.005 ng/g dry weight sediment.

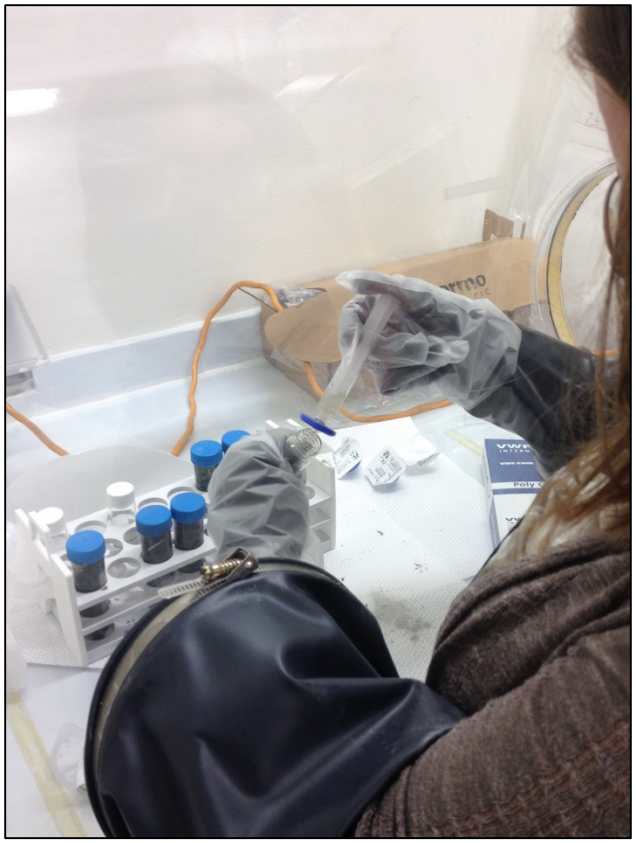

Figure 7-3. Photo of pore water extraction from sectioned cores conducted in glove box under nitrogen.

Micro depth profiles for oxygen, pH, and sulfide in pore water were measured using a Unisense micro profiling system which included a computer controlled motorized manipulator, data logger, and micro sensor capable of sub millimeter resolution (Figure 7-4). Oxygen electrodes were calibrated using two points, oxygen saturated water, and anoxic sediment (Revsbech 1989). Calibration of pH electrodes was done using a three point calibration from pH 7-9 (Revsbech and Jørgensen 1986). A five point calibration from 0 to 100 µM hydrogen sulfide was completed prior to taking sulfide measurements in cores (Jeroschewski and others, 1996).

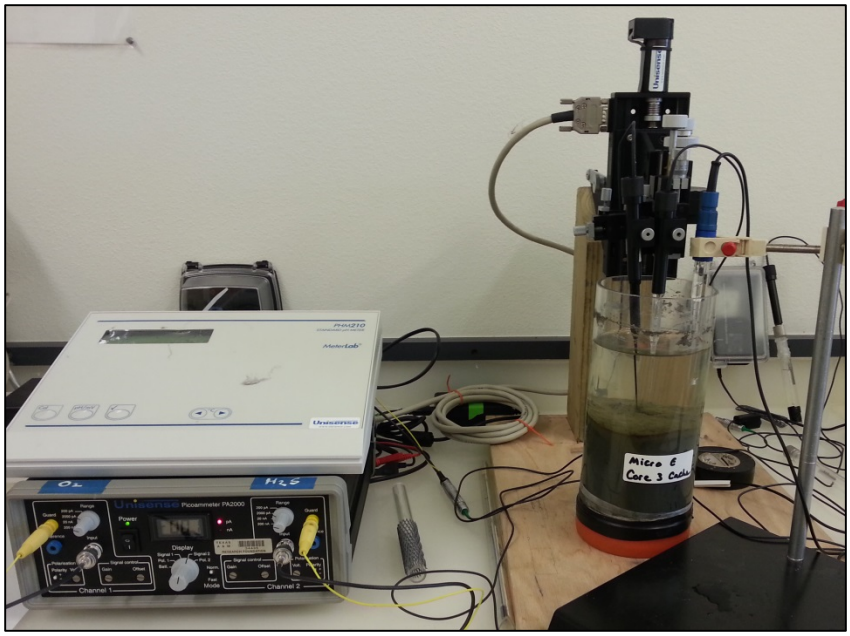

Figure 7-4. Photo of Unisense micro profiling system used for determination of fine scale depth profiles of oxygen, pH, and sulfide in sediment cores.

Sediment-water exchange fluxes (F_M) were directly measured by the time course change of Hg concentration in the incubated cores.

$$F_M = \frac{\Delta C}{\Delta t} \cdot \frac{V}{A}$$

C is the Hg concentration (ng/L), t is the incubation time (day), V is the volume of overlying water (~1 liter), and A is the surface area of the core (7.09×10^{-3} m^2).

Benthic diffusive fluxes (F_D) of mercury species were estimated using the concentration gradient between mercury in the pore water and overlying water column. According to Fick's first law, diffusive flux (F_D) is modified for application to sediments.

$$F_D = -\left(\frac{\varphi D_w}{\Theta^2}\right) \frac{\partial C}{\partial x}$$

Φ is the sediment porosity, Θ is the tortuosity, D_w is the diffusion coefficient of Hg in water without the presence of the sediment matrix, C is the concentration of Hg in pore water, and x is the sediment depth. The value of Θ^2 can be estimated from porosity by the relationship $\Theta^2 = 1 - \ln(\varphi^2)$. Porosity of surface sediments in WR and UDSW averaged 0.46 ± 0.01 (n = 6) and 0.53 ± 0.10 (n = 6) respectively. A value of 5×10^{-6} cm^2 s^{-1} was chosen for D_w for both Hg and MeHg (Li and Gregory 1974; Covelli and others, 1999a; Choe and others, 2004).

7.3. Results and Discussion

7.3.1. Analytical quality assurance and quality control (QA/QC)

For each matrix and analyte, strict QA/QC protocols were followed during analysis. For each batch of twenty samples analyzed three method blanks (MB), one reference material, one analytical duplicate pair, and two method spike duplicate pairs (aqueous MeHg analysis required 4 method spikes) were analyzed with the batch. All QA/QC samples were required to meet the data quality objective (DQO) for the batch to not be reanalyzed. All batches for all analytes and matrixes meet the DQO requirements. Results for QA/QC samples are listed in Table 7-2.

Table 7-2. Results of Analytical Quality Control Samples for THg and MeHg in Sediment and Water.

Analyte	Matrix	MB (n)	Reference Material (id, n)	Analytical Dup RPD (n)	Method Spike (n)	Method Spike Dup RPD (n)
THg	Sed	<MDL (3)	94.9% (NIST 2702, 1)	14.9% (1)	114.5% (2)	9.8% (1)
MeHg	Sed	<MDL (3)	96.8% (ERM CC580, 1)	6.92% (1)	95.4% (2)	2.62% (1)
THg	Water	<MDL (36)	100.2 ± 4.7% (NIST 1641d, 12)	1.6 ± 1.1% (12)	98.2 ± 4.7% (24)	3.3 ± 4.1% (12)
MeHg	Water	<MDL (27)	96.5 ± 3.3% (1 ppm RS, 9)	5.7 ± 3.8% (9)	91.0 ± 4.2% (36)	3.7 ± 2.6% (18)

7.3.2. Incubated core flux study

Ancillary measurements taken during the incubated core flux study are listed in the Appendix Table 7-6. Temperature was kept constant during the experiment. Average temperatures of overlying water in the WR cores were 13.86 ± 0.31 and 14.04 ± 0.34 °C and for the UDSW cores were 13.87 ± 0.97 and 13.98 ± 0.98 °C. Conductivity shows the similarity in Sacramento River water and Cache Creek between the first collection and two weeks later. Average Sacramento water conductivity was 339 ± 7 and 330 ± 25 µS/cm while Cache Creek water was 1304 ± 13 and 1480 ± 27 µS/cm. Cache Creek water conductivity was a factor of ~4 higher than Sacramento River water. Sulfate concentrations were 100 times higher in Cache Creek water (986 µM) relative to Sacramento River water (10 µM). Cache Creek water had a lower pH (7.82 ± 0.23 and 7.62 ± 0.06) relative to Sacramento River water (8.16 ± 0.21 and 8.14 ± 0.12). The measured Oxidation Reduction Potentials (ORP) show oxidizing conditions existed in overlying water of cores from both habitat types (WR and UDSW) as well as both source water types (Sacramento River and Cache Creek) during the entire incubation. Oxygen was monitored to

assure conditions in the core mimicked environmental setting and that flux of redox sensitive mercury species was not biased by creating a suboxic water column as a result of the experimental setup and duration of incubation. Oxygen depletion in overlying water was observed during incubations but concentrations always remained well above suboxic conditions (2 mg L^{-1}). The lowest oxygen concentration observed in WR cores was 7.24 mg L^{-1} (70.5% sat) and had Cache Creek overlying water. The lowest concentration measured in UDSW cores was 6.64 mg L^{-1} (62.5% sat) with Cache Creek water. Given the ability to maintain the stability of the cores longer incubation times should be possible for future experiments. These results support the incubation design and duration was appropriate and laboratory conditions did not adversely bias environmental conditions.

Table 7-3 lists mean F_M results based on triplicate measurements for the incubated core study and Tables 7-7 and 7-8 in the appendix lists raw data used to calculate fluxes. Although results were highly variable, a difference in MeHg flux between the two habitats was observed. UDSW-Sac had a higher MeHg flux than WR-Sac and UDSW-Cache had higher MeHg flux than WR-Cache. Source water did not play a clear role in controlling MeHg fluxes as Cache Creek water resulted in more negative flux (into sediments) in WR cores and more positive flux (into water) in UDSW cores. Similar results for THg were observed with UDSW having a higher flux than WR (Table 7-3). In addition, agreement between replicates was better for THg than MeHg. In WR no clear trend was observed with source water and THg flux, however, UDSW cores with Cache Creek water had factor of 3 higher flux compared to UDSW cores with Sacramento River water. The range of MeHg and THg Fluxes observed in WR and UDSW fields are similar to what has been previously reported for open water and wetlands during late winter and spring in the Sacramento Bay-Delta (Delta) and Yolo Bypass and other studies (Table 7-4).

Table 7-3. Sediment-Water Fluxes (F_M) for MeHg and THg Determined using Incubated Cores Collected from Wild Rice (WR) and Un-disked Seasonal Wetland (UDSW) Fields with Overlying Water from either the Sacramento River (Sac) or Cache Creek (Cache). Negative values Indicate Flux into the Sediment.

	MeHg F_M (ng m^{-2} d^{-1})				**THg F_M (ng m^{-2} d^{-1})**			
Treatment	*Core 1*	*Core 2*	*Core 3*	*Mean ± SD*	*Core 1*	*Core 2*	*Core 3*	*Mean ± SD*
WR - Sac	6	-1	4	3 ± 4	61	27	86	58 ± 30
UDSW - Sac	30	19	29	26 ± 6	135	156	186	159 ± 26
WR- Cache	1	-16	-24	-13 ± 13	51	45	28	41 ± 12
UDSW - Cache	35	5	67	36 ± 31	465	330	615	470 ± 142

Table 7-4. Fluxes of MeHg and THg by Location and Study. Negative Values Indicate Flux into the Sediment.

Location	MeHg (ug m^2 yr^{-1})	THg (ug m^2 yr^{-1})	Reference
Franks Tract marsh (Bay-Delta, Ca)	-3.8	128	(Choe and others, 2004)
Prospect Slough (Yolo Bypass, Ca)	16	380	(Choe and others, 2004)
Baltimore Harbor (Maryland)	0-0.4	-3-17	(Mason and others, 2006)
Gulf of Trieste (Italy/Slovenia)	-105-2,370	8-6,456	(Covelli and othes, 1999a)
Lavaca Bay (Texas)	-330-1,500	-0.9-23	(Gill and others, 1999)

7.3.3. Mercury in sediment and pore water

Figure 7-5 (Table 7-9) illustrates the distribution of MeHg in the 0-2 cm sediment interval of cores from the incubated core flux study. Solid phase MeHg concentrations were between 1.61 ± 0.14 and 4.42 ± 1.17 ng/g dry weight sediment. Variability between replicate cores was greater in cores collected from UDSW than from WR. Concentrations of MeHg were higher in UDSW relative to WR, although for the Sacramento River water treatment the difference was less clear than with the Cache Creek treatment and may be explained by spatial variability. Organic carbon was higher in UDSW (%LOI = 14.4 ± 3.4) relative to WR (%LOI = 8.4 ± 0.6) as well. The role overlying source water plays in controlling solid phase MeHg concentrations was

unclear given the variability between replicates was large in the UDSW Sacramento River treatment.

Mean concentrations of THg in surficial sediment of cores collected from WR and UDSW are shown in Figure 7-6 (Table 7-9). The range of THg measured was 274 ± 13 to 419 ± 86 ng/g and in contrast to what was observed for MeHg UDSW had lower THg concentrations relative to WR. The source of overlying water had no measureable effect on THg sediment concentrations.

The MeHg percentage of THg for surficial sediment is illustrated in Figure 7-7 (Table 7-9). We measured 0.42 ± 0.04 to 1.6 ± 0.5 percent MeHg with UDSW having a greater percentage of MeHg than WR. This was driven by both higher concentrations of MeHg and lower concentrations of THg in UDSW suggesting that UDSW was a more favorable environment for methylation relative to WR.

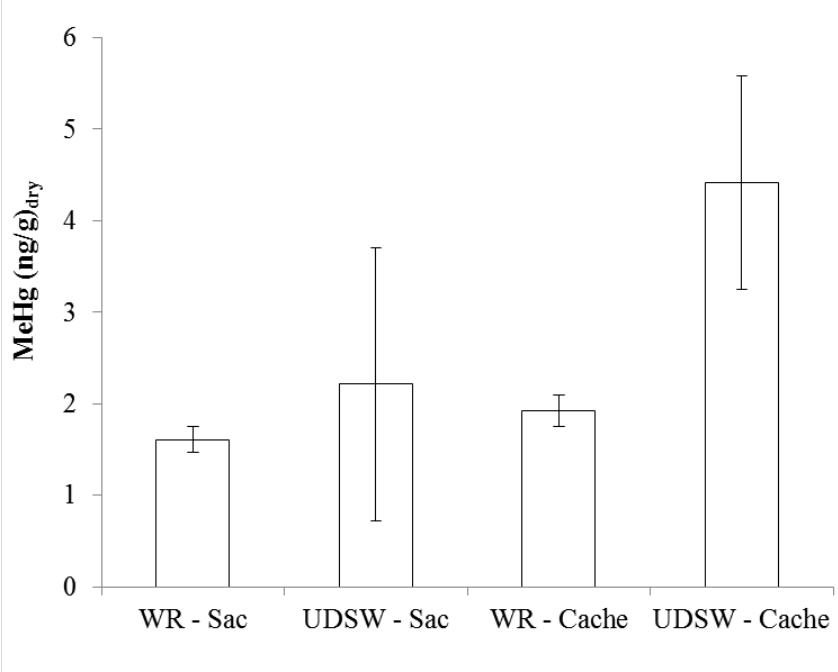

Figure 7-5. Mean surficial (0-2 cm) sediment MeHg concentrations in wild rice (WR) and un-disked seasonal wetland (UDSW) fields having either Sacramento River or Cache Creek overlying water. Error bars are standard deviation of triplicate field replicates.

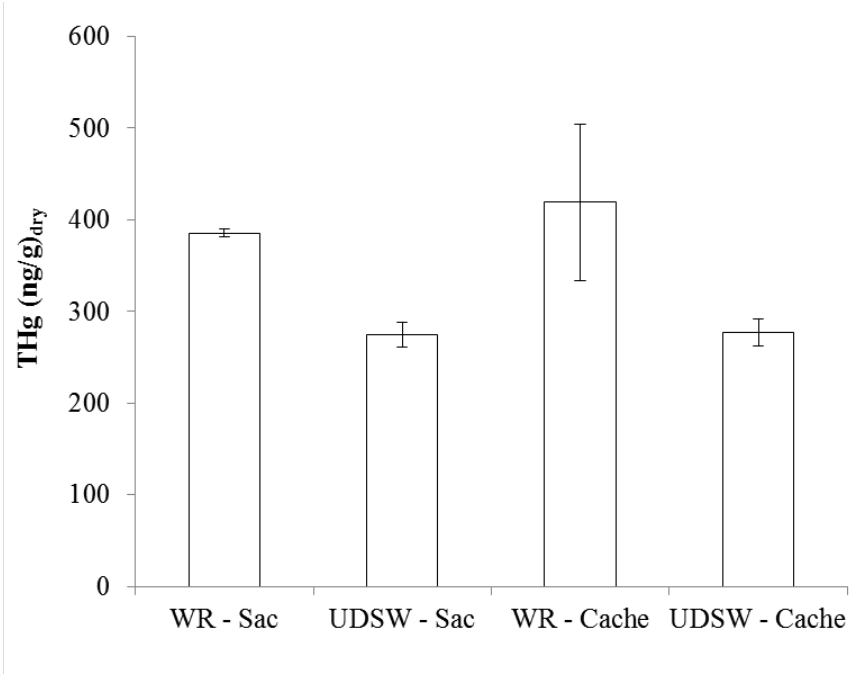

Figure 7-6. Mean surficial (0-2 cm) sediment THg concentrations in wild rice (WR) and un-disked seasonal wetland (UDSW) fields having either Sacramento River or Cache Creek overlying water. Error bars are standard deviation of triplicate field replicates.

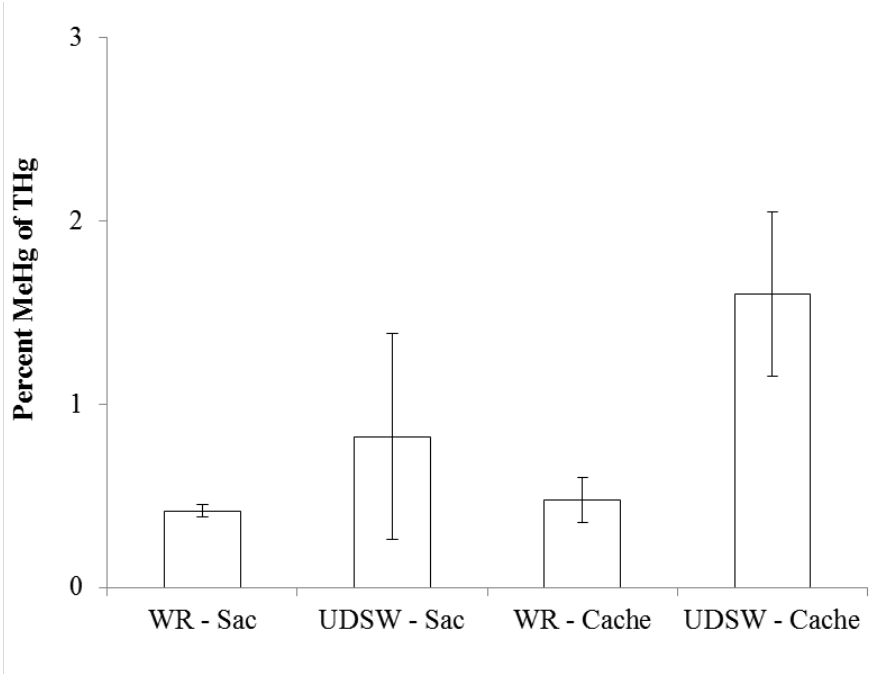

Figure 7-7. Mean MeHg percentage of THg in surficial (0-2 cm) sediment in wild rice (WR) and un-disked seasonal wetland (UDSW) fields having either Sacramento River or Cache Creek overlying water. Error bars are standard deviation of triplicate field replicates.

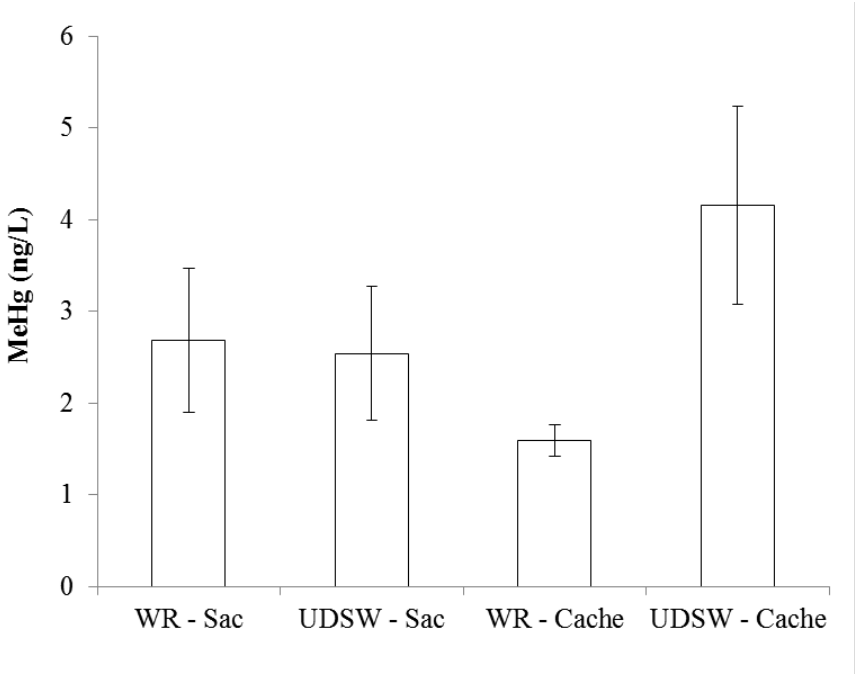

Figure 7-8. Mean Pore water MeHg concentrations in surficial (0-2 cm) sediment of sectioned cores collected from wild rice (WR) and un-disked seasonal wetland (UDSW) fields having either Sacramento River or Cache Creek overlying water. Error bars are standard deviation of triplicate field replicates.

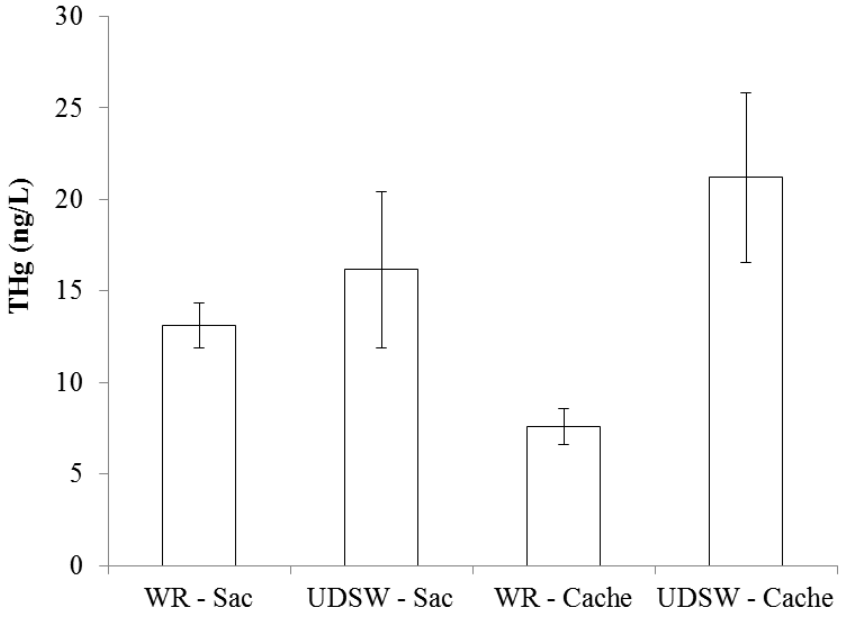

Figure 7-9. Mean Pore water THg concentrations in surficial (0-2 cm) sediment of sectioned cores collected from wild rice (WR) and un-disked seasonal wetland (UDSW) fields having either Sacramento River or Cache Creek overlying water. Error bars are standard deviation of triplicate field replicates.

Pore water concentrations for MeHg in WR and UDSW cores are shown in Figure 7-8 (Table 7-9). Mean pore water concentrations ranged from 1.59 ± 0.17 to 4.16 ± 1.08 ng/L. Traditional log particle-water partition coefficient (K_D) based on MeHg concentrations in pore water and sediment ranged from 2.79 to 3.09 L/Kg with no clear differences between WR and UDSW. Pore water MeHg concentrations in WR and UDSW with Sacramento River water were similar (2.68 ± 0.79 and 2.54 ± 0.73 ng/L respectively). Sacramento River overlying water in WR and UDSW at time of pore water collection was 0.207 ± 0.011 and 0.285 ± 0.057 ng/L or 9-13 times lower than pore water concentrations. Pore water MeHg concentration in UDSW with Cache Creek water was higher than WR with Cache Creek water by a factor of 2.6. Cache Creek overlying water MeHg concentrations in WR was 0.38 ± 0.16 ng/L and in UDSW was 0.68 ± 0.12 ng/L. Pore water MeHg was a factor of 4 higher than overlying water in WR and a factor of 6 higher in UDSW.

Pore water THg concentrations in WR and UDSW cores are shown in Figure 7-9 (Table 7-9). Pore water concentrations of THg ranged from 7.6 ± 1.0 to 21.2 ± 4.6 ng/L with higher concentrations observed in UDSW relative to WR. For THg log K_D ranged from 4.12 to 4.74 L/Kg with higher values found in WR relative to UDSW. A significant positive correlation was observed between MeHg and THg concentrations in pore water ($R^2 = 0.78$). The effect of source water on THg pore water concentrations was dependent on the receiving sediment; Cache creek water resulted in lower pore water THg concentrations in WR while the opposite was observed for UDSW. Pore water THg concentrations were a factor of 6 times higher than overlying Sacramento River water and a factor of 2-4 times higher than Cache Creek water.

7.3.4. Benthic diffusive fluxes

Benthic diffusive fluxes F_D estimated for both THg and MeHg are listed in Table 7-5. Diffusive flux estimates for THg ranged from 2.5 to 33.3 ng m^{-2}/d with higher values observed in UDSW than in WR. For MeHg F_D ranged from 0.6 to 7.2 ng m^{-2}/d and were similar in WR and UDSW with Sacramento River water but higher in UDSW relative to WR with Cache Creek water. Estimates of F_D for both WR and UDSW are similar to reported values from previous studies (Table 7-4).

Table 7-5. Sediment-Water Estimated Diffusive Fluxes (FD) for MeHg and THg Determined using Pore water to Overlying Water Gradients in Cores Collected from Wild Rice (WR) and Un-disked seasonal Wetland (UDSW) Fields with Overlying Source Water from either the Sacramento River (Sac) or Cache Creek (Cache). Negative Values Indicate Flux into the Sediment.

	MeHg F_D (ng m^{-2} d^{-1})				**THg F_D (ng m^{-2} d^{-1})**			
Treatment	*Core 1*	*Core 2*	*Core 3*	*Mean ± SD*	*Core 1*	*Core 2*	*Core 3*	*Mean ± SD*
WR - Sac	2.5	1.9	1.4	1.9 ± 0.6	9.1	8.6	7.6	8.4 ± 0.8
UDSW - Sac	0.8	2.2	3.0	2.0 ± 1.1	5.0	10.2	22.2	12.4 ± 8.9
WR- Cache	1.1	0.6	1.0	0.9 ± 0.3	4.0	2.5	3.9	3.5 ± 0.8
UDSW - Cache	7.2	3.5	2.8	4.5 ± 2.4	33.3	13.5	16.1	21.0 ± 10.7

7.3.5. Micro depth profiles

Vertical distributions of dissolved oxygen and hydrogen sulfide (H_2S) at WR and UDSW obtained with the profiling microelectrode system are shown in Figures 7-10 and 7-00. Measurements of pH using a microelectrode were also conducted for chemical equilibrium modeling of sulfide speciation (bisulfide (HS^-) and total sulfide (Stot)). Note that the depth scale for the oxygen profiles is in millimeters while the H_2S profiles are in centimeters. Dissolved oxygen in WR penetrated less than 2 mm into the sediments and showed a consistent drop with depth. Dissolved oxygen in UDSW also penetrated extremely shallow but was measured down to 3.5 mm (Figure 7-10). The deeper oxygen penetration and less linear drop in UDSW were attributed to the biological activity of oligochaetes observed by the thousands. This activity is thought to increase connectivity between overlying water and pore water of UDSW.

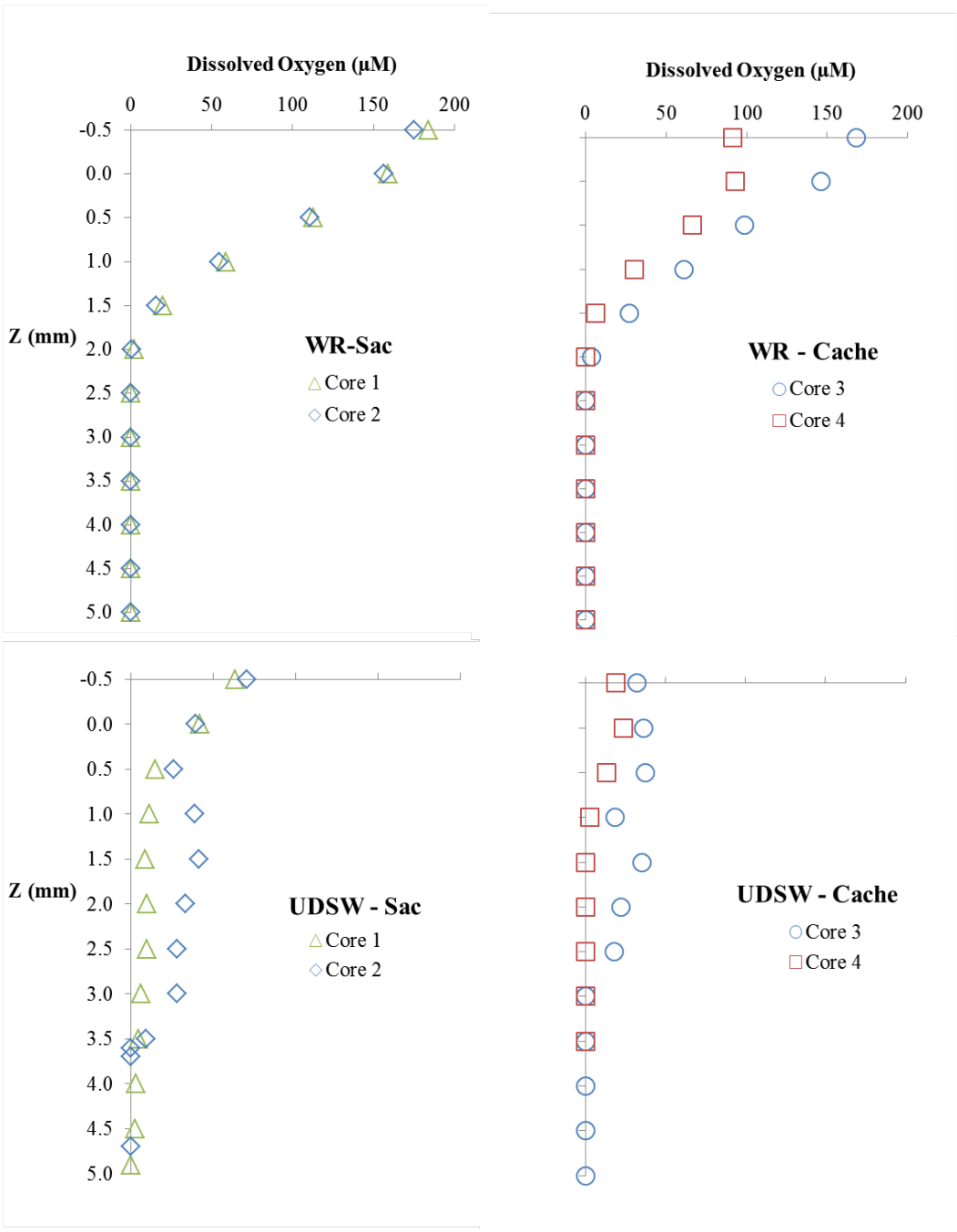

Figure 7-10. Vertical microelectrode profiles of dissolved oxygen in interstitial water at WR and UDSW having Sacramento River or Cache Creek water. Note depth scale is in millimeters.

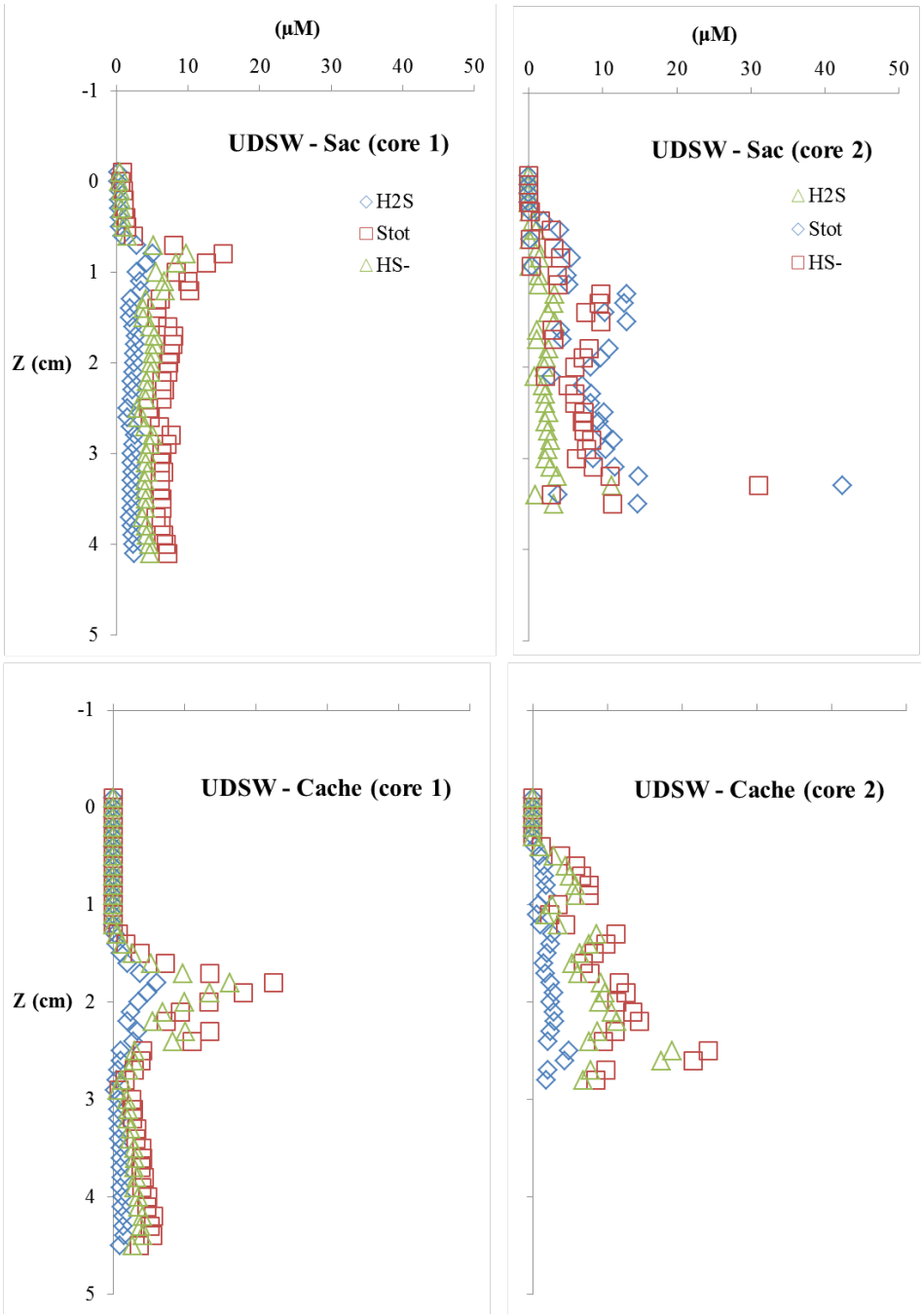

Figure 7-11. Vertical microelectrode profiles of hydrogen sulfide (H_2S), bisulfide (HS^-), and total sulfide (Stot) in interstitial water at WR and UDSW having Sacramento River or Cache Creek water. Note depth scale is in centimeters.

No measureable amounts of H_2S were found in any of the WR cores having either Sacramento River or Cache Creek overlying water. One possibility is that it may have been present at depths greater than we were able to sample with the probes. Although possible we feel this is

unlikely given no H_2S was smelled in the field while collecting the cores and the human nose is very sensitive to sulfide. For UDSW sulfide species were present, typically around 2-4 cm depth although the peak in UDSW – Sac core 1 was at 1 cm (Figure 7-11). Also, pore water (0-2 cm) sulfate concentrations were higher in UDSW with Cache Creek water (597 µM) compared to UDSW with Sacramento River water (<MDL).

In pore water MeHg was measured in the top 2 cm of sediment and oxygen never penetrated deeper than 4 mm therefore it is not possible to directly relate dissolved oxygen profiles to MeHg pore water concentrations.

The absence of measureable sulfide species in WR and the presence of sulfide species in UDSW support a link between sulfate reduction and MeHg production in UDSW. In UDSW MeHg solid phase concentrations, MeHg percent of THg, and Flux were all greater than in WR.

7.3.6. Comparison of measured and diffusive fluxes

Direct measure of flux using incubated cores produced higher THg than diffusional fluxes estimated from pore water concentration gradients. The diffusive flux accounted for 3 to 32 % of the measured flux for THg. Comparison of measured flux to diffusive flux for MeHg is less straightforward. In WR MeHg measured flux was in some cases into the sediment while diffusive flux was always into the water. For WR diffusive flux accounted for -192 to 114 %. For UDSW diffusive flux accounted for 3 to 69 % of the measured flux. It is common for reported values of diffusive and measured flux to disagree (Choe and others, 2004; Covelli and others, 1999b). We attribute the discrepancies between directly measured and calculated diffusive flux to benthic organism activities that enhance the exchange of interstitial pore water over pure diffusion, an assumed value of D_w which may not exactly represent the chemical complex of mercury present, and to an imprecise resolution of pore water concentration gradients near the sediment water interface. In this study we used a 2 cm interval to determine the gradient and a finer resolution likely would result in more accurate diffusive flux estimations.

7.3.7. Significance of sediment water exchange study

Although the authors are hesitant to make strong statements with respect to interpreting the current dataset given this is the pilot portion of an ongoing study, we are able to frame the results in broad terms and suggest directions to move forward with the study. The methods appear to provide reasonable assessments of flux based on comparison to previous studies. The data gathered to date give us insight to the chemical speciation of mercury and the biogeochemical conditions that control mercury cycling and bioavailability in the two habitat types WR and UDSW.

Solid phase THg concentration was greater in WR relative to UDSW and yet THg pore water concentrations and measured and diffusive flux at the sediment water interface were higher for UDSW than WR suggesting mercury concentration in pore water is not controlled by an exchange equilibrium between the two phases and that biogeochemical conditions at WR were less favorable for THg mobility. Production of MeHg by microbial activity has been reported to increase apparent solubility and mobility of THg (Choe and othes, 2004; Bloom and others, 1999). Pore water and solid phase MeHg concentrations, and MeHg as percent of THg were all generally higher in UDSW relative to WR suggesting conditions were more favorable for mercury methylation and possibly increased apparent solubility of THg at UDSW. Also at play may be solubilization and precipitation reactions involving iron and/or manganese which may control the solubility and mobility of THg (Covelli and others, 1999b). Measurements of oxygen at both WR and UDSW showed oxygen penetration into the sediments to be very shallow (< 4 mm) suggesting a favorable environment for iron and manganese reduction below this depth. Percent organic carbon was higher in UDSW (14 %) relative to WR (8 %). The reduction of iron or manganese (hydro) oxides at the redox boundary as a result of microbial degradation of organic matter and subsequent dissolution of Hg may explain lower pore water THg concentrations at WR relative to UDSW. Sulfide concentrations indicate sulfate reduction was occurring in sediments at UDSW but not at WR. Alternately, precipitation of insoluble mercury sulfide and the co-precipitation of mercury with iron sulphides may explain differences in THg pore water concentrations between WR and UDSW (Covelli and others, 1999b) and explain the absence of sulfide in pore water at WR as well.

Pore water MeHg concentrations were well correlated with dissolved THg concentrations (R^2 = 0.78) and were 4 to 13 times higher than water column concentrations indicating the sediments could be a source of dissolved MeHg for the water column at WR and UDSW. Rapid conversion of dissolved MeHg to particulate phase MeHg could also give rise to enhanced particulate MeHg for the water column. In addition, the possibility of methylation processes occurring in the low-oxygen portion of the water column (Figure 7-11, ≤ 32 µM), observed for UDSW just above the sediment water interface, have not been ruled out. Interpretation of MeHg results indicated UDSW to be a more favorable environment for the net production of MeHg relative to WR. Dissolved organic carbon (DOC) may play a role in controlling pore water MeHg concentrations. Although DOC in pore water was not directly measured, previous research in Yolo Bypass reported pore water DOC concentrations for agricultural (similar to WR) and nonagricultural (similar to UDSW) of 19 mg/L and 12 mg/L respectively (Marvin-DiPasquale and others, 2014).

Measured flux for both THg and MeHg were generally greater than diffusive flux estimates and this is attributed to bio pumping and other advection processes. Of particular note is the difference in oligochaete activity between WR and UDSW with much greater bio irrigation,

resulting in increased connectivity of pore water with overlying water, at UDSW. Greater measured fluxes of THg (up to 22x higher) and MeHg (up to 35x higher) at UDSW relative to WR are hypothesized to be at least partially related to biological activity in the sediment. The D-MCM model being applied to the Yolo Bypass typically uses a mass transfer coefficient for flux from the sediment that exceeds molecular diffusion rates (R. Harris unpublished).

While clear differences between WR and UDSW in mercury cycling and fluxes were observed with UDSW being more favorable for both net MeHg production and MeHg flux the effect of different sources of overlying water were less clear. Measured and diffusive fluxes at UDSW were greater with Cache Water than with Sacramento water but at WR the opposite trend was observed. Although one may expect the Cache Creek higher MeHg concentration overlying water to decrease diffusive flux relative to the lower MeHg Sacramento River water, if pore water concentrations for both treatments remain the same, this was not observed at UDSW. It is the gradient between the pore water concentration and overlying water that is important and the addition of Cache Creek water to UDSW resulted in a steeper gradient between pore water and overlying water relative to the addition of Sacramento River water. This suggests both the biogeochemical conditions of the sediment as well as the source of water are important factors to consider in the Yolo Bypass when looking at the mobility of mercury. The two waters used in this study not only brought in different amounts of mercury but also different amounts of electron acceptors such as sulfate and particulate and dissolved organic carbon that could be utilized as substrate by bacteria. When these waters were combined with the two landscape types, WR and UDSW, the resulting net MeHg production and flux were variable. We hypothesize increased sulfate and labile carbon in Cache Creek water coupled with increased bio pumping at the sediment water interface by infauna and bacteria respiration resulting in low oxygen concentrations in UDSW combined to enhance net MeHg production and increase MeHg concentrations and flux relative to other treatments.

Finally, it is important to point out some of the limitations of this study to aid discussion of possible corrections or new directions as we move out of the pilot phase of the project. Some of the results were confounded by large variability between replicates which is not unexpected for an element such as mercury which undergoes many transformations and moves by many pathways. But in many cases it was only one of three replicates that did not agree. For this report we included all data. Moving forward we may consider adding a fourth and maybe even fifth replicate to the core incubation study which should increase accuracy of all portions of this study significantly. We also only have a snap shot in time of what is happening at WR and UDSW. Cores were collected late winter with a particular biogeochemical signature indicative of that period. Flux measurements were made and results presented but the question remains as to whether the same results would be found if cores were collected earlier in the wet season. How do the sulfur and mercury cycles change seasonally on the Yolo Bypass? Would

significantly more sulfate reduction occur and change mercury cycling and fluxes in WR and UDSW if the experiments were repeated at a different time? This project is concerned with the Yolo Bypass during flood stages and floods occur at different times on the Yolo Bypass year to year, sometimes as early as late November. It may be important to add a temporal component to a subset of sample stations to determine if this is important to the program and modeling efforts. Lastly, the interpretations of the results presented here may change as we gather more information from addition habitat types in the Yolo Bypass. While some clear trends and processes emerged from the current work our sample size is relatively small and we will continue to reevaluate our findings as the study continues.

7.3.8. Summary of findings and recommendations for next set of pore water samples to be collected winter of 2015/16

- Given the pilot study results our working hypothesis that there is no difference in sediment water mercury exchange fluxes using Sacramento River and Cache Creek waters was not supported and it is important to continue work on additional habitat types using two sources of water (Low mercury concentrations – Sacramento River, High mercury concentrations – Cache Creek) in core incubation studies.
- Incubations were carried out for 12 hours with reliable results. In fulfillment of the pilot study objective to determine optimal time for incubations we recommend the next round of experiments are carried out for at least 12 hours but increasing incubation times to 18-24 hours in measured flux experiments is possible given ability to maintain stable cores during experiment. This would allow for day/night incubations to investigate effect of benthic diatoms on mercury cycling.
- Interpretation of results will be aided by increasing replication; we propose adding an additional 1 or 2 cores for each treatment moving forward which at the very least will provide a sense of the variability on a near field spatial scale.
- The working hypothesis that mercury sediment water exchange fluxes differ among the two different land uses is supported by pilot study results.
- The working hypothesis that sediment water exchange flux of mercury can be modeled by pore water and sediment chemistry measurements of MeHg, THg, total organic carbon, and grainsize currently lacks sufficient data to be evaluated as only two landscape types have been sampled.
- Diffusive flux measurements were estimated using a 0-2 cm interval. A finer resolution would allow for more accurate diffusive flux estimates and allow a more detailed comparison to THg and MeHg pore water concentrations to micro electrode work.

- Consideration should be given to temporal variation and how the timing of core collections may influence results. Collection of monthly samples to look at mercury and MeHg, net

mercury methylation, and organic carbon at a subset of sites would improve our understanding of the effect of temporal variation on mercury cycling in the Yolo Bypass.

7.4. Literature Cited

Bloom NS, Gill GA, Cappellino S, Dobbs C, Mcshea L, Driscoll C, Mason R, Rudd J (1999) Speciation and cycling of mercury in Lavaca, Bay, Texas, sediments. Environ Sci & Technol 33:7-13

Choe KY, Gill GA, Lehman RD, Han S, Heim WA, Coale KH (2004) Sediment-water exchange of total mercury and monomethyl mercury in the San Francisco Bay-Delta. Limnol Oceanogr 49 (5):1512-1527

Compeau GC, Bartha R (1985) Sulfate-reducing bacteria: Principal methylators of mercury in anoxic estuarine sediment. Appl Environ Microbiol 50 (2):498-502

Covelli S, Faganeli J, Horvat M, Brambati A (1999a) Porewater distribution and benthic flux measurements of mercury and methylmercury in the Gulf of Trieste (Northern Adriatic Sea). Estuarine Coastal and Shelf Science 48 (4):415-428

Covelli S, Faganeli J, Horvat M, Brambati A (1999b) Porewater Distribution and Benthic Flux Measurements of Mercury and Methylmercury in the Gulf of Trieste (Northern Adriatic Sea). Estuarine, Coastal and Shelf Science 48 (4):415-428. doi:http://dx.doi.org/10.1006/ecss.1999.0466

Gill GA, Bloom NS, Cappellino S, Driscoll CT, Dobbs C, Mcshea L, Mason R, Rudd JWM (1999) Sediment - water fluxes of mercury in Lavaca Bay, Texas. Environ Sci Technol 33:663-669

Gilmour CC, Riedel GS, Ederington MC, Bell JT, Benoit JM, Gill GA, Stordal MC (1998) Methylmercury concentrations and production rates across a trophic gradient in the northern Everglades. Biogeochemistry 40:327-345

Heim WA, Coale KH, Stephenson M, Choe K-Y, Gill GA, Foe C (2007) Spatial and habitat-based variations in total and methyl mercury concentrations in surficial sediments in the San Francisco Bay-Delta. Environ Sci Technol 41 (10):3501-3507

Jeroschewski P, Steuckart C, Kuhl M (1996) An amperometric microsensor for the determination of H.S in aquatic environments. Anal Chem 68:4351-4357

Kim M, Han S, Gieskes J, Deheyn DD (2011) Importance of organic matter lability for monomethylmercury production in sulfate-rich marine sediments. Science of the Total Environment 409 (4):778-784. doi:http://dx.doi.org/10.1016/j.scitotenv.2010.10.050

Kuwabara JS, Marvin-DiPasquale M, Praskins W, Byron E, Topping BR, Carter JL, Fend SV, Parchaso F, Krabbenhoft DP, Gustin MS (2002) Flux of Dissolved Mercury Across the

Sediment-water Interface in Lahontan Reservoir, Navada. vol Water Resources Investigations Report 02-4138. U.S. Geological Survey, Menlo Park, CA

Li Y-H, Gregory S (1974) Diffusion of ions in sea water and in deep-sea sediments. Geochimica et Cosmochimica Acta 38 (5):703-714. doi:http://dx.doi.org/10.1016/0016-7037(74)90145-8

Marvin-DiPasquale M, Windham-Myers L, Agee JL, Kakouros E, Kieu LH, Fleck JA, Alpers CN, Stricker CA (2014) Methylmercury production in sediment from agricultural and non-agricultural wetlands in the Yolo Bypass, California, USA. Science of the Total Environment 484:288-299. doi:http://dx.doi.org/10.1016/j.scitotenv.2013.09.098

Mason RP, Kim E-H, Cornwell J, Heyes D (2006) An examination of the factors influencing the flux of mercury, methylmercury and other constituents from estuarine sediment. Marine Chemistry 102 (1–2):96-110.

Revsbech N, Jørgensen B (1986) Microelectrodes: Their Use in Microbial Ecology. In: Marshall KC (ed) Advances in Microbial Ecology, vol 9. Advances in Microbial Ecology. Springer US, pp 293-352. doi:10.1007/978-1-4757-0611-6_7

Revsbech NP (1989) An oxygen microsensor with a guard cathode. Limnology and Oceanography 34 (2):474-478. doi:10.4319/lo.1989.34.2.0474

St. Pierre KA, Chételat J, Yumvihoze E, Poulain AJ (2014) Temperature and the Sulfur Cycle Control Monomethylmercury Cycling in High Arctic Coastal Marine Sediments from Allen Bay, Nunavut, Canada. Environmental Science & Technology 48 (5):2680-2687. doi:10.1021/es405253g

USEPA (1998) Method 7473, Mercury in solids and solutions by the thermal decomposition amalgamation, and atomic absorption spectrophotometry.

USEPA (2001) Method 1630, Methyl mercury in water by distillation, aqueous ethylation, purge and trap, and CVAFS. EPA-821-R-01-020.

USEPA (2002) Method 1631, Revision E: Mercury in water by oxidation, purge, and trap, and cold vapor atomic fluorescence spectrometry. EPA-821-R-02-019.

7.5. Appendix A

Table 7-6. Ancillary Measurements taken during the Incubated Core Flux Study and the Average and Standard Deviation for each Time Series.

Time*	**0 hr**	**3 hr**	**6 hr**	**9 hr**	**12.5 hr**	**Average**	**Stdev**
WR Sac - March 12, 2015							
T (°C)	13.7	14.4	13.7	13.6	13.9	13.9	0.3
Cond (µS/cm)	332	333	337	345	348	339	7
pH	8.28	8.28	8.34	8.02	7.86	8.16	0.21
ORP (mV)	115	101	103	68.2	64.4	90.3	22.6
DO (mg/L)	13.3	12.9	9.19	9.35	9.08	10.8	2.14
DO (%sat)	129	126	88.6	89.9	88.1	104	21.3
WR Cache - March 12, 2015							
T (°C)	14.2	14.5	13.8	13.6	14.0	14.0	0.34
Cond (µS/cm)	1323	1308	1302	1297	1290	1304	13
pH	8.11	7.81	7.82	7.89	7.48	7.82	0.23
ORP (mV)	120	105	103	50.4	63.2	88.2	29.7
DO (mg/L)	13.0	12.5	8.5	7.76	7.24	9.81	2.74
DO (%sat)	128	123	82.7	74.8	70.5	95.8	27.6
Time**	**0 hr**	**3 hr**	**6 hr**	**9 hr**	**11.5 hr**	**Average**	**Stdev**
UDSW Sac - March 26, 2015							
T (°C)	15.3	14.5	13.6	13.1	13.0	13.9	0.97
Cond (µS/cm)	305	309	325	364	345	330	25
pH	7.98	8.18	8.18	8.05	8.30	8.14	0.12
ORP (mV)	141	127	127	142	130	133	8
DO (mg/L)	9.52	9.57	9.35	8.38	9.08	9.18	0.49
DO (%sat)	95.0	94.7	89.9	79.2	83.9	88.5	6.9
UDSW Cache - March 26, 2015							
T (°C)	15.4	14.6	13.7	13.2	13.1	14.0	0.98
Cond (µS/cm)	1510	1497	1488	1444	1463	1480	27
pH	7.56	7.66	7.64	7.54	7.68	7.62	0.06
ORP (mV)	144	141	140	148	142	143	3
DO (mg/L)	8.55	7.90	7.09	6.64	7.01	7.44	0.77
DO (%sat)	85.9	78.0	68.6	62.5	64.9	72.0	9.8
*Time	10:00	13:00	16:00	19:00	22:30		
**Time	8:30	11:30	14:30	17:30	20:00		

Table 7-7. Sample Name, Time Collected, Water Volume in Core at Time of Sampling, Mercury Concentration, and Mercury Mass in Core Overlying Water for Wild Rice (WR) Incubated Core Experiment.

WR Sac – March 12, 2015							
Sample Name	Time Collected	Time (Hrs)	Water Vol (L)	MeHg (ng/L)	MeHg (ng)	THg (ng/L)	THg (ng)
Core 1 Sac T0	10:00	0.00	1.28	0.178	0.227	1.93	2.46
Core 1 Sac T1	13:00	3.00	1.23	0.188	0.239	2.01	2.56
Core 1 Sac T2	16:00	6.00	1.19	0.199	0.245	2.02	2.49
Core 1 Sac T3	19:00	9.00	1.14	0.209	0.248	2.38	2.81
Core 1 Sac T4	22:30	12.50	1.10	0.220	0.251	2.29	2.62
Core 2 Sac T0	10:00	0.00	1.20	0.179	0.216	1.84	2.22
Core 2 Sac T1	13:00	3.00	1.16	0.174	0.210	1.87	2.25
Core 2 Sac T2	16:00	6.00	1.12	0.187	0.217	1.94	2.25
Core 2 Sac T3	19:00	9.00	1.07	0.188	0.210	2.11	2.35
Core 2 Sac T4	22:30	12.50	1.03	0.198	0.212	2.14	2.29
Core 3 Sac T0	10:00	0.00	1.24	0.177	0.220	1.85	2.29
Core 3 Sac T1	13:00	3.00	1.20	0.165	0.205	1.94	2.40
Core 3 Sac T2	16:00	6.00	1.15	0.197	0.234	2.00	2.39
Core 3 Sac T3	19:00	9.00	1.11	0.196	0.226	2.31	2.65
Core 3 Sac T4	22:30	12.50	1.06	0.204	0.226	2.32	2.57
Core 1 Cache T0	10:00	0.00	1.21	0.339	0.411	2.62	3.18
Core 1 Cache T1	13:00	3.00	1.17	0.374	0.452	2.71	3.28
Core 1 Cache T2	16:00	6.00	1.12	0.377	0.440	3.10	3.60
Core 1 Cache T3	19:00	9.00	1.08	0.378	0.425	3.01	3.39
Core 1 Cache T4	22:30	12.50	1.04	0.399	0.430	3.12	3.37
Core 2 Cache T0	10:00	0.00	1.22	0.369	0.450	2.44	2.97
Core 2 Cache T1	13:00	3.00	1.18	0.393	0.478	2.78	3.37
Core 2 Cache T2	16:00	6.00	1.13	0.406	0.477	2.70	3.18
Core 2 Cache T3	19:00	9.00	1.09	0.382	0.433	2.82	3.18
Core 2 Cache T4	22:30	12.50	1.04	0.367	0.400	3.02	3.27
Core 3 Cache T0	10:00	0.00	1.23	0.408	0.500	2.54	3.11
Core 3 Cache T1	13:00	3.00	1.18	0.412	0.505	2.76	3.37
Core 3 Cache T2	16:00	6.00	1.14	0.439	0.518	2.83	3.34
Core 3 Cache T3	19:00	9.00	1.09	0.390	0.446	2.97	3.37
Core 3 Cache T4	22:30	12.50	1.05	0.385	0.422	2.97	3.25

Table 7-8. Sample Name, Time Collected, Water Volume in Core at Time of Sampling, Mercury Concentration, and Mercury Mass in Core Overlying Water for Un-disked Seasonal Wetland (UDSW) Incubated Core Experiment.

UDSW Sac – March 25, 2015							
Sample Name	Time Collected	Time (Hrs)	Water Vol (L)	MeHg (ng/L)	MeHg (ng)	THg (ng/L)	THg (ng)
Core 1 Sac T0	8:30	0.00	1.141	0.184	0.210	1.80	2.05
Core 1 Sac T1	11:30	3.00	1.091	0.220	0.249	2.18	2.47
Core 1 Sac T2	14:30	6.00	1.049	0.259	0.281	2.16	2.36
Core 1 Sac T3	17:30	9.00	1.007	0.281	0.294	2.21	2.32
Core 1 Sac T4	20:00	11.50	0.965	0.315	0.316	2.72	2.72
Core 2 Sac T0	8:30	0.00	1.141	0.153	0.175	1.69	1.93
Core 2 Sac T1	11:30	3.00	1.099	0.139	0.159	1.74	1.98
Core 2 Sac T2	14:30	6.00	1.057	0.164	0.179	1.78	1.95
Core 2 Sac T3	17:30	9.00	1.015	0.213	0.223	2.27	2.38
Core 2 Sac T4	20:00	11.50	0.973	0.219	0.222	2.37	2.40
Core 3 Sac T0	8:30	0.00	1.141	0.213	0.243	2.08	2.37
Core 3 Sac T1	11:30	3.00	1.102	0.254	0.288	2.23	2.54
Core 3 Sac T2	14:30	6.00	1.061	0.321	0.351	2.68	2.94
Core 3 Sac T3	17:30	9.00	1.018	0.343	0.363	2.80	2.97
Core 3 Sac T4	20:00	11.50	0.976	0.320	0.327	2.90	2.95
Core 1 Cache T0	8:30	0.00	1.14	0.453	0.517	2.94	3.36
Core 1 Cache T1	11:30	3.00	1.10	0.464	0.529	3.37	3.83
Core 1 Cache T2	14:30	6.00	1.05	0.537	0.586	3.97	4.33
Core 1 Cache T3	17:30	9.00	1.01	0.572	0.600	4.57	4.78
Core 1 Cache T4	20:00	11.50	0.97	0.628	0.631	4.83	4.86
Core 2 Cache T0	8:30	0.00	1.14	0.523	0.597	3.17	3.62
Core 2 Cache T1	11:30	3.00	1.10	0.476	0.545	3.44	3.91
Core 2 Cache T2	14:30	6.00	1.06	0.526	0.575	3.71	4.06
Core 2 Cache T3	17:30	9.00	1.01	0.541	0.570	4.20	4.41
Core 2 Cache T4	20:00	11.50	0.97	0.602	0.607	4.75	4.79
Core 3 Cache T0	8:30	0.00	1.14	0.515	0.588	3.07	3.50
Core 3 Cache T1	11:30	3.00	1.10	0.571	0.649	3.53	4.01
Core 3 Cache T2	14:30	6.00	1.06	0.594	0.652	4.82	5.24
Core 3 Cache T3	17:30	9.00	1.01	0.726	0.762	4.95	5.23
Core 3 Cache T4	20:00	11.50	0.97	0.813	0.820	5.46	5.51

Table 7-9. Sample Name, Date Collected, MeHg, and THg, and Percent Moisture for Pore water and Sediment Samples.

Sample Name	Date Collected	Pore Water		Sediment		Percent Moisture
		MeHg (ng/L)	THg (ng/L)	MeHg $(ng/g)_{dry}$	THg $(ng/g)_{dry}$	
WR Core 1 Sac	3/17/2015	3.54	14.5	1.64	390	44.8
WR Core 2 Sac	3/17/2015	2.52	12.5	1.73	384	47.6
WR Core 3 Sac	3/17/2015	1.99	12.3	1.45	382	45.4
Mean ± SD		2.68 ± 0.79	13.1± 1.2	1.61 ± 0.14	385 ± 4	46.0 ± 1.5
WR Core 1 Cache	3/17/2015	1.85	8.17	2.03	366	46.3
WR Core 2 Cache	3/17/2015	1.19	6.44	1.73	518	44.7
WR Core 3 Cache	3/17/2015	1.73	8.13	2.02	373	45.2
Mean ± SD		1.59 ± 0.35	7.58 ± 0.99	1.93 ± 0.17	419 ± 86	45.4 ± 0.8
UDSW Core 1 Sac	3/27/2015	1.74	12.1	0.858	289	36.8
UDSW Core 2 Sac	3/27/2015	3.17	15.8	1.98	264	45.3
UDSW Core 3 Sac	3/27/2015	2.71	20.6	3.81	269	59.4
Mean ± SD		2.54 ± 0.73	16.2 ± 4.3	2.22 ± 1.49	274 ± 13	47.1 ±11.4
UDSW Core 1 Cache	3/27/2015	5.31	26.5	5.60	268	65.6
UDSW Core 2 Cache	3/27/2015	4.01	18.0	3.27	270	53.3
UDSW Core 3 Cache	3/27/2015	3.16	19.1	4.39	294	57.6
Mean ± SD		4.16 ± 1.08	21.2 ± 4.6	4.42 ± 1.17	277 ± 14	58.8 ± 6.2

8. Model Progress

8.1. DSM2-Hg Model Development Progress

As part of the open water DMCP, two mercury models are being developed: one for the open waters of the Sacramento-San Joaquin Delta and one for the intermittently flooded Yolo Bypass (Figure 8-1). The Delta and Yolo Bypass are two very different systems: The Delta is a network of tidal channels, whereas the Yolo Bypass is a broad expanse of land that is intermittently flooded for flood control and habitat purposes. Thus two different modeling approaches were required for each of these systems, and this project will result in development of separate mercury models for the Delta and the Yolo Bypass. Results from the Yolo-Bypass model will be used as inputs to the Delta model.

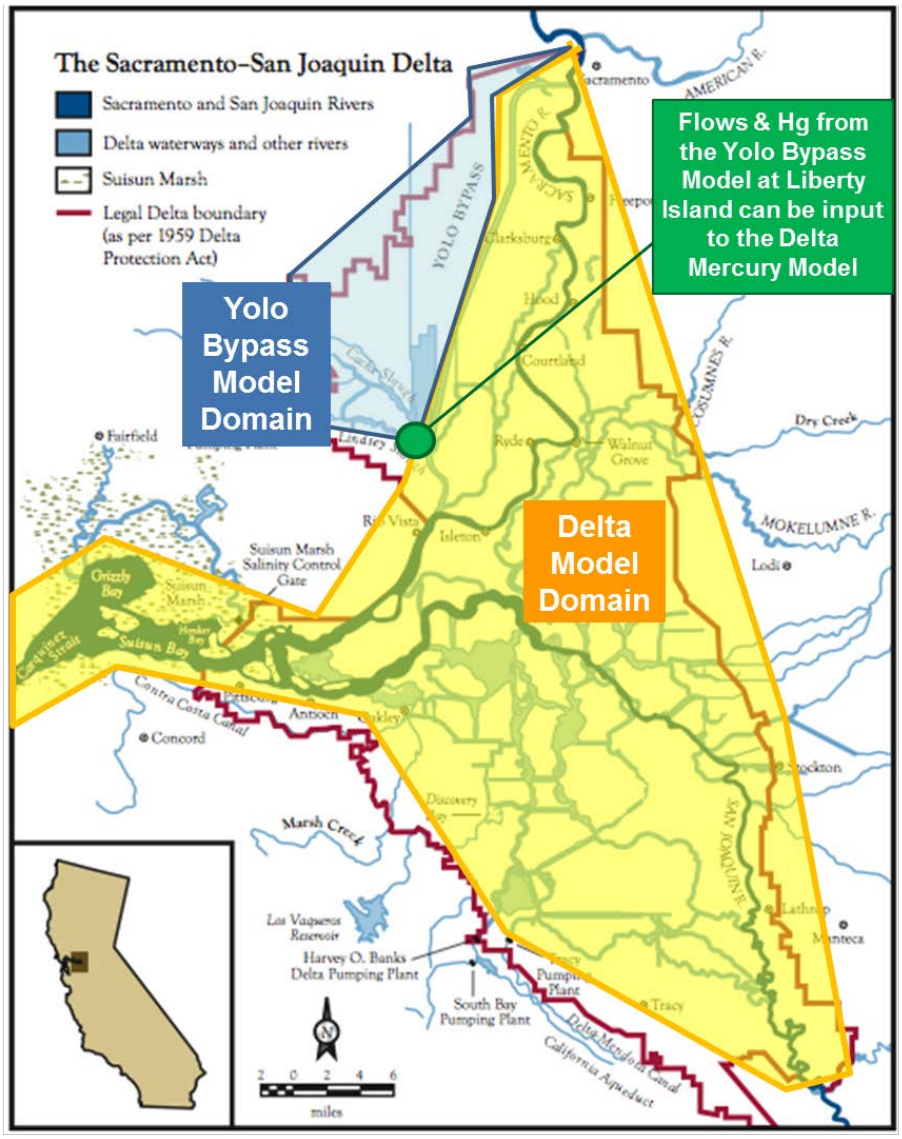

Note: Highlight model domain areas are approximate

Figure 8-1. Approximate domains for the two mercury models being developed for the open water portion of the DMCP.

8.1.1. DSM2-Hg Domain

For this project, the California Department of Water Resources' Delta Simulation Model 2 (DSM2) is being expanded to include mercury. The spatial domain of the Delta model (including mercury) will be unchanged ranging from the Sacramento River in Sacramento in the North Delta, to the San Joaquin River in Vernalis in the South Delta, and to Carquinez Strait near Martinez in the Western Delta (Figure 8-2). As shown in Figure 8-2, the model grid is represented by blue lines with yellow dots.

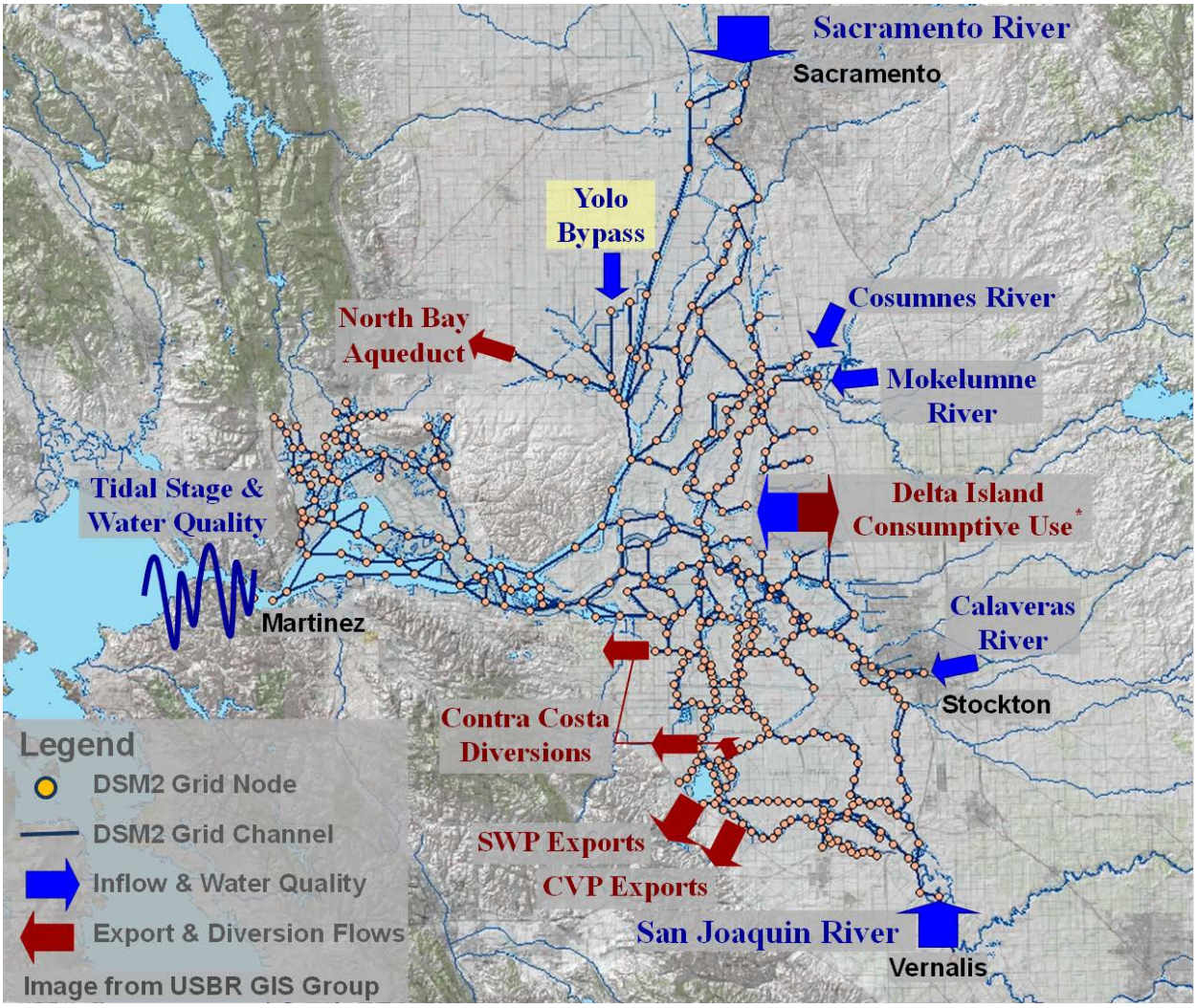

Figure 8-2. Model Domain and Boundary Data Locations for the Delta Simulation Model 2.

*Delta Island Consumptive Use is represented on each Delta Island in the model. Yellow shading indicates data that can be provided by the Yolo Bypass Mercury Model

8.1.2. Data

Data needed for mechanistic models can be grouped into two broad categories. Some types of data are needed to run a simulation. In the case of aquatic mercury simulations, this includes boundary conditions and site conditions such as bathymetry, hydrology, and water quality. Data are also needed to determine if the model is performing reasonably, e.g. measurements of THg and MeHg concentrations in water and sediments. These mercury data are compared to model outputs. If necessary the model calibration is adjusted to improve the fit to observations. Data are also desired to check if the calibrated model performs reasonably when applied to another setting (e.g. a different time period or location). This is the validation step.

Since the Dept. of Water Resources has been running DSM2 for flow and water quality simulations for over 15 years, the data sources for flow and salinity simulations are well established (see annual reports to the State Water Resources Control Board on Methodology for Flow and Salinity Estimates in the Sacramento-San Joaquin Delta and Suisun Marsh http://baydeltaoffice.water.ca.gov/modeling/deltamodeling/annualreports.cfm). For the mercury modeling project, DSM2 is being expanded to include suspended sediments, bed sediments, and mercury. Information reviewed to date for these parameters and the data types needed for mercury simulations in open waters in the Delta are shown in Table 8-1.

Table 8-1. Summary of Information Sources reviewed for Mercury Simulations in the Delta.

Model input category	Parameter	Reference
General characterization	General Descriptions	CDWR (2015l) California Department of Fish and Game (2008) Delta Methylmercury TMDL NPS Workgroup (2012)
Physical	Waterbody area and bathymetry	DSM2 (already exists in model)
	Light Intensity	Colorado State University (2015a) Colorado State University (2015b)
Hydrologic	Water inflow flowrates	DSM2 (already exists in model)
	Water outflow rates	DSM2 (already exists in model)
	Precipitation	DSM2 (already exists in model)
	Water circulation	DSM2 (already exists in model)
Water chemistry	Water temperature	USGS (2015 b-l)
	Water column DOC	Saleh and others. (2007) CDWR (2015k)
	Water column pH	USGS (2015b-l) CDWR (2015m) WDL (2015)
	TSS	USGS (2015k) Saleh and others. (2007)
	Water column Cl	CDWR (2015h)
	Water column sulfate	CDWR (2015j) WDL (2015)
	Organic Content of TSS	Saleh and others. (2007)
	Chlorophyll a	CDWR (2015i)
Sediments	Sediment porosity and density	
	Sediment organic carbon content	
	Pore water chemistry: pH / DOC/ sulfate, sulfide	
Mercury concentrations	MeHg in fish	Melwani and others. (2009) Davis and others. (2008) Melwani and others. (2007) Grenier and others. (2007)
	MeHg in zooplankton	Marvin-DiPasquale and others. (2009)
	Tribuary THg and MeHg concentrations	Foe and others. (2008)
	THg concentrations in precipitation	NADP (2015a)

Model input category	Parameter	Reference
	THg and MeHg in sediments (solids, pw useful)	Heim and others. (2008) Gehrke and others. (2011) Conoway and others. (2007)
	THg & MeHg in water column	Leatherbarrow and others. (2005)
Mercury Fluxes	Wet Hg deposition	NADP (2015a,b,c) CDWR (2015b)
	Dry Hg deposition	Gill (2008b)
	Hg evasion	Gill (2008c)
	Tributary loads	Foe and others. (2008) Bosworth and others. (2010)
	Hg sedimentation	
	Overall Hg mass balance for The Delta	Foe and others. (2008) Leatherbarrow and others. (2005)
Particle dynamics	mass sedimentation, resuspension, settling, decomposition	Morgan-King and Schoellhamer (2013) NHC (2003) Opperman (2012) Schoellhamer and others. (2012) Schoellhamer and others. (2007) Singer and Dunne (2006)

These and other data sources are being explored for use as model inputs and, calibration/validation data. Where site data are unavailable, literature information, engineering and scientific judgment will be used to estimate model input data. All such data sets and underlying assumptions will be documented. Evaluation of data for model boundary conditions, calibration and validation is an ongoing process.

8.1.3. Delta Mercury Model Development: Overview

This project uses DWR's DSM2 model to provide the platform for mercury modeling. DSM2 provides a powerful simulation package for analysis of complex hydrodynamic, water quality, and ecological conditions in riverine and estuarine systems, such as the Sacramento-San Joaquin Delta. DSM2's strength is representing flows, water quality and particle tracking in the main network of Delta channels. DSM2 can calculate water levels, flows, velocities, mass transport processes for conservative and non-conservative constituents including salts, water temperature, dissolved oxygen, and trihalomethane formation potential, and transport of individual particles. DSM2 is a one-dimensional mathematical model which means it only considers changes in the direction of flow, but not horizontally (across a channel) or vertically in the water column. This is a reasonable representation for the channelized portions of the Delta, thus is an appropriate base model for the open water Delta mercury model development.

The Delta mercury budget that was assessed as part of a multi-year CALFED Delta mercury cycling field study (Stephenson and Bonnema, 2008) showed that tributary inputs are the major sources of methyl mercury in the Delta while sedimentation is one of the major losses (Figure 8-3). DSM2 provides a solid backbone for simulating transport of constituents through the Delta, but it requires enhancements and expansion to represent mercury cycling. DSM2 currently consists of three modules: HYDRO, QUAL, and PTM. HYDRO simulates one-dimensional hydrodynamics including flows, velocities, depth, and water surface elevations. HYDRO provides the flow input for QUAL and PTM. QUAL simulates one-dimensional fate and transport of conservative and non-conservative water quality constituents given a flow field simulated by HYDRO. PTM simulates pseudo 3-D transport of neutrally buoyant particles based on the flow field simulated by HYDRO. In order to create a Delta mercury model, DSM2 enhancements include (Figure 8-4):

- Replacing the QUAL module with the General Transport Module that uses a more modern coding structure that is modular and testable.
- Adding modules for suspended sediment, bed sediment and mercury cycling.

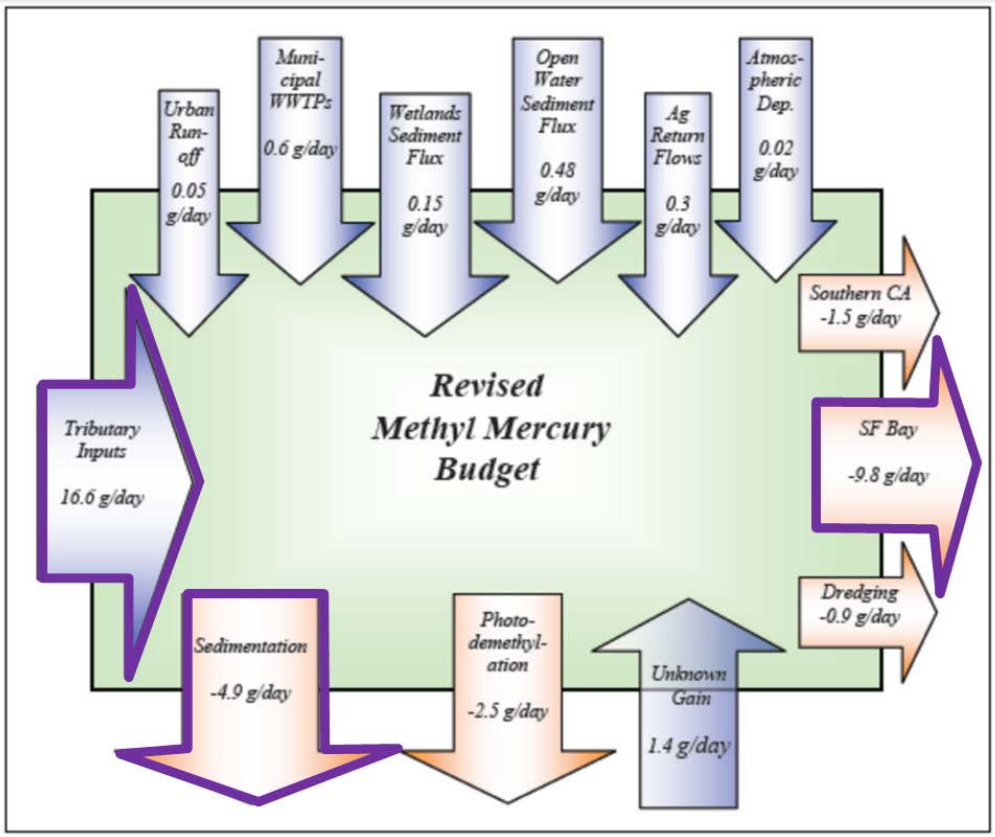

Figure 9. Revised methyl mercury mass balance model for the Delta. The revised model incorporates both some new rates for previously measured terms (tributary inputs and exports to southern California and San Francisco Bay) and rates for two previously unmeasured processes, (photo demethylation and sedimentation).

Figure 8-3. Delta methylmercury Budget with Largest Source and Sinks Highlighted (excerpted from Stephenson and others, 2008).

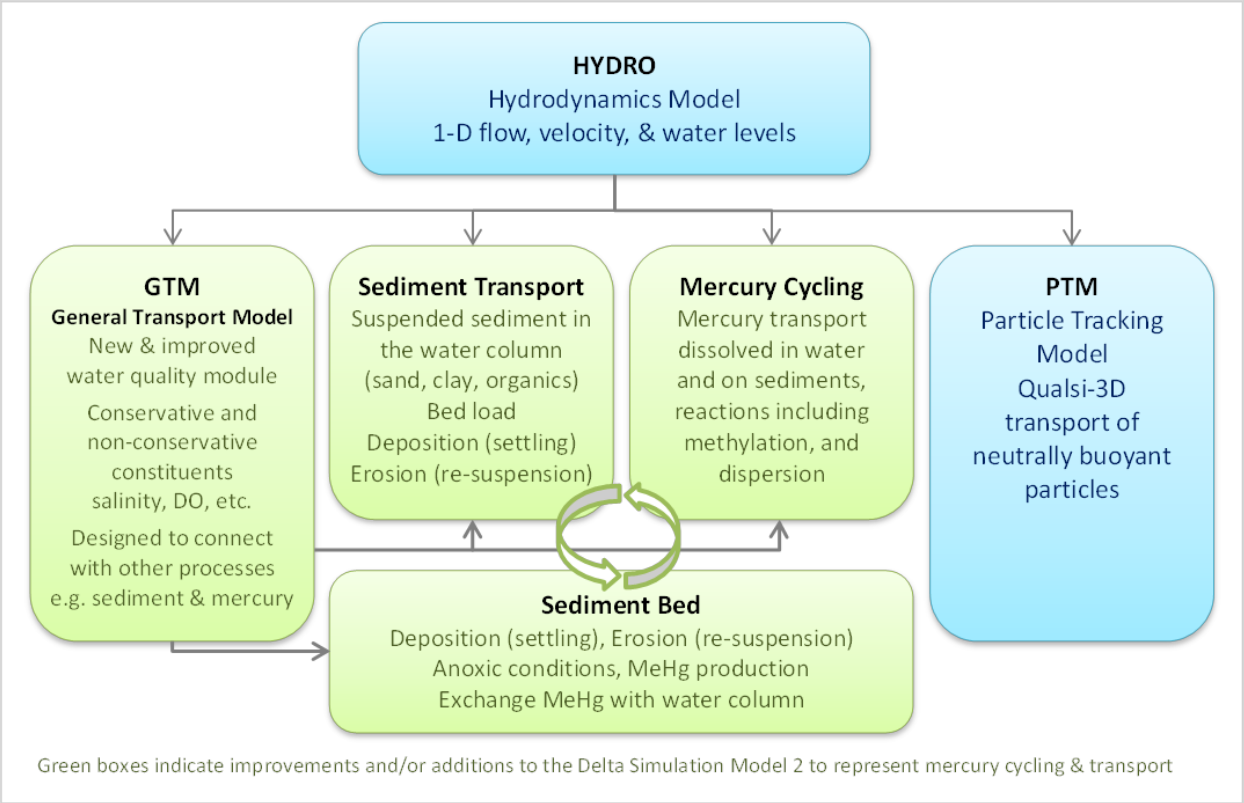

Figure 8-4. Expansion of the Delta Simulation Model 2 (DSM2) to represent Mercury Cycling and Transport.

The Delta mercury model development is being conducted by staff in DWR's Delta Modeling section and consultants from Reed Harris Environmental Ltd. Key tasks in the Delta mercury model development are summarized in Figure 8-5, and progress on those tasks is indicated by the colored shading. Current efforts focus on developing and testing the four new modules for DSM2:

- General Transport Module (transport and fate of conservative and non-conservative constituents)
- Mercury Cycling
- Suspended Sediment
- Bed Sediment

Once those modules are completed, they will be integrated into the existing DSM2 model. The integrated model will then be applied to the Delta. Field data will be used to tune the model to represent observed conditions (calibration and validation). Once the model is tuned to represent existing conditions, it can then be used for scenario analyses. Further details on the progress for each of the new modules is described in the next sections of this report.

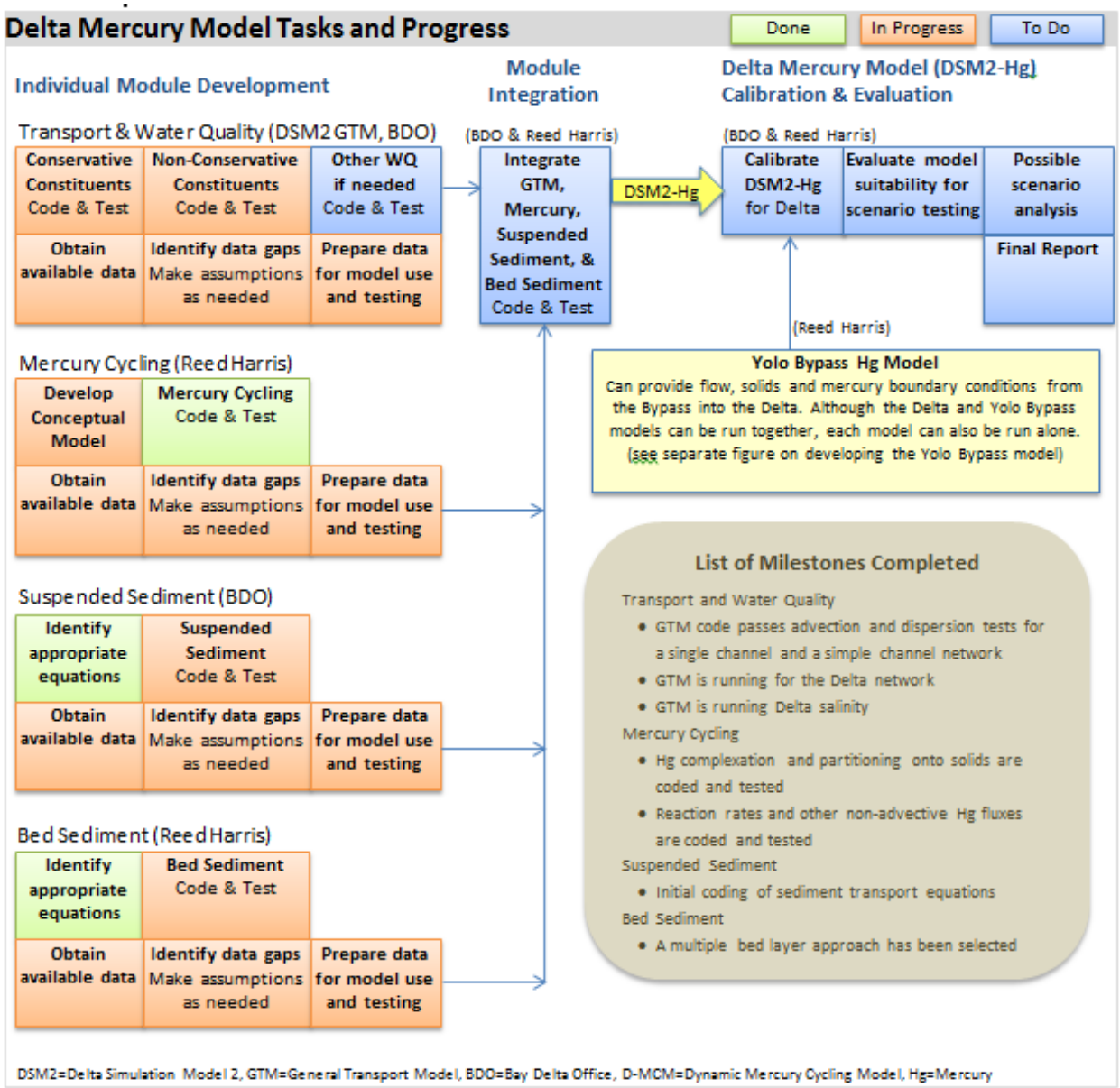

Figure 8-5. Progress and Key Steps for Development of the Delta Mercury Model.

8.1.4. Delta Mercury Model Development: General Transport Module

Development of the Delta Simulation Model 2-General Transport Module (DSM2-GTM) is described in detail in Chapter 4 of the Department of Water Resources' annual report to the State Water Resources Control Board on flow and salinity estimates (DWR, 2014). Key points and additional progress are presented here.

GTM is the backbone of the Delta mercury modeling project, since it represents advection (movement of a constituent with the flow), dispersion (spreading of a constituent due to mixing and diffusion), and reactions (transformations). Modernizing the transport code in DSM2 is analogous to remodeling a house and upgrading all of the electrical and plumbing to support the new features to be added to the house during the remodel. Thus, creating a new GTM model using modern coding and testing techniques is an essential step to building a Delta mercury model. New and expanded features that GTM will bring to the DSM2 modeling package include:

- a modular-based flexible software framework that follows computer coding best practices by creating separate groups of code for each model function or water quality constituent which facilitates:
  - Testing each piece of the code to make sure that it works properly
  - Understanding, maintaining, and enhancing the code
  - Adding complex water quality constituents such as mercury cycling
- a fixed frame of reference (known as Eulerian e.g. you are on the bank of a river watching a boat float by) instead of QUAL's moving frame of reference (known as Lagrangian e.g. you are riding on a boat as it floats downstream). With a fixed frame of reference model, it facilitates:
  - Interacting or linking with other models, including possible future coupling of GTM with DSM2-HYDRO
  - Using geo-referenced data (e.g. Geographical Information System's [GIS] data)
  - Using visualization tools to display model results
- numerical solution using a second order upwind solver with low numerical diffusion that was developed in a prior collaboration with UC Davis
  - Low numerical diffusion is desirable in water quality simulations so that modeled spreading and mixing of constituents is more reflective of physically-based mechanical dispersion than an artifact of numerical dispersion in the computational method

Major tasks and progress on developing GTM are highlighted in Figure 8-5 and are detailed in Figure 8-6. Key foundational work completed for the GTM development includes improvements to HYDRO that facilitate linking HYDRO and GTM and creating a new more efficient input/output system. The GTM development has includes enhancements to the DSM2 grid and to how DSM2 represents a network of channels, with special emphasis on reducing numerical dispersion at junctions (artificial spreading of a constituent due to the numerical solution scheme not to representation of physical mixing processes).

In keeping with the desired modular development philosophy, each function in GTM has been developed in separate code modules and each module has independent code tests. Details on the code testing approach can be found in DWR (2011). Each code test uses the code to compute the solution to a problem with a known answer. If the code produces the correct answer, then the test result is "pass". If the answer is not correct, the test result is "fail". When a code module is completed or when any changes are made anywhere in the code, the suite of code tests is run to verify that each piece of code still returns a "pass" result on for its tests. Thus these code tests are critical for building confidence in the model and are invaluable for troubleshooting coding issues.

The GTM code and tests are being developed using a building block approach to implementing and testing the code. The simplest tests are done first, and then complexity is added in terms of both the type of flow field, type of channel network (straight channel, forked channel, channel network), and in number of processes represented (advection, dispersion, and reaction). For example, the advection code was first applied and tested on a single straight channel, then on a branched channel, and then on the network of Delta channels. Code and tests have been completed for the following (see DWR 2014 for details):

- Advection of a Gaussian plume (bell shaped concentration curve) in uniform flow along a reach.
- Advection of a Gaussian plume in oscillating flow along a reach (important for representing tidal flows).
- Advection of a Gaussian plume in uniform flow along a reach with junctions.
- Advection in a Delta network.
- Dispersion and reaction tests were developed in a previous study (DWR 2011) and each test was applied to both remote and active boundary conditions.
    - Dispersion of a Gaussian plume with no flow
    - Decay of a Gaussian plume with no flow
    - Advection and dispersion of a Gaussian plume
    - Advection and reaction of a Gaussian plume
    - Advection, dispersion and reaction of a Gaussian plume

Development of GTM and its testing routines is ongoing.

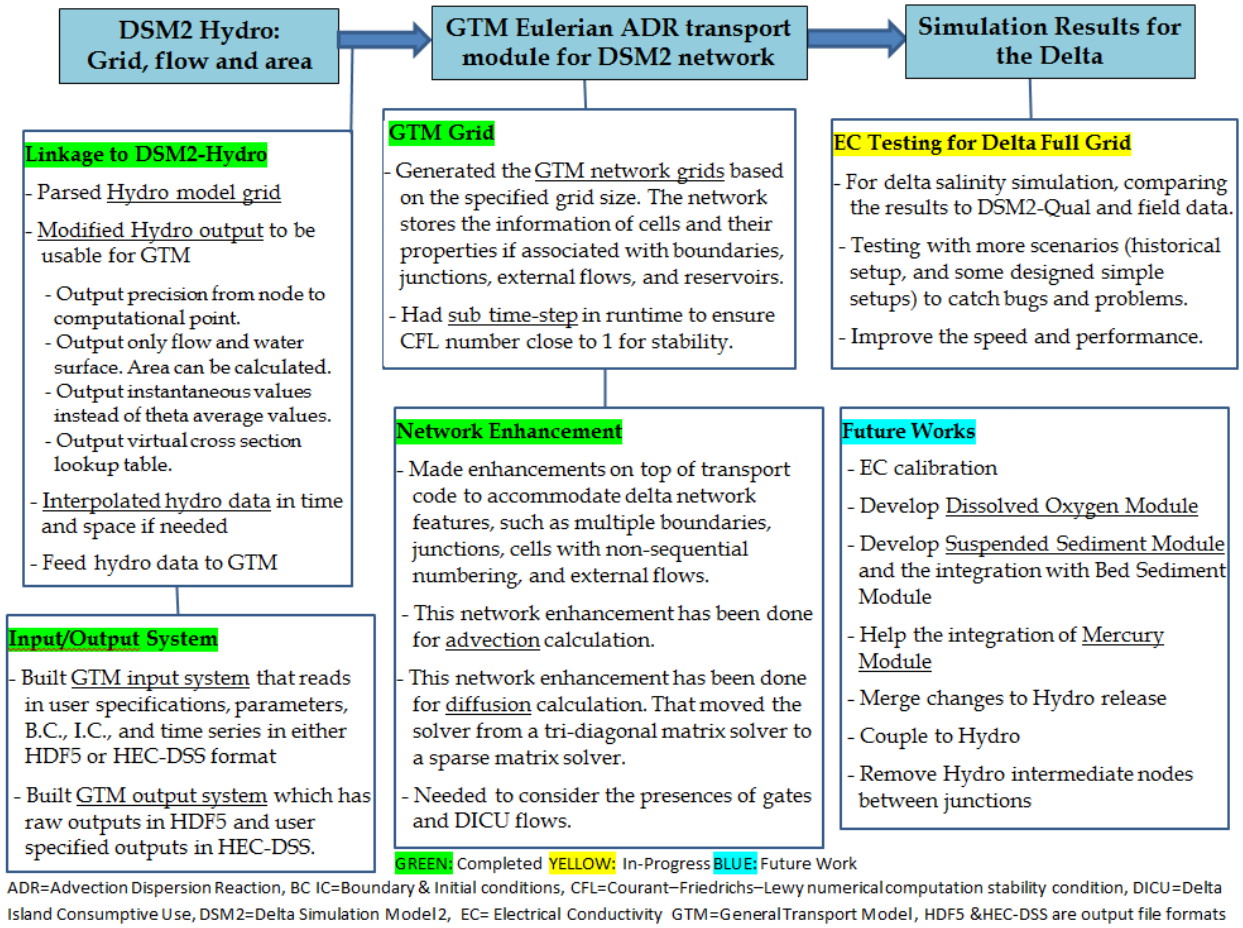

Figure 8-6. Progress on Development of the DSM2 General Transport Model (DSM2-GTM).

8.1.5. Delta Mercury Model Development: Mercury Module

The majority of this task is complete. Code test units have been developed and executed using FRUIT (FORTRAN Unit Test Framework), for all the Hg units and programming components listed below.

- **Hg complexation and partitioning onto solids** – This code unit calculates concentrations of Hg(II) and MeHg bound in dissolved complexes and on solids binding sites that easily and rapidly exchange Hg. Dissolved Hg complexes include those that form with un-protonated thiols in dissolved organic carbon, Cl^-, OH^- and HS^-. Partitioning of instantly exchangeable Hg on up to four particle types is included. Concentrations of Hg (II) and MeHg in phytoplankton are also calculated in this unit. Ancillary code for required for solving the system of non-linear algebraic equations has been developed and tested. This unit has been designed for use in the water column (filtered and solids concentrations of Hg (II) and MeHg) and in the sediment bed (pore water and sediment bed particle concentrations of Hg (II) and MeHg).

- **Reaction rates and other non-advective Hg fluxes** – Code has been written and tested to calculate Hg reaction rates based on Hg concentrations and site conditions. The following reactions/transformations have been included:

  - Biological methylation: Hg(II) → MeHg
  - Biological demethylation: MeHg → Hg(II)
  - Photochemical reduction: Hg(II) → Hg(0)
  - Photochemical demethylation: MeHg → Hg(II)
  - Oxidation: Hg(0) → Hg(II)
  - Dry deposition: (MeHg, Hg(II)
  - Wet deposition: (MeHg, Hg(II)
  - Evasion: Hg(0)
  - Rate limited adsorption/desorption of Hg(II) onto solids (freely exchangeable Hg(II) ↔ strongly sorbed Hg(II)

- Code for writing Hg fluxes to output files for user-specified time intervals has been completed and tested. Fluxes are needed for debugging and developing a detailed mercury budget for the delta.
- A unit has been created to parse input parameters passed from GTM into the appropriate variables used in the mercury model.
  A unit has been created to read time series inputs that might be required by the Hg module from dss formatted files.

8.1.6. Delta Mercury Model Development: Suspended Sediment Module

Since mercury is transported through Delta waters on suspended particles, a suspended sediment module is also being added to DSM2. This model will represent both inorganic sediments and organic solids, divided into four categories:

- Course sediments (sands and gravels)
- Fine sediments (silts and clays)
- Labile organics (easy to decompose)
- Refractory organics (slow to decompose)

Important processes that will be represented by the suspended sediment module include:

- Advection (flow based)
- Dispersion (mixing)
- Settling (deposition of sediments/organic matter out of the water column onto the bed)
- Resuspension (erosion of sediments/organic matter from the bed to the water column)

The suspended sediment module will interact with the bed sediment module through settling and resuspension.

A previous collaboration between DWR and UC Davis began the development of a suspended sediment module. That project included a technical advisory committee that provided valuable input into key sediment processes in the Delta and available data sources. The suspended sediment module is currently under continued development. The suspended sediment module is currently under development and is building upon that earlier effort.

Progress to date includes:

- Initial coding of suspended sediment transport equations
- Initial exploration of available data sources
- Coordination meetings with Reed Harris Environmental Ltd on how the suspended sediment and bed sediment modules will be integrated

8.1.7. Delta Mercury Model Development: Bed Sediment Module

A sediment bed needs to be included in aquatic mercury cycling models, to realistically represent important processes such as sediment methylation, resuspension, and long term burial. A mass balance modeling approach has been chosen for sediment bed solids. Processes include settling, resuspension, burial and decomposition. Up to four particle types can be included and the sediment bed composition can vary with time. The sediment bed module will represent an independent simulation that will run in parallel with GTM, requiring its own set of state variables, inputs, outputs, and numerical integrator. Input and output routines developed for GTM will be adopted for use with the sediment bed module. The sediment bed module will calculate solids resuspension rates for all four particle types based on the bed composition, particle characteristics, cell water depth and overlying water velocity (to be provided by GTM). These rates will be passed to the GTM. Based on rates of settling, resuspension, and decomposition, the sediment bed module will internally maintain a mass balance by solving for burial or erosion rates.

A general Runge-Kutta numerical integrator has been coded and tested. It is has the ability to optionally employ 1st order (Euler's method) through 4th order methods and also includes the Shapine-Bogaki method. Ultimately this code will enable modellers to optimize computational performance of the bed module

The following approach will be used to represent sediment bed particles in DSM2:

- Processes include settling, decomposition, resuspension, and burial (to the next sediment layer (figure 8-7).
- Up to four particle types (labile organic, refractory organic, silt, sand).
- Variable number of sediment layers with one underlying deep bed which acts as a Hg boundary condition. Hg and particles mass balance is done for Hg and particulates in the deep bed (used when overlying layer is eroding and burying).
- Sediment layer has constant thickness/volume but variable mass.
- Constant porosity in each layer.
- Mass balance on all four sediment types for each layer.
- Decomposition/mineralization is a first order temperature dependent reaction.
- Particulate mass balance for sediment layer but none for water column.
- Different settling and resuspension rates for different particle types.
- Different turnover rates for labile and refractory organic particles.

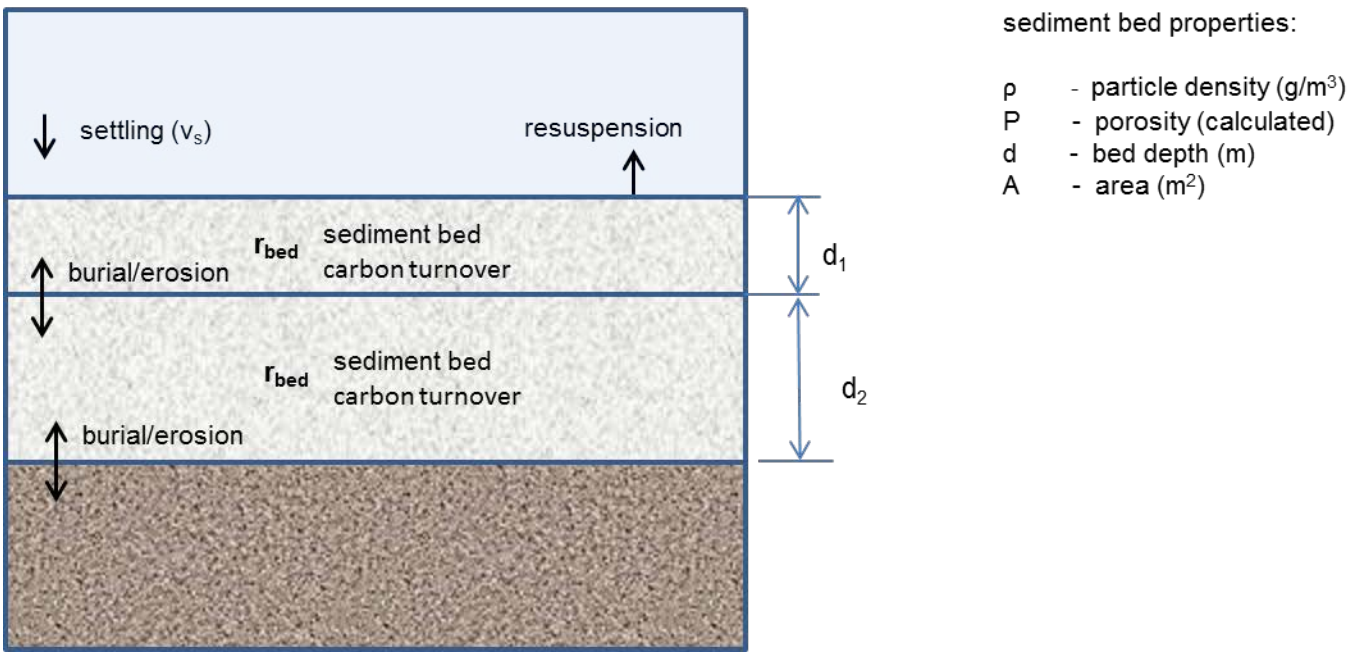

Figure 8-7. Conceptual diagram of model approach for solids in the sediment bed in DSM2.

The equations for the sediment bed model are summarized as follows:

Surface layer resuspension and settling from Garcia and Parker (1991).

$\frac{d\,V_{R,i}}{d\,t}$ volumetric resuspension rate of ith particle type

$\frac{d\,V_{S,i}}{d\,t}$ volumetric settling rate of ith particle type

$\frac{d\,V_{C,i}}{d\,t}$ volumetric mineralization rate of ith particle type $\left(\frac{d\,V_{C,i}}{d\,t} = 0 \text{ for inorganic particles}\right)$

Surface layer erosion:

$$\frac{d\,V_E}{d\,t} = \sum_j \left(\frac{d\,V_{S,j}}{d\,t} - \frac{d\,V_{R,j}}{d\,t} - \frac{d\,V_{M,j}}{d\,t}\right) < 0$$

$f_{2,i}$: volumetric fraction of ith particle type in subsurface bed layer

Erosion from subsurface layer to surface layer:

$$\frac{d\,V_E}{d\,t} = \sum_i \left(f_{2,i} \frac{d\,V_E}{d\,t} \right)$$

$$\frac{d\,V_{E,i}}{d\,t} = f_{2,i} \frac{d\,V_E}{d\,t} = f_{2,i} \sum_j \left(\frac{d\,V_{S,j}}{d\,t} - \frac{d\,V_{R,j}}{d\,t} - \frac{d\,V_{M,j}}{d\,t} \right) \text{ for i}^{th} \text{ particle type}$$

Surface layer burial:

$$\frac{d\,V_B}{d\,t} = \sum_j \left(\frac{d\,V_{S,j}}{d\,t} - \frac{d\,V_{R,j}}{d\,t} - \frac{d\,V_{M,j}}{d\,t} \right) > 0$$

$f_{1,i}$: volumetric fraction of ith particle type in surface bed layer

Burial from surface layer to subsurface layer:

$$\frac{d\,V_B}{d\,t} = \sum_i \left(f_{1,i} \frac{d\,V_B}{d\,t} \right)$$

$$\frac{d\,V_{B,i}}{d\,t} = f_{1,i} \frac{d\,V_B}{d\,t} = f_{1,i} \sum_j \left(\frac{d\,V_{S,j}}{d\,t} - \frac{d\,V_{R,j}}{d\,t} - \frac{d\,V_{M,j}}{d\,t} \right) \text{ for i}^{th} \text{ particle type}$$

8.1.8. Delta Mercury Model Development: Integration and Testing

Once the individual components of the Delta Mercury Model have been coded and tested, they will be integrated into the DSM2 framework. The two coding groups (DWR Delta Modeling Section and Reed Harris Environmental Ltd) have monthly coordination meetings. Progress has been made on specifying code interface routines and input file specifications that will facilitate integrating the mercury and sediment modules into GTM. Each group is independently creating code and the associated code tests. The Delta Modeling section is developing GTM and the suspended sediment routines, and Reed Harris Environmental Ltd is developing the mercury and bed sediment routines (Figure 8-5). In addition to verifying that each piece of code is working properly, individual routine tests will be an essential element in checking that the model components are integrated correctly. Once the routines have been integrated into DSM2, the model can then be used to simulate mercury cycling and transport in the Delta.

8.1.9. Delta Mercury Model Calibration and Application

Once the coding of the Delta mercury model is completed, then the model will be calibrated to represent observed flows, sediment, selected water quality parameters, and mercury concentrations. The model tuning consists of two stages, calibration and validation. During calibration, the model is run for a selected dataset and model constants for are adjusted as needed to improve the match between the model results and the field data. Several iterations of model runs are typically needed during calibration. Once the values of the calibration coefficients have been optimized, validation of the model involves running the model for a different dataset without adjusting any of the calibration coefficients, and then comparing the model results to field observations. If the model results are acceptable, the model is considered to be calibrated and validated. If the results of the validation simulation are not acceptable, then the calibration is revisited to see if the simulation results can be improved. A calibrated and validated model can then be used for scenario analysis. Model calibration and validation steps are meant to increase confidence that the model can be applied to other scenarios and produce reliable results.

A sensitivity analysis will also be carried out to examine which model inputs have the most effect on results, for existing conditions.

Once the Delta mercury model is calibrated and validated, it will undergo management and legal review to determine if the model performance is acceptable for scenario analysis to examine the impacts on methylmercury supply of proposed water management changes in the Delta and Yolo Bypass

This is a new model, being applied to a complex situation, and the underlying science of mercury cycling still has uncertainties regarding some key processes. If scenarios can be run, the technical team will look to the model to match observed trends (e.g. an area is a net source or sink for MeHg, or one type of land use supplies more MeHg to the water column than another), rather than expecting highly accurate results. If model performance is acceptable, then, in cooperation with DWR management and legal, possible model applications and scenarios for analysis will be developed as discussed in the open water workplan and technical memo.

8.2. Yolo Bypass Dynamic Mercury Cycling Model

The D-MCM is a 3-dimensional aquatic mercury cycling model that is being used to understand Hg processes within the Yolo Bypass under flood conditions. There are a number of steps required to apply the D-MCM model to the Yolo Bypass. Figure 8-8 provides a summary of the steps, their stage of completion, and the milestones associated with model adaption to the Yolo Bypass.

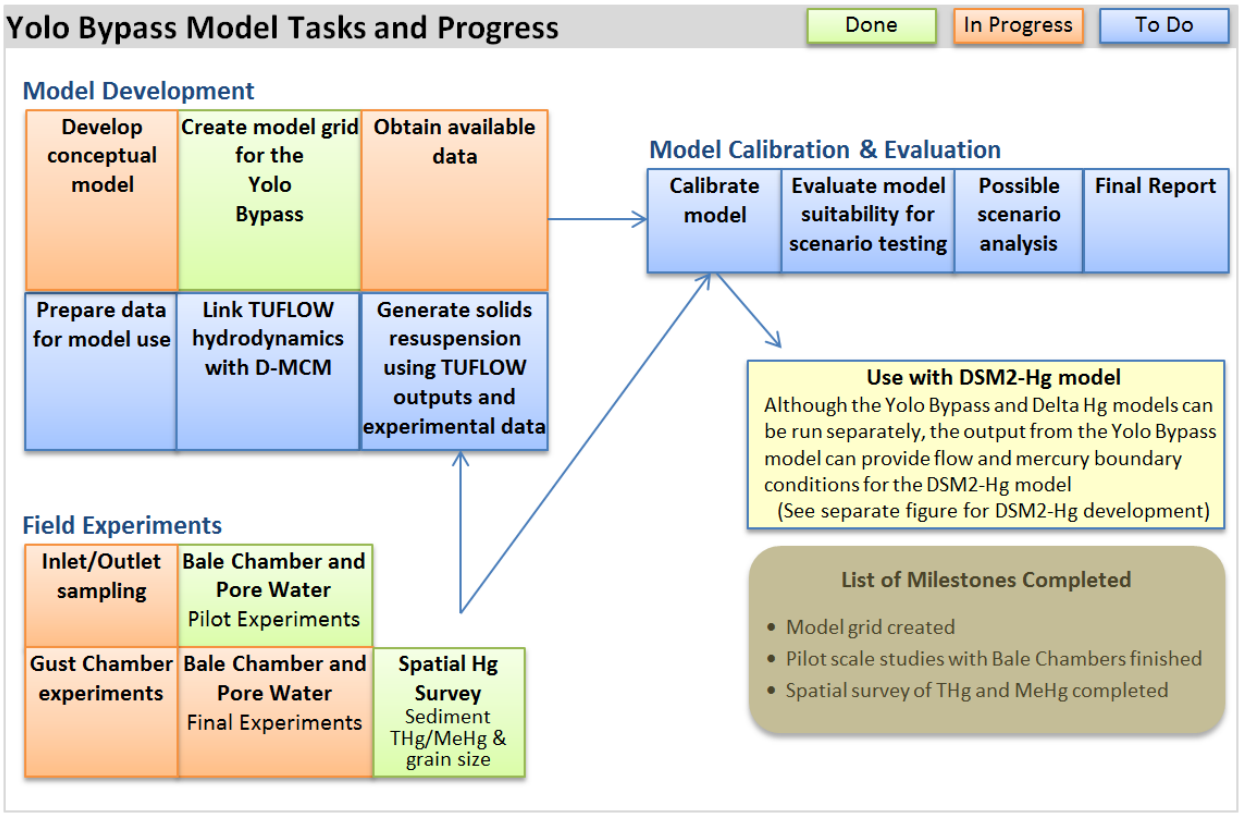

Figure 8-8. Progress and Key Steps for Development of the Yolo Bypass Mercury Model.

8.2.1. D-MCM Yolo Bypass Model Domain

The physical boundaries for the D-MCM Yolo Bypass model include the Yolo Bypass north and south subareas as defined in the DMCP. Hydrology for these simulations will be provided by spatially aggregating outputs from the TUFLOW model currently being applied to the Yolo Bypass. The DSM2 model includes a small portion of the downstream end of the Yolo Bypass near Liberty Island. This area will be simulated using D-MCM as part of the Yolo Bypass.

8.2.2. Data Assembly for D-MCM Simulations of Yolo Bypass

Similar to modeling the Delta, simulating Hg in the Yolo Bypass also requires a range of inputs, including mercury data and site conditions relevant to mercury cycling. A wide range of information sources has been (and continues to be) searched, including peer reviewed articles, on-line data sources, and unpublished data from researchers working in the Delta. Information sources reviewed to-date are summarized in Table 8-2.

Table 8-2. List of Data Sources Reviewed for use in Yolo Bypass Mercury Simulations.

Model input category	Parameter	Reference
General characterization	General descriptions	California Department of Fish and Game (2008) Delta Methylmercury TMDL NPS Workgroup (2012) Yolo Bypass Working Group and others. (2001)
Physical	Waterbody area and bathymetry	CBEC (2010b) Kirkland (2011) Schemel and others. (2002) US Army Corps of Engineers (2007)
	Light intensity	Colorado State University (2015a) Colorado State University (2015b)
	Land Use	Delta Methylmercury TMDL NPS Workgroup (2012)
Biological	Trophic structure	Natural Heritage Institute and others. (2002) Opperman (2012) Lehman and others. (2010)
	growth rates and bioenergetics	Natural Heritage Institute and others. (2002)
	dietary information	Natural Heritage Institute and others. (2002)
	Biomasses of food web compartments	Natural Heritage Institute and others. (2002)
Hydrologic	Flow rates	Schemel and others. (2002) CBEC (2010b) Kirkland (2011) USGS (2015a) California Department of Fish and Game (2008) US Army Corps of Engineers (2007) CDWR (2015a) Foe and others. (2008) Singer and others. (2008) USGS (2015b) CDWR (2015b) Singer and Aalto (2009)
	Tributary inflow rates	CDWR (2015c) USGS (2015a) USGS (2015c) USGS (2015d) USGS (2015e) Singer and Aalto (2009) USGS (2015f) USGS (2015g)
		USGS (2015h) CDWR (2015d) Louie and others (2008)

Model input category	Parameter	Reference
	Outflow Rates	CDWR (2015e) USGS (2015i) Louie and others (2008)
	Precipitation	
	General water circulation	USGS (2015j) CDWR (2015f) CDWR (2015g) USGS (2015k) US Army Corps of Engineers (2007) Natural Heritage Institute and others. (2002) CBEC (2010a) Louie and others (2008)
	Groundwater/root flows	Bachand and others. (2014)
Water chemistry	Temperature (vertical, seasonal)	USGS (2015l) Marvin-DiPasquale and others. (2009) Lehman and others. (2010) CDWR (2015g) Natural Heritage Institute and others. (2002)
	Water column DOC	Windham-Myers and others. (2010) Marvin-DiPasquale and others. (2009) Lehman and others. (2010) Schemel and others. (2002)
	Water column pH	Windham-Myers and others. (2010) Marvin-DiPasquale and others. (2009) Lehman and others. (2010)
	TSS	USGS (2015a) Windham-Myers and others. (2010) Marvin-DiPasquale and others. (2009) Lehman and others. (2010) Schemel and others. (2002) Louie and others. (2008)
	Water column Cl	Windham-Myers and others. (2010) Schemel and others. (2002) Foe and others. (2008)
		Lehman and others. (2010) Domagalski and others. (2004)
	Water column sulfate	Windham-Myers and others. (2010) Schemel and others. (2002) Domagalski and others. (2004)
	Surface light exposure	Windham-Myers and others. (2010)
	TP, N, ChlA	Windham-Myers and others. (2010) Marvin-DiPasquale and others. (2009)

Model input category	Parameter	Reference
		Lehman and others. (2010) Schemel and others. (2002)
	Organic Content of TSS	
	Dissolved oxygen	Lehman and others. (2010)
Sediments	Sediment porosity and density	Windham-Myers and others. (2010)
	Sediment organic carbon content	Windham-Myers and others. (2010) Choe and others. (2004) Marvin-DiPasquale and others. (2009) Delta Methylmercury TMDL NPS Workgroup (2012)
	Pore water chemistry: pH / DOC/ sulfate, sulfide	Windham-Myers and others. (2010) Marvin-DiPasquale and others. (2009)
Mercury concentrations	MeHg in fish	Windham-Myers and others. (2010) Foe and others. (2008)
	MeHg in lower food web	Ackerman and others. (2010)
	Inflow THg and MeHg concentrations	Marvin-DiPasquale and others. (2009) Louie and others. (2008) Domagalski and others. (2004) Lee and Jones Lee (2008) Springborn and others. (2011) Heim and others. (2008) McCord (2014)
	THg concentrations in precip	
	THg & MeHg in sediments (solids, pw useful)	Heim and others. (2008) Heim and others. (2010) Windham-Myers and others. (2010) Choe and others. (2004) Marvin-DiPasquale and others. (2009) Domagalski and others. (2004) Heim and others. (2011) Marvin-DiPasquale and others. (2014)
	THg & MeHg in water column	Windham-Myers and others. (2010) Foe and others. (2008) Marvin-DiPasquale and others. (2009) Domagalski and others. (2004)
		Gill (2008c) Heim and others. (2011) Alpers and others. (2014) Fleck and others. (2014)
Mercury Fluxes	Wet Hg deposition	
	Dry Hg deposition	
	Hg evasion	Gill (2008c)
	Inflow loads	Domagalski and others. (2004)

Model input category	Parameter	Reference
		Louie and others. (2008) Lee and Jones Lee (2008) Springborn and others. (2011) Stephenson and others. (2001)
	Hg sedimentation	Choe and others. (2004)
	THg budget	Louie and others. (2008) Springborn and others. (2011)
	MeHg Fluxes	Louie and others. (2008) Foe and others. (2008) Heim and others. (2009) Gill (2008b) Bachand and others. (2014)
	MeHg mass balance	Foe and others. (2008)
	THg & MeHg point sources	Bosworth and others. (2010)
Particle fluxes	Sediment decomposition	Windham-Myers and others. (2010)
	Resuspension	
	Sedimentation	Singer and Aalto (2009)
	Other particle fluxes	USGS (2015a) Lehman and others. (2010) Singer and Aalto (2009) Springborn and others. (2011) Louie and others. (2008)

8.2.3. Development of D-MCM Grid for the Yolo Bypass

An initial step towards simulating mercury in the Yolo Bypass with D-MCM was the development of a model grid. This process involved segmenting the Yolo Bypass into discrete well-mixed cells assumed to have uniform characteristics. Based on the objectives and scope of this modeling exercise, a grid consisting of 20 to 50 cells was targeted. Five factors identified as the most important shaping the development of the grid are listed below and shown schematically in Figure 8-9.

1. Land use
2. THg and MeHg concentrations in sediments
3. Agricultural disking
4. Hydrology -wetting frequency
5. Hydrology - wet/dry cycling

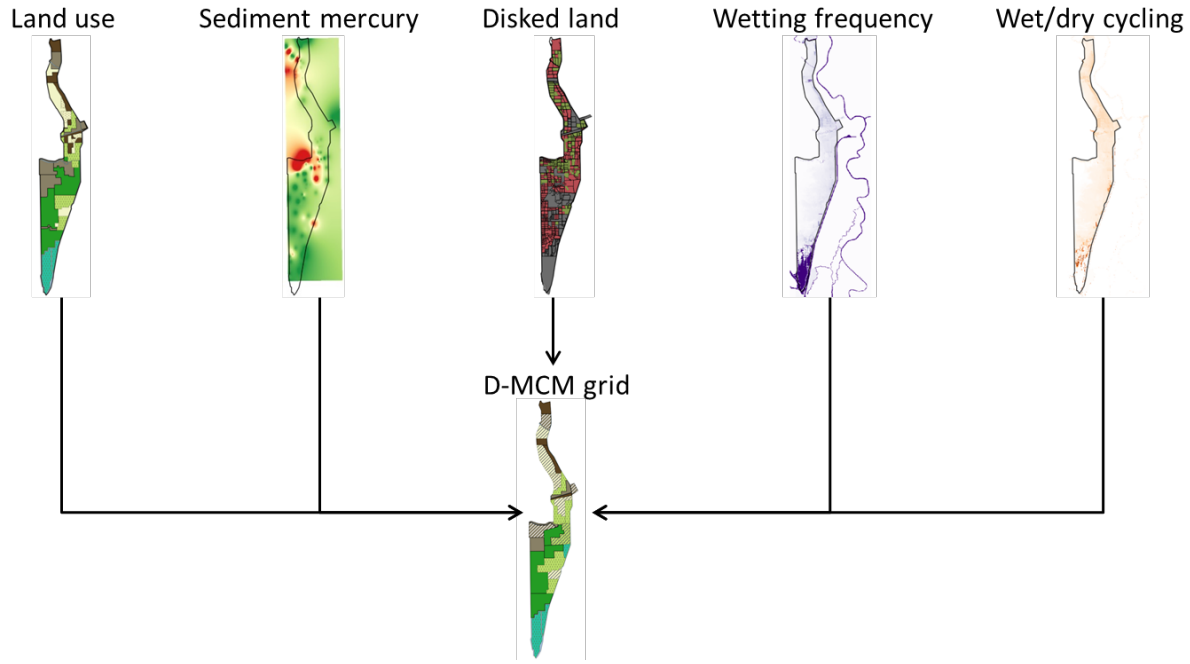

Figure 8-9. Schematic showing key factors that influenced D-MCM grid development.

8.2.3.1. Land use

Land use data were primarily drawn from a 2005-2009 survey conducted by Howitt and others (2013). This survey classified land use in the Yolo Bypass based on 35 categories (Figure 8-10a). Both the number of categories and the spatial resolution were at a higher level of detail than was suitable for this study. The five years' worth of data were averaged, aggregated and simplified into a single representative map with 8 land use categories:

1. pasture
2. fallow
3. white rice
4. wild rice
5. wetland
6. tidal marsh
7. water conveyance (permanently wet) features, and
8. remaining terrain: "mixed/other".

Wetlands are of particular interest in this study; therefore, additional datasets were examined to ensure that they were properly characterized. Recent land use data for the Yolo Bypass Wildlife Area data were obtained from Jeff Stoddard (Figure 8-10b). This dataset was used to supplement Howitt and others (2013) and further refine the model grid (Figure 8-10c). Wetland data from Ducks Unlimited and the National Wetlands Inventory were also examined, but based on the age of the data source, they were assumed to be less accurate than the more recent Yolo Bypass Wildlife Area data and were not directly used.

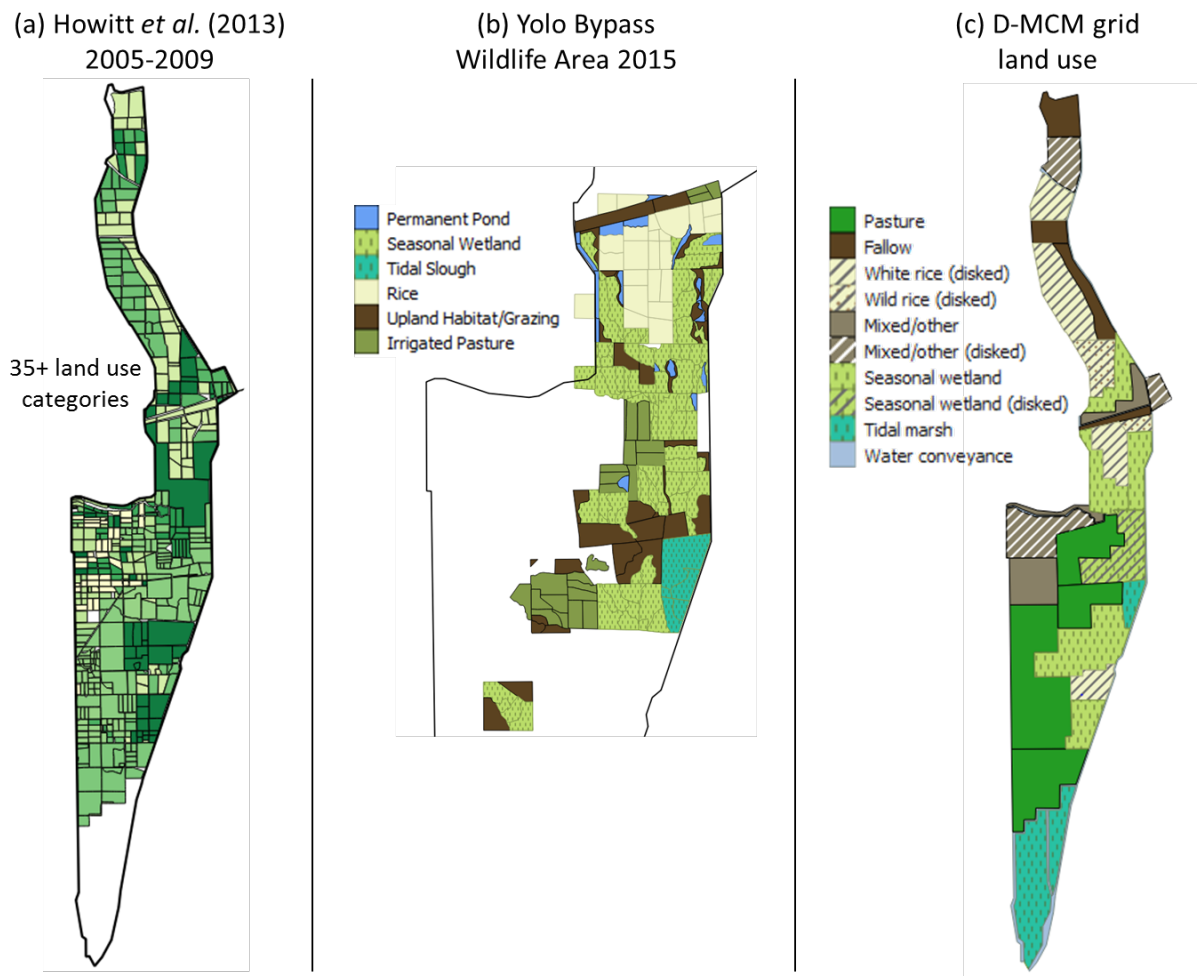

Figure 8-10. . Land use datasets used to develop the D-MCM grid. (a) 2005-2009 survey by Howitt and others. (2013), (b) more recent data for the Yolo Bypass Wildlife Area from Jeff Stoddard, (c) land use represented in the final D-MCM grid.

8.2.3.2. THg and MeHg concentrations in sediments

The initial draft of the model grid relied on THg data from June/December 2007 sampling conducted by Heim and others (2010) (N=97, 84 within the model boundary; Figure 8-11) Sampling of THg and MeHg was later conducted for this study in March-April 2015 (N=67; Figure 8-12), leading to slight revisions to the grid.

Both sediment Hg datasets were plotted using GIS software. Interpolation was also conducted using inverse distance weighting to create contour maps, which aid in visualizing the data (Figure 8-12). These maps could be overlaid with the other layers and more easily interpreted than maps of discrete points. There are however limitations to interpolation, particularly in regions where data are scarce, which were respected in this study.

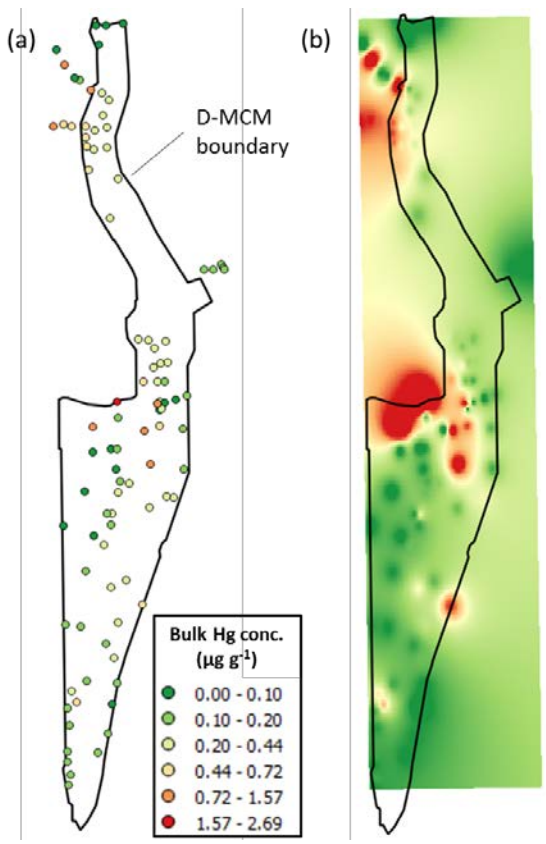

Figure 8-11. Mercury sampling conducted by Heim and others. (2010) in June/December 2007. (a) Sample sites and concentrations (N=97, 84 within model boundary), (b) interpolation using inverse distance weighting.

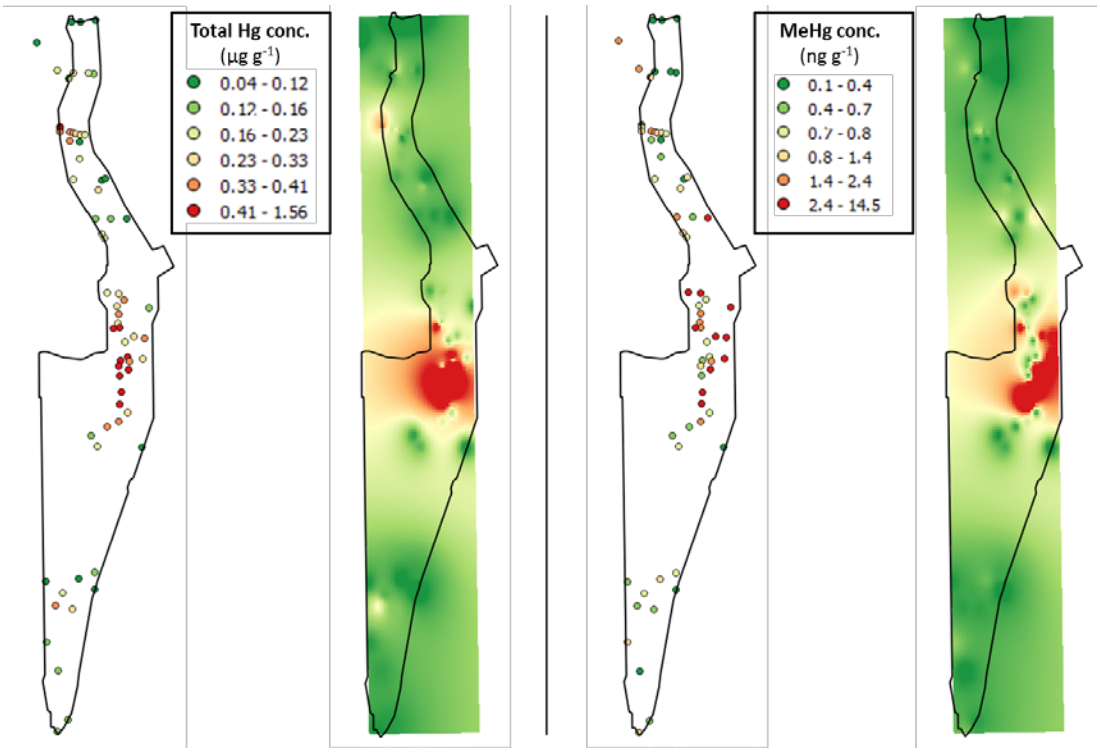

Figure 8-12. THg and MeHg sampling conducted for this study in March-April 2015. Fully shaded panels illustrate interpolation using inverse distance weighting to better visualize the data.

8.2.3.3. Agricultural disking

Agricultural disking is a common practice in the Yolo Bypass. This factor was not captured in the initial draft of the grid, but was later identified as a land management practice that potentially influences mercury dynamics. A comparison of Landsat data between August 2014 and October 2014 was conducted by D. Bosworth for this study. The result was a GIS layer showing which fields were disked or not disked (Figure 8-13 a & b)

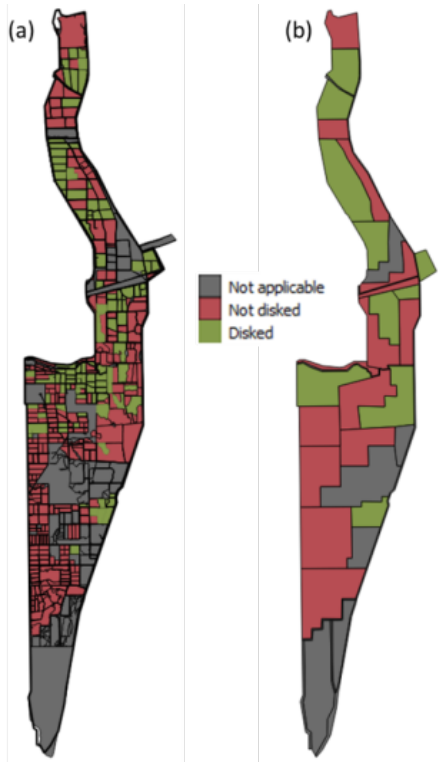

Figure 8-13. Disking in the Yolo Bypass. (a) Original analysis conducted by D. Bosworth, (b) Disking represented in the final D-MCM grid.

8.2.3.4. Hydrological factors

Two hydrological factors were considered when developing the model grid: frequency of wetting and frequency of wet/dry cycling, which may correlate with mercury methylation. These factors were characterized using data derived from TUFLOW hydrodynamic model simulations for 1997-2012 (2014 BiOP Yolo Bypass TUFLOW Hydraulic Model). Frequency of wetting was calculated as the percentage of wet days in TUFLOW simulations and the results were displayed in a raster layer (Figure 8-14a illustrates that the majority of the Yolo Bypass is wet 10-40% of the time, with the tidally-influenced area around Liberty Island being the most notable exception. A similar layer was created showing the average number of wet/dry cycles per year in TUFLOW simulations. In Figure 8-14b this analysis showed that most of the Bypass has 1-4 wet/dry cycles per year, with the Liberty Island region again being an exception. Both layers displayed a slight east to west gradient across the Bypass. The two layers were quite similar in appearance and were effectively treated as a single variable in the design of the grid.

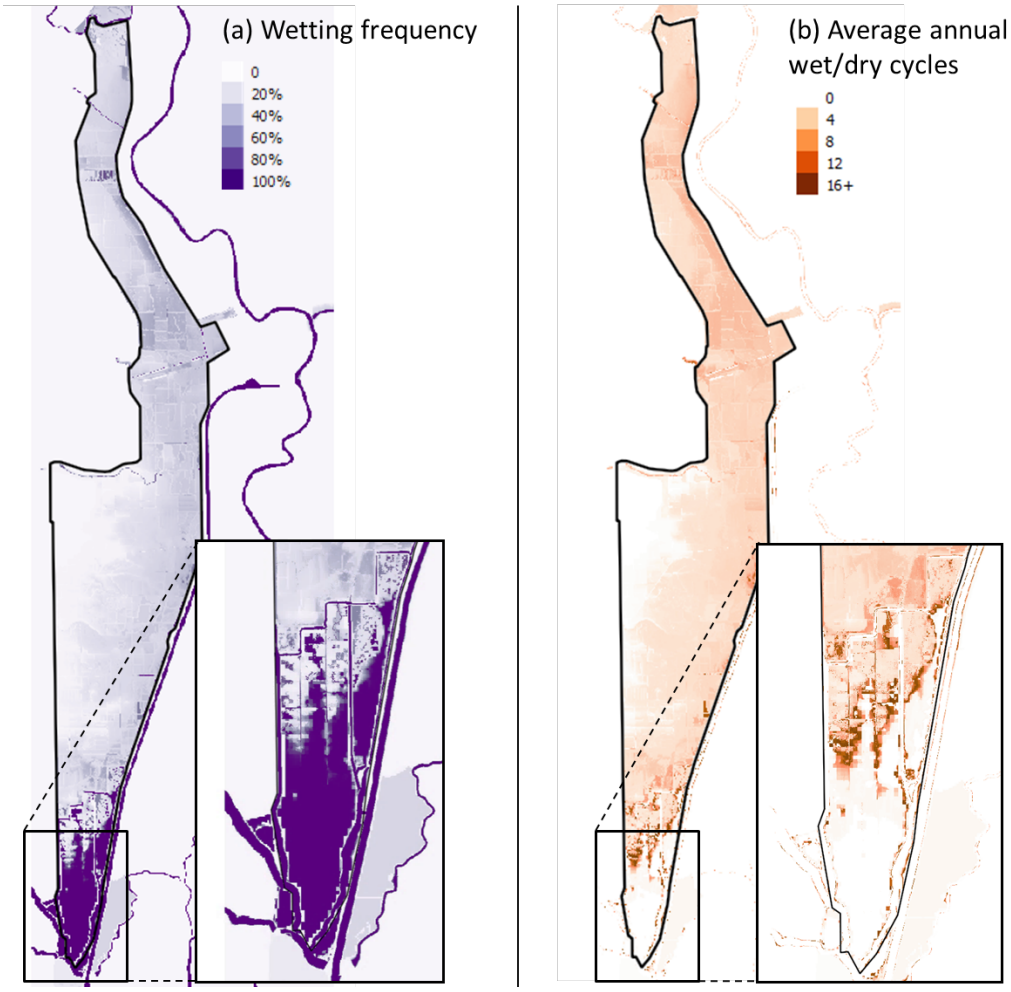

Figure 8-14. Hydrological factors included in D-MCM grid development. (a) Wetting frequency calculated as the percentage of wet days in TUFLOW simulations for 1997-2012, (b) Average number of wet/dry cycles per year in TUFLOW simulations for 1997-2012.

8.2.3.5. D-MCM grid development

The final model grid features 42 cells including 12 permanently wet cells and 30 land (seasonally wet) cells classified under 10 general land use types (Figure 8-15).

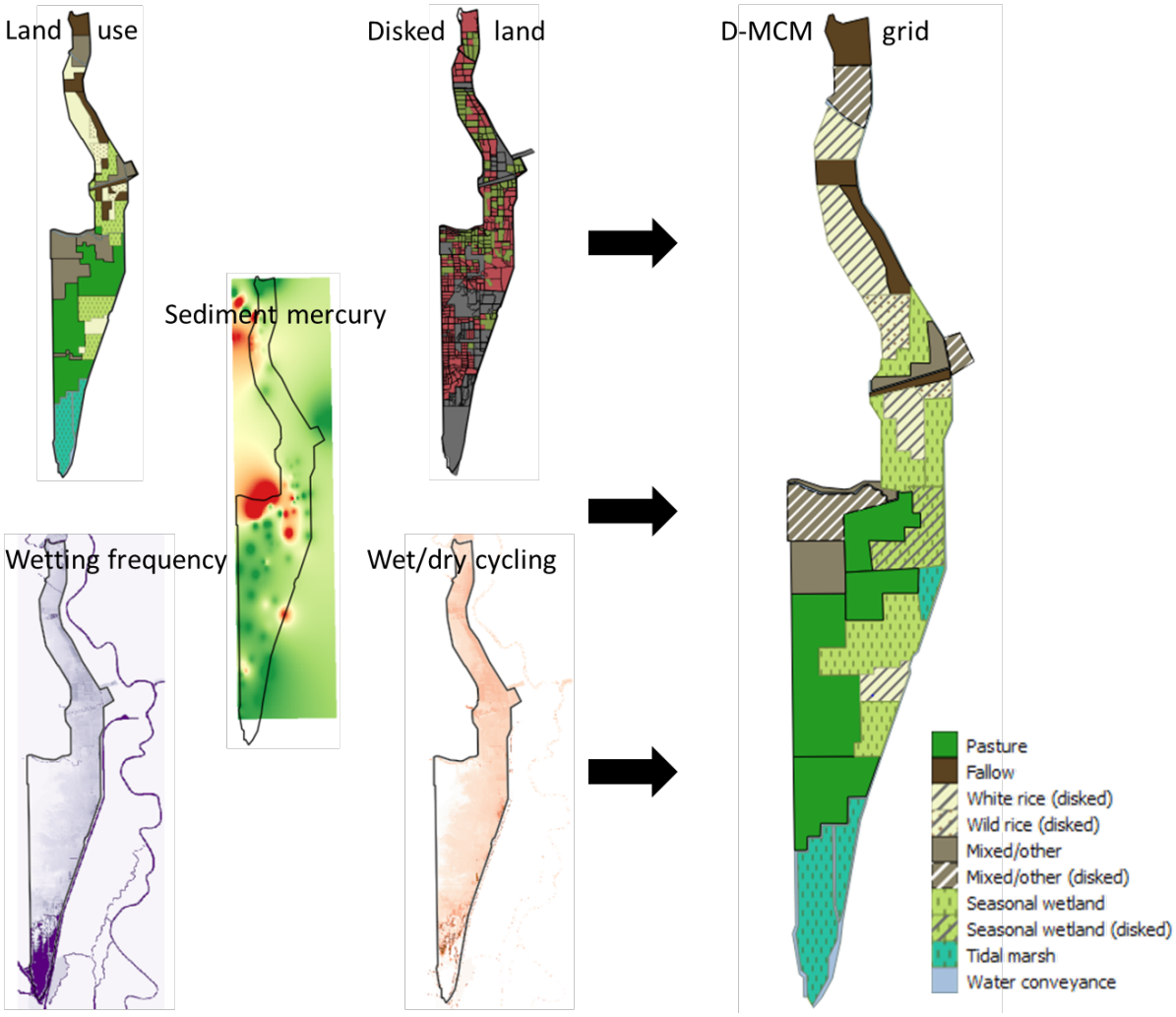

Figure 8-15. GIS layers representing five general factors contributed to the final D-MCM grid.

The model domain was defined by the TMDL boundary for the Yolo Bypass. Grid cells were first sketched out based exclusively on land use. Further simplifying and aggregating of the land use data was conducted to create cells without overly complex geometries or linkages/arrangements, which could encumber subsequent efforts to obtain hydrodynamic data from TUFLOW. Another consideration was that the grid must have built-in flexibility to accommodate new data. This was accomplished by using more, smaller cells rather than fewer, large ones.

Next, the contour maps of THg and MeHg in sediments were introduced. The contour maps were compared against the preliminary land use-based grid cells both by overlaying partially transparent layers and by toggling between layers. Some grid cell boundaries were modified and cells were divided as needed to take into account the spatial patterns in sediment mercury as well as land use.

The next factor considered was disking. This layer was overlaid with the working model grid to identify which grid cells were predominantly disked. In some cases, cell boundaries were adjusted to reflect more uniform disking conditions. The land use and disking datasets were from different time periods and some inconsistencies had to be corrected. For example, all white and wild rice fields were eventually disked in the model grid as this pattern is generally the case (M. Stephenson pers. comm.). Disked wetland was also considered to be a subcategory of interest, however there was not a single continuous area large enough to justify a dedicated cell. To address this issue, one wetland cell representing roughly 20 percent of total wetland area was taken to represent all disked wetland throughout the Bypass. This "lumping" approach was used in some other cases. The Yolo Bypass Wildlife Area dataset showed some permanent ponds, but they were not included as a model cell due to their small total area.

Frequency of wetting and wet/dry cycling were the final factors considered in grid development. Layers were again overlaid with the working grid and the grid was modified to better reflect these factors. The hydrodynamic data helped identify permanently wet areas which became water conveyance cells in the grid. The data also showed that Liberty Island was a hydrodynamically active area, therefore the highest density of cells in the grid were concentrated there. Both hydrodynamic layers showed a longitudinal gradient across parts of the Bypass which is reflected by the grid having a width of at least two cells in the relevant areas.

8.2.3.6. Using TUFLOW hydrodynamic model outputs in D-MCM simulations of Yolo Bypass.

Mercury simulations in the Yolo Bypass require estimates of water flowrates into and out of the Bypass, and between mercury model cells in the Bypass. Hourly to daily flows between cells will be based on results of the TUFLOW model for the period 1997-2012. The mercury model is using a much coarser grid than TUFLOW, which uses cells roughly 25' x 25'. Discussions have occurred between the TUFLOW and mercury modellers to develop a plan to aggregate flows to a scale that fits the mercury model. To maintain a mass balance for water, TUFLOW will provide D-MCM with the following information for each time step:

- Water flows across all cell boundaries
- Water surface elevation/ mean cell depth
- Wetted surface area of cell
- Cell volume

TUFLOW outputs will also be used in calculations to estimate the resuspension of solids in the Yolo Bypass, to use as an input in mercury simulations. Shear stresses calculated by TUFLOW

will be used in equations predicting mass erosion rates (See USGS discussion in this report). This will be done for each TUFLOW segment within a mercury model cell, and then summed to estimate the erosion for a mercury model cell. This post processing of TUFLOW outputs to estimate mass resuspension will be carried out by Reed Harris Environmental Ltd. This task requires funding for DWR and supporting hydrological modeling consultants that is not yet in place.

8.3. Linkage Analysis between DSM2-Hg and D-MCM

For scenario analyses, the two models can be run separately or combined into a single model framework. There are advantages and disadvantages to each approach. For this modeling effort, the technical team has determined that the most feasible approach is to run each model separately. Outputs from the Yolo Bypass model (flow, solids, and mercury concentrations from) will be used as inputs into Delta simulations.

The geographic overlap between the two models is at the south end of the Yolo Bypass (Figure 8-16). Thus, as shown in Figure 8-17, the results from running the Yolo Bypass Model for a given scenario could potentially provide flow, solids and mercury concentrations from the Yolo Bypass into the Delta from locations such as:

- Shag Slough
- Liberty Cut
- Prospect Slough (including Toe Drain flow into Prospect Slough)

The technical team settled upon running the models separately because although running the models sequentially is conceptually straight forward, the reality of using the models together is more challenging. Since the Yolo Bypass model is a two-dimensional model and the Delta model is a one-dimensional model, the way that information is represented by each model is not the same. For example, the Yolo Bypass is represented by two-dimensional grid cells (e.g. rectangle or triangle) in its model and the Delta is represented by lines and nodes (Figure 8--2). The D-MCM Yolo Bypass model uses a finer resolution grid for the flow simulation (millions of grid cells) and a coarser grid for mercury simulation (42 grid cells). The Delta model uses the same grid for both flow and mercury simulation (several hundred grid channels/nodes). The two model domains have a relatively small geographical overlap in the southern Yolo Bypass (Figure 8-16). To run the models sequentially, a method would need to be developed that would convert the Yolo Bypass Model's simulated flows, solids and mercury concentrations in the southern end of the Yolo Bypass into a format that could be used as input for the Delta model (step 3 of Figure 8-17). The Delta model also requires point source information at its boundaries, so flow and mercury fluxes from the D-MCM's Yolo Bypass model's grid cell boundaries will likely need to be aggregated and converted into time series flows and concentrations at specific points, for example such as the end points of each of the channels represented in both models (Shag Slough, Liberty Cut, and Prospect Slough).

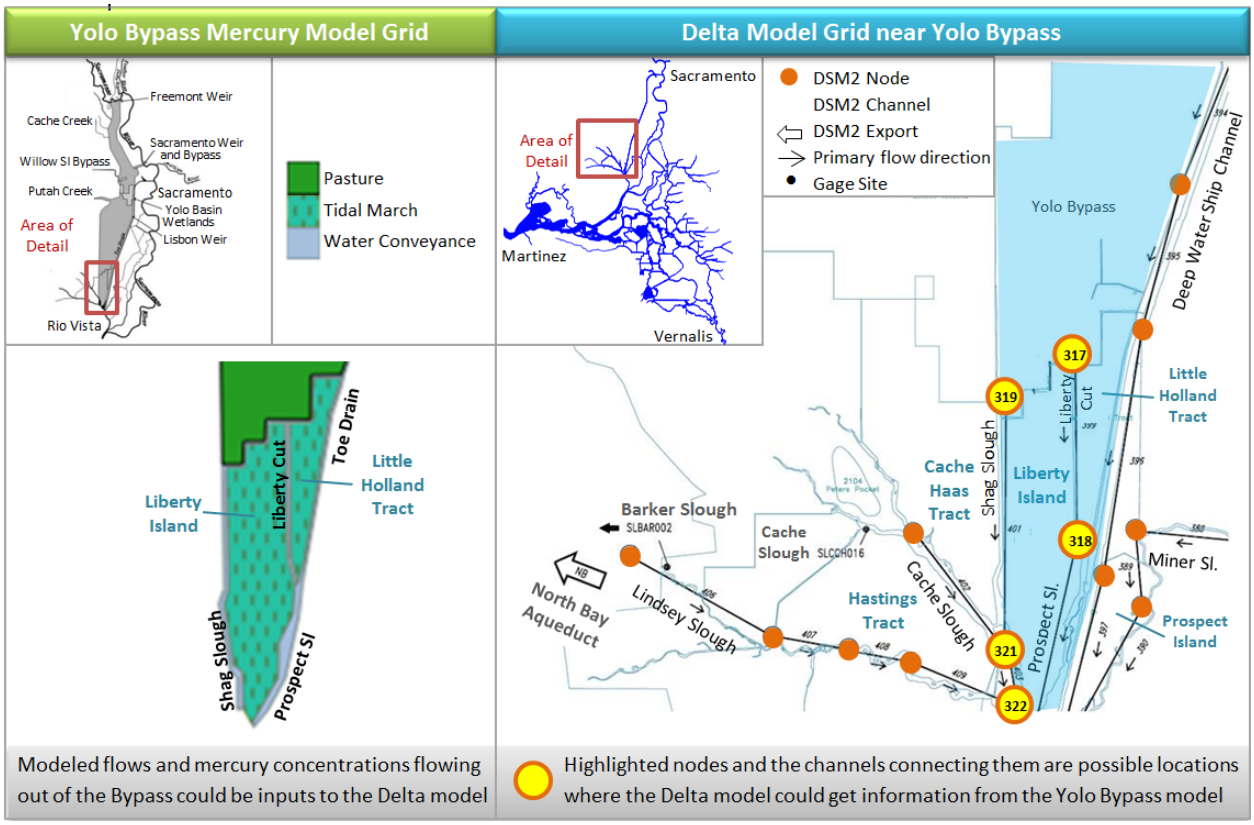

Figure 8-16. Geographic overlap between the Yolo Bypass and Delta Mercury models.

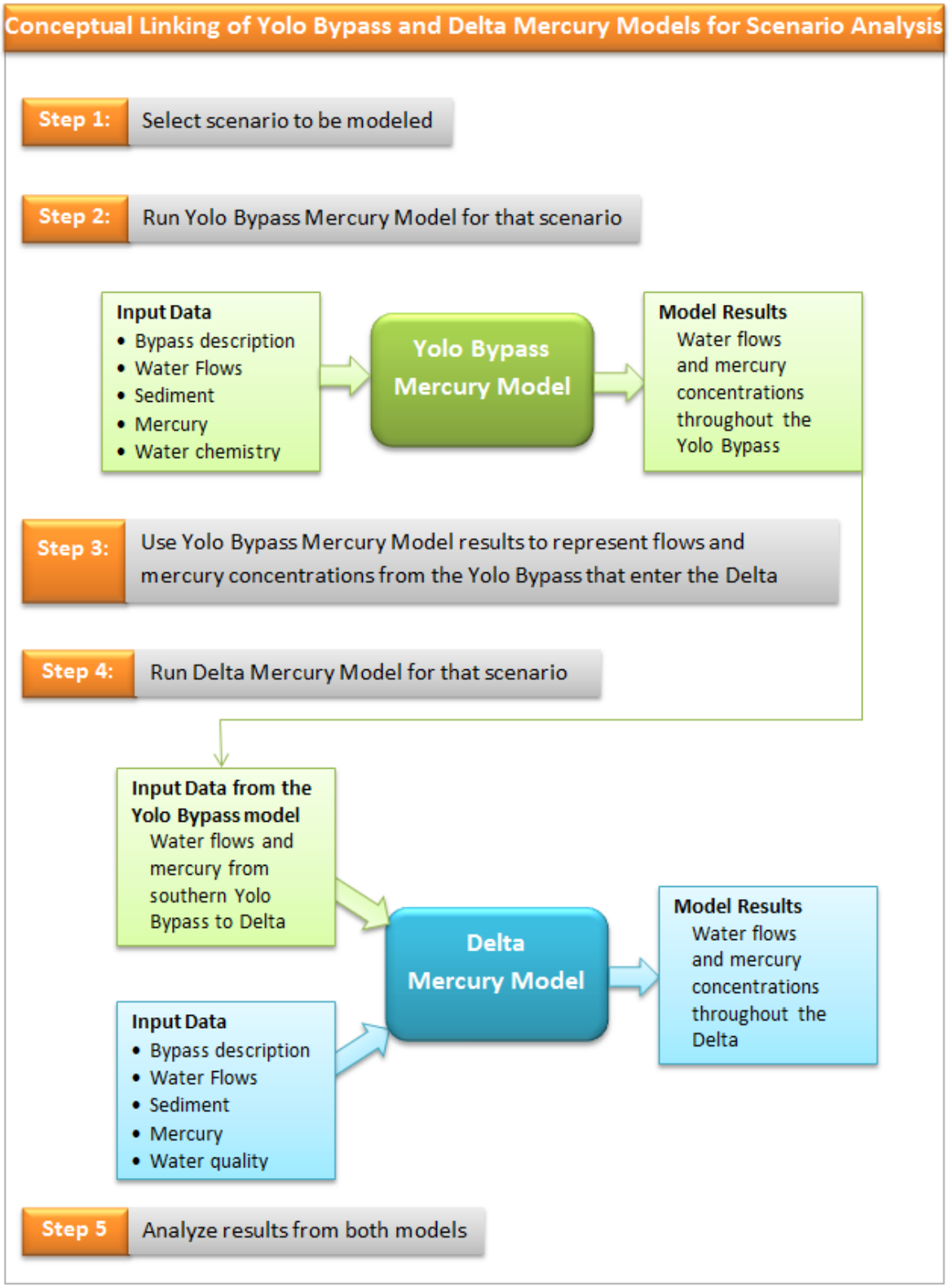

Figure 8-17. How the Yolo Bypass and Delta Mercury models could be linked for Scenario Analysis.

8.4. Literature Cited

Ackerman, J.T., A.K. Miles and C.A. Eagles-Smith (2010). Invertebrate mercury bioaccumulation in permanent, seasonal, and flooded rice wetlands within California's Central Valley. Science of the Total Environment 408: 666–671.

Alpers, C.N., J.A. Fleck, M. Marvin-DiPasquale, C.A. Stricker, M. Stephenson and H.E. Taylor (2014). Mercury cycling in agricultural and managed wetlands, Yolo Bypass, California: Spatial and seasonal variations in water quality. Science of the Total Environment 484: 276–287.

Bachand, P.A.M., S.M. Bachand, J.A. Fleck, F. Anderson and L.M. Windham-Myers (2014). Differentiating transpiration from evaporation in seasonal agricultural wetlands and the link to advective fluxes in the root zone. Science of the Total Environment 484: 232–248.

Bosworth, D.H., S.J. Louie, M.L. Wood, D.J. Little and H. Kulesza (2010). A Review of Methylmercury and Inorganic Mercury Discharges from NPDES Facilities in California's Central Valley Staff Report. California Environmental Protection Agency. Regional Water Quality Control Board. Central Valley Region. March 2010.

California Department of Fish and Game (2008). Yolo Bypass Wildlife Area Land Management Plan. Retrieved from https://nrm.dfg.ca.gov/FileHandler.ashx?DocumentID=84924&inline

California Department of Water Resources (2010). Central Valley Flood Management Program. State Plan of Flood Control. November 2010.

California Department of Water Resources (2011). "Chapter 6 Using Software Quality and Algorithm Testing to Verify a One-dimensional Transport Model", Methodology for Flow and Salinity Estimates in the Sacramento-San Joaquin Delta and Suisun Marsh, 32th Annual Progress Report to the State Water Resources Control Board, Prepared by the Delta Modeling Section, Bay-Delta Office, California Department of Water Resources, Natural Resources Agency, August 2011. http://baydeltaoffice.water.ca.gov/modeling/deltamodeling/AR2011/Method_2011_Ch6.pdf

California Department of Water Resources (2014). "Chapter 4 DSM2-GTM from Methodology for Flow and Salinity Estimates in the Sacramento-San Joaquin Delta and Suisun Marsh", 35th Annual Progress Report to the State Water Resources Control Board, Prepared by the Delta Modeling Section, Bay-Delta Office, California Department of Water Resources, Natural Resources Agency, June 2014. http://baydeltaoffice.water.ca.gov/modeling/deltamodeling/AR2014/Method_2014_Ch4.pdf

California Department of Water Resources (2015a). Sacramento River at Fremont Weir (FRE), California Data Exchange Center [Database]. Retrieved from http://cdec.water.ca.gov/cgi-progs/selectQuery?station_id=FRE&sensor_num=&dur_code=M&start_date=1980-01-01&end_date=2013-01-01

California Department of Water Resources (2015b). Sacramento River at Verona (VON), California Data Exchange Center [Database]. Retrieved from http://cdec.water.ca.gov/cgi-progs/selectQuery?station_id=VON&sensor_num=&dur_code=M&start_date=1980-01-01&end_date=2013-01-01

California Department of Water Resources (2015c). Cache Creek at Yolo (CCY), California Data Exchange Center [Database]. Retrieved from http://cdec.water.ca.gov/cgi-progs/selectQuery?station_id=CCY&sensor_num=&dur_code=M&start_date=1980-01-01&end_date=2013-01-01

California Department of Water Resources (2015d). Ridge Cut Slough at Knights Landing (RCS), California Data Exchange Center [Database]. Retrieved from http://cdec.water.ca.gov/cgi-progs/selectQuery?station_id=RCS&sensor_num=&dur_code=M&start_date=1980-01-01&end_date=2013-01-01

California Department of Water Resources (2015e). Liberty Island at Approximate Center South End (LIB), California Data Exchange Center [Database]. Retrieved from http://cdec.water.ca.gov/cgi-progs/staMeta?station_id=LIB

California Department of Water Resources (2015f). Yolo Bypass near Woodland (YBY), California Data Exchange Center [Database]. Retrieved from http://cdec.water.ca.gov/cgi-progs/staMeta?station_id=YBY

California Department of Water Resources (2015g). Yolo Bypass at Lisbon (LIS), California Data Exchange Center [Database]. Retrieved from http://cdec.water.ca.gov/cgi-progs/staMeta?station_id=LIS

California Department of Water Resources (2015h) California Data Exchange Center. Station search for chloride http://cdec.water.ca.gov/cgi-progs/staSearch?sensor_chk=on&sensor=148

California Department of Water Resources (2015i) California Data Exchange Center. Station search for chlorophyll a. http://cdec.water.ca.gov/cgi-progs/staSearch?sensor_chk=on&sensor=28

California Department of Water Resources (2015j) California Data Exchange Center. Station search for sulfate. http://cdec.water.ca.gov/cgi-progs/staSearch?sensor_chk=on&senso

California Department of Water Resources (2015k) California Data Exchange Center. Station Search for TOC. http://cdec.water.ca.gov/cgi-progs/staSearch?sensor_chk=on&sensor=179

California Department of Water Resources (20151) Sacramento – San Joaquin Delta Overview. http://baydeltaoffice.water.ca.gov/sdb/tbp/deltaoverview/index.cfm

California Department of Water Resources (2015m) California Data Exchange Center. Station Search for pH. http://cdec.water.ca.gov/cgi-progs/staSearch?sensor_chk=on&sensor=

California Regional Water Quality Board (2010). Central Valley Region. Resolution No. R5-2010-0043 Amendments to the Water Quality Control Plan for the Sacramento River and San Joaquin River Basins for the Control Of Methylmercury and Total Mercury in the Sacramento-San Joaquin Delta Estuary.

CBEC (2010a). Yolo Bypass Two-Dimensional Hydrodynamic Modeling. Prepared for Metropolitan Water District of Southern California. May 2010. Project # 08-1015

CBEC (2010b). BDCP Effects Analysis: 2D Hydrodynamic Modeling of the Fremont Weir Diversion Structure. Prepared for SAIC and the California Department of Water Resources. November 2010.

Choe, K.Y., G.A. Gill, R.D. Lehman, S. Han, W.A. Heim and K.H. Coale (2004). Sediment–water exchange of total mercury and monomethyl mercury in the San Francisco Bay–Delta. Limnol. Oceanogr. 49(5): 1512–1527.

Colorado State University (2015a). UV-B Monitoring and Research Program, Natural Resource Ecology Laboratory. Photosynthetically Active Radiation (PAR) [Database]. Retrieved from http://uvb.nrel.colostate.edu/UVB/da_queryPar.jsf

Colorado State University (2015b). UV-B Monitoring and Research Program, Natural Resource Ecology Laboratory. Erythemal Radiation [Database]. Retrieved from http://uvb.nrel.colostate.edu/UVB/da_queryErythemal.jsf

Conoway, C., J. R.M. Rossb, R. Lookerc, R. P. Masond, A. R. Flegala (2007). Decadal mercury trends in San Francisco Estuary sediments. Environmental Research 105 (2007): 53–66.

Davis, J.A., B.K. Greenfield, G. Ichikawa, and M. Stephenson (2008). Mercury in sport fish from the Sacramento-San Joaquin Delta region, California, USA. Science of the Total Environment 391: 66-75.

Delta Methylmercury TMDL Nonpoint Sources Workgroup (2012). Memo submitted to D. Beaulaurier, Central Valley Regional Water Control Board. August 17, 2012.

DiGiorgio, C. (2013). Yolo Bypass tour September 2013 [Map].

Domagalski, J.L., C.N. Alpers, D.G. Slotton, T.H. Suchanek and S.M. Ayers (2004). Mercury and methylmercury concentrations and loads in the Cache Creek watershed, California. Science of the Total Environment 327: 215–237.

Fleck, J.A., G. Gill, B.A. Bergamashci, T.E.C. Kraus, B.D. Downing and C.N Alpers (2014). Concurrent photolytic degradation of aqueous methylmercury and dissolved organic matter. Science of the Total Environment 484:263–275.

Foe, C., S. Louie and D. Bosworth (2008). Task 2 Methyl mercury Concentrations and Loads in the Central Valley and Freshwater Delta. In: Stephenson M., C. Foe, G. A. Gill, and K. H. Coale (2008). Transport, Cycling, and Fate of Mercury and Monomethyl Mercury in the San Francisco Delta and Tributaries: An Integrated Mass Balance Assessment Approach, CALFED Mercury Project Final Report, September 15, 2008.

Gehrke G.E., J. D. Blum and M. Marvin-DiPasquale (2011). Sources of mercury to San Francisco Bay surface sediment as revealed by mercury stable isotopes. Geochimica et Cosmochimica Acta 75 (2011): 691–705.

Gill, G.A. (2008a). Task 5.3, Atmospheric Mercury Deposition Studies. In: Stephenson M., C. Foe, G. A. Gill, and K. H. Coale (2008). Transport, Cycling, and Fate of Mercury and Monomethyl Mercury in the San Francisco Delta and Tributaries: An Integrated Mass Balance Assessment Approach, CALFED Mercury Project Final Report, September 15, 2008.

Gill, G.A. (2008b). Task 5.1 Monomethylmercury Photodegradation Studies. In: Stephenson M., C. Foe, G. A. Gill, and K. H. Coale (2008). Transport, Cycling, and Fate of Mercury and Monomethyl Mercury in the San Francisco Delta and Tributaries: An Integrated Mass Balance Assessment Approach, CALFED Mercury Project Final Report, September 15, 2008.

Gill, G.A. (2008c). Task 5.4. Air-Water Exchange Studies. In: Stephenson, M. C. Foe, G.A. Gill, and K.H. Coale (2008). Transport, Cycling, and Fate of Mercury and Monomethyl Mercury in

the San Francisco Delta and Tributaries: An Integrated Mass Balance Assessment Approach, CALFED Mercury Project Final Report, September 15, 2008.

Grenier, L., A. Melwani, J. Hunt, S. Bezalel, J. Davis, G. Ichikawa, B. Jakl, W. Heim, A. Bonnema, and M. Gassel (2007). California Bay-Delta Authority Fish Mercury Project Year 1 Annual Report Sport Fish Sampling and Analysis. California Office of Environmental Health Hazard Assessment CBDA Project # ERP 02D-P67 29. May 2007.

Heim, W.A., K. Coale, and M. Stephenson (2008). Methyl and Total Mercury Spatial and Temporal Trends in Surficial Sediments of the San Francisco Bay-Delta. CALFED Mercury Project Final Report.

Heim, W.A., S. Deverel, T. Ingram, W. Piekarski and M. Stephenson (2009). Assessment of Methylmercury Contributions from Sacramento-San Joaquin Delta Farmed Islands. Final report submitted to Chris Foe and the Central Valley Regional Water Quality Control Board.

Heim, W.A., A. Newman, A. Byington, B. Hughes and M. Stephenson (2010). Spatial Distribution of Total Mercury in the Yolo Bypass: Implications for Land Use Management of Mercury Contaminated Floodplains. May 2010. Final report submitted to Chris Foe and the Central Valley Regional Water Quality Control Board.

Heim, W.A., M. Stephenson, A. Bonnema, A. Byington, A. Newman, D. Feliz, Levi Sousa and K. Coale (2011) Methylmercury Concentrations and Exports from Seasonal Wetlands in the Yolo Wildlife Area, California. Draft manuscript.

Howitt, R., MacEwan, D., Garnache, C., Azuara, J.M., Marchand, P., Brown, D., Six, J., Lee, J. 2013. Final Report. Agricultural and Economic Impacts of Yolo Bypass Fish Habitat Proposals. Prepared for Yolo County. April 2013.

Kirkland, M. (2011). Early Yolo Bypass Inundation Modeling Results. Presentation to BDCP Yolo Bypass Fishery Enhancement Planning Team. June 30, 2011.

Leatherbarrow J.E., L.J. McKee, D.H. Schoellhamer, N.K. Ganju and A. R. Flegal (2005). Concentrations and Loads of Organic Contaminants and Mercury associated with Suspended Sediment Discharged to San Francisco Bay from the Sacramento-San Joaquin River Delta, California. San Francisco Estuary Regional Monitoring Program for Trace Substances.

Lee, G.F. and A. Jones Lee (2008). Runoff of Mercury from UCD/DOE LEHR Superfund Site – Putah Creek Mercury Issues. Delta Tributary Council [Presentation]. December 2, 2008.

Lehman, P.W., T. Somer and L. Rivard (2007). The influence of floodplain habitat on the quantity and quality of riverine phytoplankton carbon produced during the flood season in San Francisco Estuary. Aquat. Ecol. DOI 10.1007/s10452-007-9102-6.

Lehman, P.W., S. Mayr, L. Mecum and C. Enright (2010). The freshwater tidal wetland Liberty Island, CA was both a source and sink of inorganic and organic material to the San Francisco Estuary. Aquat. Ecol. 44: 359–372.

Louie, S., C. Foe and D. Bosworth (2008). Task 2 Mercury and Suspended Sediment Concentrations and Loads in the Central Valley and Freshwater Delta. In: Stephenson, M., C. Foe, G.A. Gill and K. H. Coale (2008). Transport, Cycling, and Fate of Mercury and Monomethyl Mercury in the San Francisco Delta and Tributaries: An Integrated Mass Balance Assessment Approach, CALFED Mercury Project Final Report, September 15, 2008. https://mercury.mlml.calstate.edu/wp-content/uploads/2008/10/16_task2_deposition.pdf.

Marvin-DiPasquale, M., R. Stewart, N.S. Fisher, P. Pickhardt, R.P. Mason, A. Heyes, and L. Windham-Myers (2007). Evaluation of Mercury Transformations and Trophic Transfer in the San Francisco Bay/Delta: Identifying Critical Processes for the Ecosystem Restoration Program. The California Bay-Delta Authority (CBDA). ERP-02-P40 Progress Report April 2, 2007.

Marvin-DisPasquale, M., C.N. Alpers and J.A. Fleck (2009). Mercury, Methylmercury, and Other Constituents in Sediment and Water from Seasonal and Permanent Wetlands in the Cache Creek Settling Basin and Yolo Bypass, Yolo County, California, 2005−06. USGS open file report 2009-1182.

Marvin-DisPasquale, M., L. Windham-Myers, J.L. Agee, E. Kakouros, Le H. Kieu, J.A. Fleck, C.N. Alpers and C.A. Stricker (2014). Methylmercury production in sediment from agricultural and non-agricultural wetlands in the Yolo Bypass, California, USA. Science of the Total Environment 484: 288–299.

McCord, S. (2014). Yolo Bypass Primer.

Melwani, A., S. Bezalel, J. Hunt, L. Grenier, J. Davis, G. Ichikawa, B. Jakl, W. Heim, A. Bonnema, and M. Gassel (2007). California Bay - Delta Authority Fish Mercury Project Year 2 Annual Report Sport Fish Sampling and Analysis. San Francisco Estuary Institute.

Melwani, A.R., S.N. Bezalel, J.A. Hunt, J.L. Grenier, G. Ichikawa,W. Heim, A. Bonnema, C. Foe, D.G. Slotton and J.A. Davis (2009). Spatial trends and impairment assessment 1 of mercury in sport fish in the Sacramento-San Joaquin Delta Watershed.

Morgan-King, T., and D.H. Schoellhamer (2013). Suspended-Sediment Flux and Retention in a Backwater Tidal Slough Complex near the Landward Boundary of an Estuary. Estuaries and Coasts 36: 300–318. DOI 10.1007/s12237-012-9574-z

NADP (National Atmospheric Deposition Program) (2015a). Retrieved from http://nadp.isws.illinois.edu/data/sites/siteDetails.aspx?id=CA88&net=NTN

NADP (National Atmospheric Deposition Program) (2015b). Mercury Deposition Network data from Site CA72 (San Jose) from 2000- 2006. Retrieved from http://nadp.sws.uiuc.edu/sites/siteinfo.asp?id=CA72&net=MDN

NADP (National Atmospheric Deposition Program) (2015c). Mercury Deposition Network data from Site CA97 1997-2000. Retrieved from http://nadp.sws.uiuc.edu/sites/siteinfo.asp?id=CA97&net=MDN

Natural Heritage Institute, California Department of Water Resources, California Department of Fish and Game, Yolo Basin Foundation, Northwest Hydraulic Consultants, G. Yates, P. Kiel, and Jones & Stokes (2002). Habitat Improvement for Native Fish in the Yolo Bypass. December 2002.

NHC (Northwest Hydraulic Consultants) (2003). Assessment of sediment budget of Sacramento-San Joaquin Delta. Report prepared for the California Department of WaterResources, Sacramento, California, July 2003, 36 p.

Opperman, J.J. (2012). A Conceptual Model for Floodplains in the Sacramento-San Joaquin Delta. San Francisco Estuary & Watershed Science. October 2012.

Saleh, D.K, J. L. Domagalski, C.R. Kratzer, and D.L. Knifong (2007). Organic Carbon Trends, Loads, and Yields to the Sacramento-San Joaquin Delta, California, Water Years 1980 to 2000, Second Edition. U.S. Geological Survey. Water Resources Investigation Report 03-4070, Second Edition. Sacramento, California 2007.

Schemel, L.E., M.H. Cox, S.W. Hager and T.R. Sommer (2002). Hydrology and Chemistry of Floodwaters in the Yolo Bypass, Sacramento River System, California, During 2000. U.S. Geological Survey Water Resources Investigations Report 02-4202.

Schoellhamer D.H., S.A. Wright, J.Z. Drexler and M. Stacy (2007). Sedimentation conceptual model. Sacramento, CA: Delta Regional Ecosystem Restoration Implementation Plan.

Schoellhamer, D.H., S.A. Wright, and J.Z. Drexler (2012). Conceptual Model of Sedimentation in the Sacramento-San Joaquin River Delta. San Francisco Estuary and Watershed Science. October 2012.

Singer, M.B. and T. Dunne (2006). Modeling the influence of river rehabilitation scenarios on bed material sediment flux in a large river over decadal timescales. Water Resources Research, Vol 42, W12415.

Singer, M.B., R. Aalto and L.A. James (2008). Status of the Lower Sacramento Valley Flood-Control System within the Context of Its Natural Geomorphic Setting. Natural Hazards Review 9(3): 104–115.

Singer, M.B. and R. Aalto (2009). Floodplain development in an engineered setting. Earth Surf. Process. Landforms 34: 291–304.

Springborn, M., M.B. Singer and T. Dunne (2011). Sediment-adsorbed total mercury flux through Yolo Bypass, the primary floodway and wetland in the Sacramento Valley, California. Science of the Total Environment 412-413: 203–213.

Stephenson, M., K. Coale, G. Gill and M. Puckett (2001). Transport, Cycling, and Fate of Mercury and Monomethyl Mercury in the San Francisco Delta and Tributaries – An Integrated Mass Balance Assessment Approach [Proposal].

Stephenson and Bonnema (2008). Task 5.3a. Methylmercury Loss in the Delta through Particulate Deposition. In: Stephenson and Bonnema (2008). Transport, Cycling, and Fate of Mercury and Monomethyl Mercury in the San Francisco Delta and Tributaries: An Integrated Mass Balance Assessment Approach, CALFED Mercury Project Final Report, September 15, 2008. https://mercury.mlml.calstate.edu/wp-content/uploads/2008/10/16_task5_3a_deposition.pdf

US Army Corps of Engineers (2007). Yolo Bypass 2-D Hydraulic Model Development and Calibration. Sacramento District. May 2007.

US Geological Survey (2013). Sacramento River at Freeport, National Water Information System. Retrieved from http://waterdata.usgs.gov/usa/nwis/uv?site_no=11447650

US Geological Survey (2015a). USGS Sediment Portal [Database]. Retrieved from http://cida.usgs.gov/sediment

US Geological Survey (2015b). Sacramento River at Verona, National Water Information System [Database]. Retrieved from http://waterdata.usgs.gov/nwis/inventory?agency_code=USGS&site_no=11425500

US Geological Survey (2015c). Cache Creek at Yolo, National Water Information System [Database]. Retrieved from http://waterdata.usgs.gov/usa/nwis/uv?11452500

US Geological Survey (2015d). Cache Creek Overflow Weir from Settling Basin near Woodland, National Water Information System [Database]. Retrieved from http://waterdata.usgs.gov/nwis/inventory?agency_code=USGS&site_no=11452800

US Geological Survey (2015e). Cache Creek total flow from Settling Basin near Woodland, National Water Information System [Database]. Retrieved from http://waterdata.usgs.gov/nwis/inventory?agency_code=USGS&site_no=11452901

US Geological Survey (2015f). Putah Creek near Winters, National Water Information System [Database]. Retrieved from http://waterdata.usgs.gov/nwis/inventory?agency_code=USGS&site_no=11454000

US Geological Survey (2015g). Willow Slough Bypass near Davis, National Water Information System [Database]. Retrieved from http://waterdata.usgs.gov/nwis/inventory?agency_code=USGS&site_no=383525121434383

US Geological Survey (2015h). Sacramento Weir Spill to Yolo Bypass near Sacramento, National Water Information System [Database]. Retrieved from http://waterdata.usgs.gov/nwis/inventory?agency_code=USGS&site_no=11426000

US Geological Survey (2015i). Cache Slough at South Liberty Island near Rio Vista, National Water Information System [Database]. Retrieved from http://waterdata.usgs.gov/nwis/inventory?agency_code=USGS&site_no=11455315

US Geological Survey (2015j). Yolo Bypass near Woodland, National Water Information System [Database]. Retrieved from http://waterdata.usgs.gov/usa/nwis/uv?11453000

US Geological Survey (2015k). Yolo Bypass at I-80 near West Sacramento, National Water Information System [Database]. Retrieved from http://waterdata.usgs.gov/nwis/inventory?agency_code=USGS&site_no=11453120

US Geological Survey (2015l). Yolo Bypass near Woodland, National Water Information System [Database]. Retrieved from http://waterdata.usgs.gov/nwis/inventory?agency_code=USGS&site_no=11453000

US Geological Survey (2015k). http://waterdata.usgs.gov/nwis/monthly?referred_module=sw&site_no=11447650&por_11447650_4=2209860,80154,4,1956-10,2014-09&format=html_table&date_format=YYYY-MM-DD&rdb_compression=file&submitted_form=parameter_selection_list

WDL (Water Data Library) (2015). Retrieved from http://www.water.ca.gov/waterdatalibrary

Windham-Myers, L.M, M. Marvin-DiPasquale, J. Fleck, C.N. Alpers, J. Ackerman, C. Eagles-Smith, C. Stricker, M. Stephenson. D. Feliz, G. Gill, P. Bachand, A. Brice, and R. Kulakow (2010). Methylmercury cycling, bioaccumulation, and export from agricultural and non-agricultural wetlands in the Yolo Bypass. Final Report. September 30, 2010.

Windham-Myers, L.M. and J.T. Ackerman (2012). A Synthesis of Mercury Science to Support TMDL Implementation (Phase 1 Control Studies) for San Francisco Bay - Delta Wetlands and Irrigated Agriculture [Presentation].

Windham-Myers, L.M. (2014a). Methylmercury cycling in wetlands managed for rice agriculture and wildlife: Implications for methylmercury production, transport, and bioaccumulation. Science of the Total Environment 484: 219–220.

Windham-Myers, L.M., M. Marvin-DiPasquale, E. Kakouros, J.L. Agee, Le H. Kieu, C. A. Stricker, J. A Fleck and J.T. Ackerman (2014b). Mercury cycling in agricultural and managed wetlands of California, USA: Seasonal influences of vegetation on mercury methylation, storage, and transport. Science of the Total Environment 484: 308–318.

Windham-Myers, L.M., J.A. Fleck, J.T. Ackerman, M. Marvin-DiPasquale, C.A. Stricker, W.A. Heim, P.A.M. Bachand, C.A. Eagles-Smith, G. Gill, M. Stephenson and C.N. Alpers (2014c). Mercury cycling in agricultural and managed wetlands: A synthesis of methylmercury production, hydrologic export, and bioaccumulation from an integrated field study. Science of the Total Environment 484: 221–231.

Wood, M.L., C.G. Foe, J. Cooke, and S.J. Louie (2010). California Environmental Protection Agency, Regional Water Quality Control Board, Central Valley Region. Sacramento – San Joaquin Delta Estuary TMDL for Methylmercury. Staff Report. April 2010.

Yolo Bypass Working Group, Yolo Basin Foundation, and Jones & Stokes (2001). A Framework for the Future: Yolo Bypass Management Strategy. Prepared for the CALFED Bay-Delta Program.

9. Next Steps

This progress report covers open water progress through approximately June 2015. Figure 9-1 provides an updated draft schedule on remaining tasks described in more detail in the subsections below.

9.1. Field and Laboratory Experiments

9.1.1. Next Steps—Inlet/Outlet Study

Inlet/outlet samples are scheduled to be collected in the winter of 2015/16 during mini-flood and major flooding events. However, sample collection is predicated on the weather and hydrology to create the appropriate flooding regimes in the Yolo Bypass. Data from flooding events will be provided to the Yolo Bypass D-MCM model for use in either calibration or validation model runs.

9.1.2. Next Steps—Gust Chamber

The technical team will evaluate final approaches, however; it is anticipated that Gust Chamber analyses will be performed at the 5-6 additional land-use sites used by the D-MCM Yolo Bypass model. These potentially include (1) fallow or irrigated pasture, (2) below CCSB, (3) Liberty Island, (4) Toe Drain near Lisbon Weir, and (5) Toe Drain near Little Holland tract (Liberty Cut). Most of these sites are continuously submerged and will be sampled from a boat, helping reduce any dependency on weather conditions. At higher velocities, and in vegetated areas, the Gust Chamber is not capable of providing erosion characteristics for the D-MCM Yolo Bypass model. Since Bale Chamber pilot experiments indicated that our studies should rely on Gust Chamber results for the erosion rates of solids, the technical team will investigate approaches that could be used under these circumstances. Some of the approaches to be evaluated may include whether literature values can be used to extrapolate Gust Chamber erosion characteristics at higher velocities, or whether the Bale Chamber could be used to provide a relative indicator of erosion characteristics between vegetated and non-vegetated sites.

9.1.3. Next Steps—Bale Chamber

Pilot experiments indicate that the Bale Chamber could not reliably provide erosion information at velocities > 1ft/sec. The technical team is evaluating if the Bale Chamber can still provide the Gust Chamber with relative information on the erosion characteristics of vegetated and non-vegetated land uses. The technical team is also evaluating if the Bale Chamber can still provide useful Hg concentration information for the D-MCM Yolo Bypass calibration and validation runs.

9.1.4. Next Steps—Pore Water Diffusive Flux

Results of the pilot pore water diffusion experiments successfully demonstrated their ability to provide the D-MCM Yolo Bypass model with mercury flux estimates, pore water concentrations, and Kd values. Final approaches will be determined by the technical team, but next steps potentially include conducting pore water diffusion experiments on the remaining land uses covered by the D-MCM Yolo Bypass Model. Samples will be collected from the same locations sampled by USGS in the winter of 2014/15 and winter 2015/16 for Gust Chamber analysis. These land-uses are: (1) white rice, (2) seasonal wetland-disked, (3) below Putah Creek, (4) fallow or irrigated pasture, (5) below CCSB, (7) Liberty Island, (8) Toe Drain near Lisbon Weir, and (9) the Toe Drain near Little Holland tract (Liberty Cut). Besides conducting pore water diffusional flux experiments on these land uses, the pilot experiments suggest that we may wish to adapt our upcoming experiments to incorporate more replicates, and potentially add a temporal component to a subset of sample station to determine if flux measurements change depending on whether pore water experiments are conducted at different times during the flood season.

9.2. Next Steps—Modeling

9.2.1. Next Steps--DSM2-Hg Modeling

The updated schedule for open water modeling tasks is shown in Figure 9-1. Modeling efforts to-date for DSM2-Hg have focused on refinement of the conceptual model, coding routines for Hg cycling in the water column, and data assembly. These tasks are well underway or largely completed. The next tasks involve linking the new Hg routines to DSM2, adjusting the DSM2 model interface to accommodate the new Hg routines, adding code to DSM2 to represent the sediment bed (particles and mercury), and developing model inputs from the available data and literature.

The development of the DSM2-Hg model is also dependent on the GTM upgrade to DSM2. This upgrade is being developed in parallel with the development of DSM2-Hg modules. The next step in the GTM development process is to complete a Delta-wide simulation of salinity using the GTM. This simulation will demonstrate that the GTM can correctly simulate Delta salinity processes. Secondly, as part of the GTM development, output model results need to be written to HECDSS and HDF5 formats.

While the workgroup's modeling team is making every effort to create a modeling product within the DMCP's deadline, it has become apparent that the schedule provided in the original workplan did not fully represent the tasks or complexity associated with building a Delta Hg model and a timeline extension will be required to complete modeling tasks. Figure 9-1 provides an updated draft timeline. To the best of the modeling team's ability, the schedule

incorporates a timeline that reflects the time to complete the modeling steps listed in the updated schedule. The increase in time is required due to the following:

- Workplan approval vs. DMCP deadline—The open water workplan was submitted by the April 20, 2013 deadline. The updated schedule reflects approval of the workplan in February 2014. Losing a year of modeling effort, due to the uncertainty of workplan approval, created an a priori time-induced handicap that cannot be overcome with the current level of resources.

- Addition of Bed Sediment module—We did not originally anticipate that a bed sediment module would be required in addition to a Hg module. The need for this module was only discovered once modeling tasks got underway and data gaps were examined. The updated schedule has built time into the schedule to complete and test this module.

- Addition of Other Water Quality Constituents—The updated schedule has included time to research relationships of additional water quality constituents (sulfate and pH) that may be needed by the mercury model. Currently sulfate and pH are not modeled in DSM2. Modeling these constituents would require modeling their reactions, along with other non-modeled, non-conservative constituents. Adding these parameters would be a significant task on its own so, early on, the decision was made to use sulfate and pH data directly as inputs. To use this approach, the focus has been to try and find relationships between sulfate and pH and other parameters such as location, time of year, hydrology, or other water quality conditions. This effort is ongoing and has now been included in the updated schedule.

- Development and testing of water quality modules—The mercury modeling effort has been added to a much larger DWR modeling project to modernize the water quality (QUAL) portion of DSM2. Known as the GTM module, the updated schedule now includes time for testing the GTM as a standalone module. The updated schedule also includes time to test individual modules required for Hg modeling (for example, the suspended sediment, bed sediment and Hg modules) as well as time to test their interaction with the GTM. This type of “unit testing” is a testing process done in computer programing to make sure that the code works correctly.

- Calibration and validation of water quality modules—The original schedule did not include time for calibration, and validation for salinity, non-conservative water quality, and sediment modules that interact with the mercury module. The updated schedule now provides time to complete these tasks. Currently, DSM2-Qual has been calibrated

and validated for salinity and non-conservative constituents. However, Qual is being replaced by the GTM and will need to be recalibrated. This replacement is necessary in order for all the modules to interact properly. For modeling salinity, a simple conservative substance, dispersion coefficients for hundreds of channels are adjusted and observed data and model output are compared. Tools, such as the Parameter Estimation Tool (PEST), are used to help streamline the process. Recalibration time increases significantly with the addition of non-conservative water quality, and sediment and mercury parameters.

- Scenario Analysis—Validation studies will help assess whether the models are robust enough to predict previously collected data, and move forward to scenario or predictive testing. While the original schedule included time for modeling scenarios, the updated schedule now includes time to select and vet scenarios from both a policy and technical perspective.
- Reporting—Based on the complexity of the review process, additional time has been added for review by technical, legal, and management participants.

9.2.2. Next Steps--D-MCM Yolo Bypass Modeling

Yolo Bypass activities to-date have focused on the following.

- Development of the conceptual model
- Data assembly
- Discussions with DWR hydrodynamic modelers about inputs for the mercury model related to flows
- Discussions with DWR and the USGS about options and field/laboratory studies to estimate particle fluxes (e.g. resuspension and settling), and
- Development of a model grid for D-MCM mercury simulations in the Yolo Bypass.

The next steps for the Yolo Bypass modeling are obtain TUFLOW hydrodynamic data from DWR's consultants, necessary for model inputs related to flow, and also needed to estimate resuspension rates in different areas of the Yolo Bypass. As described in the Gust Chamber section, shear stress outputs from DWR's TUFLOW model will be used to estimate resuspension rates. This task will be carried out by Reed Harris Environmental Ltd. In parallel with those activities, other inputs needed for Yolo Bypass mercury simulations will be developed. The full set of Yolo Bypass modeling tasks is shown in Figure 9-1.

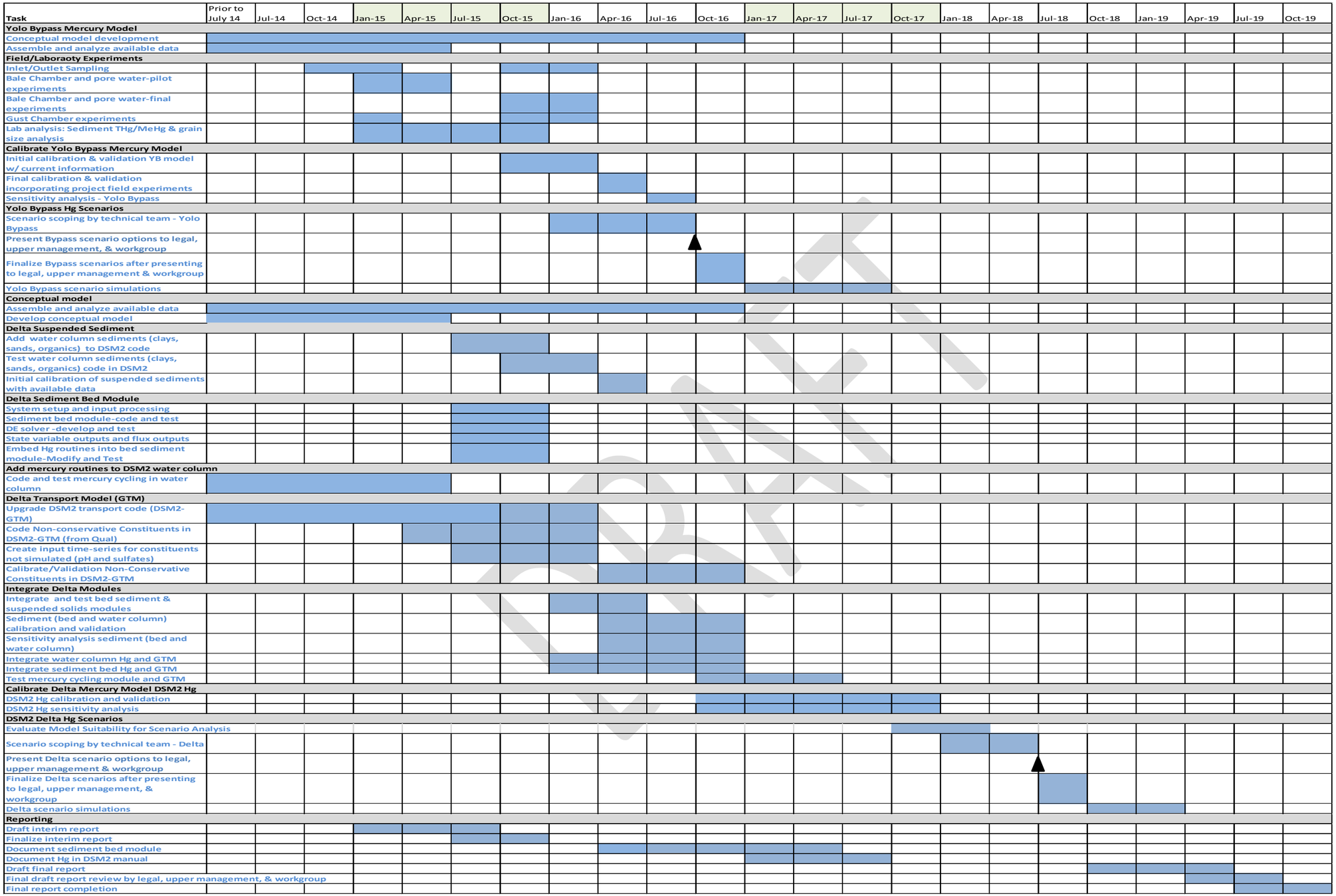

Figure 9-1. Draft revised open water modeling and field/laboratory schedule.